

International Atomic Energy Agency

INDC(NDS)-412
Distr. G+RP

INDC

INTERNATIONAL NUCLEAR DATA COMMITTEE

**Measurement, Calculation and Evaluation of
Photon Production Data**

Final Report of a Coordinated Research Project

Edited by

P. Obložinský
IAEA Vienna, Austria

F.S. Dietrich
LLNL Livermore, U.S.A.

A. Mengoni
ENEA Bologna, Italy

December 1999

IAEA NUCLEAR DATA SECTION, WAGRAMERSTRASSE 5, A-1400 VIENNA

Reproduced by the IAEA in Austria
December 1999

Measurement, Calculation and Evaluation of Photon Production Data

Final Report of a Coordinated Research Project

Edited by

P. Obložinský
IAEA Vienna, Austria

F.S. Dietrich
LLNL Livermore, U.S.A.

A. Mengoni
ENEA Bologna, Italy

Abstract

The report summarizes results of the Coordinated Research Project (CRP) devoted to photon production in neutron-induced reactions. The report presents 25 original contributions that reflect accomplishments achieved in measurement, calculation and evaluation of photon production under the project in 1994-1997. Major results are highlighted and a list of the CRP publications is given.

December 1999

Preface

Over a period of several last years, the IAEA Nuclear Data Section conducted a series of Coordinated Research Projects (CRPs) devoted to specific aspects of nuclear reaction data. These projects focused either on improvements of nuclear data evaluation methodology and related tools, or on development of actual databases. An example of the former would be the reference input parameter library for nuclear model calculations (RIPL, completed in 1998). Example of the latter would be the charged-particle cross section database for medical radioisotope production (completed in 1999), and the photonuclear data library (to be completed in 2000). Both aspects, evaluation methodology and data development, were present in the project devoted to photon production in nuclear reactions.

Photons (γ rays) produced in nuclear reactions are of substantial practical interest. Photons represent an important part of energy released in nuclear power generation facilities, and they must be tracked in photon transport calculations to establish heating of various reactor components. Photons must be considered in designing biological shielding of nuclear facilities, and discrete gamma rays provide information about the nucleus from which they originate and thus about the isotope composition of an emitting material.

Photon production in nuclear reactions was traditionally somewhat neglected topic. A need to improve the evaluation methodology and related databases represented a motivation to initiate a CRP on "Measurement, Calculation and Evaluation of Photon Production Data".

The response to this initiative was appreciable and ten laboratories from 9 countries took part in the project during 1994-1997: Austria (IRK Vienna - H.K. Vonach assisted by A. Pavlik), Germany (TU Dresden - S. Unholzer), Italy (ENEA Bologna - A. Mengoni), Japan (JAERI Tokai - K. Shibata), Netherlands (JUKO Alkmaar - J.Kopecky), Russia (IPPE Obninsk - S.P. Simakov), Slovakia (IP SAS Bratislava - E. Běták assisted by S. Hlaváč), Slovenia (IJS Ljubljana - F. Cvelbar assisted by A. Likar), and USA (LLNL Livermore - F.S. Dietrich, and ORNL Oak Ridge - J.K. Dickens). The group met at 3 Research Coordination Meetings (14-17 November 1994 in Bologna, 21-24 May 1996 in Vienna and 29 September-3 October 1997 in Bled).

The CRP produced several useful and interesting results. Among them are new and better measurements of photon production including very important benchmark experiments, improved procedures to calculate photon production, and several new evaluations. Furthermore, the CRP provided an overall assessment of photon production, produced compilations of photon data, and prepared recommendations for future evaluations.

The CRP was formally completed in 1997, with the intention to prepare an extensive final report in 1998. This appeared to be too ambitious and had to be replaced by a more realistic collection of papers that would sufficiently illustrate results of the project. Thus, with some delay, we offer the nuclear data community the present Final Report of the CRP.

The report is organized as follows. Chapter 1 explains main elements and accomplishments of the project. This is followed by 25 papers highlighting specific results obtained under the project. Chapter 2 is devoted to experimental studies, including actual measurements and benchmarking analyses. Then, Chapter 3 deals with calculations, codes and recommended procedures. Finally, Chapter 4 explains compilations and evaluations. The list of CRP publications is given in Appendix A, followed by the list of CRP participants in Appendix B.

Pavel Obložinský, Vienna, December 1999

Frank Dietrich, Livermore, December 1999

Alberto Mengoni, Bologna, December 1999

CONTENTS

1. Introduction	7
Scope of the CRP	7
Accomplishments of the CRP	8
2. Measurements and Benchmarking Analyses	11
Cross Sections for Discrete γ Ray Production in Interactions of 14.6 MeV Neutrons with Light and Medium Heavy Nuclei <i>S. Hlaváč et al</i>	12
Measurement of gamma-ray production cross sections in $^{27}\text{Al}(n,xn\gamma)$ and $^{208}\text{Pb}(n,pxn\gamma)$ reactions for neutron energies up to 400 MeV <i>A. Pavlik et al</i>	27
Gamma Ray Production Following Spallation Reactions in ^{27}Al and ^{56}Fe Induced by 800 MeV Protons <i>H. Vonach et al</i>	32
Analysis of Gamma-Ray Emission Spectra from Spherical Piles with a 14 MeV Neutron Source <i>F. Maekawa</i>	36
Measurement of Gamma-Ray Spectra and Heating Rates in Cylindrical Assemblies <i>F. Maekawa et al</i>	43
New Analysis of Photon Flux Spectra from an Iron Slab Benchmark Experiment <i>U. Fischer et al</i>	52
Neutron Induced Photon Flux Spectra Inside an ITER Shield Mockup <i>H. Freiesleben et al</i>	57
3. Calculations, Codes and Recommended Procedures	63
Modeling 14 MeV Neutron Radiative Capture <i>F. Cvelbar et al</i>	64
Comparison of Discrete Gamma Calculations with GNASH and DEGAS <i>E. Běták</i>	72
Extension of the Direct-Semidirect Model for Calculating the High Energy Component of Fast-Nucleon Induced Gamma Spectra <i>F.S. Dietrich</i>	77
Mass Dependence of the Complex Coupling in the DSD Model Generated by the Consistency Requirement <i>A. Likar and T. Vidmar</i>	88
Calculation of Photon Production in Light Nuclei <i>A. Mengoni</i>	95
Computer Programs and Data Libraries Pertaining to Photon Production Data <i>J.E. White et al</i>	101

Pre-Equilibrium Codes for Gamma Emission <i>E. Běták</i>	104
Direct-Semidirect (DSD) Codes <i>F. Cvelbar</i>	109
Recommended Gamma Ray Strength Functions <i>J. Kopecky</i>	119
Recommendations for Pre-Equilibrium Calculations <i>E. Běták</i>	134
Recommendations for DSD Model Calculations <i>F. Cvelbar</i>	139
4. Compilations and Evaluations	143
Status of Experimental and Evaluated Data for Discrete Gamma-Ray Production at 14.5 MeV Neutron Incident Energy <i>S.P. Simakov et al</i>	144
Atlas of Neutron Capture Cross Sections (NGATLAS) <i>J. Kopecky</i>	151
Review of Experimental Capture Gamma Spectra for Neutrons above 10 MeV <i>F.S. Dietrich</i>	154
Experimental Database for Gamma-Ray Strength Functions <i>J. Kopecky</i>	163
Evaluations of Radiative Capture on C, O, and Li <i>A. Mengoni et al</i>	184
Evaluation of Photon Production Data for Fe and Ni <i>K. Shibata</i>	195
Review of Evaluations of Photon Production for ${}^7\text{Li}$ and ${}^{52}\text{Cr}$ <i>J.K. Dickens</i>	200
Appendices	
Appendix A: List of Publications produced by the CRP	205
Appendix B: Participants of the CRP	213

1 Introduction

Photons (γ rays) accompany practically all nuclear interactions and are of substantial practical interest for two reasons. First, they represent an important part of energy released in nuclear power generation facilities. In a fusion reactor, for example, photons from $(n, x\gamma)$ reactions constitute the major part of energy released. Energy output calculations require precise knowledge of γ production cross sections, γ ray spectra and whenever possible also their angular distributions. These γ rays must be tracked in photon transport calculations to establish heating of various reactor components. Another major concern refers to biological shielding and, more generally, to transport of radiation through material.

Second, γ rays yield important information about the nucleus from which they originate and thus about the isotope composition of an emitting material. This aspect can be used as a very efficient tool to identify production of stable, long-lived and also short-lived nuclei. This is important for example in assessment of environmentally critical material activation of nuclear energy as well as non-energy facilities, for nuclear waste transmutation and nuclear geophysical applications.

A considerable progress has been achieved in recent years in understanding the physics of photon emission in nuclear reactions, in developing sophisticated techniques for their measurements, and in assessment of importance of photon production for a number of applications (see conclusions of the 1990 Specialists' Meeting, where the idea of the photon CRP was formulated for the first time [1]). This provides for a sufficient background to address necessary improvements in evaluation procedures and methods and related accuracy and quality of photon production data in the evaluated nuclear data files. This effort should take into account understanding and theoretical modelling of photon emission primarily in $(n, x\gamma)$ and capture reactions, the substantial new amount of measured photon data especially in discrete spectral energy range, and the growing variety of applications.

1.1 Scope of the CRP

The CRP aimed to examine the current status of measurements, calculations and evaluations of photon production with the emphasis on neutron-induced reactions, work out procedures and methods to be recommended for future evaluation procedures of photon production data, and improve selected photon production cross sections in internationally recognized general purpose nuclear data libraries.

The following topics were covered:

- Experimental photon data: Assessment of status, selected own measurements, recommendations for future measurements. Included was capture

(at very low energies and at 14 MeV), $(n, x\gamma)$ reactions (at 14 MeV, from threshold to 20 MeV, and above 20 MeV), and integral experiments for data testing.

- Theoretical photon data: Status, selected improvements, recommendations. Included was physics of capture, physics of $(n, x\gamma)$ reactions, assessment of computer codes for photon production and input parameters for its calculations.
- Evaluations: Specific developments, status, recommendations. Developmental activities included atlas of neutron capture cross sections, compilation of discrete gamma production at 14 MeV, and a file of recommended gamma-ray strength functions. Further included was status of evaluations and benchmarking of evaluated photon production libraries.

1.2 Accomplishments of the CRP

Measurements and Benchmarks. Experimental developments were primarily concerned with measurements of discrete γ -ray production cross sections. Several careful measurements on medium-heavy nuclei were done at the 14-MeV neutron facility in Bratislava. Measurements at the Los Alamos WNR facility of gamma production induced by a white neutron source up to 200-400 MeV proved to provide data for sensitive testing of nuclear reaction model calculations. Of special interest is a new multidetector array (GEANIE) for continuing these measurements. In addition, an extensive set of benchmark measurements was performed in Tokai and partly in Dresden. Benchmark tests of gamma production were performed for a number of materials for the evaluated libraries JENDL-3.2, JENDL Fusion File and FENDL, providing an important assessment of the quality of these files. A specific effort was devoted to an integral test of neutron-induced photon production for Fe and comparison with Monte Carlo calculations using the EFF-1 library.

Calculations. New developments in the calculation of gamma spectra were largely concerned with the modeling of high energy (> 10 MeV) gamma rays. These include an extension of the direct-semidirect (DSD) model to treat unbound final states that was successfully tested on a data set of 34-MeV proton capture. The direct radiative capture model was successfully applied to explain observed capture on ^{12}C and ^{16}O for $E_n < 1$ MeV, with results already included into the Japan Evaluated Nuclear Data Library JENDL-3.2. Of interest are attempts to understand the origin of the imaginary coupling in the semidirect form factor and the phenomenological separation of the DSD from multistep mechanisms. A consistent preequilibrium exciton model that includes spin effects was tested against $(n, x\gamma)$ data and compared with the recommended code GNASH.

Compilations and Evaluations. Completed was an interesting Atlas of Neutron Capture Cross Sections comprising 737 target nuclei for neutrons up

to 20 MeV. An update of the status of gamma-ray strength functions was done and the file of recommended strength functions was prepared. Compilation of discrete γ ray production for all practically important elements with 14 MeV neutrons was prepared. New evaluations for ^{12}C and ^{16}O , and for Ni and Fe were done for the JENDL library.

Publications. 4 interim reports illustrate the progress of the project [2-5]. A total of 82 technical and scientific papers were produced in the course of the CRP as listed in the Appendix A of the present report. Specifically mentioned should be two extensive and user oriented publications, a comprehensive atlas of neutron capture cross sections [6], and a summary of computer programs for photon data [7]. In addition, a useful overview was prepared on experimental and evaluated discrete γ -ray production with 14 MeV neutrons [8]. In support of the CRP an atlas of energy-angular distributions of gamma rays was published [9].

References

- [1] Ed. N.P. Kocherov, "Measurement, Calculation and Evaluation of Photon Production Cross Sections", Proc. IAEA Specialists' Meeting, Smolenice, Czechoslovakia, 5-7 February 1990. (Report INDC(NDS)-238, IAEA Vienna, September 1990).
- [2] Ed. P. Obložinský, 1-st Research Coordination Meeting, Report INDC(NDS)-330 (IAEA, Vienna, Mar 1995).
- [3] Ed. P. Obložinský, "Measurement, Calculation and Evaluation of Photon Production Data", Report INDC(NDS)-334 (IAEA, Vienna, May 1995).
- [4] Ed. P. Obložinský, 2-nd Research Coordination Meeting, Report INDC(NDS)-357 (IAEA, Vienna, December 1996).
- [5] Ed. P. Obložinský, 3-rd Research Coordination Meeting, Report INDC(NDS)-375 (IAEA, Vienna, January 1998).
- [6] J. Kopecky et al. "Atlas of Neutron Capture Cross Sections (NGATLAS)", Report INDC(NDS)-362 (IAEA, Vienna, April 1997), 369 pages. See also <http://www-nds.iaea.or.at/ngatlas>.
- [7] J. White et al. "Computer Programs and Data Libraries Pertaining to Photon Production Data", Report ORNL/RSIC-57 (ORNL, Oak Ridge, 1997), 160 pages.
- [8] S.P. Simakov, A. Pavlik, H. Vonach and S. Hlaváč, "Status of Experimental and Evaluated discrete γ -ray production at $E_n = 14.5$ MeV", Report INDC(CCP)-413 (IAEA, Vienna, September 1998), 61 pages.
- [9] A.I. Blokhin et al. "Atlas of Energy-Angular Distribution of Gamma Rays Produced in Neutron Reactions", Report INDC (CCP)-387 (IAEA, Vienna, February 1996), 140 pages.

2 Measurements and Benchmarking Analyses

Among the tasks accomplished by the CRP were measurements and benchmark analysis of γ -ray production cross sections. As described in several contributions to this chapter, the experimental developments were primarily concerned with measurements of discrete γ -ray production cross sections. Reports are given here on several careful measurements on medium-heavy nuclei done at the 14-MeV neutron facility in Bratislava. Measurements of γ production induced by a white neutron source up to 200-400 MeV (Los Alamos WNR facility) provided data for sensitive test of nuclear reaction model calculations. Of special interest for continuing this kind of measurements is the multidetector array GEANIE.

Reports on additional benchmark measurements of neutron flux as well as photon flux recently performed in JAERI (Japan) and Dresden (Germany) documents the most relevant initiatives taken by the CRP on this field.

The present Chapter includes 7 papers to be found in the following pages.

Cross Sections for Discrete γ Ray Production in Interactions of 14.6 MeV Neutrons with Light and Medium Heavy Nuclei

S. Hlaváč, M. Benovič, E. Běták, L. Dostál, I. Turzo
*Institute of Physics SAS,
842 28 Bratislava, Slovakia*

S. P. Simakov
*Institute of Physics and Power Engineering,
Obninsk, Russian Federation*

Abstract

We measured cross section of prompt discrete γ ray transitions produced in 14.6 MeV neutron interactions with ^{23}Na , ^{27}Al , ^{28}Si , ^{31}P , ^{39}K , ^{51}V , ^{55}Mn and ^{nat}Mo . Cross sections were measured relative to reference cross sections with low uncertainties using a dedicated experimental setup with a 244 cm³ HPGe photon detector and associated α particle timing. In addition to photons from inelastic scattering we observed discrete transitions from (n,p), (n,n'p), (n, α), and (n,2n) reactions. Discrete γ transitions in $^{28}\text{Si}(n,n'p)^{27}\text{Al}$, the majority of transitions in Mn+n, and all transitions in Mo+n reactions were observed for the first time. Where available, our experimental data are compared with existing data. This comparison shows that existing data are in disagreement with present data in many cases, a finding which stresses the necessity of standardization of measurement procedure. For some reactions we compared our results with statistical model predictions, calculated with the advanced code GNASH as well as with a technically simpler code DEGAS, developed in our lab. In several instances, mostly in reactions where only a single nucleon is emitted, the statistical model calculations describe the observed cross sections well. In other cases, where several nucleons are emitted sequentially or in a cluster, the agreement is less satisfactory.

1 Introduction

Production cross section of prompt discrete γ transitions are interesting from many different aspects. Population of discrete levels reflect physical processes

leading to their population and may bring new information concerning reaction mechanisms as well as properties of the nuclei involved. Discrete γ ray cross sections give us information on population of discrete levels with definite spins and parities, which is analogous to the measurement of isomeric ratios – a useful quantity obtained using the activation technique. However, data measured by using discrete γ transitions are more detailed, because population of several levels in all reactions may be measured simultaneously.

Apart from interesting physics, cross sections of discrete γ transitions are important for a growing number of applications.

During the fusion programme, many reaction cross sections were necessary for evaluation of different aspects of fusion technology, including such diverse fields as energy balance of the reactor, safety considerations, and long term environmental impact. The required data include in some instances reactions leading to product nuclei which are stable or have a very long half-life. In such cases, which are difficult or impossible to measure with conventional activation techniques, the prompt γ ray alternative may bring an estimation of the required reaction cross sections.

We measured discrete prompt γ ray production cross sections in reactions induced by 14.6 MeV neutrons with ^{23}Na , ^{27}Al , ^{28}Si , ^{31}P , ^{39}K , ^{51}V , ^{55}Mn , and ^{nat}Mo . The selection of measured nuclei was to a great extent influenced by requests for experimental data included in WRENDA [1], compiled and carefully reviewed in a paper [2] included in this report.

Cross sections on ^{27}Al were measured with the collaboration of IRK Vienna to obtain absolute values at 14.6 MeV for the normalization of their white source measurements. The γ ray production measurements in $^{28}\text{Si}(n,n'\text{p}\gamma)^{27}\text{Al}$ and $^{39}\text{K}(n,p\gamma)^{39}\text{Ar}$ reactions was motivated by the conclusions of the IAEA Consultants Meeting [3] on activation cross sections.

In the following we briefly describe the experimental setup used in the measurements. Then we will subsequently present measured cross sections of discrete γ transitions in individual reactions. In the discussion we compare our experimental data with the available literature data as well as with the theoretical calculations performed within the statistical model of nuclear reactions.

2 The experimental procedure

The measurements were performed at the 14 MeV neutron source of the Institute of Physics, Bratislava. A detailed description of the neutron source [4] and the whole experimental facility [6] was recently published. The setup consists of a neutron source with an associated α particle detector, neutron shielding, HPGe photon detector and a CAMAC based data acquisition system. A schematic drawing of the experimental setup is shown in Fig. 1. The neutron source is based on an 300 keV deuteron accelerator with momentum analysis of the accelerated deuteron beam. Typical separated D^+ beam current and energy were about 80 μA and 150 keV, respectively. The D^+ beam strikes a TiT

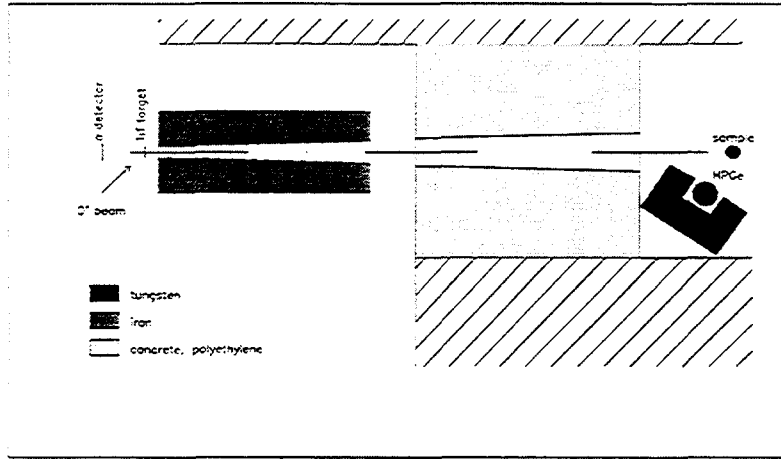


Figure 1: Schematic drawing of the experimental setup.

target and the alpha particles from the $T(D,n)\alpha$ reaction are detected in a fast plastic scintillation detector, which defines by its solid angle the electronically collimated neutron beam as well as the timing for neutrons. The uncollimated part of the neutron beam is shielded by a massive concrete/polyethylene collimator. The neutron energy at the target position was 14.6 ± 0.3 MeV and the total neutron flux at the sample was up to 10^4 n cm $^{-2}$ s $^{-1}$, depending on the TiT target conditions.

The sample was located behind the collimator at a distance of 2.75 m from the TiT target. A HPGe detector with an active volume of 244 cm 3 and resolution of 2.2 keV at 1332 keV was placed at an angle of 125 $^\circ$ with respect to the neutron beam at the distance of 17.8 cm from the sample. The HPGe detector was shielded by a tungsten shield to reduce further the background from the scattered neutrons as well as from photons. We determined the relative efficiency curve of the HPGe detector using standard sources ^{60}Co and ^{152}Eu . For higher energy we used ^{24}Na , which we produced by the reaction $^{27}\text{Al}(n,\alpha)^{24}\text{Na}$ during the experiment. For data acquisition a CAMAC based multiparameter system was used. The main parameters were photon energy and time-of-flight, which were stored in a list mode file during the experiment. As a rule, several runs with different samples (pure and mixed with reference nuclei) as well as background measurement were performed. Background in the photon detector is produced mainly by neutrons scattered from the sample. It was measured with a target having a similar number of different nuclei as in the measured sample. A typical run time for a single cross section as well as background measurement was around 50 hours. Net prompt photon energy spectra were obtained from the the two-parameter spectra using the standard procedure of subtracting the uncorrelated part of the spectrum from the prompt window in the time domain.

We determined areas of the individual single peaks by simply integrating

Reaction	Transition	Energy (keV)	Cross section (mb)
$^{28}\text{Si}(n,n'\gamma)$	$2^+ \longrightarrow 0^+$	1778.9	406 ± 19
$^{52}\text{Cr}(n,n'\gamma)$	$2^+ \longrightarrow 0^+$	1434.1	683 ± 38
$^{56}\text{Fe}(n,n'\gamma)$	$2^+ \longrightarrow 0^+$	846.8	609 ± 31

Table 1: Gamma transitions and their cross sections at 14.6 MeV used as a reference in the present experiments.

the peak area and subtracting the background determined on both sides of the peak. To resolve several closely spaced lines in the spectrum, the areas of individual components was obtained by a fit, where the fitting function was a sum of Gaussians superimposed on a linear background.

In order to reduce uncertainties we measured cross sections relative to well known cross sections. All transitions we used for reference were $2^+ \longrightarrow 0^+$ transitions in even-even nuclei excited by inelastic neutron scattering. Transitions and their cross sections at 14.6 MeV incident neutron energy are summarized in Table 1. The cross section for production of the 1778.9 keV γ transition in the $^{28}\text{Si}(n,n'\gamma)$ reaction was taken from a recent compilation [7] at 14.5 MeV (403 ± 18 mb) and a gradient of 30.5 ± 13.7 mb/MeV, obtained by the fit to the existing experimental data [8]. Cross sections were calculated according to the formula

$$\sigma_i = \frac{N_i \times \epsilon_{ref} \times C_{ref} \times f_i \times n_{ref}}{N_{ref} \times \epsilon_i \times C_i \times f_{ref} \times n_i} \times \sigma_{ref}, \quad (1)$$

where σ is the cross section, N is the peak area observed in the spectrum, ϵ is the relative full energy peak efficiency, C is the correction for γ ray absorption in the sample, f is the correction for multiple neutron scattering in the sample and n is the number of nuclei in the sample. Subscripts i and ref refer to the measured individual and reference γ transitions, respectively. Corrections for multiple scattering were calculated as described in previous work [5]. For the Na, P, V and Mn experiments, corrections for multiple scattering were calculated using the MCNP-4a code.

The properties of samples used in these measurements, their chemical form, weight and geometry are summarized in Table 2. Uncertainties in the measured cross sections are influenced mainly by statistical uncertainties of the net peak areas, uncertainties of the reference cross sections, and other uncertainties, which are summarized in Table 3. Uncertainty of the normalization of the Cr reference cross section applies only in the case where we measured the reference cross section in a separate run, *i.e.* in the cases of ^{23}Na , ^{31}P , and ^{51}V . In all other cases we used combined samples and we measured the reference cross section simultaneously.

Sample	Form	Size (mm)	Weight (g)	No. of nuclei $\times 10^{24}$
Na	$\text{Na}_4\text{P}_2\text{O}_7$	$\varnothing 44 \times 70$	118.5	1.074
Al	metallic Al	$80 \times 80 \times 5$	86.2	1.924
Al+Fe	metallic Al + metallic Fe	$80 \times 80 \times (5.7+1.3)$	98.1+67.7	2.190 + 0.670
Si	crystalline Si	$\varnothing 120 \times 10; \varnothing 120 \times 5$	258.5, 129.6	5.542, 2.778
K	$\text{KOH} + \text{Cr}_2\text{O}_3$	$\varnothing 84 \times 12.5$	56.1+51.9	1.01+0.29
P	$\text{Na}_4\text{P}_2\text{O}_7$	$\varnothing 44 \times 70$	118.5	0.537
V	metallic V (hollow cyl.)	$\varnothing 30/20 \times 50$	120.3	1.542
Mn	metallic Mn	$\varnothing 84 \times 12.5$	218.0	2.39
Mn+Cr	metallic Mn+ Cr_2O_3	$\varnothing 84 \times 12.5$	120.2+80.0	1.32 + 0.63
Cr	metallic Cr (hollow cyl.)	$\varnothing 44/35 \times 60$	133.1	1.542
Mo+Cr	metallic Mo + Cr_2O_3	$\varnothing 84 \times 12.5$	131.3+20.1	0.82+0.16

Table 2: Characteristics of samples used in the present work.

Source of uncertainty	Value (%)
Net peak area	3-20
Reference cross section	4-5
Relative detector efficiency	3
Neutron multiple scattering	<3
Correction for γ absorption	1.5
Normalization to Cr reference cross section	4
Total	7-22

Table 3: Uncertainties in measured $(n,x\gamma)$ cross sections.

3 Experimental results

In this chapter we present results of our experiments in tabular form. For each observed transition we give the transition energy, spin, and parities of initial and final states, the reaction, and the measured cross section. In several reactions also cross sections calculated within the statistical model of nuclear reactions using codes GNASH and DEGAS are shown.

In measurements with ^{23}Na and ^{31}P we used the combined sample (see Table 2) and normalization to ^{52}Cr was performed in a separate run with a metallic Cr sample. Results of these measurements for ^{23}Na and ^{31}P are summarized in Table 4 and Table 7, respectively.

In the ^{27}Al experiments we used two samples. A pure Al sample was used for relative cross section measurements in reactions on Al. The second combined Al+Fe sample was used for measurement of cross sections of strong γ transitions relative to $2^+ \rightarrow 0^+$ in ^{56}Fe . Results of the measurements are summarized in Table 5.

Measurements of γ ray production cross sections in $^{28}\text{Si} + n$ reactions were performed using crystalline samples of semiconductor purity relative to the cross section for $2^+ \rightarrow 0^+$ in ^{28}Si . Results are given in Table 6.

We identified also two weak γ transitions with energies of 843.6 keV and 1014.4 keV from the $^{28}\text{Si}(n,n'\text{p}\gamma)^{27}\text{Al}$ reaction. Because of the decay pattern of the even-odd nucleus ^{27}Al , where all observed excited levels decay directly to the ground state, the cross section for the $^{28}\text{Si}(n,n'\text{p}\gamma)$ reaction is the sum of both observed cross sections which yields the value 20.9 ± 3.6 mb.

The measurements on ^{39}K were performed with a combined K+Cr sample. The photon production cross sections were determined relative to the 1434.1 transition in ^{52}Cr . Results are given in Table 8. Here we observed a strong $2^+ \rightarrow 0^+$ transition from the $^{39}\text{K}(n,n'\text{p})^{38}\text{Ar}$ reaction, which is important for nuclear waste assessment [3]. Cross sections for this transition in even-even nucleus ^{38}Ar may serve as an estimate of the reaction cross section.

Measurements on V were performed using a pure metallic sample. The reference cross section measurement of the $2^+ \rightarrow 0^+$ transition in ^{52}Cr was performed in a separate run using a metallic Cr sample. Results are displayed in Table 9.

For cross section measurements of n+Mn reactions two samples were used. A combined Mn+Cr sample was used for cross section measurements of strong γ transitions relative to the $2^+ \rightarrow 0^+$ transition in ^{52}Cr , whereas a pure Mn sample served for relative cross section measurements in n+Mn reactions. Results are summarized in Table 10.

We measured for the first time the photon production on ^{nat}Mo using a mixed metallic powder Mo+Cr sample, using Cr as a monitor. We observed photons from inelastic neutron scattering as well as from the (n,2n) reaction. ^{nat}Mo consists of a chain of 5 closely spaced isotopes with masses 94-98 and two isolated isotopes with $A = 92$ and 100. For discrete γ production in these nuclei we measured the sum of the contributions of both $^{A}\text{Mo}(n,n'\gamma)$ and

E_γ (keV)	Transition	Reaction	Cross section (mb)
627.5	$9/2^+ \rightarrow 7/2^-$	$^{23}\text{Na}(n,n')^{23}\text{Na}$	26 ± 5
656.0	$3^+ \rightarrow 2^+$	$^{23}\text{Na}(n,\alpha)^{20}\text{F}$	45 ± 6
822.7	$4^+ \rightarrow 2^+$	$^{23}\text{Na}(n,\alpha)^{20}\text{F}$	13 ± 2
1274.5	$2^+ \rightarrow 0^+$	$^{23}\text{Na}(n,n'p)^{22}\text{Ne}$	194 ± 14
1636.0	$7/2^+ \rightarrow 5/2^+$	$^{23}\text{Na}(n,n')^{23}\text{Na}$	149 ± 11

Table 4: Cross sections of discrete γ rays observed in $n+^{23}\text{Na}$.

E_γ	Transition	Reaction	Cross section (mb)
843.7	$1/2^+ \rightarrow 5/2^+$	$^{27}\text{Al}(n,n')^{27}\text{Al}$	35.9 ± 5.9
984.6	$3/2^- \rightarrow 1/2^+$	$^{27}\text{Al}(n,p)^{27}\text{Mg}$	32.2 ± 2.7
1014.4	$3/2^+ \rightarrow 5/2^+$	$^{27}\text{Al}(n,n')^{27}\text{Al}$	72.1 ± 5.6
1697.9	$5/2^+ \rightarrow 1/2^+$	$^{27}\text{Al}(n,p)^{27}\text{Mg}$	27.8 ± 2.7
1808.6	$2^+ \rightarrow 0^+$	$^{27}\text{Al}(n,n'p)^{26}\text{Mg}$	244 ± 21
2211.1	$7/2^- \rightarrow 5/2^-$	$^{27}\text{Al}(n,n')^{27}\text{Al}$	176 ± 13
2981.8+3004.2	$3/2^+, 9/2^+ \rightarrow 5/2^+$	$^{27}\text{Al}(n,n'p)^{26}\text{Mg}$	137 ± 12

Table 5: Discrete γ ray production cross sections in the reaction $^{27}\text{Al}(n,x\gamma)$ measured at 14.6 MeV incident neutron energy.

Reaction	E_γ (keV)	Experiment (mb)	GNASH (mb)	DEGAS (mb)
(n,n' γ)	2838.8	99 ± 10	98.3	85.0
(n,p γ)	941.7	18 ± 3	16.2	5.4
	983.0	23 ± 3	23.3	13.1
	1013.6	28 ± 4	14.5	8.1
	1589.2	25 ± 4	13.6	6.3
(n, $\alpha\gamma$)	585.1	75 ± 10	36.3	
	389.7	26 ± 4	13.3	
	974.7	41 ± 5	13.8	
(n,n'p γ)	843.6	9.4 ± 1.9	6	4
	1014.4	11.5 ± 3.0	6	22

Table 6: Cross sections of discrete γ transitions measured in the $^{28}\text{Si}(n,x\gamma)$ experiment.

E_γ (keV)	Transition	Reaction	Cross section (mb)
1266.1	$3/2^- \longrightarrow 1/2^-$	$^{31}\text{P}(n,n')^{31}\text{P}$	186 ± 15
2148.3	$7/2^+ \longrightarrow 3/2^+$	$^{31}\text{P}(n,n')^{31}\text{P}$	51 ± 9
2233.6	$3/2^+ \longrightarrow 1/2^+$	$^{31}\text{P}(n,n')^{31}\text{P}$	390 ± 30

Table 7: Cross sections of discrete γ rays observed in $n+^{31}\text{P}$.

E_γ (keV)	Transition	Reaction	Cross section (mb)	GNASH (mb)	DEGAS (mb)
788.4	$3^+ \longrightarrow 2^-$	$^{39}\text{K}(n,\alpha\gamma)^{36}\text{Cl}$	20.1 ± 2.2	10.9	
1164.7	$1^+ \longrightarrow 2^+$	$^{39}\text{K}(n,\alpha\gamma)^{36}\text{Cl}$	17.3 ± 1.6	5.1	
1267.2	$3/2^- \longrightarrow 7/2^-$	$^{39}\text{K}(n,p\gamma)^{39}\text{Ar}$	19.3 ± 2.2	25.7	16.8
1769.0	$2^+ \longrightarrow 2^-$	$^{39}\text{K}(n,n'p\gamma)^{38}\text{Ar}$	6.7 ± 1.4	-	-
1951.0	$2^- \longrightarrow 2^+$	$^{39}\text{K}(n,\alpha\gamma)^{36}\text{Cl}$	9.7 ± 1.6	3.4	-
2167.6	$2^+ \longrightarrow 0^+$	$^{39}\text{K}(n,n'p\gamma)^{38}\text{Ar}$	193 ± 14	491	149
2813.8	$7/2^- \longrightarrow 3/2^+$	$^{39}\text{K}(n,n'\gamma)^{39}\text{K}$	74 ± 5	104	37.2
3597.6	$9/2^+ \longrightarrow 3/2^+$	$^{39}\text{K}(n,n'\gamma)^{39}\text{K}$	23 ± 3	24.3	5.6
3680.0	$(?) \longrightarrow 7/2^-$	$^{39}\text{K}(n,p\gamma)^{38}\text{Ar}$	98 ± 10	-	-

Table 8: Discrete γ ray production cross sections in the reaction $^{39}\text{K}(n,x\gamma)$ measured at 14.6 MeV incident neutron energy.

E_γ (keV)	Transition	Reaction	Cross section (mb)
815.	$? \longrightarrow 4^+$	$^{51}\text{V}(n,2n)^{50}\text{V}$	18.9 ± 4.9
836.3	$5^+ \longrightarrow 6^+$	$^{51}\text{V}(n,2n)^{50}\text{V}$	36.0 ± 3.3
909.8+912.9	$7^+ \longrightarrow 6^+, 2^+ \longrightarrow 2^+$	$^{51}\text{V}(n,2n)^{50}\text{V}$	85 ± 6
928.7	$3/2^- \longrightarrow 7/2^-$	$^{51}\text{V}(n,n')^{51}\text{V}$	46 ± 4
946.0	$2^+ \longrightarrow 3^+$	$^{51}\text{V}(n,2n)^{50}\text{V}$	20.9 ± 2.9
1090	$3/2^+ \longrightarrow 1/2^+$	$^{51}\text{V}(n,2n)^{50}\text{V}$	61 ± 5
1121.1	$4^+ \longrightarrow 2^+$	$^{51}\text{V}(n,n'p)^{50}\text{Ti}$	14.5 ± 2.3
1173.1	$2^+ \longrightarrow 2^+$	$^{51}\text{V}(n,2n)^{50}\text{V}$	22.2 ± 2.9
1437	unassigned	$^{51}\text{V}(n,n')^{51}\text{V}$	25.1 ± 3.3
1492.9	$9/2^- \longrightarrow 5/2^-$	$^{51}\text{V}(n,n')^{51}\text{V}$	12.5 ± 2.2
1553.8	$2^+ \longrightarrow 0^+$	$^{51}\text{V}(n,n'p)^{50}\text{Ti}$	34.0 ± 3.4
1608.9	$11/2^- \longrightarrow 7/2^-$	$^{51}\text{V}(n,n')^{51}\text{V}$	212 ± 15
1776.7	$13/2^- \longrightarrow 11/2^-$	$^{51}\text{V}(n,n')^{51}\text{V}$	49.0 ± 3.5
1813.1	$9/2^- \longrightarrow 7/2^-$	$^{51}\text{V}(n,n')^{51}\text{V}$	70.0 ± 6.0
2004.7	$? \longrightarrow 11/2^-$	$^{51}\text{V}(n,n')^{51}\text{V}$	12.6 ± 2.9
2334.9	$5/2^- \longrightarrow 11/2^-$	$^{51}\text{V}(n,n')^{51}\text{V}$	14.5 ± 3.2

Table 9: Discrete γ production cross sections observed in reactions $n+^{51}\text{V}$.

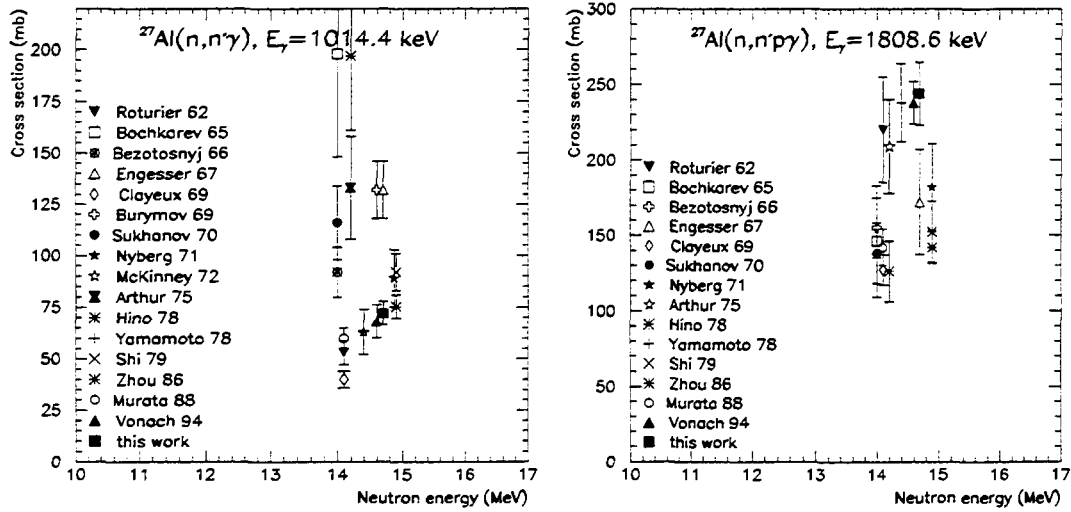


Figure 2: Cross sections of two discrete γ transitions of 1014.4 keV and 1808.8 keV from (n,n') and $(n,n'p)$ reactions, respectively, and their comparison with other experimental data around 14 MeV.

$(A+1)\text{Mo}(n,2n\gamma)$ cross sections and report these as the elemental cross section. The results are summarized in Table 11.

4 Discussion

We measured discrete γ ray production on a number of nuclei, and now we compare our experimental results with the available data and in the cases of Si (Table 6), K (Table 8, and Mo (Table 11), also with the calculated values.

The availability of literature data is very different for individual reactions. In the case of Al (Table 5) there are many literature data available; however these are often extremely contradictory. The situation is best demonstrated in Fig. 2, where our results for two discrete lines of 1014.4 keV and 1808.6 keV from $(n,n'\gamma)$ and $(n,n'p\gamma)$ reactions, respectively, are shown together with published data [9].

The contradictory character of existing data is clearly visible, especially for the 1014.4 keV transition, where the difference between extreme values is a factor of six. Observed differences greatly exceed quoted experimental errors and are difficult to explain. However, the majority of recent measurements are centered around 70 mb in good accord with our experimental value. Slightly better is the situation for the 1808.6 keV gamma in the $(n,n'p)$ channel, where the experimental results differ by a factor of two.

Few experimental data are available for reactions on ^{39}K . There is a single measurement using a NaI(Tl) spectrometer by Engesser, and our cross sections

E_γ (keV)	Transition	Reaction	Cross section (mb)
125.9	$7/2^- \rightarrow 5/2^-$	$^{55}\text{Mn}(n,n')^{55}\text{Mn}$	383 ± 27
156.2	$4^+ \rightarrow 3^+$	$^{55}\text{Mn}(n,2n)^{54}\text{Mn}$	542 ± 38
212.0	$5^+ \rightarrow 4^+$	$^{55}\text{Mn}(n,2n)^{54}\text{Mn}$	299 ± 19
304.+308.1	$5/2^- \rightarrow 9/2^-, 11/2^- \rightarrow 9/2^-$	$^{55}\text{Mn}(n,n')^{55}\text{Mn}$	26 ± 4
407.6	$3^+ \rightarrow 3^+$	$^{55}\text{Mn}(n,2n)^{54}\text{Mn}$	26 ± 3
470.5	$4^+ \rightarrow 5^+$	$^{55}\text{Mn}(n,2n)^{54}\text{Mn}$	66 ± 7
704.9	$6^+ \rightarrow 5^+$	$^{55}\text{Mn}(n,2n)^{54}\text{Mn}$	108 ± 8
768.7	$5^+ \rightarrow 5^+$	$^{55}\text{Mn}(n,2n)^{54}\text{Mn}$	28 ± 4
834.9	$2^+ \rightarrow 0^+$	$^{55}\text{Mn}(n,n'p)^{54}\text{Cr}$	83 ± 7
839.00	$4^+ \rightarrow 3^+$	$^{55}\text{Mn}(n,2n)^{54}\text{Mn}$	58 ± 5
858.2	$9/2^- \rightarrow 7/2^-$	$^{55}\text{Mn}(n,n')^{55}\text{Mn}$	95 ± 7
1019.4	$13/2^- \rightarrow 11/2^-$	$^{55}\text{Mn}(n,n')^{55}\text{Mn}$	67 ± 6
1164.0+1166.3	$5/2^- \rightarrow 7/2^-, 11/2^- \rightarrow 7/2^-$	$^{55}\text{Mn}(n,n')^{55}\text{Mn}$	107 ± 9
1528.4	$3/2^- \rightarrow 5/2^-$	$^{55}\text{Mn}(n,n')^{55}\text{Mn}$	48 ± 5

Table 10: Discrete γ production cross sections observed in n+Mn reactions.

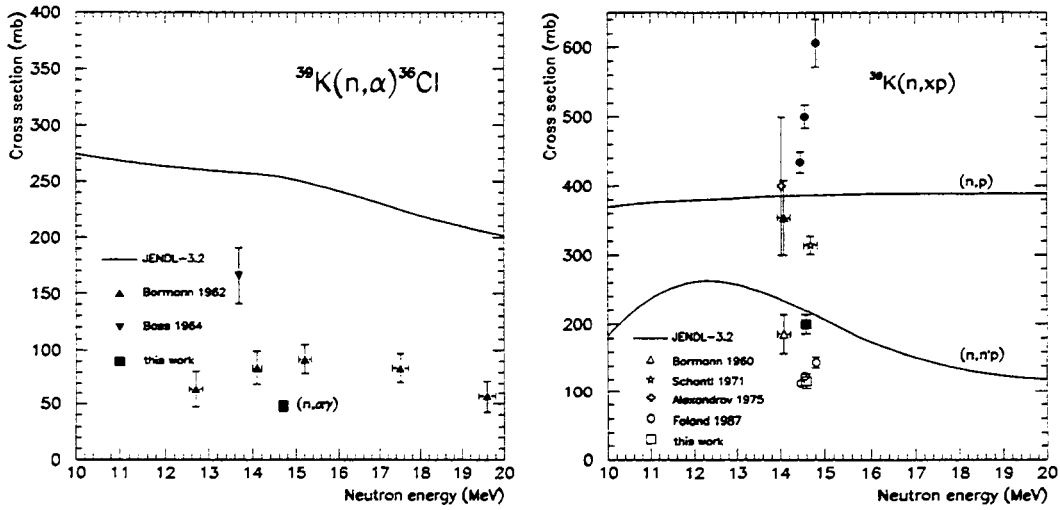


Figure 3: Experimental cross sections for neutron induced reactions on ^{39}K compared with our $(n,x\gamma)$ results. On the left side is the cross section for the (n,α) reaction. On the right side the cross section of (n,p) (open points) and $(n,n'p)$ (full points of the same shape) reaction are given. Solid lines in both parts represent the JENDL-3.2 evaluated cross sections, and the dashed line on the right side represents the new IRDL recommendation.

Product	E_γ (keV)	Transition	σ_{exp} (mb)	GNASH(mb)			DEGAS(mb)		
				sum	(n,n')	(n,2n)	sum	(n,n')	(n,2n)
^{92}Mo	773.0	$4^+ \rightarrow 2^+$	53 ± 6	75	75		43	43	
	1509.7	$2^+ \rightarrow 0^+$	88 ± 10	99	99		77	77	
^{93}Mo	943.3	$1/2^+ \rightarrow 5/2^+$	14 ± 2	4		4	12		12
	1477.1	$9/2^+ \rightarrow 5/2^+$	47 ± 6	27		27	4		4
^{94}Mo	702.6	$4^+ \rightarrow 2^+$	148 ± 16	198	30	167	63	13	51
	849.7*	$6^+ \rightarrow 4^+$	140 ± 16	98	17	81	6	3	3
	871.1	$2^+ \rightarrow 0^+$	241 ± 26	266	40	226	226	26	200
^{95}Mo	204.1	$3/2^+ \rightarrow 5/2^+$	11.7 ± 1.7	42	4	38	84	4	81
	765.8	$7/2^+ \rightarrow 5/2^+$	41 ± 5	66	11	55	22	3	19
	947.7	$9/2^+ \rightarrow 5/2^+$	95 ± 11	95	17	78	11	3	8.0
	1073.7	$7/2^+ \rightarrow 5/2^+$	28 ± 4	14	2	12	11	3	8
^{96}Mo	778.2	$2^+ \rightarrow 0^+$	192 ± 16	174	36	138	156	37	119
	812.6	$6^+ \rightarrow 4^+$	28 ± 4	28	7	21			
	849.9*	$4^+ \rightarrow 2^+$	140 ± 16	67	14	53	30	10	20
^{97}Mo	480.9	$3/2^+ \rightarrow 5/2^+$	54 ± 6	38	1	37	74	1	73
	658.1	$7/2^+ \rightarrow 5/2^+$	80 ± 9	115	6	108	41	1	40
	719.5	$5/2^+ \rightarrow 5/2^+$	40 ± 5	16	1	15	32	1	31
	720.9	$3/2^+ \rightarrow 5/2^+$	24 ± 4	14	1	13	42	1	41
	1024.5	$7/2^+ \rightarrow 5/2^+$	40 ± 5	21	1	20	20	1	19
	1116.6	$9/2^+ \rightarrow 5/2^+$	81 ± 9	92	1	91	13	1	12
^{98}Mo	722.6	$4^+ \rightarrow 2^+$	43 ± 5	24	24		18	18	
	787.4	$2^+ \rightarrow 0^+$	88 ± 8	32	32		42	42	
^{100}Mo	535.6	$2^+ \rightarrow 0^+$	46 ± 5	12	12		16	16	
^{91}Nb	1082.9	$5/2^- \rightarrow 1/2^-$	3 ± 1	7			32		
	1108.1	$3/2^- \rightarrow 1/2^-$	8 ± 2	4			19		

Table 11: Experimental and theoretical cross sections of discrete γ transitions observed in $^{nat}\text{Mo}(n,x\gamma)$ reactions. Most of the experimental cross sections are the sum of (n,n' γ) and (n,2n γ) reactions. * - *unresolved doublet at 849.7 and 849.9 keV*.

are systematically lower than his results. Comparison of published reaction cross sections [10] with our $(n,x\gamma)$ data for $n+^{39}\text{K}$ reactions is shown in Fig. 3 for the reactions (n,α) , (n,p) and $(n,n'p)$. The $(n,x\gamma)$ cross section is always shown as the sum of all observed discrete γ transitions which populate the ground state of the final nucleus. In an even-even final nucleus it is typical that the $(n,x\gamma)$ cross section is approximately given by the cross section of the last $2^+ \rightarrow 0^+(\text{g.s.})$ transition; in an odd-odd final nucleus usually the abovementioned sum is used as the $(n,x\gamma)$ cross section. In the reaction $^{39}\text{K}(n,p\gamma)^{39}\text{K}$ we observed two discrete γ transitions to the ground state. Their sum 117 ± 11 mb is our lower bound estimate of the $^{39}\text{K}(n,p)^{39}\text{K}$ reaction cross section. Fig. 3 shows that our $(n,x\gamma)$ cross sections are always lower than the corresponding reaction cross sections and therefore these two data sets are consistent. However, the JENDL-3.2 evaluation shown as the solid line is not in accord with recent experimental values, whereas the new evaluation started by the IAEA [13] agrees better with the measured values.

In the reactions on Mn only a single cross section for the γ transition with energy 858.2 keV from inelastic scattering $^{55}\text{Mn}(n,n')^{55}\text{Mn}$ has been reported so far. All other transitions given in Table 10 were measured for the first time. Our value for the 858.2 keV transition differs from literature data by a factor of approximately 20.

The extreme case represents Mo where no experimental data on γ ray production were measured so far. Experimental cross sections can be checked only by comparison with the calculations shown together with experimental results in Table 11. This comparison shows that the agreement is reasonable for all lighter Mo nuclei, being slightly better for even-even reaction products. For the two heavy isotopes ^{98}Mo and ^{100}Mo the situation is different and the theoretical values underestimate the experimental values approximately by a factor of 2-4.

For several cases we compare our experimental results with the theoretical values. Calculations were performed within the statistical model of nuclear reactions using advanced codes GNASH [11] and DEGAS, which is an improved version of a code released earlier [12]. Both codes incorporate equilibrium (*e.g.* compound nucleus) as well as pre-equilibrium particle and γ emission, however not within the same formalism. The code GNASH uses more specific input for every reaction and therefore it usually reproduces the data better than the code DEGAS, which is (at least for input and available options) of much simpler structure. For the calculations we used recommended input parameters without special adjustments to individual nuclei. The agreement is generally acceptable, in some cases within a factor of two, which shows the limits of the present (even if using rather advanced) calculational methods.

The general situation of photon cross section measurements presented here shows that the situation is far from being satisfactory. This shows that the experiment with neutrons both in the input as well as in the output channel is rather difficult and may be a source of serious systematic errors. To avoid this difficulty and to improve the general consistency of experimental data it is desirable to measure cross section relative to well known and accepted cross

sections. In measurements only a high resolution detector with good timing properties should be used. As a general standard we recommend using the cross section of the 1434.1 keV $2^+ \rightarrow 0^+$ transition excited in inelastic scattering on ^{52}Cr .

References

- [1] N. Kocherov, P. K. McLaughlin, eds., WRENDA 93/94, Report INDC(SEC)-104, IAEA Vienna, 1993.
- [2] S. P. Simakov, A. Pavlik, H. Vonach and S. Hlaváč, in this report.
- [3] A. Paschenko, ed., Report IAEA-NDS, (1994) SLR-32-94.
- [4] J. Pivarč and S. Hlaváč, Nucl. Sci. Eng. 106, 266 (1990).
- [5] S. Hlaváč, L. Dostál, I. Turzo, A. Pavlik and H. Vonach, Nucl. Sci. Eng. 64, 1332 (1996).
- [6] S. Hlaváč and P. Obložinský, Nucl. Instr. Meth. 206, 127 (1983).
- [7] S. P. Simakov, A. Pavlik, H. Vonach, S. Hlaváč, Status of Experimental and Evaluated Data for Discrete γ -ray Production at 14.5 MeV Neutron Incident Energy, Obninsk 1997, unpublished.
- [8] Experimental data on 1778.9 keV production in $^{28}\text{Si}(n,n'\gamma)$ scattering around 14 MeV:
 - P. W. Martin *et al.*, J. Nucl. Energy, 19, 447 (1965).
 - T. Roturier, Comp. Rendus 262, 1738 (1966).
 - F. C. Engesser, W. E. Thompson, J. Nucl. Energy 21, 487 (1967).
 - U. Abbondano *et al.*, J. Nucl. Energy 27, 227 (1973).
 - G. Grenier, Neutron Physics, Obninsk 3, 215 (1974).
 - D. M. Drake *et al.*, Nucl. Sci. Eng. 65, 49 (1978).
 - Zong Reng *et al.*, Chinese J. of Nuclear Physics 1, 45 (1979).
 - V. M. Bezotosny *et al.*, Proc. Conf. on Neutron Physics, Kiev 1980, vol. 2, p. 21.
 - I. Murata *et al.*, Proc. Int. Conf. on Nuclear Data for Science and Technology, Mito 1988, p. 275.
 - F. Guoying, Z. Hongyu *et al.*, Proc. Int. Conf. on Nuclear Data for Science and Technology, Jülich 1991, p. 332.
 - M. Drog, D. M. Drake *et al.*, Proc. Int. Conf. on Nuclear Data for Science and Technology, Jülich 1991, p. 304.
 - A. A. Lychagin *et al.*, Report FEI-2281, FEI Obninsk, 1992.
 - Z. Hongyu *et al.*, Proc. Int. Conf. on Nuclear Data for Science and Technology, Gatlinburg 1994, v. 1., p. 166.
- [9] Experimental data on 1014.4 keV and 1808.6 keV production in $n+\text{Al}$ around 14 MeV:

- **Roturier 62**– J. Roturier, *Comp. Rendus* 262, 1763 (1962).
- **Bochkarev 65**– V. N. Bochkarev and V. V. Nefedov, *Sov. J. Nucl. Phys.* 1, 574 (1965).
- **Bezotosnyj 65**– V. M. Bezotosnyj, V. G. Vershin, L. M. Surov and M. S. Shvestov, *Sov. J. Nucl. Phys* 3, 632 (1966).
- **Engesser 67**– F. C. Engesser and W. H. Thompson, *J. Nucl. Energy* 21, 487 (1967).
- **Clayeux 69**– G. Clayeux and G. Grenier, CEA Report, CEA-R-3807, CEA 1969.
- **Burymov 69**– E. M. Burymov, *Sov. J. Nucl. Phys* 9, 546 (1969).
- **Sukchanov 70**– B. I. Sukchanov and N. P. Tkach, *Sov. J. Nucl. Phys.* 11, 17 (1970).
- **Nyberg 71**– K. Nyberg-Ponnert, B. Joensson and I. Bergquist, *Phys. Scripta* 4, 165 (1971).
- **McKinney 72**– H. O. McKinney, EXFOR 13034.
- **Arthur 75**– E. D. Arthur, D. M. Drake, M. G. Silbert and P. G. Young, *Proc. Int. Conf. Neutron Cross Sections for Science and Technology*, Washington 1975, Vol. 2, p. 770, NBS 1975.
- **Hino 78** –Y. Hino, T. Yamamoto, T. Saito, Y. Arai, S. Itagaki and K. Sugiyama, *J. Nucl. Sci. Technology* 15, 85 (1978).
- **Yamamoto 78**– T. Yamamoto, Y. Hino, S. Itagaki and K. Sugiyama, *J. Nucl. Sci. Technology* 15, 797 (1978).
- **Shi 79**– Z. Shi, X. Shi, X. Zeng, Y. Lu, J. Xing, R. Shen and D. Ding, *Chin. J. Nucl. Phys.* 1, 45 (1979).
- **Zhou 86**– H. Zhou, L. Tang, Y. Yan, S. wen, L. Lan, S. Zhang, Q. Wang, S. Sun, C. Han, X. Ding and W. Wang, INDC(CPR)-10, IAEA (1986).
- **Murata 88**– I. Murata, J. Yamamoto and A. Takahashi, *Proc. Int. Conf. Nucl. Data for Science and Technology*, Saikon Publishing Company (1988), p. 275.
- **Vonach 94**– H. Vonach, A. Pavlik, M. B. Chadwick, R. C. Haight, R. O. Nelson, S. A. Wender and P. G. Young, *Phys. Rev. C* 50, 1952 (1994).

[10] Experimental data on $^{39}\text{K}(n,x\gamma)$ reactions cross sections:

- **Borman 1960** – M. Borman, H. Jarmie, G. Andersson-Lindström, H. Heuert and H. Pollehn, *Z. Naturforschung* 15, 200 (1960), EXFOR 21668.
- **Schantl 1971** – W. Schantl, IRK Vienna 1971, unpublished thesis, EXFOR 21846.
- **Alexandrov 1975** – D. V. Alexandrov, L. I. Klochkova, B. S. Kovrigin, *Yad. Energia* 39 137 (1975) in Russian, EXFOR 40433.

- **Foland 1987** – K. A. Foland, R. J. Borg, M. G. Mustafa, Nucl. Sci. Eng. 95, 128 (1987), EXFOR 13109.
- [11] P. G. Young, E. D. Arthur, M. B. Chadwick, Report LA-12343-MS (UC-13), Los Alamos 1992.
- [12] E. Běták, P. Obložinský, Report INDC(SLK)-001, IAEA Vienna 1993.
- [13] R. Forrest, A. Ignatyuk, A. Pashchenko, Contribution to the Int. Conf. on Nuclear Data for Science and Technology, Trieste 1997.

Measurement of gamma-ray production cross sections in $^{27}\text{Al}(n,x\gamma)$ and $^{208}\text{Pb}(n,px\gamma)$ reactions for neutron energies up to 400 MeV

A. Pavlik, H. Vonach, and H. Hitzemberger-Schauer
Institut für Radiumforschung und Kernphysik, Universität Wien
A-1090 Wien, Austria

and

M. B. Chadwick, R. O. Nelson, R. C. Haight, S. A. Wender, and P. G. Young
Los Alamos National Laboratory, Los Alamos, NM 87545, U.S.A.

Abstract: The prompt γ -radiation from the interaction of fast neutrons with samples of Al and enriched ^{208}Pb was measured using the white neutron beam of the LANSCE/WNR facility at the Los Alamos National Laboratory. From the aluminum γ -ray spectra excitation functions for prominent γ -ray transitions in various residual nuclei (in the range from F to Al) were determined for neutron energies up to 400 MeV. In addition to the primary purpose of the ^{208}Pb experiment, the study of $(n,x\gamma)$ reactions leading to various lead isotopes. γ -ray transitions in residual Tl nuclei were analyzed and cross sections were derived in the neutron energy range from the effective threshold to 200 MeV. In the neutron energy range up to 200 MeV all experimental results were compared with nuclear model calculations using the code GNASH.

1. Introduction

One method to measure photon-production cross sections in neutron induced reactions is the use of a "white" neutron spallation source and high-resolution γ -ray spectroscopy. The incident neutron energy is determined by the time-of-flight method and γ -ray production cross sections can be measured simultaneously for a wide neutron energy range.

As a part of the program for white neutron source $(n,x\gamma)$ measurements at the LANSCE/WNR facility [1] of the Los Alamos National Laboratory γ -ray production cross sections for Al and $^{207,208}\text{Pb}$ were investigated. In the course of this CRP we reported the γ -ray production cross sections for discrete γ -ray transitions in Tl nuclei produced by $^{208}\text{Pb}(n,px\gamma)$ reactions. In our study of $\text{Al}(n,x\gamma)$ reactions production cross sections were measured for γ -ray transitions in 11 residual nuclei in the element range F to Al.

Al was chosen to be studied as this element is monoisotopic and thus well suited for testing of model calculations. In continuation of a study of $(n,x\gamma)$ reactions on $^{207,208}\text{Pb}$ [2,3] less intense γ -rays related to the $^{208}\text{Pb}(n,px\gamma)$ reactions were identified in the already measured spectra and analyzed. In the energy range up to 200 MeV the experimental cross sections were compared with the results of model calculations performed with the code GNASH [4].

Table I: Nuclear reactions and γ transitions investigated in $^{27}\text{Al}(n,x\gamma)$ reactions.

Reaction	Residual nucleus	γ Transition investigated	Energy (keV)
$^{27}\text{Al}(n,n'\gamma)$	^{27}Al	$9/2^+ \rightarrow 7/2^+$	793.0
		$3/2^+ \rightarrow \text{gs}$	1014.4
		$5/2^+ \rightarrow 3/2^+$	1720.3
		$7/2^+ \rightarrow \text{gs}$	2211.1
		$9/2^+ \rightarrow \text{gs}$	3004.2 ^a
$^{27}\text{Al}(n,2n\gamma)$	^{26}Al	$3^+ \rightarrow \text{gs}$	416.9
		$1^+ \rightarrow 0^+$	829.4
$^{27}\text{Al}(n,p\gamma)$	^{27}Mg	$5/2^+ \rightarrow 3/2^+$	955.3
		$3/2^+ \rightarrow \text{gs}$	984.6
		$5/2^+ \rightarrow \text{gs}$	1697.9
$^{27}\text{Al}(n,pn\gamma)$ $^{27}\text{Al}(n,d\gamma)$	^{26}Mg	$3_1^+ \rightarrow 2_1^+$	1002.4
		$2_2^+ \rightarrow 2_1^+$	1129.7
		$2_1^+ \rightarrow \text{gs}$	1808.6
$^{27}\text{Al}(n,p2n\gamma)$ $^{27}\text{Al}(n,dn\gamma)$	^{25}Mg	$3/2^+ \rightarrow 1/2^+$	389.7
		$3/2^+ \rightarrow \text{gs}$	974.8
$^{27}\text{Al}(n,p3n\gamma)$ $^{27}\text{Al}(n,d2n\gamma)$	^{24}Mg	$2^+ \rightarrow \text{gs}$	1368.6
$^{27}\text{Al}(n,2p3n\gamma)$ $^{27}\text{Al}(n,\alpha n\gamma)$	^{23}Na	$5/2^+ \rightarrow \text{gs}$	440.0
$^{27}\text{Al}(n,3p3n\gamma)$ $^{27}\text{Al}(n,\alpha pn\gamma)$	^{22}Ne	$2^+ \rightarrow \text{gs}$	1274.5
$^{27}\text{Al}(n,3p4n\gamma)$ $^{27}\text{Al}(n,\alpha p2n\gamma)$	^{21}Ne	$5/2^+ \rightarrow \text{gs}$	350.5
$^{27}\text{Al}(n,3p5n\gamma)$ $^{27}\text{Al}(n,\alpha p3n\gamma)$	^{20}Ne	$2^+ \rightarrow \text{gs}$	1633.8
$^{27}\text{Al}(n,4p6n\gamma)$ $^{27}\text{Al}(n,\alpha 2p4n\gamma)$ $^{27}\text{Al}(n,2\alpha 2n\gamma)$	^{18}F	$3^+ \rightarrow \text{gs}$	937.1

^a This line was not resolved from the 2981.8 keV ($3/2^+ \rightarrow \text{gs}$) transition.

2. Experiment and Data Reduction

The experimental set-up and the data reduction procedures are described in Refs. [3,5,6] and only a short summary is given here. Al samples (2 mm and 6 mm thick plates) were positioned at distances of 20.0 m and 41.5 m from the neutron production target. The prompt γ -radiation was detected with high-purity Ge detectors with tungsten collimators positioned at γ -ray emission angles of 90° and 125° . At 125° the angle-integrated γ -ray production cross section is approximately given by 4π times the measured cross section. For the isotopically enriched Pb sample (99.56% ^{208}Pb) only the position at the distance of 41.5 m from the neutron production target was used. Only results measured with the Ge detector at 125° are given in this paper. The transitions chosen for analysis are summarized in Tables I and II.

Two-dimensional spectra, neutron TOF versus gamma pulse-height, were recorded for the Ge detector. The neutron energy range between 3 and 400 MeV for the Al measurement and between 3 and 200 MeV for the lead measurement, respectively, was divided into energy groups with increasing widths

(0.25 to 50 MeV) according to the neutron energy resolution of the experiment. Then a one-dimensional γ pulse-height spectrum was derived from the two-dimensional spectrum for each neutron energy group and γ -peak areas were determined. Corrections were applied for the attenuation of the γ rays within the samples. For reactions with low thresholds the contributions of multiply scattered neutrons were estimated [6].

The neutron fluence was measured with a fission chamber containing a ^{238}U fission foil using $^{238}\text{U}(n,f)$ cross sections given by Lisowski et al. [7].

Because of uncertainty in our knowledge of the Ge detector dead time, experiments in the 14-MeV neutron energy range were performed at the Institute of Physics of the Slovak Academy of Sciences to determine better absolute normalizations of the cross sections [8,9].

A major problem in such white source experiments might be the presence of isomers with half-lives exceeding a few nanoseconds in the residual nuclei. When isomers are present in the cascade preceding the γ -ray transitions investigated (as in the nuclei ^{205}Tl and ^{201}Tl studied in the present experiment), the measured γ -radiation is not emitted promptly. Such delayed transitions may be detected in this type of experiment but they cannot be properly correlated with the neutron energy because the measured TOF includes the decay delay. For the measured γ -ray production cross sections for transitions in ^{205}Tl and ^{201}Tl corrections were estimated to be small (see Ref. [5]) and neglected. The measured cross sections give in good approximation the cross sections indicated in the last column of Table II.

Table II: Nuclear reactions and gamma transitions investigated in $^{208}\text{Pb}(n,pxn\gamma)$ reactions.

Reaction investigated	γ Transition (Level energies in keV)	γ Energy	Isomers in γ cascade			Measured cross section
			$J\pi$	E[keV]	$t_{1/2}$	
$^{208}\text{Pb}(n,pn\gamma)^{207}\text{Tl}$	1682.7 \rightarrow 351.0	1331.7	none			total
$^{208}\text{Pb}(n,p3n\gamma)^{205}\text{Tl}$	203.7 \rightarrow gs	203.7	3/2 ⁺ 11/2 ⁻ 25/2 ⁺	203.7 1484.0 3290.6	1.46 ns 4.5 ns 2.6 μs	approx. total
$^{208}\text{Pb}(n,p3n\gamma)^{205}\text{Tl}$	923.8 \rightarrow 203.7	720.1	11/2 ⁻ 25/2 ⁺	1484.0 3290.6	4.5 ns 2.6 μs	approx. total
$^{208}\text{Pb}(n,p5n\gamma)^{203}\text{Tl}$	680.5 \rightarrow 279.2	401.3	none			total
$^{208}\text{Pb}(n,p7n\gamma)^{201}\text{Tl}$	331.2 \rightarrow gs	331.2 ^a	(9/2 ⁻) (13/2 ⁻)	919.5 2015.0	2.035 ms 2.9 ns	appr. sum of prompt part of $\sigma(332.2)$
$^{208}\text{Pb}(n,p7n\gamma)^{201}\text{Tl}$	1571.7 \rightarrow 1238.8	332.9 ^a	(13/2 ⁻)	2015.0	2.9 ns	and total $\sigma(332.9)$

^a The 331.2-keV and 332.9-keV γ lines in ^{201}Tl were not resolved.

3. Results and Discussion

All measured cross sections can be found in graphical representation in Refs. [5,6] and in numerical form in the CSISRS (EXFOR) data library (entries 13643 and 13645). In the energy range up to 200 MeV the measured cross sections were compared with the results of model calculations performed with the code GNASH [4]. The calculations for the $^{208}\text{Pb}(n,pxn\gamma)$ reactions were performed using the same models and parameters which had been successfully used to describe γ -ray production cross sections in $^{207,208}\text{Pb}(n,xn\gamma)$ reactions [2]. For aluminum, the calculations were carried out with two different options for modeling multiple preequilibrium emission: the earlier model (MPE1) used for lead which determines the emission of a second preequilibrium particle from the dominant $1p1h$ states using an exciton model; and the more recent generalized multiple preequilibrium model (MPE2) [10], which determines second-particle emission from all preequilibrium particle-hole states. For the majority of the measured $\text{Al}(n,x\gamma)$ reaction there is reasonable agreement between experiment and model calculation. Only for the 440.0-keV transition in ^{23}Na and 937.1-keV transition in ^{18}F there is disagreement which is not understood yet. Generally the experimental cross sections are better reproduced by the earlier model

(MPE1), which is difficult to understand since the physical assumptions used are less accurate. Comparisons of the predictions from these models with experimental emission spectra data available from the literature, on the other hand, indicate a preference for the more recent model (MPE2). Figs. 1 and 2 show as examples the measured and the calculated cross sections for the 440.0-keV transition in ^{23}Na and the 1274.5-keV transition in ^{22}Ne .

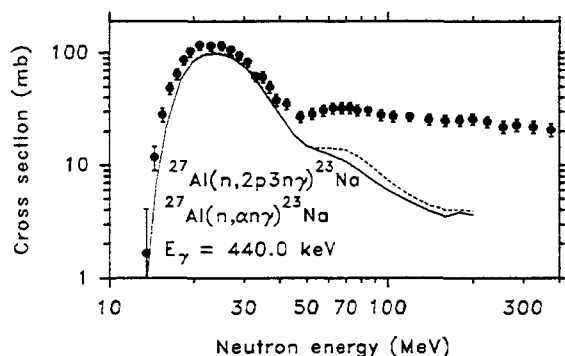


Fig. 1: The γ -ray production cross section for the 440.0-keV transition in ^{23}Na . \bullet experimental results. — GNASH calculation (MPE1), ---- GNASH calculation (MPE2).

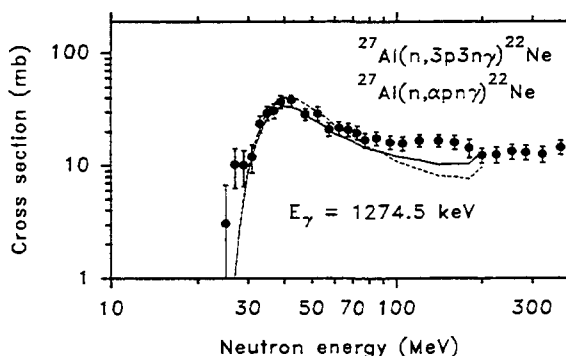


Fig. 2: The γ -ray production cross section for the 1274.5-keV transition in ^{23}Na . Same symbols as in Fig. 1.

For the $^{208}\text{Pb}(n,pxn\gamma)$ reactions there is, other than in the case of reactions with neutron emission only [2], no agreement between experimental results and model calculations for the majority of the transitions analyzed. For the analyzed transitions in ^{207}Tl and ^{205}Tl the model calculation overestimates the measured cross section for neutron energies above about 70 MeV. There is rather good agreement for the 401.3-keV transition in ^{203}Tl and the calculated cross sections are smaller than the experimental results for γ -ray transitions in ^{201}Tl for high neutron energies. It seems that our calculation gives a spectrum of the emitted protons that is too hard. Proton emission is important for the preequilibrium stage of the reaction only, as proton emission from compound nucleus decay is strongly suppressed by the Coulomb barrier. An average energy of the emitted protons from the preequilibrium stage that is too high results in higher cross sections for reactions with the subsequent emission of only a few neutrons, and in lower cross sections for reactions with multiparticle emission as less energy is available after emission of the proton, which is observed in the present study. It should also be mentioned that the experimental information on discrete levels and γ -ray branching in Tl nuclei is not as good as for Pb, and incomplete level scheme information might also contribute to some of the observed discrepancies. As examples we give the measured and calculated γ -ray production cross sections for transition in the nuclei ^{207}Tl and ^{201}Tl in Figs. 3. and 4.

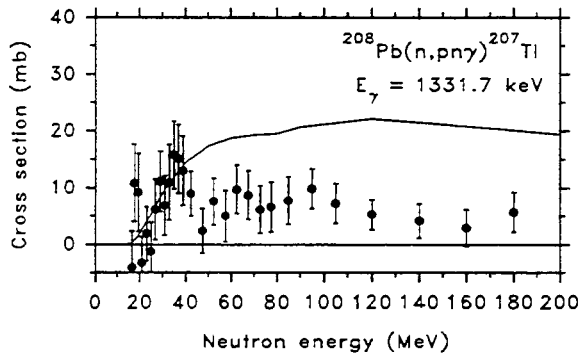


Fig. 3: The γ -ray production cross section for the 1331.7-keV transition in ^{207}Tl . • experimental results, — GNASH calculation.

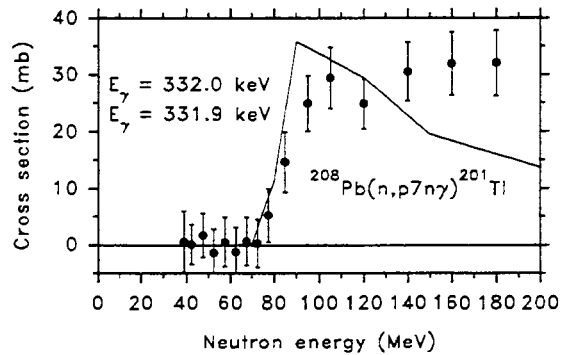


Fig. 4: The sum of the γ -ray production cross sections for the 332.9-keV transition and the prompt part of the 331.2-keV in ^{201}Tl . Same symbols as in Fig. 3.

References

- [1] P. W. Lisowski, C. D. Bowman, G. J. Russell, and S. A. Wender, Nucl. Sci. Eng. **106**, 208 (1990).
- [2] H. Vonach, A. Pavlik, M. B. Chadwick, R. C. Haight, R. O. Nelson, S. A. Wender, and P. G. Young, Phys. Rev. C **50**, 1952 (1994).
- [3] A. Pavlik, H. Vonach, M. B. Chadwick, R. C. Haight, R. O. Nelson, S. A. Wender, and P. G. Young, in *Proceedings of the International Conference on Nuclear Data for Science and Technology*, Gatlinburg, U.S.A., 1994, edited by J. K. Dickens (American Nuclear Society, La Grange Park, 1994), p. 363.
- [4] P. G. Young, E. D. Arthur, and M. B. Chadwick, "Comprehensive Nuclear Model Calculations: Introduction to the Theory and Use of the GNASH Code" (Los Alamos National Laboratory report No. LA-12343-MS, Los Alamos, 1992).
- [5] A. Pavlik, H. Vonach, R. O. Nelson, R. C. Haight, S. A. Wender, P. G. Young, and M. B. Chadwick, in *Measurement, Calculation and Evaluation of Photon Production Data* (Text of Papers presented at the 1st Research Co-ordination Meeting), Bologna, Italy, 1994, compiled by P. Oblozinsky (International Nuclear Data Committee Report No. INDC(NDS)-334, IAEA, Vienna, 1995), p. 39.
- [6] A. Pavlik, H. Hitzengerger-Schauer, H. Vonach, M. B. Chadwick, R. C. Haight, R. O. Nelson, and P. G. Young, " $^{27}\text{Al}(n,\gamma)$ reactions for neutron energies from 3 to 400 MeV", submitted to Phys. Rev. C
- [7] P. W. Lisowski *et al.*, in *Proc. Specialists' Meeting on Neutron Cross Section Standards for the Energy Region above 20 MeV*, Uppsala, Sweden, 1991, (Nuclear Energy Agency Nuclear Data Committee report NEANDC-305 'U', Paris, 1991), p. 177.
- [8] S. Hlavác, P. Oblozinský, I. Turzo, L. Dostál, H. Vonach, A. Pavlik, S.P. Simakov, Nucl. Sci. Eng. **119**, 195 (1995).
- [9] S. Hlavác, I. Turzo, L. Dostál, A. Pavlik, H. Vonach, Nucl. Sci. Eng. **125**, 196 (1997).
- [10] M. B. Chadwick, P. G. Young, D. C. George and Y. Watanabe, Phys. Rev. C **50**, 996 (1994).

Gamma Ray Production Following Spallation Reactions in ^{27}Al and ^{56}Fe Induced by 800 MeV Protons

H. Vonach¹, A. Pavlik¹, A. Wallner¹, M. Drosig², R.C. Haight³, D.M. Drake³, S. Chiba⁴

¹Institut für Radiumforschung und Kernphysik, Wien, Austria, ²Institut für Experimentalphysik, Wien, Austria, ³Los Alamos National Laboratory, USA, ⁴JAERI, Japan

1. Introduction

The mass and charge distributions of the reaction products from spallation reactions induced by protons in the energy range from several hundred MeV to several GeV have been investigated in a number of experiments (see, *e.g.*, references in [1]). Cross sections for the formation of radioactive residual nuclei with half-lives exceeding some hours have been investigated by conventional γ -ray spectroscopy and accelerator mass spectrometry (AMS), and the production of stable isotopes of noble gases has been measured by gas production measurements and mass analysis. Much less information, however, exists about the production of stable isotopes from elements other than noble gases, and for short-lived residual nuclei. Only one experiment has been reported, in which the full mass and charge distribution of the spallation products has been measured by detection of the recoiling nuclei in so-called inverse kinematics at $E = 600$ MeV [2]. Although the results of this experiment are in reasonable overall agreement with the above mentioned activation, AMS, and gas production measurements, there are a number of discrepancies exceeding experimental errors [1]. The present experiment was performed using in-beam γ -ray spectroscopy. This method, which so far has not been used in the study of spallation reactions, allows the determination of cross sections for formation of stable and very short-lived isotopes, both of which cannot be measured by conventional activation techniques.

Two nuclei, ^{27}Al and ^{56}Fe , have been selected for this study because they have been studied before in a number of papers [1,2]. These nuclei are well suited for the goal of obtaining a rather complete mass and charge distribution of the residual nuclei by combining our results with the existing data base. In addition, checks of the results obtained by very different methods become possible for a number of residual nuclei.

2. Experiment

Thin foils of ^{27}Al and ^{56}Fe ($12.13 \pm 0.27 \text{ mg/cm}^2$ and $6.82 \pm 0.24 \text{ mg/cm}^2$) were irradiated with the 800 MeV proton beam of the WNR facility of the Los Alamos National Laboratory [3]. The foils were irradiated in a scattering chamber located in the beam line from the accelerator to the neutron producing target of WNR.

The γ -radiation from the targets was measured with a high-purity Ge-detector at a distance of about 30 m from the targets at an angle of 150° relative to the proton beam. The WNR beam consisted of 40 macro-pulses per second separated by either 16.66 or 33.33 ms. Each macropulse had a length of 600 μs . Within each macro-pulse the beam consisted of narrow micro-pulses of a width of about 1 ns at intervals of 1.8 μs . Accordingly, the prompt γ -radiation originating from the so-called γ -cascade deexciting the final residual nucleus was observed by its time correlation to the micro-pulses. In this way the prompt γ -radiation could also be separated from the γ -radiation produced in and near the Ge-detector by the neutrons also produced in the spallation reactions. The γ -radiation from the decay of the short-lived residual nuclei formed in spallation reactions was measured between the macro-pulses by setting a time window of 15 ms after the end of each macro-pulse. After the experiment the irradiated Al and Fe foils were transferred to the Institut für Radiumforschung und Kernphysik in Vienna and the γ -radiation from all long-lived activities produced in the samples was measured with a calibrated high-purity Ge-detector. From the measured short- and long-lived activities the production cross sections for the respective nuclei were derived. In the prompt γ -ray spectrum it was possible to observe the transitions from the first excited 2^+ state to the ground state for all even-even nuclei strongly populated in the spallation reactions and to deduce the production cross sections of these mostly stable nuclei from these data. In this way production cross sections for 36 nuclides from the proton interactions with ^{56}Fe and for 12 nuclides in case of ^{27}Al could be measured; in addition meaningful upper limits were obtained for a number of further nuclides in both cases.

3. Results and Discussion

The present data as well as the results of all previous measurements have been compared with the predictions of the semi-empirical systematics of Tsao and Silberberg [4] and with calculations according to the quantum molecular dynamics model (QMD) followed by statistical decay (SDM) [5,6] (see Figs. 1 - 4). Figure 1 shows that for Al the quality of the theoretical description by the QMD model is now approximately as good as that of the semiempirical systematics, although the QMD model does not contain any parameters fitted to the existing data on nuclide production cross sections. For ^{56}Fe (Figs. 2 - 4) the QMD model does not work quite so well. In this case the model seems to systematically underestimate the production of nuclides with low ΔZ and to overestimate the production of higher ΔZ values and does not give a description as good as the systematics. However, there are for both targets still deviations up to a factor of two between the experimental data and both calculations, even in the peaks of the mass distributions. Unfortunately the

overall spread even of the more recent data is still so large that it is difficult to draw general conclusions on possible systematic dependencies of the observed discrepancies on Z and A . A complete version of this work including numerical results has recently been published [7].

References:

1. R. Michel *et al.*, Nucl. Inst. Meth. B **103**, 183 (1995).
2. W.R. Webber, J.C. Kish and D.A. Schrier, Phys. Rev. C **41**, 547 (1990).
3. P.W. Lisowski, C.D. Bowman, G.J. Russell and S.A. Wender, Nucl. Sci. Eng. **106**, 208 (1990).
4. R. Silberberg and C.H. Tsao, Astrophys. J. **220**, 335 (1973); R. Silberberg, C.H. Tsao and M.M. Shapiro, in Spallation Nuclear Reactions and Their Applications, eds. B.S. P. Shen and M. Merker (Reidel, Dordrecht, 1976) p. 49; C.H. Tsao and R. Silberberg, in Proc. 16th Int. Cosmic Ray Conf. (Kyoto, 1979), vol. 2, p. 202; R. Silberberg, C.H. Tsao and J.R. Letaw, Ap. J. Suppl. Ser. **58**, 873 (1985); R. Silberberg, C.H. Tsao and J.R. Letaw, in Proc. 20th Int. Cosmic Ray Conf. (Moscow, 1987) vol. 2, p. 133.
5. K. Niifa *et al.*, Phys. Rev. C **52**, 2620 (1995).
6. S. Chiba *et al.*, Phys. Rev. C **54**, 285 (1996).
7. H. Vonach *et al.*, Phys.Rev. C **55**, 2458 (1997).

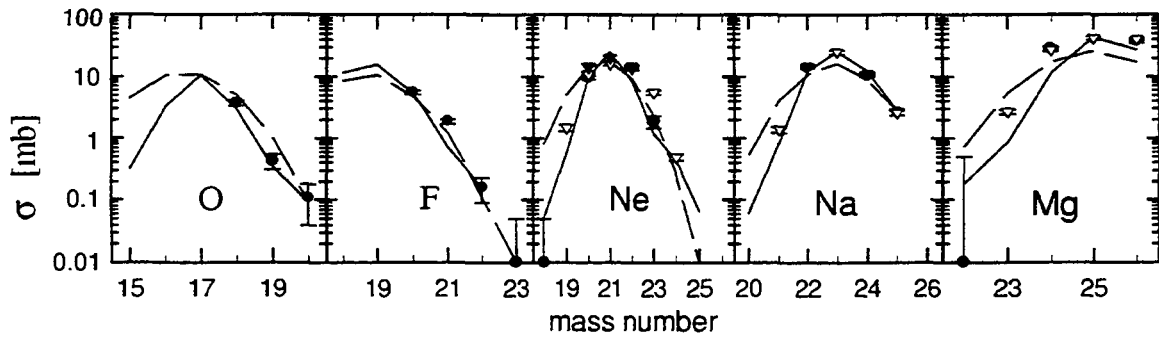


Fig. 1: Incident production cross sections for Mg, Na, Ne, F and O isotopes in the interaction of 600-800 MeV protons with Al. Closed circles: this work, open triangles: Webber [2], closed triangles: Michel [1], closed diamonds: other experiments, solid line: QMD calculation, dotted line: Tsao-Silberberg systematics.

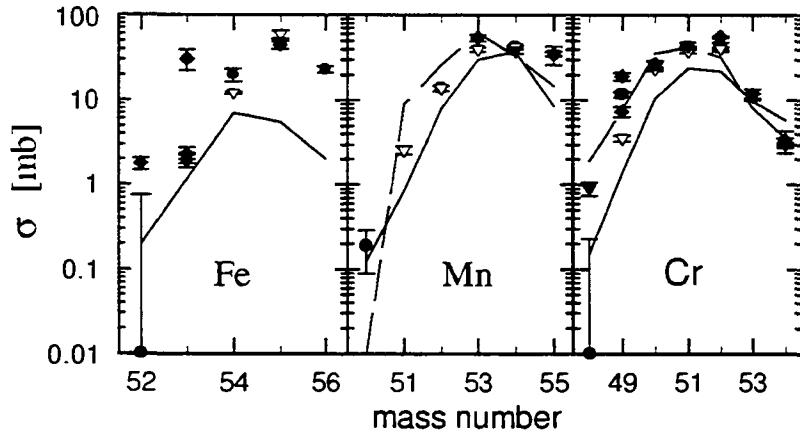


Fig. 2: Independent production cross sections for Fe, Mn and Cr isotopes from the interaction of 600-800 MeV protons with ^{56}Fe . The notation is the same as in Fig. 1.

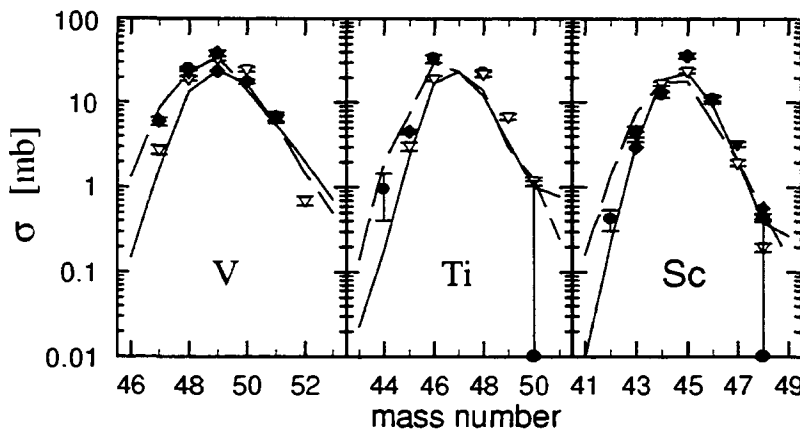


Fig. 3: Independent production cross sections for V, Ti, and Sc isotopes from the interaction of 600-800 MeV protons with ^{56}Fe . The notation is the same as in Fig. 1.

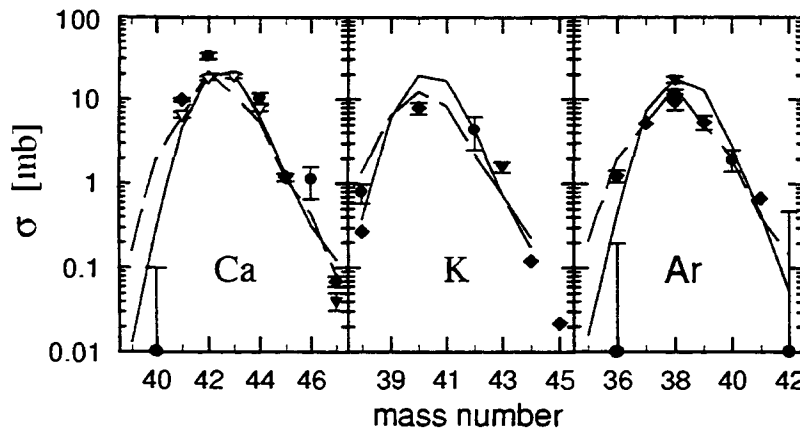


Fig. 4: Independent production cross sections for Ca, K, and Ar isotopes from the interaction of 600-800 MeV protons with ^{56}Fe . The notation is the same as in Fig. 1.

Analysis of Gamma-Ray Emission Spectra from Spherical Piles with a 14-MeV Neutron Source

F. Maekawa

High Energy Neutron Laboratory, Japan Atomic Energy Research Institute
Tokai, Ibaraki, 319-11 Japan

1. Introduction

The benchmark experiment of gamma-ray emission spectrum measurements conducted at the OKTAVIAN facility at Osaka university provides a valuable experimental data base for validating secondary gamma-ray data in evaluated nuclear data libraries. Benchmark tests of secondary gamma-ray data in the JENDL-3.2, JENDL Fusion File and FENDL/E-1.0 were performed through analysis of the OKTAVIAN experiment.

2. Experiment

The experiment was performed by Yamamoto *et al.* at the OKTAVIAN facility [1-3]. Specifications of the spherical sample piles used in the experiment are given in Table 1. All the samples except for lead were powder or granular contained in soft-steel or stainless steel containers, while the lead pile was made of solid metal. Pulsed D-T neutrons were generated at the center of the spherical pile. Gamma-ray events were detected by a NaI(Tl) scintillation detector at 5.8 m from the source. Neutron events were discriminated by the arrival time difference at the detector. The measured pulse height spectrum was unfolded to derive the gamma-ray spectrum. Details of the experimental procedure are described in the three references.

3. Analysis

Experimental analysis was performed with the continuous energy Monte Carlo transport code MCNP-4A [4]. Three evaluated nuclear data files, JENDL-3.2 [5], JENDL Fusion File [6] and FENDL/E-1.0 [7], were used. The measured source neutron spectrum was used as a source term. The gamma-ray spectra were measured in a limited time period of 60 ~ 80 ns to separate neutron events. To take the time cutoff effect into account, a surface crossing estimator was placed at the same distance from the D-T neutron source as the experiment, and the time cut-off was considered in the calculations. The D-T neutron source also emits gamma-rays produced by interactions of source neutrons with the structural materials of the target. Another series of calculations was performed starting with the target gamma-rays. Calculated gamma-ray spectra with the neutron and the target gamma-ray sources are summed up to compare with the experimental spectrum. Details of the analysis are given in references [8,9].

Table 1. Specification of the sample piles.

Material	Container		Weight [kg]	Density [g/cm ³]	Thickness [#]		Time Cutoff [ns]	Purity [%]
	Type	Diam.			[cm]	[mfp]		
LiF	I	61	198.0	1.79	27.5	3.5	65	98.07*
Teflon	II	40	34.7	1.30	9.8	0.7	69	> 99.9
Al	II	40	32.8	1.22	9.8	0.5	69	> 99.7
Si	III	60	138.05	1.29	20.0	1.1	70	99.9
Ti	II	40	41.20	1.54	9.8	0.5	70	> 99.4
Cr	II	40	99.7	3.72	9.8	0.7	56	> 99.78
Mn	I	61	480.0	4.37	27.5	3.4	65	> 99.95
Co	II	40	52.0	1.94	9.8	0.5	70	> 99.5
Cu	I	61	675.0	6.23	27.5	4.7	65	> 99.993
Nb	IV	28	47.7	4.39	11.2	1.1	65	> 99.8
Mo	I	61	236.0	2.15	27.5	1.5	65	> 99.9
W	II	40	118.6	4.43	9.8	0.8	56	> 99.9
Pb	---	40	NA	11.34	10.0	1.8	65	NA

Thickness is indicated in both centimeters and mean-free-paths (mfp).

* Fluorine of 1.83 % is contained.

4. Discussion

According to the analysis, it is found that most of the observed gamma-rays, approximately 60 ~ 80 %, are produced by 14-MeV neutrons [9]. Hence the OKTAVIAN experiments give us knowledge about gamma-ray production cross sections mainly at 14 MeV. Figure 1 compares the calculated gamma-ray spectra with the experimental data for the 13 materials. In general, although there are some small discrepancies between the measured and calculated gamma-ray spectra, all the calculated spectra reproduce adequately the measured ones, and no serious problem is found.

The measured and calculated gamma-ray spectra are integrated in two ways to compare numerically to each other:

$$I_E = \int E \cdot \phi_\gamma(E) \cdot dE \quad (1)$$

$$I_N = \int \phi_\gamma(E) \cdot dE \quad (2)$$

The integral I_E corresponds to the total gamma-ray energy observed while I_N means just a total number of gamma-rays. Table 2 summarizes the I_E and I_N values for the measured

gamma-ray spectra, and Figs. 2 and 3 show calculated to experimental (C/E) ratios for the I_E and I_N values, respectively. Upper energies of the integration for the LiF, CF₂, Nb and W samples are limited to 5 or 6.5 MeV because, above these energies, gamma-rays produced in the sample materials are much less than gamma-rays produced in the container of the sample piles and target gamma-rays [9].

In the comparisons of the I_E and I_N values in Figs. 2 and 3, most of the C/E ratios lie in the range of 0.8 ~ 1.2. There is no C/E ratio which is greater than 1.31 or less than 0.74. From the viewpoint of engineering use of secondary gamma-ray data, the I_E values are more important than the I_N values because most engineering parameters related to gamma-rays, such as gamma-ray heating, gamma-ray dose and radiation damage, are in proportion to total deposited energies to surrounding materials. If we concentrate on the I_E values rather than the I_N values, the agreement of the integral values becomes better. All the C/E ratios of the I_E values range from 0.73 to 1.18. In particular, the agreement of the I_E values for JENDL-3.2 and JENDL Fusion File is excellent since all the C/E ratios are in the range of 0.79 ~ 1.17.

Table 2. Integrals of the measured gamma-ray spectra.

Material	Integration Range [MeV]	Total Flux I_N	Total Energy I_E
LiF	0.5- 6.5	0.210	0.400
CF ₂	0.5- 6.5	0.207	0.460
Al	0.5-20	0.389	0.999
Si	0.5-20	0.491	1.416
Ti	0.5-20	0.466	1.082
Mn	0.7-20	0.191	0.440
Cr	0.5-20	0.386	0.888
Co	0.5-20	0.318	0.658
Cu	0.5-20	0.107	0.192
Nb	0.7- 5	0.361	0.604
Mo	0.5-20	0.394	0.649
W	0.5- 5	0.192	0.320
Pb	0.5-20	0.082	0.162

5. Conclusions

Although there are some disagreements between the measured and calculated gamma-ray spectra and energy integrals, the calculations with JENDL-3.2, JENDL Fusion File and FENDL/E-1.0 predict adequately the experimental data. Most of the recent secondary gamma-ray data for high energy neutrons are evaluated with statistical model calculation codes, such as GNASH [10] and TNG [11]. We can conclude,

therefore, that such an evaluation method with statistical model calculation codes provides energetically reasonable secondary gamma-ray data if calculation parameters are well adjusted with investigating secondary neutron and charged particle emission cross sections.

References

- [1] J. Yamamoto, I. Murata and A. Takahashi, "Gamma-Ray Emission Spectra from Spheres with 14 MeV Neutron Source," JAERI-M 89-026, pp. 232-242 (1989).
- [2] J. Yamamoto, "Integral Experiment on Gamma-Ray Production at OKTAVIAN," JAERI-M 91-062, pp. 118-125 (1991).
- [3] J. Yamamoto *et al.*, "Gamma-Ray Energy Spectra Emitted from Spheres with 14 MeV Neutron Source," JAERI-M 94-014, pp. 32-62 (1994).
- [4] J. F. Briesmeister (Ed.), "MCNP - A General Monte Carlo N-Particle Transport Code, Version 4A", LA-12625-M (1993).
- [5] T. Nakagawa *et al.*, "Japanese Evaluated Nuclear Data Library Version 3 Revision-2: JENDL-3.2," J. Nucl. Sci. Technol., 32, 1259 (1995).
- [6] S. Chiba, B. Yu and T. Fukahori, "Evaluation of JENDL Fusion File," JAERI-M 92-027, pp. 35-44 (1992).
- [7] S. Ganesan and P. K. McLaughlin, "FENDL/E Evaluated Nuclear Data Library of Neutron Nuclear Interaction Cross-Sections and Photon Production Cross-Sections and Photon-Atom Interaction Cross Sections for Fusion Applications Version 1.0 of May 1994," IAEA-NDS-128 (1995).
- [8] F. Maekawa and Y. Oyama, "Benchmark Test of Gamma-Ray Production Data in JENDL-3.2 and FENDL-1," Proc. 1st Research Co-ordination Meeting on Measurement, Calculation and Evaluation of Photon Production Data," Nov. 14-17, 1994, Bologna, Italy, pp. 139-145 (1995).
- [9] F. Maekawa and Y. Oyama, Nucl. Sci. Eng., 123, 272 (1996).
- [10] P. G. Young and E. D. Arthur, "GNASH: A Preequilibrium, Statistical Nuclear-Model Code for Calculation of Cross sections and Emission Spectra," LA-6947 (1977).
- [11] K. Shibata and C. Y. Fu, "Recent Improvements of the TNG Statistical Model Code," ORNL/TM-10093 (1986).

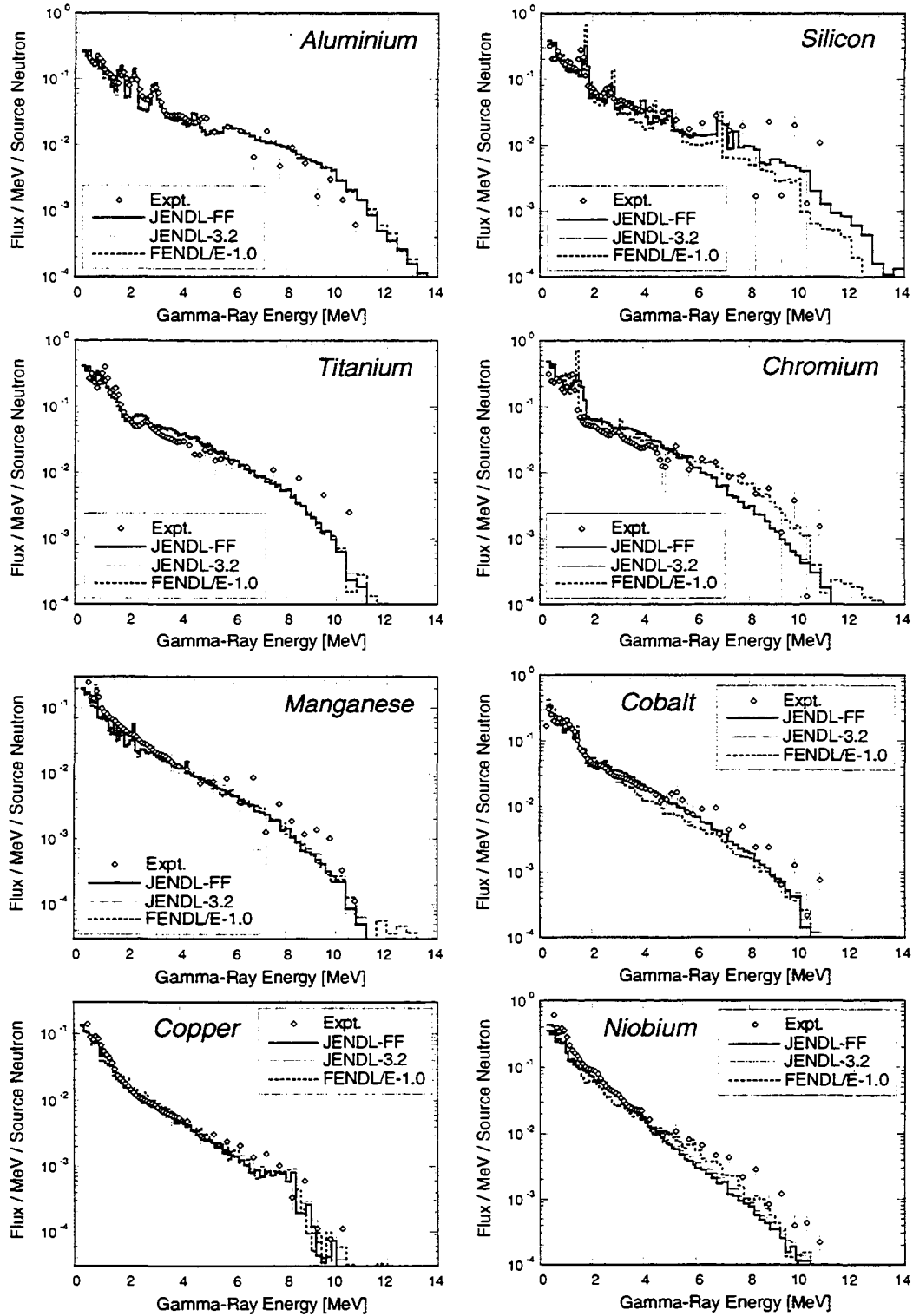


Fig. 1, Part 1. Measured gamma-ray spectra leaking from the sample piles compared with calculations with JENDL Fusion File, JENDL-3.2 and FENDL/E-1.0.

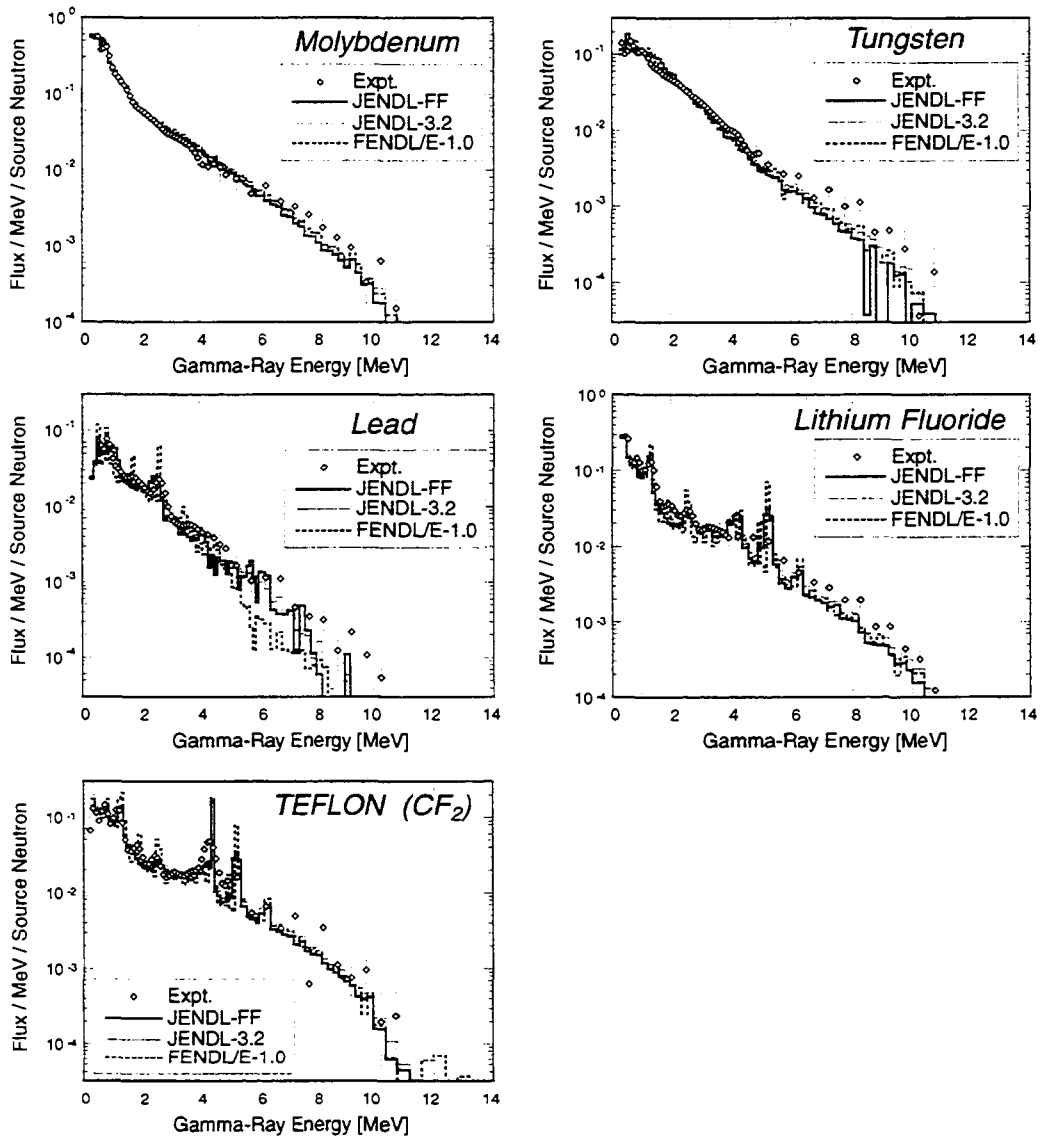


Fig. 1. Part 2. Measured gamma-ray spectra leaking from the sample piles compared with calculations with JENDL Fusion File, JENDL-3.2 and FENDL/E-1.0.

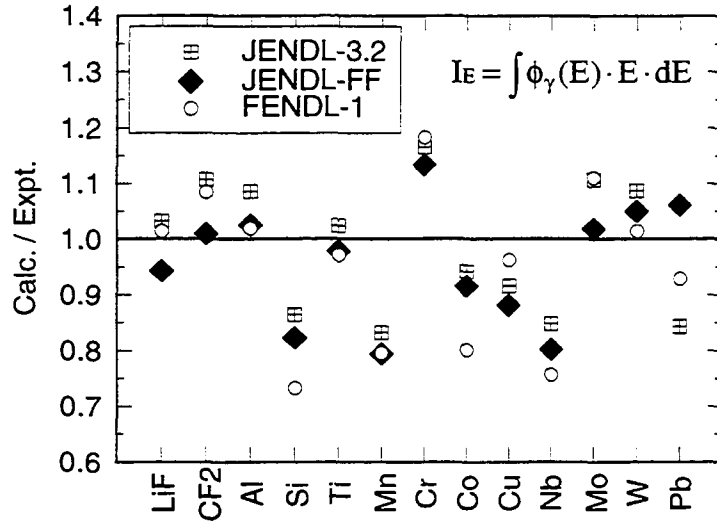


Fig. 2. Calculated to experimental ratios for integrated gamma-ray energies, I_E .

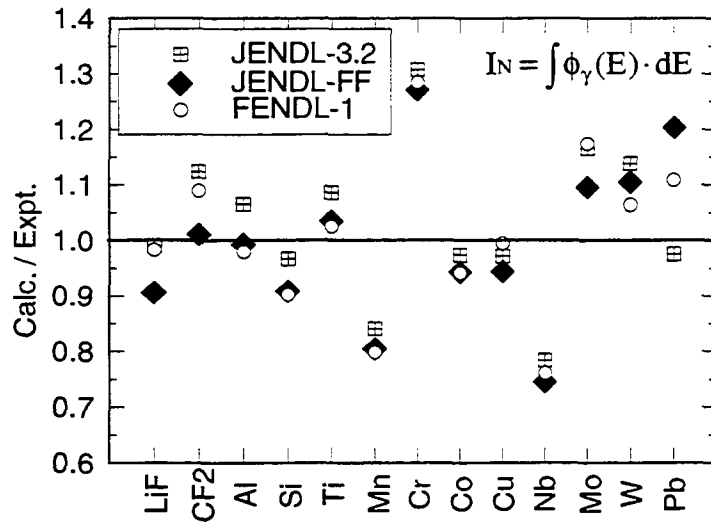


Fig. 3. Calculated to experimental ratios for integrated gamma-ray fluxes, I_N .

Measurement of Gamma-Ray Spectra and Heating Rates in Cylindrical Assemblies

F. Maekawa, Y. Oyama and M. Wada

High Energy Neutron Laboratory, Japan Atomic Energy Research Institute
Tokai, Ibaraki, 319-11 Japan

1. Introduction

A series of fusion neutronics clean benchmark experiments has been conducted at the FNS facility in JAERI. Gamma-ray spectra and heating rates were measured in cylindrical experimental assemblies made of iron, copper, tungsten and type 316 stainless steel (SS-316). These experimental data are compared with calculations with JENDL-3.2, JENDL Fusion File, FENDL/E-1.0 and EFF-3.

2. Experimental Configuration

All the experimental assemblies are in cylindrical shapes to allow two-dimensional (R-Z) modeling for transport calculations. One of the cylindrical experimental assemblies is placed at distances of 200 or 300 mm from the D-T neutron source. Both neutrons and gamma-rays are measured inside the experimental assembly with various measuring techniques during D-T neutron irradiation. As for gamma-ray related quantities, gamma-ray spectra and heating rate were measured. Table 1 summarizes dimensions, chemical composition, weight density and detector locations for each experimental assembly. Detailed information about the experiments is described in the references: iron [1], copper [2,3], tungsten [4] and SS-316 [4-6].

It should be remarked that the experimental gamma-ray data can be used for validation of gamma-ray production cross sections for high energy neutrons to induce threshold reactions as well as for low energy neutrons to induce (n, γ) reactions. Gamma-rays at the detector positions near the D-T neutron source are dominated by the threshold reactions, while those at deep inside the experimental assembly are mainly produced by the (n, γ) reactions.

3. Measurement of Gamma-Ray Heating Rate and Spectrum

Here a brief explanation is given. See reference [1] for a more detailed description.

(a) Gamma-ray heating rate

Three types of thermoluminescence dosimeters (TLD) were used: Mg_2SiO_4 (effective atomic number: $Z_{eff}=11.1$), Sr_2SiO_4 ($Z_{eff}=32.5$) and Ba_2SiO_4 ($Z_{eff}=49.9$). These TLDs were inserted in the experimental assembly at several positions and irradiated by D-T neutrons. Total (neutron + gamma) responses of the TLDs were read by a TLD

reader. Neutron contributions to the total responses were estimated with semi-experimental neutron-energy-dependent response functions for each type of TLD and calculated neutron spectra at the detector positions, and subtracted from the total responses to obtain heating rates by gamma-rays only. The gamma-ray heating rate increases monotonically as a function of atomic number of the probe material [7]. Based on this principle, gamma-ray heating rates of the material of the experimental assembly were deduced by interpolating the measured gamma-ray heating by the three types of TLD in terms of their atomic numbers. Typical experimental uncertainties are ~ 10 %. Numerical data for the measured gamma-ray heating rates for the four materials are given in Table 2.

(b) Gamma-ray spectrum

The gamma-ray spectrometer was a 40 mm ϕ spherical deuterated liquid organic scintillator (BC-537) contained in a quartz glass, which was specially designed to reduce gamma-ray emission by the spectrometer itself. The spectrometer was inserted in the experimental assembly, and a pulse height spectrum due to prompt gamma-rays was measured during a neutron irradiation. Neutron events were rejected by the pulse-shape discrimination technique. Gamma-rays associated with disintegration of induced radioactivities were also rejected by the pulse-shape discrimination method. The gamma-ray energy spectra were obtained by unfolding the measured pulse height spectra.

The spectrometer size is rather large for the in-situ measurement. The measured spectrum fluxes in these assemblies were observed to be larger than those with an ideal infinitesimal detector because attenuation of gamma-ray fluxes in the detector is smaller, typically ~ 30 %, than that in the materials of the assemblies. To facilitate the transport calculation without modeling of the spectrometer, the measured spectrum fluxes are normalized so as to be consistent with the measured gamma-ray heating rates by the TLDs, for which detector size is negligibly small.

4. Analysis

Experimental analyses were performed with the continuous energy Monte Carlo transport code MCNP-4A [8]. Three evaluated nuclear data files, i.e., JENDL-3.2 [9], JENDL Fusion File [10] and FENDL/E-1.0 [11], were used. For the iron experiment, an analysis with the latest EFF-3 evaluation for Fe-56 [12] was also performed. In this analysis, the FENDL/E-1.0 evaluation was used for the rest of iron isotopes, i.e., Fe-54, Fe-57 and Fe-58. This combination of iron data is to be adopted in FENDL/E-2.0.

5. Discussion

Calculated to experimental (C/E) ratios for the gamma-ray heating rates are shown in Fig. 1. Calculated gamma-ray spectra are compared with the measured ones in Figs. 2 - 5 for iron, copper, tungsten and SS-316, respectively.

In the gamma-ray spectra of iron, copper and SS-316, a clear trend of changing spectral shape is clearly seen. At the detector position close to the D-T neutron source, low energy gamma-rays around 1 MeV are dominant because these gamma-rays are mainly produced by threshold reactions exciting lower levels of interacting nuclei. At deeper detector positions far from the D-T neutron source where low energy neutrons are dominant, clear peaks at ~ 8 MeV are observed in the gamma-ray spectra. This energy just corresponds to the binding energy of a neutron, indicating that these peaks are produced by radiative neutron capture reactions.

The C/E ratios for copper, tungsten and SS-316 in Fig. 1 indicate that most of the calculated gamma-ray heating rates agree within $\pm 30\%$ with the experiment. In the case of iron, however, calculations with JENDL-3.2 and EFF-3 predict considerably larger gamma-ray heating rates at the positions near the D-T source. This fact implies that the gamma-ray production cross sections of iron at 14-MeV in the two evaluations are given larger. Figure 6 compares the measured gamma-ray production cross section of iron with the evaluations. Although some scattering is seen among the experimental data, the cross sections in the JENDL Fusion File and FENDL/E-1.0 follow the experimental data. However, the cross sections in JENDL-3.2 and EFF-3 are apparently larger than the measured cross sections. The present integral experiment and the differential cross section measurement are consistent with each other at this point.

6. Conclusions

Benchmark experimental data for secondary gamma-rays produced by threshold reactions with high energy neutrons as well as by neutron capture reactions with low energy neutrons were obtained for iron, copper, tungsten and SS-316. A serious problem was found through the experimental analysis that significantly large gamma-ray production cross sections were given for natural iron by JENDL-3.2 and iron-56 by EFF-3. Since iron is one of the most important structural materials, these gamma-ray production cross sections should be re-evaluated as soon as possible.

References

- [1] F. Maekawa *et al.*, "Measurement of Gamma-Ray Spectra and Heating Rates in Iron and Stainless Steel Shields Bombarded by Deuterium-Tritium Neutrons and Validation of Secondary-Gamma-Ray Data in Evaluated Nuclear Data Libraries." to be published in Nucl. Sci. Eng. (June, 1997).
- [2] F. Maekawa *et al.*, "Benchmark Experiment on a Copper Slab Assembly Bombarded by D-T Neutrons," JAERI-M 94-038 (1994).
- [3] F. Maekawa *et al.*, Fusion Eng. Des., 28, 753 (1995).
- [4] F. Maekawa *et al.*, "Benchmark Experiment on Tungsten Assembly Bombarded with D-T Neutrons," Proc. Intl. Conf. on Nucl. Data for Sci. and Technol., May 19-24, 1997, Trieste, Italy, to be published (1997).

- [5] C. Konno *et al.*, Fusion Technol., 21, 2169 (1992).
- [6] C. Konno *et al.*, "Bulk Shielding Experiment on Large SS-316 Assemblies Bombarded by D-T Neutrons Volume I: Experiment," JAERI-Research 94-043 (1994).
- [7] S. Tanaka and N. Sasamoto, "Gamma-ray Absorbed Dose Measurements in Media with Plural Thermoluminescent Dosimeters Having Different Atomic Numbers," J. Nucl. Sci. Technol., 22, 109 (1985).
- [8] J. F. Briesmeister (Ed.), "MCNP - A General Monte Carlo N-Particle Transport Code, Version 4A", LA-12625-M (1993).
- [9] T. Nakagawa *et al.*, "Japanese Evaluated Nuclear Data Library Version 3 Revision-2: JENDL-3.2," J. Nucl. Sci. Technol., 32, 1259 (1995).
- [10] S. Chiba, B. Yu and T. Fukahori, "Evaluation of JENDL Fusion File," JAERI-M 92-027, pp. 35-44 (1992).
- [11] S. Ganesan and P. K. McLaughlin, "FENDL/E Evaluated Nuclear Data Library of Neutron Nuclear Interaction Cross-Sections and Photon Production Cross-Sections and Photon-Atom Interaction Cross Sections for Fusion Applications Version 1.0 of May 1994," IAEA-NDS-128 (1995).
- [12] A. J. Koning and H. Gruppelaar, EFF-DOC-426 (1995).

Table 1. Specifications of the experimental assemblies used for the cylinder experiments.

Iron	
Dimension	1000 mm ϕ x 950 mm 200 mm from the D-T source
Chemical Composition*	Fe: 98.83 %, C: 0.19 %, Si: 0.15 %, Mn: 0.83 %
Weight Density	7.849 [g/cm ³]
Detector Location	heating: 0, 50, 100, 200, 300, 400, 500, 600, 700, 800 mm spectrum: 100, 300, 500, 700 mm
Copper	
Dimension	629 mm ϕ x 608 mm 200 mm from the D-T source
Chemical Composition	Cu: 100 %
Weight Density	8.93 [g/cm ³]
Detector Location	heating: 0, 58, 210, 356, 508 mm spectrum: 76, 228, 380, 532 mm
Tungsten	
Dimension	629 mm ϕ x 507 mm 200 mm from the D-T source
Chemical Composition	W: 94.8 %, Ni: 3.1 %, Cu: 2.1 %
Weight Density	18.05 [g/cm ³]
Detector Location	heating: 0, 76, 228, 380 mm spectrum: 76, 228, 380 mm
Stainless Steel-316	
Dimension	1200 mm ϕ x 1118 mm 300 mm from the D-T source Source reflector of 200 mm in thickness that surrounds the D-T neutron source is attached in front of the cylindrical assembly.
Chemical Composition	Fe: 67.37 %, Cr: 16.86 %, Ni: 11.95 %, Mo: 2.11 %, Mn: 1.13 %, Si: 0.58 %
Weight Density	7.926 [g/cm ³]
Detector Location	heating: 0, 102, 229, 356, 533, 711, 914 mm spectrum: 102, 356, 711, 914 mm

*Note: Chemical compositions are given in units of weight percentages.

Table 2. Measured gamma-ray heating rates in the vanadium, iron, copper, tungsten and SS-316 assemblies.

Material	Position [mm]	Gamma-Ray Heating [Gy/source]	Error [%]
Iron	0	9.10e-16	25.7
	50	1.17e-15	10.8
	100	5.30e-16	10.5
	200	1.32e-16	9.3
	300	3.55e-17	10.0
	400	1.36e-17	10.2
	500	7.18e-18	10.6
	600	4.92e-18	8.5
	700	3.08e-18	8.2
	800	2.00e-18	8.0
Copper	0	1.20e-15	24.5
	58	8.35e-16	22.2
	210	1.12e-16	13.2
	356	2.69e-17	14.5
	508	7.48e-18	11.1
Tungsten	0	5.41e-16	58.1
	76	5.95e-16	19.0
	228	9.38e-17	16.7
	380	1.26e-17	17.6
SS-316	0	9.48e-16	18.1
	102	3.93e-16	13.6
	229	1.28e-16	14.5
	356	5.85e-17	12.6
	533	2.31e-17	13.5
	711	8.47e-18	13.0
	914	2.27e-18	12.9

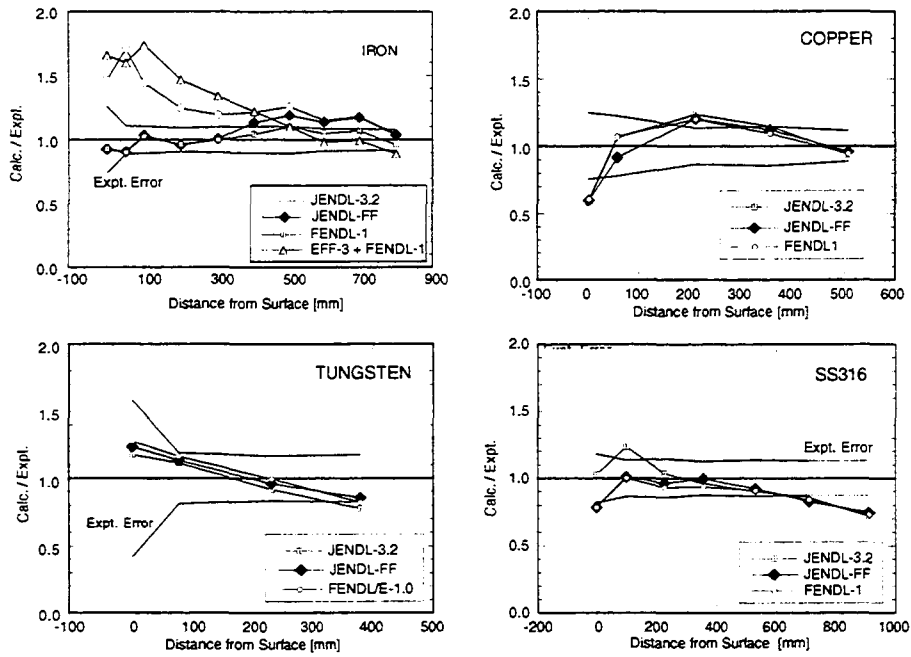


Fig. 1. Calculated to experimental ratios for the gamma-ray heating rates.

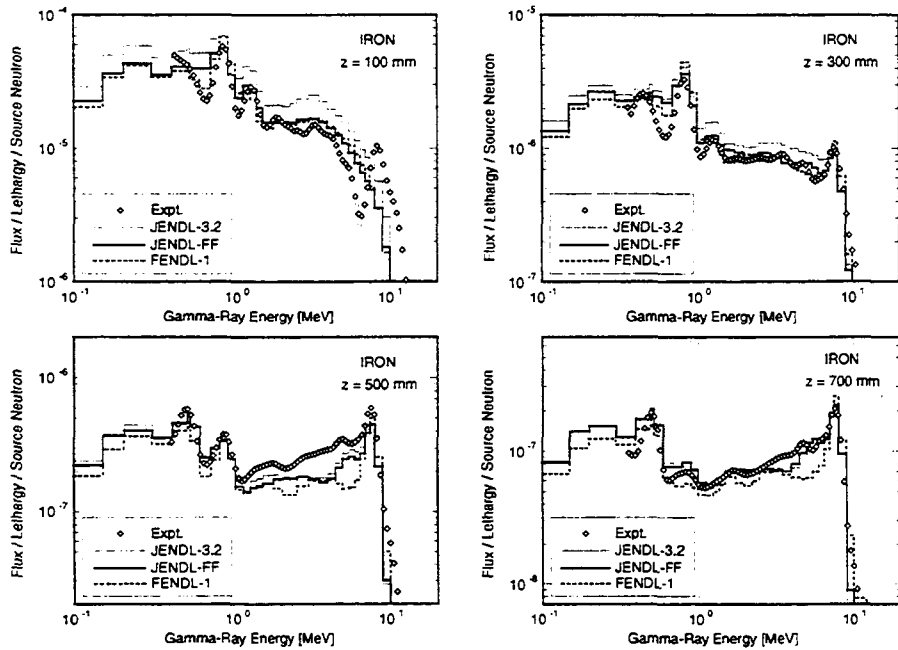


Fig. 2. Measured gamma-ray spectra in the iron assembly compared with calculations.

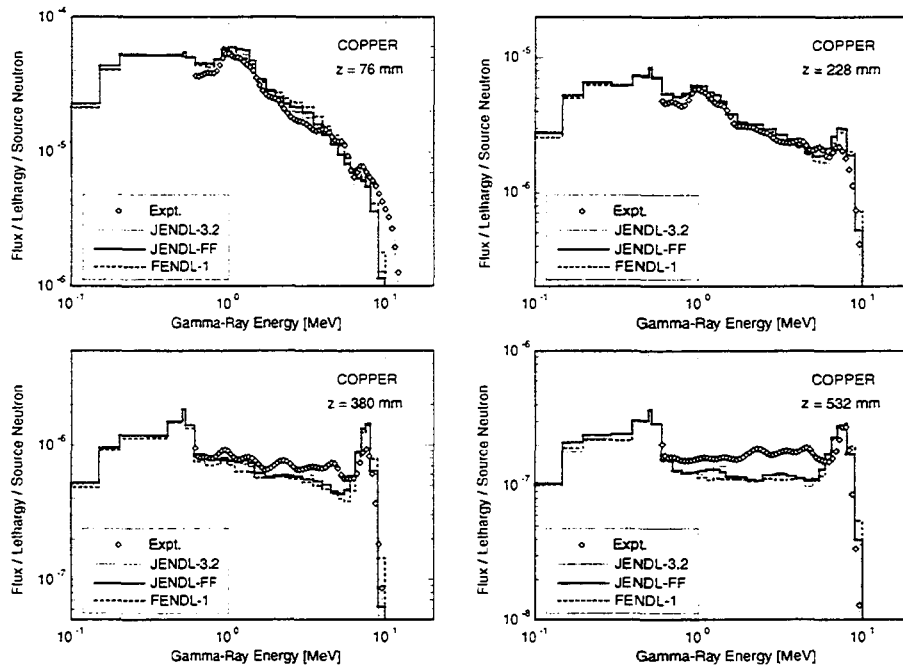


Fig. 3. Measured gamma-ray spectra in the copper assembly compared with calculations.

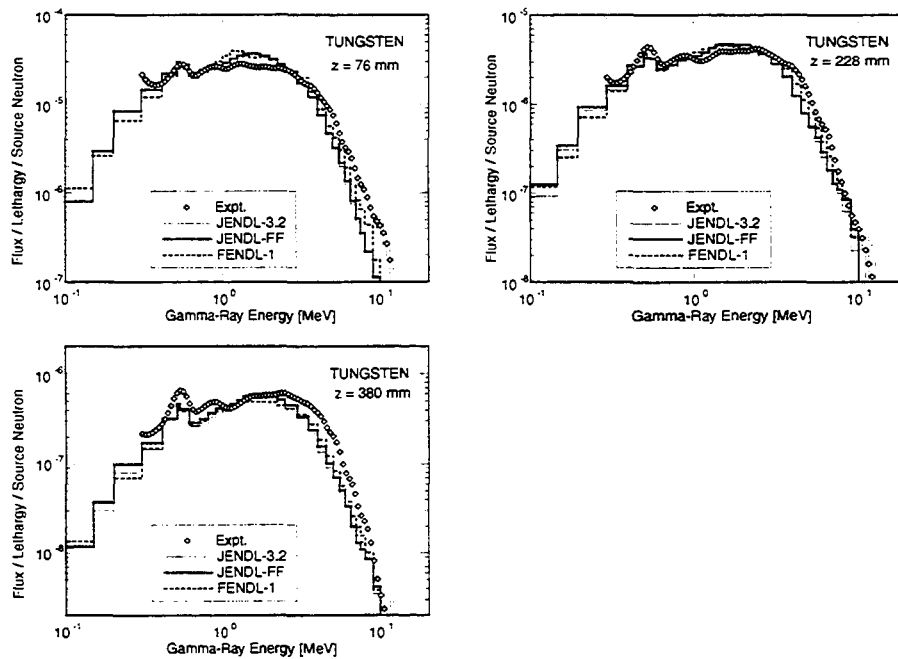


Fig. 4. Measured gamma-ray spectra in the tungsten assembly compared with calculations.

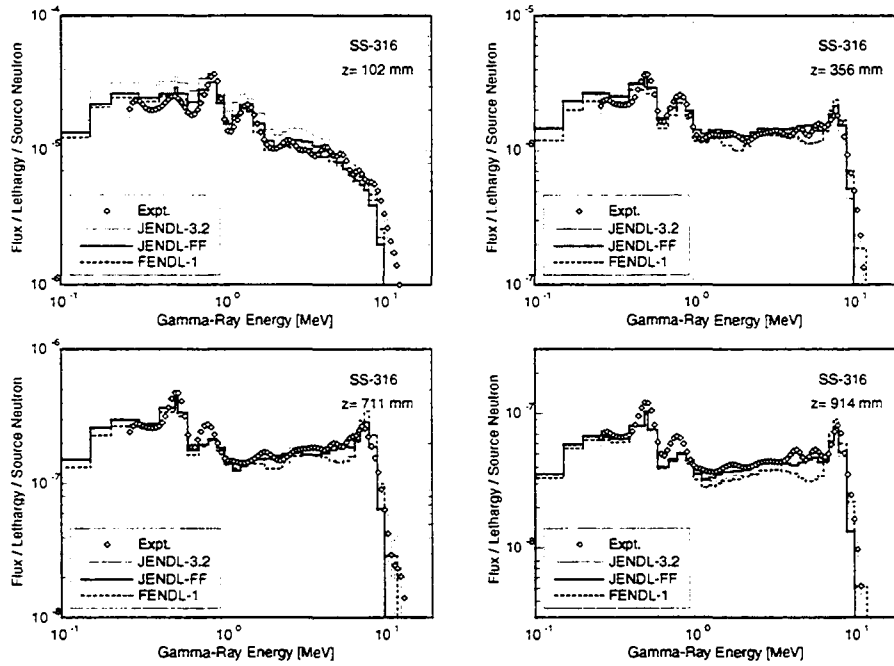


Fig. 5. Measured gamma-ray spectra in the SS-316 assembly compared with calculations.

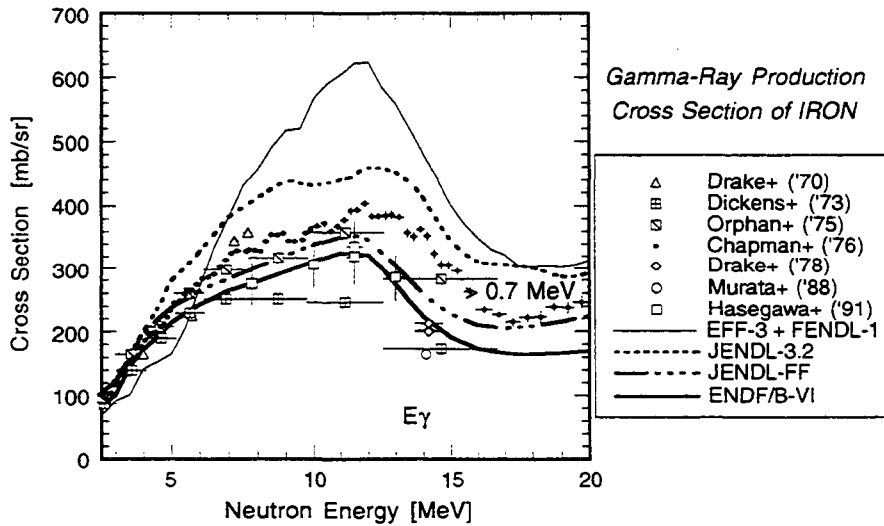


Fig. 6. Gamma-ray production cross section of natural iron ($E_{\gamma} > 0.7$ MeV).

NEW ANALYSIS OF PHOTON FLUX SPECTRA FROM AN IRON SLAB BENCHMARK EXPERIMENT

U. Fischer*, H. Freiesleben, K. Seidel, S. Unholzer

Technische Universität Dresden, Institut für Kern-und Teilchenphysik, D-01062 Dresden,
Germany, *Forschungszentrum Karlsruhe, Institut für Neutronenphysik und
Reaktortechnik, D-76021 Karlsruhe, PF 3640, Germany

Abstract

Neutron induced photon flux spectra from an iron slab irradiated with 14 MeV neutrons and the corresponding neutron flux spectra were analysed by use of the EFF-3 nuclear data file containing new measured and re-evaluated iron data. The EFF-3 data file was also tested against evaluations from the EFF-2 data library. The influence of uncertainties related to neutron data on the calculated neutron flux spectra producing the photon flux is considered for the first time.

1. Introduction

Iron is the basic structural and shielding material in fusion reactors. The 10% accuracy level required for shielding related nuclear responses is not achieved with the currently available iron cross-section data.

2. Experiment

A thick iron slab of dimensions $1\text{ m} \times 1\text{ m} \times 0.3\text{ m}$ was irradiated with 14 MeV neutrons. The benchmark experiment is characterised by the simultaneous measurement of both neutron and photon flux spectra two-dimensionally in time-of-arrival and pulse height as recommended [1] for the measurement of photon flux spectra from thick assemblies. The experiment is described in more detail elsewhere [2].

3. Database

The data base for calculations has been improved by re-evaluation of the Fe-56 cross-section data of the European Fusion File EFF-2 [3]. Improvements in the EFF-3 evaluation refer to newer precise measurements of neutron cross-section data. The evaluation for all MF=3 cross section data was carried out jointly with the Bayesian code GLUCS [4] starting from the EFF-2 evaluation and its covariances as a primary data set. The new Fe-56 data file was processed with NJOY [5] for subsequent use with the MCNP Monte Carlo Transport code [6]. Data-related uncertainties of the calculated neutron flux spectra inducing the prompt photon spectra have been estimated by two-dimensional

uncertainty analysis. The required covariance data were processed with NJOY from the basic Fe-56 data. For all comparisons the new evaluated EFF-3 data file [7] was used, where the processing error of the previous version [8] was corrected.

4. Results and discussion

The measured photon flux spectrum is compared with MCNP calculations using EFF-3 and EFF-2 data in Fig. 1 and Table 1. In contrast to the EFF-2 calculation, which underestimates the measured prompt photon flux by about 19% in the entire range, the new EFF-3 calculation gives a strong increase of 47% in the photon flux spectrum, resulting now in an overestimation of 19% in comparison with the experimental data. The reason for this jump is obscure at the moment, because it is not accompanied by the same tendency in the calculated neutron flux spectrum that produces the prompt photons.

Table 1. Photon fluence in cm^{-2} per source neutron for selected photon energy ranges.

E (MeV)	0.4 - 1.0	1.0 - 8.0	> 0.4
Experiment	$1.07 \pm 0.06 \text{ E-8}$	$1.15 \pm 0.06 \text{ E-8}$	$2.22 \pm 0.12 \text{ E-8}$
EFF-2	0.93 E-8	0.89 E-8	1.81 E-8
EFF-3	1.25 E-8	1.39 E-8	2.64 E-8
FENDL-1	0.89 E-8	0.81 E-8	1.69 E-8

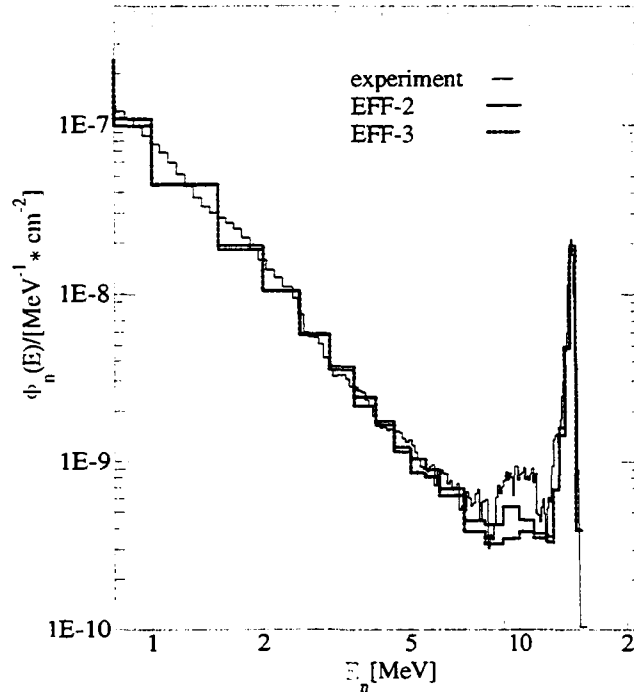


Fig. 1. Measured and calculated spectral photon fluences per source neutron.

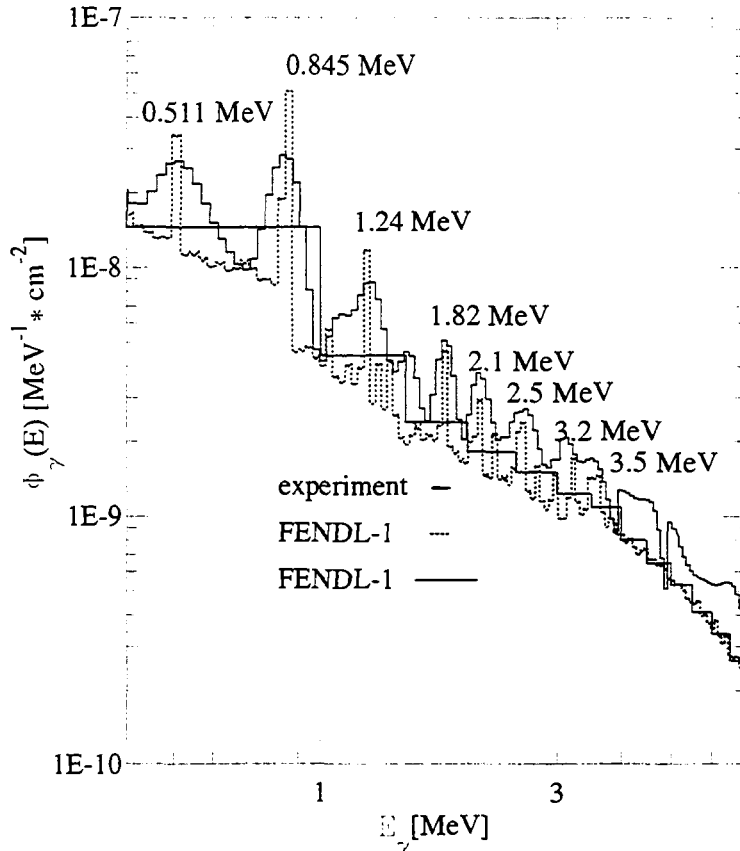


Fig. 2. Measured photon fluence and photon fluence calculated on the basis of FENDL-1 data per source neutron.

The experiment is compared in Fig. 2 with a new FENDL-1 calculation of high resolution to give a more detailed description of the calculated photon spectrum. This kind of MCNP calculation is strongly time consuming. Prominent gamma lines are stated above in the picture. The spectrum consists of 2 parts, a discrete line shaped part and a continuous spectral part. It can be seen that the experiment is underestimated in both components.

For comparison the wide-meshed structure used for the calculations of Fig. 1 is also given here for a second FENDL-1 calculation describing the mean energy dependence of the photon flux spectrum. The measured photon flux spectrum is altogether underestimated by 24% (see also Table 1). The calculated neutron flux spectrum using FENDL-1 data is underestimated compared with EFF-2 calculations (see Table 2).

Neutron flux spectra from the various calculations are compared in Fig. 3 and Table 2. Estimates of data-related uncertainties are shown. The replacement of EFF-2 by EFF-3 iron data in the range 1-5 MeV, where the fluctuating elastic and inelastic scattering cross sections have been newly introduced, results in the minor improvement of a 1.8% increase

in the neutron flux, explaining fully the remaining discrepancy of 2 % between calculation and experiment. On the other hand, the EFF-3 data evaluation gives a larger underestimate of the experiment between 5-10 MeV, which is an actual drawback with regard to EFF-2. The deviation is now outside the data-related and experimental error limits. With EFF-3 the calculated mean neutron flux between 5-10 MeV (5-8 MeV) is reduced by 18% (12%) with respect to EFF-2, and for $E > 10$ MeV the calculated mean flux is reduced by 4.8% .

Table 2. Neutron fluence in cm^{-2} per source neutron for selected neutron energy ranges, with experimental and data-related uncertainties.

E (MeV)	1.0 - 5.0	5.0 - 8.0	5.0 -10.0	> 10.0
Experiment	$4.51 \pm 0.15 \text{ E-}8$	$2.30 \pm 0.09 \text{ E-}9$	$3.42 \pm 0.13 \text{ E-}9$	$1.59 \pm 0.05 \text{ E-}8$
EFF-2	$4.40 \pm 0.33 \text{ E-}8$	$2.11 \pm 0.53 \text{ E-}9$	$3.07 \pm 0.58 \text{ E-}9$	$1.45 \pm 0.46 \text{ E-}8$
EFF-3	$4.48 \pm 0.08 \text{ E-}8$	$1.86 \pm 0.20 \text{ E-}9$	$2.53 \pm 0.22 \text{ E-}9$	$1.38 \pm 0.15 \text{ E-}8$
FENDL-1	$4.26 \text{ E-}8$		$3.63 \text{ E-}9$	$1.31 \text{ E-}8$

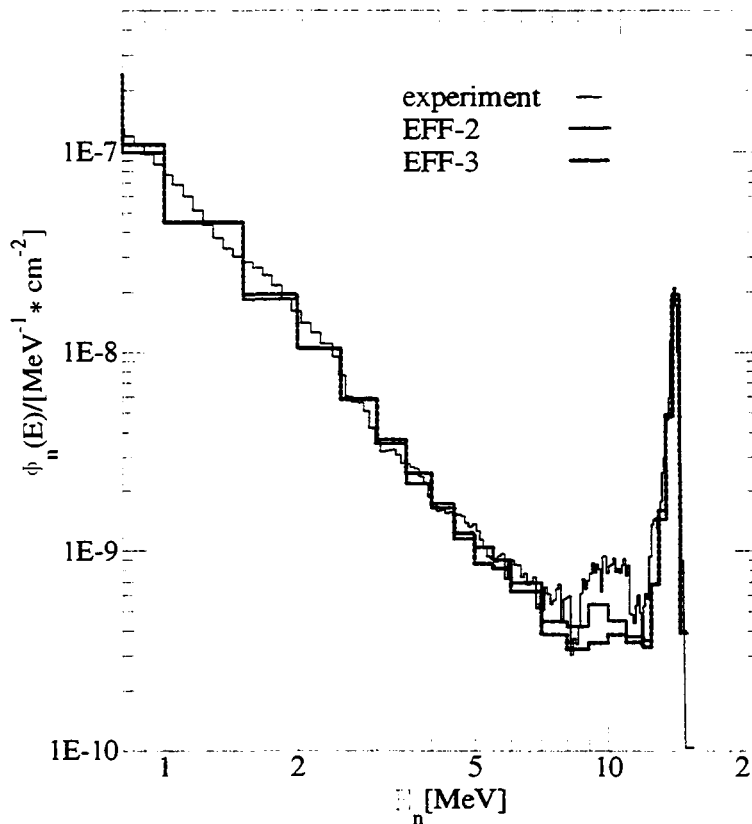


Fig. 3. Measured and calculated spectral neutron fluences per source neutron.

The latter problems are currently under investigation. It appears that the observed underestimate is a result of a processing error when converting the secondary energy-angle distribution of MT=91 to the Kalbach-Mann representation by NJOY/ACER. Actually, it was found [9] that this discrepancy disappears when using file 6 from ENDF/B-6 for MT=91 instead of EFF-3. The observed overestimate of the photon production may be related to this problem. Work is in progress to investigate this possibility.

5. Summary and conclusions

When compared with EFF-2 calculations, the measured neutron flux spectrum that produces the photon flux is well described within the error limits, with a weak tendency toward underestimation by 2% but not larger than 10%. The measured photon flux spectrum is clearly underestimated on average by about 19% but not larger than 23%. Larger discrepancies are observed with the new EFF-3 data, both in the calculated neutron and photon flux spectra. The calculated photon flux spectrum shows a clear overestimate by 20%. The calculated neutron flux is lower by 20% in the range 5-8 MeV, which is outside the error limits.

The discrepancies show that the new EFF-3 data file still needs further revisions before it can be applied with confidence. Possibly this is true only for the processed file, whereas the basic data file may need no corrections. With the reduced uncertainties associated with the neutron cross section data a substantial improvement was achieved.

6. References

- [1] 1st CRP Meeting on Photon Production, Bologna, 1995.
- [2] H. Freiesleben *et al.*, Report TUD-PHY-94/2, Dresden, 1994.
- [3] H. Vonach *et al.*, Physics Data, No.13-7, 1992 and No 13-8, 1996.
- [4] D. M. Hetric and C. Y. Fu, Report ORNL/TM-7341, Oak Ridge, 1980 and S. Tagesen and D. M. Hetric: Proc. Int. Conf. on Nuclear Data, Gatlinburg (USA), May 9-15, 1994, ed. J. K. Dickens, p.589.
- [5] R. E. MacFarlane and D. W. Muir., Report LA-12740, Los Alamos, 1994.
- [6] J. F. Briesmeister (ed.), Report LA-12625-M, Los Alamos, 1993.
- [7] A. J. Koning, H. Gruppelaar, Report EFF-DOC-426 (1995).
- [8] A. Hogenbirk *et al.*, Report EFF-DOC-382 (1995).
- [9] A. Trkov, EFF Fusion Data & Neutronics Monitoring Meeting, NEA Data Bank, Paris, June 19-20, 1997.

NEUTRON INDUCED PHOTON FLUX SPECTRA INSIDE AN ITER SHIELD MOCKUP

H.Freiesleben , K. Seidel, S. Unholzer

Technische Universität Dresden, Institut für Kern- und Teilchenphysik,
D-01062 Dresden, Germany

Abstract

Neutron and photon flux spectra were measured at two different positions deep inside a fusion reactor bulk shield mock-up in the framework of the International Thermonuclear Experimental Reactor project ITER. The measured spectra were analysed by MCNP calculations using nuclear data from the European Fusion File libraries EFF-3, EFF-2, the Fusion Evaluated Nuclear Data Library FENDL-1, and the Japanese Evaluated Nuclear Data Library JENDL-FF.

1. Introduction

Following benchmarking iron data files, different libraries were tested against an ITER shield mock-up experiment performed at the Frascati 14 MeV neutron generator. The experiment is part of the joint investigations of the simulated ITER-inboard shield system [1]. The measurement of neutron flux spectra is of basic importance for the calculation of all neutron flux related nuclear responses, such as nuclear heating, material activation, gas production, and radiation damage. The simultaneous measurement of neutron induced photon flux spectra is a direct measurement of an important function of the neutron flux and can be used as a test of photon production data in nuclear data files. In addition it allows the direct estimation of gamma heating and the calculation of radiation effects on materials induced by photons.

2. Experiment and database

The bulk shield mock-up simulating the reactor first wall, shielding blanket and vacuum vessel of ITER consists of a sequence of thin Perspex and SS-316 stainless-steel layers of thickness 2.5 cm and 5 cm with a total dimension of 1 m × 1 m × 0.943 m. Photon and neutron flux spectra were measured on the central axis inside the bulk in 2 different positions. Position A at a distance of 41.5 cm from the front corresponds to the back plate of the ITER shield blanket, and position B at 87.6 cm is close to the boundary of the ITER vacuum vessel.

The neutron flux between 50 KeV and 1 MeV was measured with proton recoil proportional counters. For the measurement of neutron flux spectra between 1 MeV and 15 MeV and for the simultaneous measurement of neutron-induced photon flux spectra

between 0.4 and 10 MeV, a NE-213 scintillation spectrometer was used as both a proton recoil and Compton gamma spectrometer. The detector response matrices of the 1.5-inch \times 1.5-inch scintillation detector are well described for both neutron and photon events. The measured pulse height spectra were unfolded to give the neutron and photon energy spectra, which were then compared with calculations. The Frascati neutron generator operates in the stationary beam mode only. The measured photon spectra are thus induced by all interacting neutrons. Background-related events from outside the assembly are strongly reduced inside the assembly and have been neglected. The remaining gamma-ray background from activated nuclei inside the assembly was on the order of 2% of the total photon flux and was separately measured for subtraction.

Neutron and photon spectra measured were analysed by three-dimensional coupled neutron-gamma transport calculations with the Monte Carlo code MCNP-4A [2] using the nuclear data files EFF-3 [3] Version 2, EFF-2 [4] Version 2, FENDL-1 [5], and JENDL-FF [6].

3. Results and discussion

Photon flux spectra measured in positions A and B are compared in Fig. 1 with calculations using the EFF-2 and FENDL-1 nuclear data libraries and for selected energy-integrated intervals, including also EFF-3 and JENDL-FF calculations, in Table 1.

Intercomparing the measured photon spectra in positions A and B, it is found that the intensity is reduced by a constant factor of 1.43×10^{-3} within 1% precision, independent of the selected energy intervals shown in Table 1. It can be seen in more detail (see Fig. 1) that also the spectral shape in either case is nearly the same. Local differences in the bulk shield composition (specifically, a double Perspex layer before Position A) result only in an enhanced 2.225 MeV gamma line from neutron capture on hydrogen.

Table 1. Photon fluence in cm^{-2} per source neutron for selected photon energy ranges inside the ITER shield mock-up in position A and position B.

	E (MeV)	0.4 - 1.0	1.0 - 10.0	>0.4
Position A	Experiment	$3.18 \pm 0.18 \text{ E-6}$	$4.29 \pm 0.24 \text{ E-6}$	$7.47 \pm 0.42 \text{ E-6}$
	EFF-3	3.66 E-6	5.11 E-6	8.74 E-6
	EFF-2	3.34 E-6	4.63 E-6	8.00 E-6
	FENDL-1	3.15 E-6	4.50 E-6	7.62 E-6
	JENDL-FF	3.31 E-6	4.80 E-6	8.14 E-6
Position B	Experiment	$4.50 \pm 0.24 \text{ E-9}$	$6.20 \pm 0.33 \text{ E-9}$	$1.07 \pm 0.06 \text{ E-8}$
	EFF-3	4.77 E-9	6.51 E-9	1.13 E-8
	EFF-2	4.32 E-9	6.08 E-9	1.04 E-8
	FENDL-1	4.00 E-9	5.58 E-9	0.95 E-8
	JENDL-FF	4.32 E-9	6.14 E-9	1.05 E-8

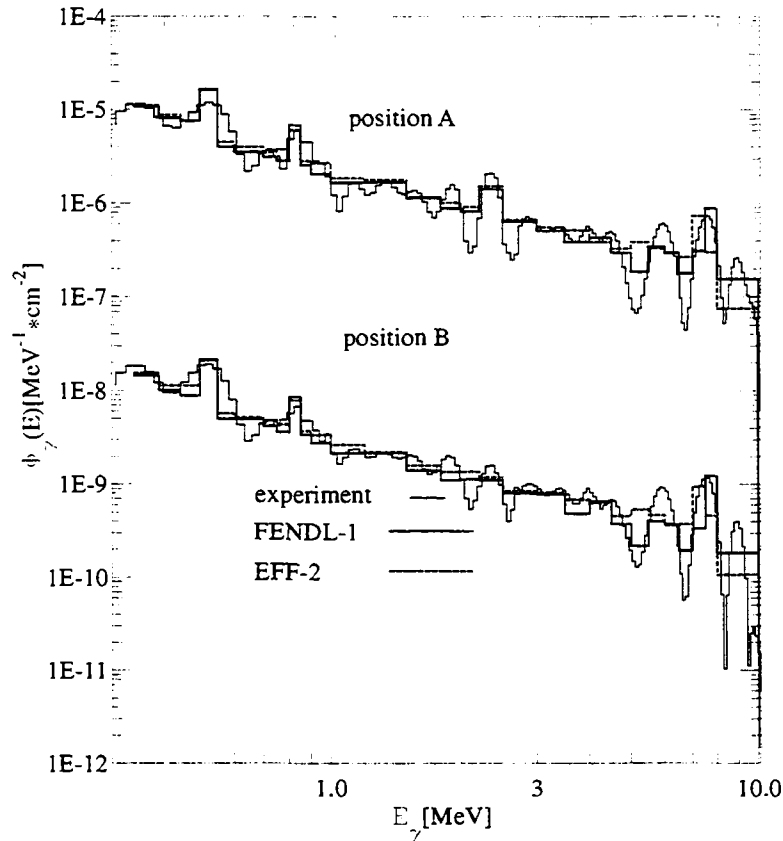


Fig.1. Measured and calculated photon flux spectra per source neutron inside the ITER shield mock-up in position A and position B.

In position A the experiment is overestimated by about 19% by the EFF-3 calculations. This value is significantly larger than those using other nuclear data files and lies outside of the experimental error limits. The same tendency was already found in the analysis of the TUD iron benchmark experiment using the new evaluated EFF-3 iron data [7] and is probably attributable to a processing error in the new EFF-3 photon production data for iron. For EFF-2, FENDL-1, and JENDL-FF the mean differences compared to the experiment are smaller than 10%. The measured flux is generally larger than the calculated flux.

Neutron flux spectra are compared with each other in Fig. 2 and Table 2. The high energy part ($> 5\text{MeV}$) of the measured neutron flux in position A is well described by all data files within 2% - 4%. The low energy spectral part is underestimated by 10%. Altogether, a sufficiently accurate description of the experiment within the 10% level is obtained in position A for both neutron and photon spectra. This is true for all data files used in the calculations, with the exception of the photon flux for EFF-3.

Table 2. Neutron fluence in cm^{-2} per source neutron for selected neutron energy ranges inside the ITER shield mock-up in position A and position B.

	E (MeV)	0.1 -1.0	1.0 -5.0	5.0 -10.0	> 10.0
Position A	Experiment	$2.76 \pm 0.28 \text{ E-6}$	$1.43 \pm 0.08 \text{ E-6}$	$2.47 \pm 0.13 \text{ E-7}$	$5.42 \pm 0.14 \text{ E-7}$
	EFF-3	2.48 E-6	1.36 E-6	2.52 E-7	5.37 E-7
	EFF-2	2.51 E-6	1.42 E-6	2.52 E-7	5.31 E-7
	FENDL-1	2.37 E-6	1.30 E-6	2.57 E-7	5.37 E-7
	JENDL-FF	2.46 E-6	1.27 E-6	2.40 E-7	5.42 E-7
Position B	Experiment	$8.78 \pm 0.89 \text{ E-9}$	$2.37 \pm 0.13 \text{ E-9}$	$2.69 \pm 0.14 \text{ E-10}$	$5.79 \pm 0.15 \text{ E-10}$
	EFF-3	6.41 E-9	1.99 E-9	2.88 E-10	5.04 E-10
	EFF-2	6.50 E-9	2.04 E-9	2.88 E-10	5.04 E-10
	FENDL-1	5.97 E-9	1.82 E-9	2.66 E-10	4.69 E-10
	JENDL-FF	6.41 E-9	1.85 E-9	2.61 E-10	4.81 E-10

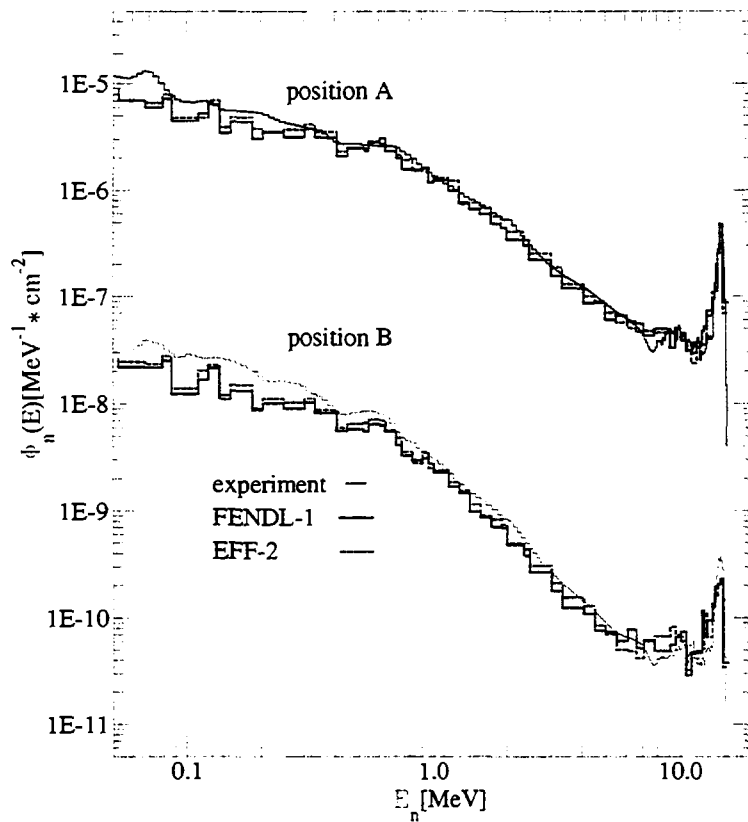


Fig. 2. Measured and calculated neutron flux spectra inside the ITER shield mock-up in position A and position B.

Larger discrepancies are observed for position B deeper inside the bulk, where the measured neutron flux is generally underestimated by all calculations with the exception of the energy range between 5 and 10 MeV. Between 0.1 MeV and 1 MeV the experiment is underestimated by 27 %. Differences up to 19% are observed above 10 MeV for FENDL-1 calculations and up to 13% for EFF-2 and EFF-3.

In comparing the calculated and measured photon spectra in position B, good agreement is still found among all calculations with differences between 2 and 11 %, but the experiment is now generally underestimated by all calculations (except for EFF-3), following the same tendency observed in the calculated neutron flux spectra.

4. Summary and conclusions

The measured photon flux spectra inside the ITER shield mock-up are well described for both positions within the 10% level. Larger discrepancies are observed with EFF-3 calculations, where the measured spectra are always overestimated in position A by 15-20% and in position B by 6%. Such a tendency was already found in the analysis of the TUD iron benchmark experiment with the new evaluated EFF-3 iron data file. The problem is currently under investigation.

The measured neutron flux spectrum in position A is well described by all calculations within the 10% level or better, depending on the data file employed. Larger discrepancies are found in position B, where the experiment is generally underestimated, particularly by FENDL-1 calculations. This requires further investigation.

5. References

- [1] P. Batistoni *et al.*, Proc. 19th Symp. on Fusion Technology, Lisbon, 1996, in press.
- [2] J.F. Briesmeister (ed.), Report LA-12625-M, Los Alamos, 1993.
- [3] A. J. Koning, H. Gruppelaar, Report EFF-DOC-426 (1995).
- [4] H. Vonach *et al.*, Physics Data, No.13-7, 1992, and No.13-8, 1996.
- [5] S. Ganesan and P.K. Mc Laughlin, Report IAEA-NDS-128, Vienna, 1994.
- [6] S. Chiba *et al.*, Report JAERI-M 92-027, Tokai-mura, 1992.
- [7] U. Fischer *et al.*, previous contribution in this report.

3 Calculations, Codes and Recommended Procedures

New developments in the calculation of gamma spectra were largely concerned with the modeling of high energy (> 10 MeV) gamma rays. These include an extension of the direct-semidirect (DSD) model to treat unbound final states that was successfully tested on a data set of 34-MeV proton capture. The direct radiative capture model was successfully applied to explain observed capture on ^{12}C and ^{16}O for $E_n < 1$ MeV, with results already included into the Japan Evaluated Nuclear Data Library JENDL-3.2. Of interest are attempts to understand the origin of the imaginary coupling in the semidirect form factor and the phenomenological separation of the DSD from multistep mechanisms. A consistent preequilibrium exciton model that includes spin effects was tested against $(n, x\gamma)$ data and compared with the recommended code GNASH.

Three overviews of codes related to photon production were prepared. An overview of general photon production codes is followed by a summary of preequilibrium codes, and by direct-semidirect (DSD) codes for fast nucleon capture. Afterwards, recommendations are given on a key ingredient of photon production calculations – photon strength functions, followed by recommendations on preequilibrium and DSD calculations.

The present Chapter includes 11 papers to be found in the following pages.

Modeling 14 MeV Neutron Radiative Capture

F.Cvelbar, A.Likar, T. Vidmar and M.Hočevar

*"J.Stefan" Institute and Faculty of Mathematics and Physics,
University of Ljubljana, Slovenia*

Abstract

Integrated cross sections (sum of the transitions to the bound states) for the radiative capture of 14 MeV neutrons, which have been measured rather systematically, are calculated using the two most reasonable models, which have recently been improved: the direct-semidirect (DSD) model and the pre-equilibrium-equilibrium (PEEQ) model. DSD results, obtained without free parameters and taking into account the transitions to the experimentally observed and additional tentatively introduced bound states, agree with the experimental results only for heavier nuclei, while the PEEQ results reproduce the experimental data in the entire mass region only after the introduction of an effective energy for the GDR and a slight adjustment of the cascade transition matrix element. As an example calculations of the γ -ray spectrum from 14 MeV neutron capture on ^{89}Y using the DSD model are presented.

1 Introduction

In 14 MeV neutron radiative capture there are available, besides the experimental activation cross sections σ_{act} (e.g.[1, 2]) also the prompt gamma-ray spectra measured at about 90° relative to the neutron direction, (e.g. [3, 4, 5]) or integrated approximately over 2π , (4π) solid angle [9]. Sum of the parts of these spectra, which belong to the noncascade transitions to the bound states, represent the energy integrated cross section σ_{int} . The activation cross section σ_{act} differs from the integrated one only by the cascade transitions via the unbound region.

Noncascade primary dipole transitions to the bound states (and corresponding sums) are treated within the framework of the original DSD (direct-semidirect) model [10, 11] which has recently been improved by Likar [12] and extended by Dietrich, Chadwick and Kerman [13, 14].

The semiclassical preequilibrium (PE) model [16, 17] competes with the rather accurate semimicroscopic DSD model mostly in the description of the capture process in nuclei far from magic numbers.

In the following both models are presented and calculated results are compared to the experimental σ_{int} data.

2 DSD model

The transition matrix element in the DSD model [10, 11] is the sum of the direct term and the semi-direct one:

$$T_{if} \propto \langle \psi_f | d | \chi^+ \rangle + \frac{\langle \psi_f | D | \chi_d \rangle \langle \chi_d | H_\tau | \chi^+ \rangle}{E - E_R + i\Gamma/2} . \quad (1)$$

The first term describes the direct radiative transition of the projectile to the selected final state. In the two-step semidirect process the incoming nucleon, while scattered inelastically to the same final single particle state, excites a giant dipole resonance collective motion. Its deexcitation yields the capture γ -ray. To reproduce in general the experimental cross sections, the interaction of the incident nucleon and the dipole oscillations of the target nucleus H_τ is taken in the form of a complex function with the real and imaginary strength V_1 and W_1 , respectively [11]. These strengths appear as free parameters in the classical DSD model. Their values used in the computations are often selected rather intuitively.

Recently Likar [12] has reconsidered the source of W_1 and found that due the fact that the more complicated processes than the two step ones are not taken into account in the DSD model, an effective (dressed) direct dipole (multipole) operator $H_{eff}(\tau)$ instead of the classical one has to be used. It seems that in this approach one of the DSD model drawbacks has been removed. Calculations presented here were done using this CDSD (consistent direct-semidirect) model.

The extension of the DSD model to cover also the transitions to unbound states ([13]) is discussed in another contribution by F. Dietrich to this report. An additional model, the so-called pure resonance model (PRM) as a specific case of DSD model has been proposed [18, 19]. This model is also discussed in the same contribution by F. Dietrich.

3 PEEQ model

The primary capture γ - ray emission energy spectrum is given by [16]

$$\frac{d\sigma_\gamma}{d\epsilon_\gamma} = \sigma_R \sum_n \int \tau(n, E') \lambda_\gamma^c(n, E', \epsilon_\gamma) dE' , \quad (2)$$

where σ_R is the nucleon absorption cross section, λ_γ^c is the γ -emission rate from an n -exciton state and $\tau(n, E)$ stands for the total time spent by a nucleus in an n -exciton state. It is obtained from the system of master equations.

In the PEEC model used here [16, 17] all nuclear states are, as is usually the case, treated as continuum ones. Originally equidistant single particle levels with a density of $g = A/13$ were assumed.

4 Discussion

4.1 Experimental σ_{int} data

It is usually assumed that the experimental σ_{int} values cover only primary γ - ray transitions. This is not far from reality if the bombarding energy is much higher than the binding energy of the projectile as, for example, at 14 MeV neutron capture. In this case the dominating primary transitions to the excitation energy region just above the neutron binding energy, enhanced due to the factor E_γ^3 , are well separated from the secondaries belonging to the deexcitation from this energy region to the bound states. If, on the other hand, the energy of the projectile (especially proton) is comparable to its binding energy (*e.g.* 8 MeV), it can happen that after the primary γ -ray transition of the energy of approximately 7 MeV to the unbound region, which does not enter by definition into the σ_{int} , one may observe the secondary transition to the ground state ($E_\gamma = 9$ MeV), which is included in the σ_{int} . The result might be that the low energy slope of the broad peak of the σ_{int} excitation function is erroneously enhanced.

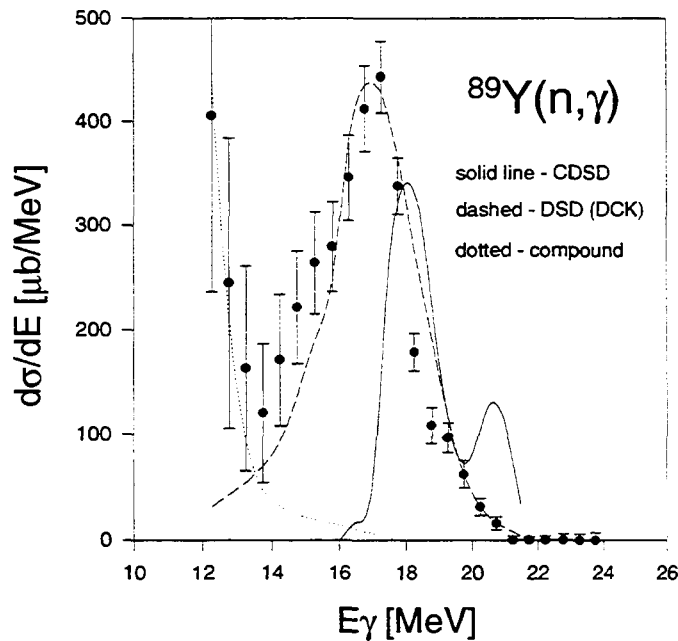


Figure 1: Comparison of the experimental spectrum and DSD model calculations for the reaction $^{89}\text{Y}(n,\gamma)$ at 14 MeV neutron bombarding energy. a) approach of Dietrich, Chadwick and Kerman (EDSD, see the contribution of F. Dietrich to this report), b) CDS approach of Likar *et al.* (see the contribution of A. Likar) in which only the experimentally known levels are taken into account.

4.2 DSD model calculation

In the past the DSD model usually has been used to calculate the radiative transitions to the isolated single particle states known experimentally. Sometimes such calculations were applied to such states generated with a nuclear potential with less adequate results. There has not been an analytical method known to treat transitions to the region of the loosely bound dense states until the very recent solution of Dietrich, Chadwick and Kerman (called extended DSD (EDSD) model [13],[14]), calculating the wave functions of these states by the use of the complex nuclear potential (see Fig.1.). Additional analyses of this type should be carried out.

In the CDSD calculations reported here, there are no free parameters. Even the real strength of the interaction V_1 is fixed at 135 MeV, equal to the values used in other types of nuclear reactions. To study the adequacy of this model, one should calculate radiative transitions to realistic states, *i.e.* to the experimentally identified bound levels with known spectroscopic factors S_i . A physically sound approach is to calculate the wave functions of such states using single-particle potentials with a depth that reproduces the experimental energy value. The final cross section is obtained after the multiplication of the calculated value assuming unit spectroscopic factor with the spectroscopic factor S_i . Thereby the single-particle strength of the state is taken into account.

However, spectroscopic data (E_i, n_i, l_i, j_i, S_i) are usually known only up to an excitation energy E approximately equal to $E \simeq \frac{2}{3}B_0$. For the region $\frac{2}{3}B_0 \leq E \leq B_0$ (let us call it the upper interval) missing single-particle levels (with $S = 1$) were generated using a nuclear potential which (in most cases) reproduces the ground-state binding energy. The spectroscopic sum rule for the levels in the lower energy interval has been, for the present purpose, taken as equal to 1.

In the calculation of the capture cross section both models require the experimental data for the peak energy the width of the GDR and its strength. Sometimes it is sufficient to use the corresponding model data (see e.g. [20]).

The experimental spectrum and results of DSD model calculations for the reaction $^{89}\text{Y}(n, \gamma)$ at 14 MeV neutron bombarding energy based partly on experimentally determined and partly on estimated levels are compared in Fig. 1. The experimental data are taken from Ref. [9]. The DSD calculations shown employ the CDSD model and the EDSD model as described elsewhere in this report. The difference between the two DSD model results and experimental data could be explained (*i.e.*, roughly disappears) if the experimental spectral intensity and EDSD model calculations are shifted by approximately 1 MeV toward lower energies and if some additional states in the roughly treated upper excitation energy interval are missing in the CDSD calculation. Results of the CDSD calculations of σ_{int} are shown in Fig. 2.

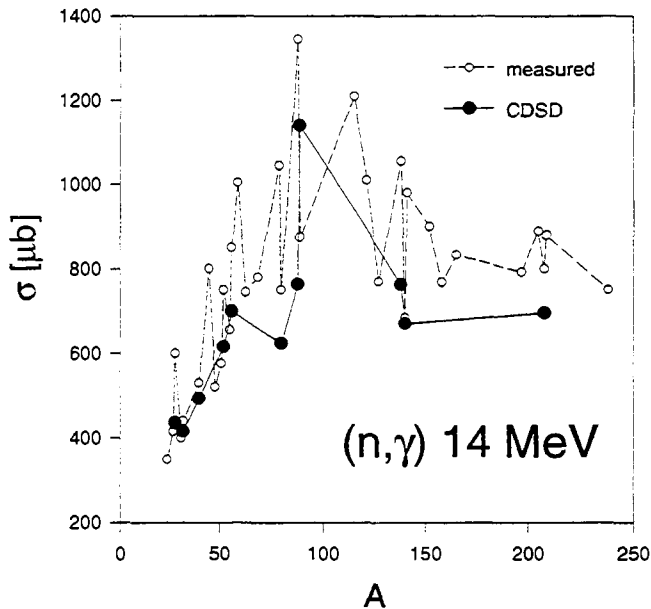


Figure 2: Comparison of the experimental mass dependence of σ_{int} at 14 MeV neutron bombarding energy and CDS model calculations. Experimental data are taken from Refs. [3, 4, 5, 9]. Data from Refs. [6, 7, 8] were not considered due to the fact that the corresponding γ -ray spectra differ essentially from the results of other groups (see also the review of capture spectra above 10 MeV by F. Dietrich in this report).

4.3 PEEQ model calculation

Due to its assumption of independence of the radiative matrix elements on spins, the PEEQ model is too crude to yield spectra comparable to the experimental ones, especially for light nuclei [15]. We therefore concentrated on the computation of the σ_{int} data. To get a better insight into these calculations at 14 MeV neutron energy, we studied separately the σ_{int} excitation functions in *e.g.* the $^{208}\text{Pb}(n, \gamma)^{209}\text{Pb}$ reaction (see Fig.3.). The calculated peak appears at an excitation energy that is about 2 MeV too high in comparison with the experimental one.

From the detailed analysis we get an indication that this effect stems (at least partly) from the fact that the γ -ray spectrum, assumed in the PEEQ model to be continuous, is numerically calculated in bins, *i.e.* discretized. Due to many numerical steps in which the integer values are extracted from the continuous ones, the content of the two highest channels is moved to lower energies.

To eliminate this drawback in the algorithm, we tried to use in the computations the effective GDR energy, equal to E_D reduced by 2 MeV (Fig. 3). In this way the agreement between the experimental σ_{int} excitation function and the one calculated by the PEEQ model is improved considerably.

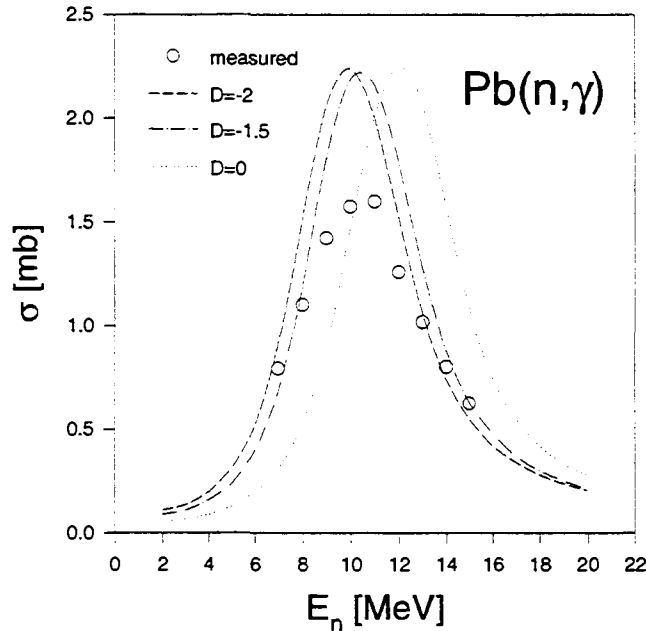


Figure 3: Comparison of the experimental and calculated PEEQ-model excitation functions of σ_{int} for radiative neutron capture in ^{208}Pb , showing the displacement of the PEEQ model peak energy relative to the experimental one. Also the effect of lowering the GDR energy by 2 MeV in these calculations is presented.

As an additional study of the usefulness of the concept of the effective E_D , we analysed the mass dependence of σ_{int} for 14-MeV neutron radiative capture. The agreement of calculated and experimental data is improved significantly by using this approach. Additional improvement is obtained if the mass dependence of the square of the nuclear cascade matrix element, which is usually taken in a form proportional to A^{-3} (see Kalbach [21]), is replaced with a slightly different form proportional to $\frac{125}{A^3}(1 + \frac{A}{150})^{-1}$. The quality of such a fit is shown in Fig. 4. Let us recall that this effective A dependence corresponds to a single particle level density of the form $g = A/13$.

5 Conclusion

As there are no available known spectroscopic data for the whole region of bound states in final nuclei, one cannot expect to reproduce well the prompt primary capture γ -ray spectra by the DSD model used here. New hope in addressing this problem is brought by the extended DSD model [13, 14], but some additional effort is needed to test its predictive power. In this contribution the main effort is therefore concentrated

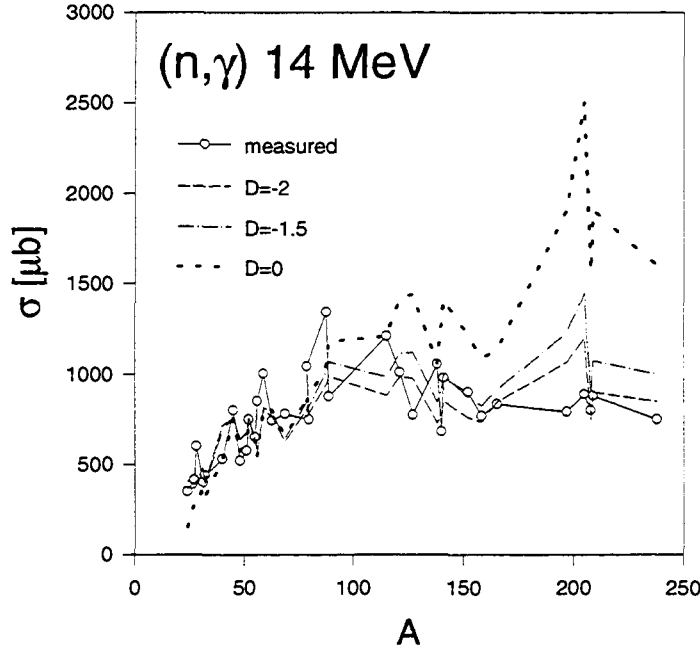


Figure 4: Comparison of the experimental and PEEQ-model mass dependence of σ_{int} at 14MeV neutron bombarding energy, showing the fit obtained by the use of cascade matrix element of the form $\sim \frac{125}{A^3} (1 + \frac{A}{150})^{-1}$ and with the GDR energy lowered by 2 MeV.

on the comparison of the calculated and experimental 14-MeV neutron capture σ_{int} data, which are less sensitive to the details of the levels in question. The result is that values obtained from the consistent DSD model, without any free parameters, agree with the experimental results only for heavier nuclei, while the PEEQ results reproduce the experimental data in the whole mas region only after the introduction of an effective energy for the GDR and somewhat adjusted cascade transition matrix elements. Since the difference between σ_{act} and σ_{int} at 14 MeV neutron energy is within the experimental error, the conclusions are roughly valid also for σ_{act} [15].

References

- [1] J. Kantele, and M. Valkonen, Phys. Lett. **B39**, 625 (1972).
- [2] G. Magnuson, P. Anderson, I. Bergqvist, Lund F6/(NFFR-3032), 1-22, 1979.
- [3] I. Bergqvist, D. M. Drake, and D. K. McDaniels, Nucl. Phys. **A191**,250 (1972).

- [4] I. Bergqvist, B. Pålsson, L. Nilsson, A. Lindholm, D. K. McDaniels, P. Varghese, Nucl. Phys. **A295**, 256 (1978).
- [5] H. Dinter, Nucl. Phys. **A11**, 360 (1968).
- [6] F. Rigaud *et al.*, Nucl. Phys. **A154**, 243 (1970).
- [7] F. Rigaud *et al.*, Nucl. Phys. **A173**, 551 (1971).
- [8] F. Rigaud *et al.*, Nucl. Phys. **A176**, 545 (1971).
- [9] M. Budnar *et al.*, INDC(YUG)-6/L (1977).
- [10] C. L. Clement, A. M. Lane and J. A. Rook, Nucl. Phys. **66**, 273,293 (1965).
- [11] M. Potokar, Phys. Lett. **B46**, 346 (1973).
- [12] A. Likar and T. Vidmar, Nucl. Phys. **A591**, 458 (1996).
- [13] W. E. Parker *et al.*, Phys. Rev. **C52**, 252 (1995).
- [14] F. S. Dietrich, M. B. Chadwick and A. K. Kerman, INDC(NDS)-357 1996.
- [15] F. Cvelbar and E. Běták, Z. Phys. **332**, 163 (1998).
- [16] J. M. Akkermans and H. Gruppelaar, Phys. Lett. **157B**, 95 (1985).
- [17] E. Běták, Report INDC(CSR)-016/LJ, IAEA Vienna 1989.
- [18] F. S. Dietrich and A. K. Kerman, Phys. Rev. Lett. **43**,114 (1979).
- [19] M. Potokar, Phys. Lett. **B92**, 1 (1980).
- [20] J. Speth and A. Van der Woude, Rept. Prog. Phys. **44**, 719 (1981).
- [21] C. Kalbach Z. Phys. **A287**, 319 (1987).

COMPARISON OF DISCRETE GAMMA CALCULATIONS WITH GNASH AND DEGAS

E. Běták

Institute of Physics, Slov. Acad. Sci., 84228 Bratislava, Slovakia

Abstract

A comparison of calculations performed by the code DEGAS, which combines pre-equilibrium plus equilibrium parts within a single formalism, and those performed by GNASH, which combines various approaches to specific parts of the reaction, is given. The main emphasis is put on the production of discrete gammas.

1 Introduction

Two pre-equilibrium codes include pre-equilibrium γ emission and they are able to consider the discrete γ transitions as well, namely GNASH and DEGAS. GNASH [1] combines various approaches to specific parts of the reaction, whereas DEGAS (developed within this CRP) [2] is built on a single formalism, namely that of pre-equilibrium plus equilibrium parts, extended from the very beginning of the reaction until the very late de-excitation stages. Both codes have a many common features, but also a many differences. Both of them belong to the class of sophisticated codes with pre-equilibrium emission and inclusion of discrete states.

2 Common features

The codes GNASH and DEGAS both

- calculate only spectra and cross sections, but not angular distributions;
- both models are assumed to work reasonably up to about 150 or 200 MeV of incident (or excitation) energy;
- include pre-equilibrium emission;
- are able to calculate subsequent emission;
- include discrete states;
- include pre-equilibrium γ emission.

3 Main differences

Apart from many common features listed above, the codes also significantly differ in many aspects. The main differences in the physics are

- GNASH uses different approaches for the pre-equilibrium part (either the exciton model or the FKK approach), whereas DEGAS solves the exciton master equations for all parts of the reaction, thus eliminating any need to "glue" together different approaches;
- pre-equilibrium γ emission in GNASH does not take account of angular momentum coupling; however, angular momentum variables are fully taken into account for equilibrium γ emission (this makes only a very small difference in results for γ emission);
- DEGAS does not consider the parity variable;
- GNASH has (as an option) also the possibility for including direct reactions as a contributing mechanism;

However, there are also other differences, which may be important in detailed analyses of specific reactions, namely

- GNASH has a reasonably wide variety of different types of level densities and γ strength functions;
- as an option, GNASH enables the use of various "charge factors" (which are responsible for proton/neutron composition of the ejectile as an approximate and effective replacement of the two-component formalism), and can also switch among several mechanisms of complex particle formation;

From the point of view of the user, some additional aspects become of interest:

- GNASH includes the mass table as an input, and does not therefore need any specific additional information on binding energies, as DEGAS does;
- DEGAS is capable of handling only a very limited number of discrete states, whereas the capacity of GNASH in this respect is more than currently needed. This difference, however, will disappear rather soon, as the dimensions of DEGAS arrays are to be increased;
- both input and output data (transmission coefficients, energy spectra, etc.) of DEGAS are given in an equidistant energy-spacing scheme. This may not be suitable, if one is interested in low-energy part of the spectrum (neutrons) and in the case of (relatively) high excitations.

Table 1.
Observed (Ref. [3]) and calculated discrete γ lines in $^{27}\text{Al}+n$ at 14.6 MeV

Reaction	Energy (keV)	Transition	Cross section (mb)		
			Exper.	GNASH	DEGAS
$(n, n'\gamma)$	844	844 \rightarrow g.s.	36 ± 6	31	27
	1014	1014 \rightarrow g.s.	72 ± 6	55	62
	1720	2735 \rightarrow 1014	(54, 60)	16	14
	2211	2211 \rightarrow g.s.	176 ± 13	98	24
	≈ 3000	$\approx 3000 \rightarrow$ g.s.	137 ± 12	85	20
$(n, p\gamma)$	985	985 \rightarrow g.s.	32 ± 3	17	32
	1698	1698 \rightarrow g.s.	28 ± 3	23	27

- the running time of GNASH is much shorter than that of DEGAS (typically, by an order of magnitude);
- GNASH incorporates some machine-dependent instructions in subroutines yielding information about the run time, and cannot be straightforwardly run on another computer ¹;
- it is not easy to prepare the input files for GNASH and to understand the output. The input files are significantly larger (and in some places of an unusual data structure, for example in the ordering of transmission coefficients) than they are in the case of DEGAS. The output is a huge file using 132-column lines (and special commands to give new pages etc.). This is somewhat impractical today, when a standard output medium is the computer screen (typically 80 columns) and/or a laser (or jet) printer using the A4/letter-size paper (which under default circumstances, also does not produce the "wide format").

4 Comparison

In order to compare the codes, I consider the proper way to calculate a reaction without application of the specific features offered by GNASH. In other words, a reaction without complex particle channels and without inclusion of the contribution from the direct reaction part.

We have done several calculations of this type. An example is given in Table 1 (taken from [3]).

Although the table is not representative of all cases, we can see some comparison of the predictive power of the codes. More detailed and systematic studies, such as

¹However, these subroutines can be deleted without any harmful consequences.

international code intercomparisons [4, 5], give a more complete picture. Generally the agreement of GNASH with the data is better than that of DEGAS, though there are some (and not extremely rare) exceptions to this rule. Usually, GNASH (with all necessary options included) is one of the codes which are best for reproducing the data (and, of even more importance, to predict the cross section when no data are available).

5 Conclusions

GNASH is to be clearly recommended in practical applications (*i.e.* fitting and evaluation of data and reasonably reliable predictions of the cross sections in region(s) where no data exist or where there is wide scatter in the available data). This is probably the main consideration for a computer code to be used in evaluations and/or predictions. Another typical domain of clear preference of GNASH over DEGAS is for reactions with significant contributions from direct mechanisms, since DEGAS does not envisage such a possibility.

On the other hand, the mere fact that GNASH "glues" together different mechanisms and model approaches used for different stages of a reaction is a potential source of ambiguities. The transition from one mechanism to the other is very well treated in standard situations, but if one is aiming to test new ideas and formalisms, the results obtained by GNASH can be to some extent distorted by the interplay of the new formalism itself and of its gluing to the other parts of the calculation, whereas such new ingredients appear in a clear form if DEGAS is used. Therefore, this is the task where DEGAS is better suited.

References

- [1] P.G. Young, E.D. Arthur, M.B. Chadwick, Report LA-12343-MS (UC-413) (Los Alamos 1992); updated 22 Sept., 1995; M.B. Chadwick, P.G. Young, private communication.
- [2] E. Běták, P. Obložinský, *Code PEGAS*, Report INDC(SLK)-001 (IAEA Vienna 1993) and its later development (unpublished).
- [3] E. Běták, S. Hlaváč, "Production of continuum and discrete gamma rays in (n,x γ) reactions". Progress report on IAEA Research Contract No. 7811/R2/RBF (September 1996).
- [4] M. Blann, H. Gruppelaar, P. Nagel, J. Rodens, "International Code Comparison for Intermediate Energy Nuclear Data" (OECD Paris 1994).

- [5] R. Michel, P. Nagel, "International Codes and Model Intercomparison for Intermediate Energy Activation Yields" Report NSC/DOC(97)-1 = NEA/P& T No. 14 (NEA 1997).

EXTENSIONS OF THE DIRECT-SEMIDIRECT MODEL FOR CALCULATING THE HIGH ENERGY COMPONENT OF FAST- NUCLEON INDUCED GAMMA SPECTRA

FRANK S. DIETRICH

Lawrence Livermore National Laboratory
P. O. Box 808, Livermore, CA 94550, USA

ABSTRACT

This section reviews extensions and variations of the direct-semidirect (DSD) model for understanding the high-energy component of gamma spectra resulting from radiative capture of fast nucleons; i.e., the part of the spectrum that is not amenable to standard statistical model (Hauser-Feshbach) treatments. We describe recent results on the extension of the DSD model to unbound final states, including comparison with proton and neutron capture data. The importance of including convective-current magnetic radiation to explain proton capture angular distributions in the 30 MeV region is shown. We conclude with a brief discussion of a model closely related to the DSD, the pure-resonance model.

1. Introduction

In radiative capture of nucleons above a few MeV incident energy, the most energetic gammas are well understood as arising from direct reaction processes. Since its introduction 30 years ago, the direct-semidirect (DSD) model [1,2] has been the principal theoretical tool for interpreting this component of the gamma spectrum. In this model, direct radiative capture is supplemented by additional coherent amplitudes in which the incident nucleon excites giant resonances that subsequently decay by gamma emission. While both types of amplitudes are required for a full description of the capture process, semidirect excitation of the giant-dipole resonance (GDR) is dominant over a wide energy region about the position of the GDR. In addition to the dominant E1 multipolarity, higher multipolarities (M1, E2, E3) have also been included in DSD calculations.

Until recently, DSD calculations have been limited to capture to bound final states, and consequently only the portion of the gamma spectrum between the incident nucleon energy and the endpoint (approximately 8 MeV higher) has been available to this model. Consequently, the portion of the spectrum above the region where Hauser-Feshbach calculations apply (less than approximately 10-12 MeV) and below the region of bound final states has been calculated only with semiclassical pre-equilibrium models [3], or with multistep compound models that yield conflicting results [4,5]. A recent extension of the DSD model to unbound final states [6] that significantly expands the region of applicability of this model is reviewed in Section 2. This extended model is also applicable

to a portion of the bound final-state region where conventional DSD calculations are of limited usefulness because of fragmentation of the final single-particle orbitals among a dense background of complicated neighboring states.

Magnetic radiation of multipolarity higher than M1 has not previously been incorporated in DSD calculations. In Section 3 calculations are shown for the angular distributions of 34-MeV protons on medium and heavy nuclei that indicate the importance of convective current M2 and M3 radiation in the direct terms.

Difficulties in applying the DSD model to certain transitions in heavy nuclei (particularly neutron and proton capture on ^{208}Pb) led to the development of a closely related model, the pure-resonance model (PRM). This model [7,8], which is an approximation to DSD, was developed in the course of an examination of the consistency of the DSD model. A current view of this model and a recent application of it are presented in Section 4.

2. The Extended DSD Model for Capture to Unstable Final States

The direct-semidirect model has recently been extended to allow calculation of radiative capture to unstable final states [6]. Two types of unstable final states are included: 1) states in which the single-particle configuration following capture are unbound and may therefore decay into the continuum, and 2) single-particle states that are bound, but subsequently damp into the compound nucleus. In both cases, the correct treatment of the compound-nuclear damping is critical for the success of the model. The extended model was tested and shown to be successful by performing an experiment on radiative capture of 19.6-MeV polarized protons on ^{89}Y [6]. More recently, this model has been used to interpret 34-MeV proton-induced gamma spectra and angular distributions [9], as well as spectra from 14-MeV neutron capture [10].

The principal difference between the extended treatment and the standard DSD model is in the handling of the final state. In the standard DSD model, the final state of the captured particle is described by a bound-state wave function, usually obtained by solution of the Schrödinger equation for a Woods-Saxon well. In the extension of the model, all necessary information on the final state is determined by a complex (i.e., optical) potential, which is defined for both unbound and bound final-state single-particle configurations. For unbound final states, the imaginary potential describes damping of the simple single-particle state following capture into the compound nucleus. Similarly, for bound final states, the imaginary potential represents the spreading of the single-particle configuration into a dense spectrum of complicated states in the neighborhood of the final-state energy. The extended model reduces to the standard DSD calculation in the limit of vanishing final-state imaginary potential.

In the extended model for capture to unbound final-state configurations, the double-differential inclusive cross section (i.e., in which only the outgoing gamma is measured) is

$$\frac{d\sigma}{dE_\gamma d\Omega_\gamma} = \sigma_1 + \sigma_2 . \quad (1)$$

in which the first term on the right-hand side is

$$\sigma_1 = -\frac{1}{\phi_{inc}} \frac{2}{\hbar} \left(\frac{1}{\hbar c} \right)^3 E_\gamma^2 \langle \bar{\Psi}_i^{(+)} | H_\gamma G^{(+)} W G^{(+)} H_\gamma | \bar{\Psi}_i^{(+)} \rangle, \quad (2)$$

and the second is

$$\sigma_2 = \frac{1}{\phi_{inc}} \frac{2\pi}{\hbar} \left(\frac{1}{\hbar c} \right)^3 E_\gamma^2 \sum_p \left| \langle \tilde{\chi}_p^{(-)} | H_\gamma | \bar{\Psi}_i^{(+)} \rangle \right|^2 \delta(E - E_p). \quad (3)$$

For bound final-state configurations, the corresponding expression is

$$\frac{d\sigma}{dE_\gamma d\Omega_\gamma} = -\frac{1}{\phi_{inc}} \frac{2}{\hbar} \left(\frac{1}{\hbar c} \right)^3 E_\gamma^2 \text{Im} \langle \bar{\Psi}_i^{(+)} | H_\gamma G^{(+)} H_\gamma | \bar{\Psi}_i^{(+)} \rangle. \quad (4)$$

In these expressions, $\bar{\Psi}_i^{(+)}$ is the energy-averaged incident wave function at energy E_i ; it is the optical-model wave function, plus resonant terms representing coupling to giant resonances that give rise to the semidirect amplitude. E_f and E_γ are the energies of the final nuclear state and gamma ray, respectively, while E is $E_i - E_\gamma$. H_γ is the electromagnetic operator. ϕ_{inc} is the flux of incident particles. $G^{(+)}$ is a Green's function (with appropriate boundary conditions) for the interaction of the captured nucleon with the target via a complex optical potential. W is the imaginary part of the optical potential, defined for both continuum and bound final states, and $\tilde{\chi}_p^{(-)}$ is an optical-model wave function for continuum final states. For the unbound case, Eq. (3) is the straightforward extension of the conventional DSD calculation. The additional term, Eq. (2), represents damping of the final-state configuration following capture, and in fact is the dominant term [6].

Calculations using the extended DSD model are shown in Figs. 1 and 2 and are compared to the results of the $^{89}\text{Y}(p,\gamma)$ experiment with 19.6-MeV polarized protons. Direct E1, E2, and E3 radiation as well as semidirect E1 were included.

Fig. 1 shows the measured 90° differential cross section, together with the extended DSD calculations and with Hauser-Feshbach calculations using the GNASH code [11] of the equilibrium statistical emission using two different prescriptions for the gamma-ray transmission coefficient [12,13]. The peak at 15.11 MeV is due to inelastic scattering on a carbon impurity in the target. The combination of DSD and Hauser-Feshbach calculations reproduces the data reasonably well, and additional multistep reaction mechanisms are not required. The DSD calculations were made with Eqs. (2) and (3) in the unbound region below 19.6 MeV gamma energy, and with Eq. (4) in the bound-state region above that energy. There is no discontinuity between these two regions. The DSD calculations were carried out to only 26 MeV, since the ground-state peak near 28 MeV is more appropriately treated by a conventional DSD calculation. The calculations show a transition between compound and direct processes in the region near 16 MeV.

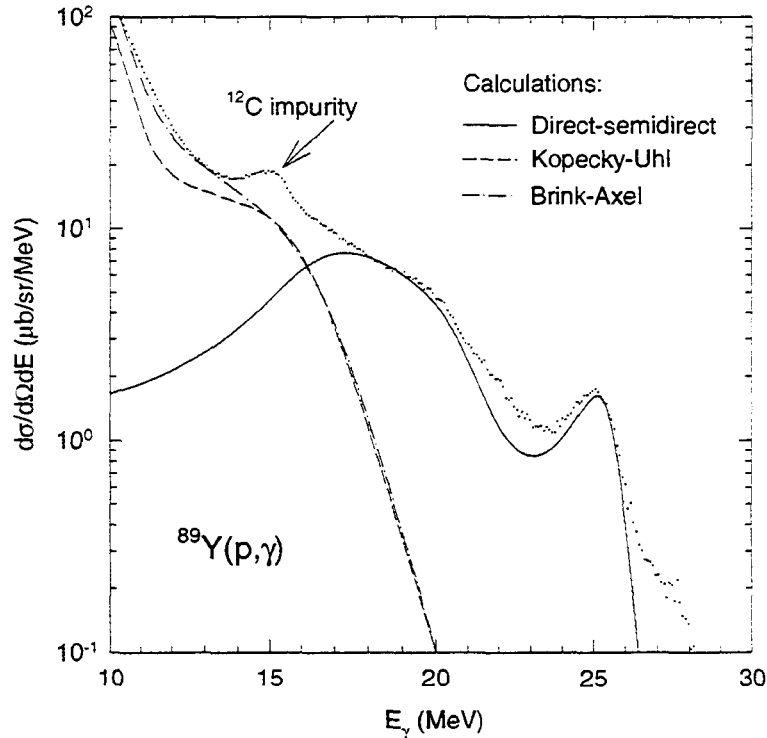


Figure 1. Unpolarized differential cross section at 90° . The data (dots) are shown together with the extended DSD model calculation (solid line), and with Hauser-Feshbach calculations using Kopecky-Uhl (dashed line) and Brink-Axel (dot-dashed line) gamma transmission coefficients. The calculations were folded with experimentally determined lineshapes before presentation with the data.

In Fig. 2 the extended DSD calculations are compared with the measured analyzing powers at the five angles for which data were taken. The data are well reproduced by the calculations, including the reversal in the sign of the asymmetries between the forward and backward hemispheres.

The calculations shown in Figs. 1 and 2 suggest that multistep contributions may not be important at energies up to approximately 20 MeV. To further investigate this issue, the model has been applied to gamma-production data [9] taken with 34 MeV protons on targets of Cu, Ag, and Au. Fig. 3 shows the spectrum at 75° for the Cu target. The parameters and calculational details were very similar to those in the $^{89}\text{Y}(p,\gamma)$ case with appropriate variations taking into account the incident and final state energies as well as the target Z and A. However, the calculations have not been smeared with the experimental lineshapes, which should make little difference since the part of the spectrum of interest varies rather slowly with energy. The falloff in the spectrum below 10 MeV is due to an electronic cutoff. No further adjustment was made except for the final state well depth which was chosen to match known single-particle energies. In addition to direct E1.

E2, and E3 radiation as well as E1 semidirect, we have included convective-current direct M1 and M2. The importance of the magnetic radiation is shown in the next section.

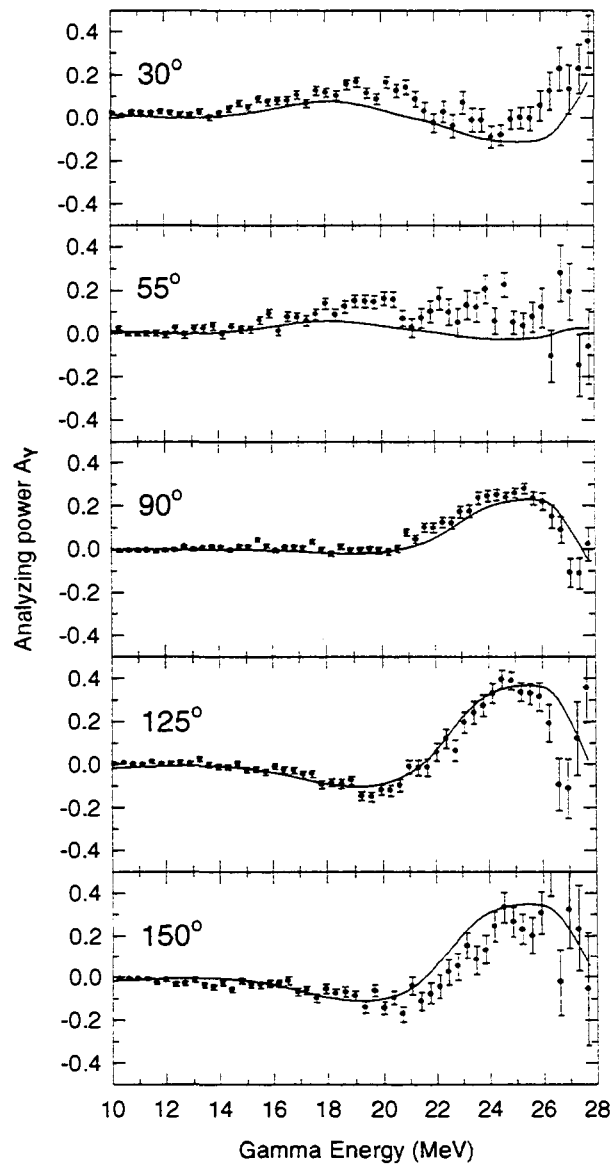


Figure 2. Measured analyzing powers compared with the extended DSD calculations. The calculations have been folded with the experimentally-determined lineshapes.

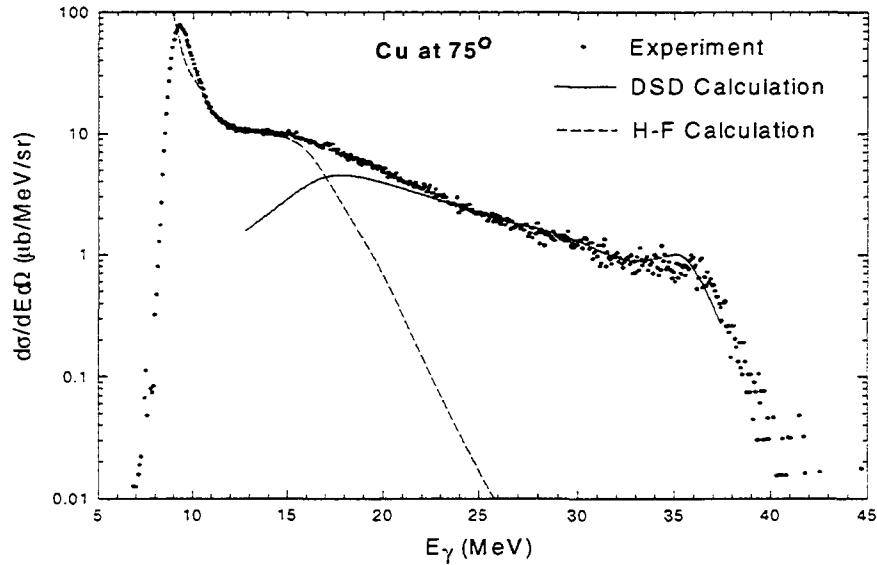


Figure 3. Spectrum of gammas at 75° from 34-MeV proton bombardment of Cu compared with extended DSD and Hauser-Feshbach calculations.

As was the case for $^{89}\text{Y}(p,\gamma)$ at 19.6 MeV, there is no apparent need for additional mechanisms to explain the spectrum. The results for Ag are of similar quality. The DSD calculation for Au lies below the data by about a factor of 2, which is likely due to the fact that no attempt was made to optimize the parameters for the higher mass region.

Additional tests have been performed for neutron capture near 14 MeV. The results for 14-MeV neutron capture on ^{89}Y , compared with the data of Budnar *et al.* [10], are shown in Fig. 4, together with a Hauser-Feshbach calculation. Parameters were similar to those for 19.6-MeV $^{89}\text{Y}(p,\gamma)$. The solid line is the DSD calculation, while the dashed line is the same calculation smeared by the experimental resolution. The combination of the smeared DSD and Hauser-Feshbach calculations is in excellent agreement with the experiment. In particular, the dip near 14 MeV gamma energy is reproduced. However, the experimental data of Rigaud *et al.* [14] are very different in magnitude and shape; there is neither a peak near 17 MeV nor a dip near 14 MeV. The disagreement between experimental data sets severely hampers tests of capture models at 14 MeV. These disagreements are discussed in Section B.3.2.2 of this report, together with an illustration of the differences between Refs. [10] and [14] for capture on ^{89}Y .

3. Effect of Higher Magnetic Multipolarities on Angular Distributions

Apart from occasional attempts to include M1 radiation, magnetic multipolarities have been ignored in DSD calculations. Although direct radiation higher than dipole of both magnetic and electric multipolarities is suppressed by effective charge factors for neutron

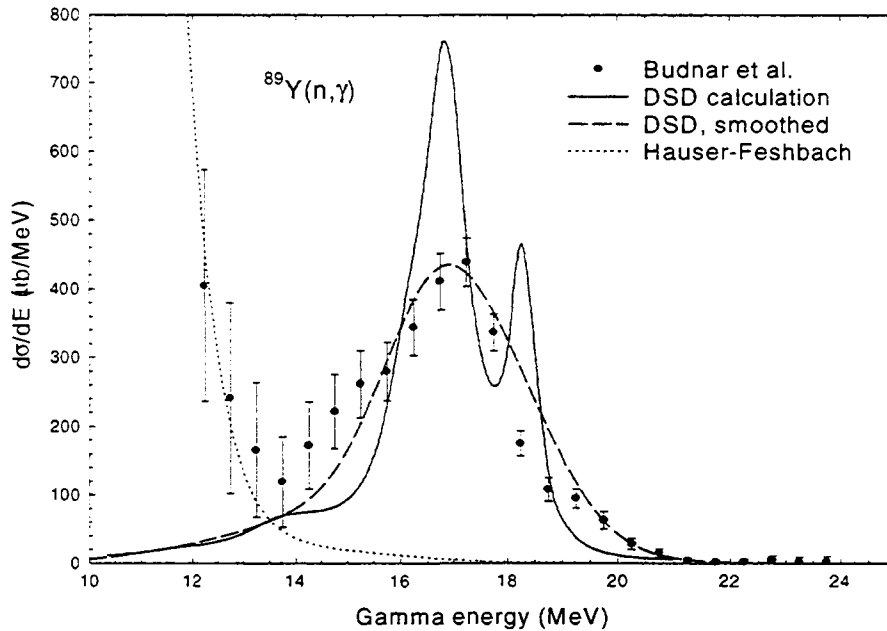


Figure 4. Comparison of extended DSD and Hauser-Feshbach calculations with the data of Ref. [10] for 14-MeV neutron capture on ^{89}Y . The calculations are shown both smeared by the experimental resolution and unsmeared. See text for a discussion of inconsistencies between experimental data sets for this reaction.

capture, this is not the case for capture of charged particles. Analysis of the 34-MeV proton capture data of Ref. [9] using the extended DSD model required investigation of this question. Convective current M1 through M4 direct capture amplitudes were incorporated in the code used to analyze these data. The spin current contributions were not included, since the convective currents are expected to be dominant because of the large orbital angular momenta (up to 8 or 10) required at these high energies.

Fig. 5 shows calculations that demonstrate the importance of the higher magnetic radiations on angular distributions in proton capture. The calculations are for 30.8 MeV gamma rays from capture on Au at 34 MeV proton energy. The curve labeled "E only" includes direct E1, E2, and E3 radiation as well as semidirect E1. The remaining curves show the effect of adding the magnetic radiations of orders M1 through M3. The calculations show that magnetic radiations are very important at forward and backward angles. While the magnetic radiations have a significant effect on the angular distributions, their effect on the angle-integrated cross sections is small. In the present case it appears that including M1 and M2 is sufficient. At still higher energies additional multipoles, both electric and magnetic, should be required.

In Fig. 6 angular distributions calculated with the extended DSD model are compared with the 34-MeV proton capture data of Ref. [9]. Both calculations and experimental data have been integrated over a gamma-ray energy interval of 25 to 33 MeV.

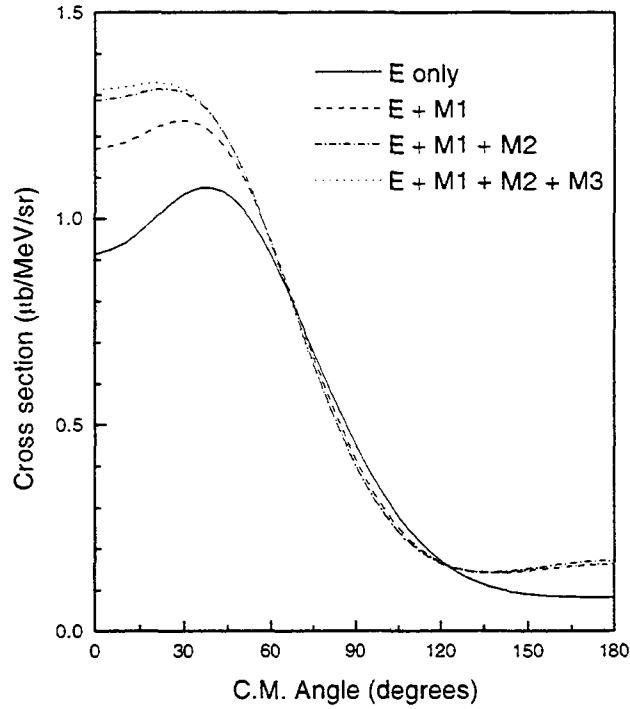


Figure 5. Angular distributions calculated with the extended DSD model for $^{197}\text{Au}(p,\gamma)$ at an incident energy of 34 MeV and a gamma energy of 30.8 MeV. The calculation labeled "E only" includes direct E1 through E3 and semidirect E1. The remaining curves show the effect of adding additional direct convective-current magnetic radiation.

4. The Pure-Resonance Model

The pure-resonance model (PRM) was developed to address questions of consistency between the two terms in the direct-semidirect model [7,8]. It was based on the two observations that 1) in the photoejection reaction (which is inverse to radiative capture) experimental data show symmetric resonant peaks without an obvious nonresonant contribution; and that 2) the direct amplitude in DSD contains a giant-resonance contribution, since the incident optical-model wave function is not orthogonal to the giant resonance.

The PRM results from reformulating the capture model so that the continuum wave function appearing in its matrix elements no longer contains giant-resonance components. This is accomplished by using projection operator techniques as developed for the photonuclear problem by Wang and Shakin [15]. Using these techniques, the direct-semidirect amplitude

$$c_1 + \frac{c_2}{E_\gamma - E_{GDR} + \frac{1}{2}i\Gamma_{GDR}} \quad (5)$$

may be formally rearranged (neglecting an unimportant small term) as

$$\frac{c_3 - c_4}{E_\gamma - E_{SP} + \frac{1}{2}i\Gamma_{SP}} + \frac{c_5}{E_\gamma - E_{GDR} + \frac{1}{2}i\Gamma_{GDR}}$$

(6) in which c_1 through c_5 are matrix elements calculated with ordinary optical wave functions in the DSD case (Eq. (5)), or projected wave functions for the PRM (Eq. (6)). E_{SP} and Γ_{SP} are the position and width of a single-particle resonance in the entrance channel, and are computed from the optical potential. The single particle resonance lies in the region of approximately 8 to 10 MeV. E_{GDR} and Γ_{GDR} are the position and width of the giant dipole resonance.

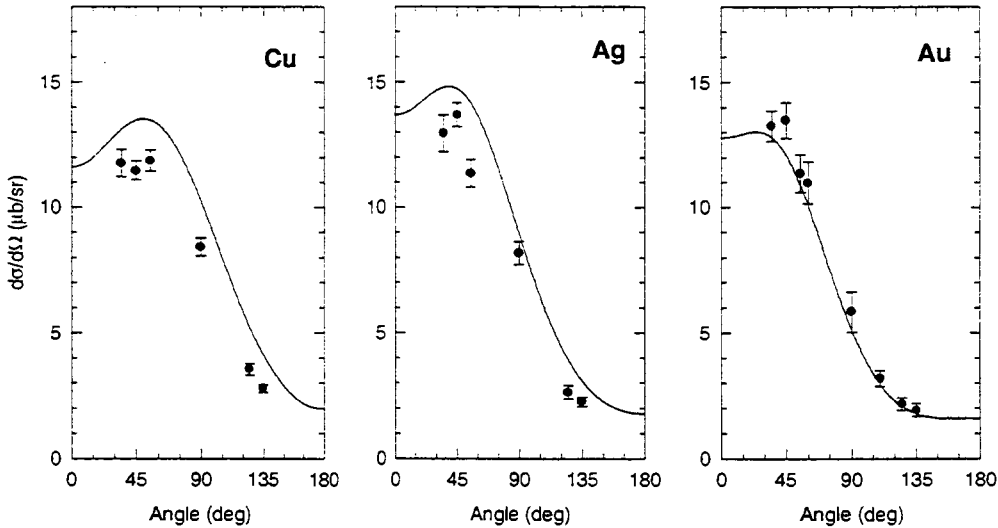


Figure 6. Extended DSD calculations and experimental data for angular distributions of 25 to 33 MeV gammas from 34-MeV proton capture on Cu, Ag, and Au.

In Eq. (6), c_3 and c_4 are both large and nearly cancel. Thus, a potential instability that is implicit in the DSD model is exhibited explicitly in the PRM formulation. In the pure-resonance model this instability is eliminated by assuming that this cancellation is exact, leaving only the giant resonance term.

A recent experiment [16] on the $^{40}\text{Ca}(n,\gamma_0)$ reaction, which was performed to search for the isovector quadrupole giant resonance, shows the usefulness of the PRM. Fig. 7 shows the data for this reaction, together with two calculations that included E1 and E2 radiation. The right-hand panel shows the 90° differential cross section, while the left-hand shows the fore-aft asymmetry $A(55^\circ)$, defined as $[\sigma(55^\circ) - \sigma(125^\circ)] / [\sigma(55^\circ) + \sigma(125^\circ)]$, where σ is the differential cross section. The solid curves used DSD for both E1 and E2, whereas the dashed curves were calculated using PRM for E1 and DSD for E2.

In the case shown in Fig. 7, it is apparent that the PRM yields a better reproduction of the experiment than the DSD. However, it should be noted that the approximation of neglecting the first term in Eq. (6) may be extreme, and that this approximation may not

be necessary if the consistency between the direct and semidirect terms in the DSD model is better understood than at present. Further work should be done in this direction.

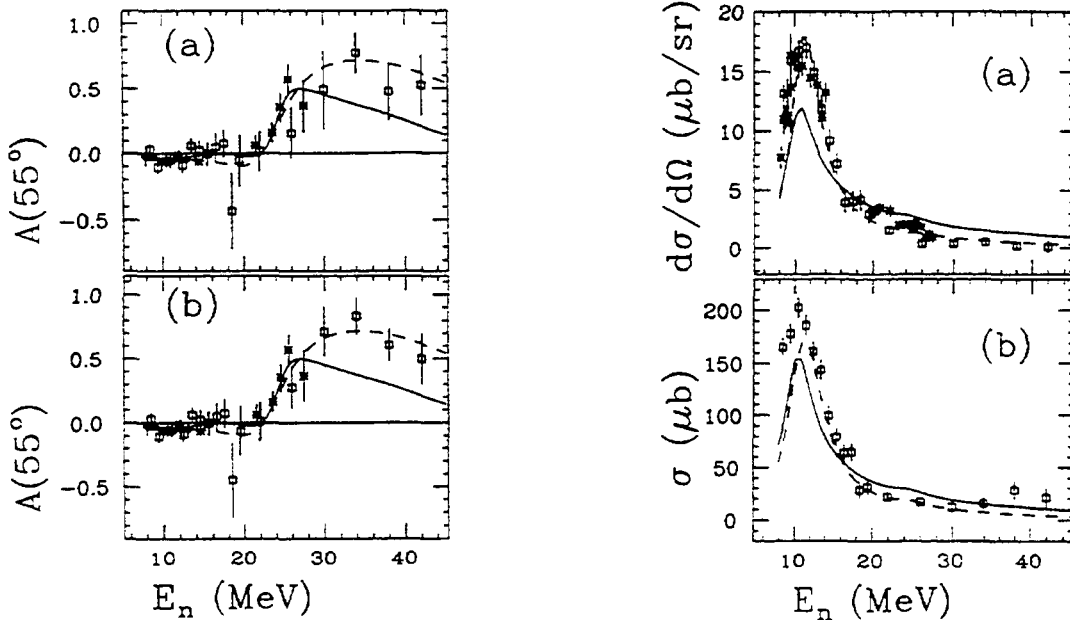


Figure 7. Fore-aft asymmetry (left panel) and 90° differential cross section (right panel) in the $^{40}\text{Ca}(n,\gamma)$ reaction [16]. Calculations were made with DSD for E1 and E2 amplitudes (solid curves), and with PRM for E1 and DSD for E2 (dashed curves).

5. Acknowledgments

The calculations in this section were performed in collaboration with Dr. Mark Chadwick (Los Alamos National Laboratory) and Prof. Arthur Kerman (Massachusetts Institute of Technology). Dr. S. John Luke (Lawrence Livermore National Laboratory) supplied the data on 34-MeV proton capture. This work was performed by Lawrence Livermore National Laboratory under U.S.D.O.E. Contract No. W-7405-Eng-48.

6. References

1. G. E. Brown, Nucl. Phys. **57**, 339 (1964).
2. C. F. Clement, A. M. Lane, and J. R. Rook. Nucl. Phys. **66**, 273,293 (1965).
3. E. Betak, contributions to this report and references therein.
4. P. Oblozinsky and M. Chadwick, Phys. Rev. **C42**, 1652 (1990).
5. M. Herman, A. Höring, and G. Reffo, Phys. Rev. **C46**, 2493 (1992).
6. W. E. Parker *et al.*, Phys. Rev. **C52**, 252 (1995).

7. F. S. Dietrich and A. K. Kerman, Phys. Rev. Lett. **43**, 114 (1979).
8. F. S. Dietrich, in AIP Conference Proceedings No. 125, Capture Gamma-Ray Spectroscopy, Knoxville, TN, 1984, p. 445.
9. S. J. Luke, Ph.D. thesis, University of Washington, 1992 (unpublished).
10. M. Budnar *et al.*, IAEA report INDC(YUG)-6 (1979).
11. P. G. Young, E. D. Arthur, and M. B. Chadwick, Los Alamos National Laboratory Report LA-12343-MS (1992).
12. D. M. Brink, Ph. D. thesis, Oxford University (1955); P. Axel, Phys. Rev. **126**, 671 (1962).
13. J. Kopecky and M. Uhl, Phys. Rev. **C41**, 1941 (1990).
14. F. Rigaud *et al.*, Nucl. Phys. **A154**, 243 (1970).
15. W. L. Wang and C. M. Shakin, Phys. Rev. **C5**, 1898 (1972).
16. C. M. Laymon, R. O. Nelson, S. A. Wender, and L. R. Nilsson, Phys. Rev. **C46**, 1880 (1992).

Mass Dependence of the Complex Coupling in the DSD Model Generated by the Consistency Requirement

A. Likar and T. Vidmar

*J. Stefan Institute and Department of Physics
University of Ljubljana, Ljubljana, Slovenia*

Abstract

The complex form factor in the DSD model is determined in terms of consistency requirements for the dipole operator. It is shown that in the region of the giant dipole resonance the form factors can be in most cases parametrised as a real volume term with strength V_1 and an imaginary surface-peaked term with strength W_1 , as suggested previously. The mass dependence of the parameters V_1 and W_1 is extracted for the $^{208}\text{Pb}(n, \gamma)$, $^{89}\text{Y}(n, \gamma)$ and $^{40}\text{Ca}(n, \gamma)$ reactions where the neutron is captured to the ground state and several well resolved excited states. The mass dependence of the imaginary parameter W_1 is compared with the one obtained from the analysis of the integrated spectra.

1 Introduction

The direct-semidirect (DSD) model for nucleon radiative capture reproduces well the cross sections and angular distributions for nuclei in a wide mass region if the complex coupling between nucleon and giant multipole resonance motion is introduced. The imaginary part of the coupling is strongly mass dependent, being small for nuclei with low mass numbers, and surprisingly high for lead. It has been shown [1] that a part of the Hilbert space, which is eliminated from the formalism, requires imaginary coupling. A procedure to calculate the coupling has been suggested as well. It is based on difference between potentials generating the initial and final wave functions. In this work we confront the complex coupling of the old DSD model deduced from the experiments and the one obtained by the new approach. It is shown that the shapes of the couplings agree rather well. The corresponding parameters V_1 and W_1 depend on mass of the target nucleus as well as on the spin of the state to which the nucleon is captured.

2 Theory

The starting point for the discussion is the formal result for the transition matrix for radiative capture:

$$T = \langle 0 | \mathcal{H}_\gamma P | \Psi^+ \rangle + \langle 0 | \frac{1}{E - E_R + i \frac{\Gamma_R}{2}} \mathcal{H}' P | \Psi^+ \rangle \quad (1)$$

The $|0\rangle$ is the state of the captured nucleon in one of the unoccupied orbits of the target nucleus. The state $P|\Psi^+\rangle$ is approximated by the optical model state of the nucleon plus the target nucleus.

The transition amplitude in the DSD model has two terms. The first one is responsible for the direct radiative multipole transition of the incoming nucleon to a bound state of the target nucleus. The nucleus in this process acts only as a potential well for the nucleon. The second term describes the excitation of the target nucleus by the incoming nucleon to the giant dipole resonance state (GDR) with energy E_R and width Γ_R and a subsequent radiative de-excitation of the excited nucleus.

In [1] the consistent version of the DSD [2] model (CDSD) was introduced. The complex form factor [3] of the original DSD model is interpreted as a remedy for violation of the continuity equation when the optical model states are used.

The effective multipole operator \mathcal{H}_γ and effective form factor \mathcal{H}' arise as a consequence of explicit elimination of complicated states $Q|\Psi^+\rangle$ from the formalism.

We parametrise the effective interaction as

$$\mathcal{H}_\gamma = H_\gamma(1 + F(r)), \quad (2)$$

r being the relative coordinate of the incoming nucleon. The complex function $F(r)$ is determined by requiring that the continuity equation relating the matrix elements of the projectile current and density operators is preserved:

$$\nabla \mathbf{j} = -\frac{\partial \rho}{\partial t}. \quad (3)$$

In the case where the initial- and final-state Hamiltonians are identical eq. (3) holds automatically. The Siegert theorem is based on this observation. The function $F(r)$ is therefore determined from a differential equation which ensures that either form of the electromagnetic interaction, namely, $\mathbf{j} \cdot \nabla \epsilon r$ and $i \frac{E_\gamma}{\hbar} \epsilon r$, yield the same transition matrix. Here ϵ is the polarisation vector of the emitted radiation.

The differential equation for $F(r)$ can be found in [1]. The difference $\Delta V = V_{opt} - V_{nlj}^*$ of the potentials for the initial (V_{opt}) and the final captured state (V_{nlj}^*) is the generator of the $F(r)$. The regular solution of the equation is used which ensures that $F(r)$ vanishes when the difference ΔV is zero.

The procedure can be generalised to include any specific shape $\varphi(r)Y_{l,m}^*(\hat{r})$ of the form factor \mathcal{H}' . The function $\varphi(r)F_{SD}(r)$ can be obtained if we require that $\mathbf{j} \cdot \nabla(\varphi(r)Y_{l,m}^*(\hat{r}))$ and $i \frac{E_\gamma}{\hbar} \varphi(r)Y_{l,m}^*(\hat{r})$ yield the same matrix elements. It can be shown

that the functions $rF(r)$ and $\varphi(r)F_{SD}(r)$ are similar when the function $\varphi(r)$ is similar to the function r in the interval where the ΔV is concentrated. This justifies our simplified approach to the effective form factor \mathcal{H}' where we set

$$\mathcal{H}' = H'(1 + F(r))^2$$

using the free form factor of the volume shape [5, 6]:

$$H' = -\tau_{03} \frac{2NZ}{A^2} f^{sum} \frac{\hbar^2}{2mE_R} \frac{V_1}{4} \left(\frac{5}{R^2} r f(r) \right) Y_{1\mu}^*(\mathbf{r}) = -\tau_{03} \frac{2NZ}{A^2} f^{sum} \frac{\hbar^2}{2mE_R} \frac{5}{R^2} h(r) Y_{1\mu}^*(\mathbf{r}) \quad (4)$$

with the range of Fermi function $f(r)$ extended by 20% beyond the original radius. The f^{sum} is determined from the experimental value for the energy weighted photo-absorption cross section σ_{-1} from:

$$\sigma_{-1} = 4\pi^2 \alpha f^{sum} \frac{\hbar^2}{2mE_R} \frac{NZ}{A} \approx f^{sum} 6 \frac{NZ}{AE_R} \text{fm}^2, \quad (5)$$

where E_R is the energy of the dipole resonance (GDR) in MeV. The value of the parameter V_1 is taken to be 135 MeV independent of the mass of the target nucleus. It was also found that the surface shaped form factor

$$H' = -\tau_{03} \frac{2NZ}{A^2} f^{sum} \frac{\hbar^2}{2mE_R} \frac{V_1}{4} \left(-\frac{df(r)}{dr} \right) Y_{1\mu}^*(\hat{\mathbf{r}}) \quad (6)$$

with a proper function $F_{SD}(r)$ reproduced the experimental data well. The model favours the use of the optical model sets proposed by Rosen et al. [7] and recently by Olsson *et al.* [8] and Varner *et al.* [9] referred to as the compilation CH89. The predictive power of the modified model is significantly improved regarding the excitation functions for the capture to individual states of the final nucleus, angular distributions and integrated cross sections.

3 Results

It is of interest to find a connection between the old DSD model with the complex interaction and the new one. Since the function $F(r)$ depends on the photon energy E_γ , the bound state to which the nucleon is captured, and even on the partial wave quantum numbers of the incoming neutron, such a connection can only be done in an approximate way. We have chosen the energy of the incoming neutron to be 10 MeV which for all cases considered maximally excites the GDR. Only transitions to the ground state and in some cases to low lying excited states were considered.

Fig. 1 shows the situation for neutron capture to the ground state of ^{209}Pb . The form factor of the new model (CDS) has been expanded by the usual form factors, $rf(r)$ for the real part and $-4ar \frac{df}{dr}$ for the complex one, as used by the DSD model:

$$h(r) = r \left(\frac{V_1}{4} f(r) - i \frac{W_1}{4} 4a \frac{df(r)}{dr} \right).$$

The equivalent parameters V_1 and W_1 are thus obtained which can be used in the DSD model. The parameters of the Fermi function $f(r)$, radius R , and diffuseness a , are the same as for the optical model employed, in our case the set of Rosen *et al.* [7]. The shapes of the CDSO form factors agree well with the old ones. Exceptions were observed only for transitions between the states with the same values of the total angular momentum j which are strongly hindered due to angular momentum algebra.

Nucleus	state	V_1^+	V_1^0	V_1^-	W_1^+	W_1^0	W_1^-
		[MeV]	[MeV]	[MeV]	[MeV]	[MeV]	[MeV]
^{209}Pb	$2g_{9/2}$	111.6	76.1	108.4	104.7	164.3	112.3
	$1i_{11/2}$	146.2	152.8	148.4	144.9	90.8	132.7
	$1j_{15/2}$	80.0	-99.0	75.0	97.1	46.7	103.2
^{141}Ce	$4s_{1/2}$	91.7	83.1		111.2	124.0	
	$2f_{7/2}$	85.6	56.2	81.4	78.1	104.1	83.0
	$3p_{3/2}$	64.9	50.1	59.8	69.8	78.5	73.2
	$1i_{13/2}$	46.6	-35.8	41.0	61.3	-1.3	63.2
^{90}Y	$1h_{9/2}$	108.0	122.2	112.2	111.3	75.5	102.5
	$2d_{5/2}$	74.1	49.3	68.9	63.5	77.4	67.2
^{40}Ca	$1f_{7/2}$	52.9	-0.3	45.1	43.3	40.2	45.1

Table 1: The extracted equivalent parameters V_1 and W_1 for different nuclei and capturing states. V_1^+ refers to the values for the transitions $j_i \rightarrow j_f + 1$, V_1^0 to the transitions $j_i \rightarrow j_f$ and V_1^- to the transitions $j_i \rightarrow j_f - 1$, where j_f refers to the angular momentum number j of the final bound state and j_i to the continuum state. The same holds for W_1 .

Table 1 gives the values of the equivalent parameters V_1 and W_1 for different target nuclei and capturing states. Fig. 2 shows the A -dependence of the parameters for transitions considered excluding the $j \rightarrow j$ transitions. Although the variation of parameters for different capturing states is not negligible, the curve proportional to $A^{1/3}$, as suggested in [1], can be drawn through the points. The trend for the imaginary interaction has been noted previously [10] based on the analysis of the measured excitation functions. The real part of the potential has been fixed in that work to $V_1 = 70$ MeV.

References

- [1] A. Likar and T. Vidmar, Nucl. Phys. **A591** (1995) 458, **A593** (1995) 69, **A615** (1997) 18.
- [2] G. E. Brown, Nucl. Phys. **57** (1964) 339.

- [3] M. Potokar, Phys. Lett. **46B** (1973) 346.
- [4] W. L. Wang and C. M. Shakin, Phys. Rev. **C5** (1972) 1898.
- [5] C. F. Clement, S. M. Perez, Nucl. Phys. **A165** (1971) 569.
- [6] G. Longo, S. Saporetti, Phys. Lett. **42B**.
- [7] L. Rosen, J. G. Beery, A. M. Goldhaber, E. M. Auerbach, Ann. of Phys. **34** (1965) 96.
- [8] N. Olsson, B. Trostell, E. Ramström, B. Holmqvist, F. S. Dietrich, Nucl. Phys. **A472** (1987) 237.
- [9] R. L. Varner, W. J. Thompson, T. L. McAbee, E. J. Ludwig and T. B. Clegg, Phys. Rep. **201** (1991) 57.
- [10] F. Cvelbar, R. Martinčič and A. Likar, Atomkernenergie-Kerntechnik **45** (1984) 179.

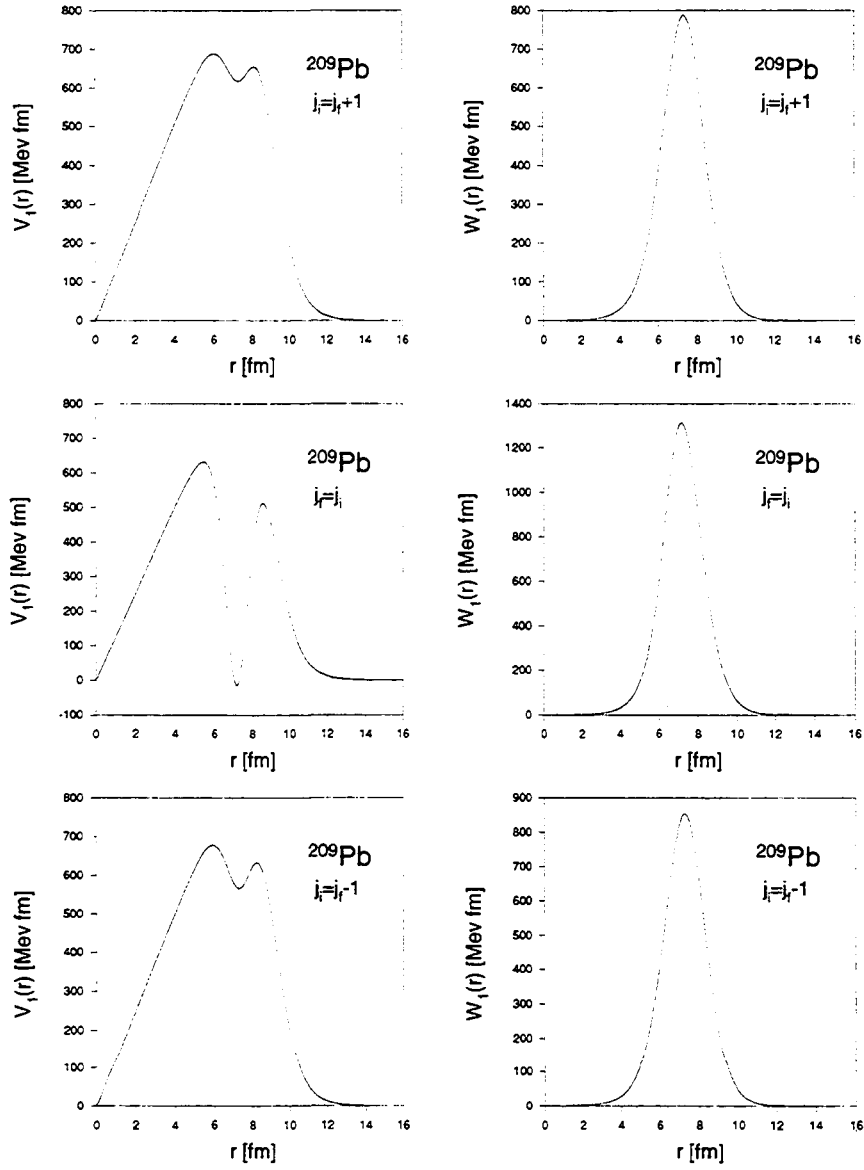


Figure 1: Comparison of CSDS (solid lines) and equivalent DSD (dashed lines) real and imaginary form factors for indicated transitions to the ground $2g_{9/2}$ state in ^{209}Pb . The parameters of the DSD form factors are from the optical model parameters of Rosen et al. [7]. The incident neutron energy was 10 MeV.

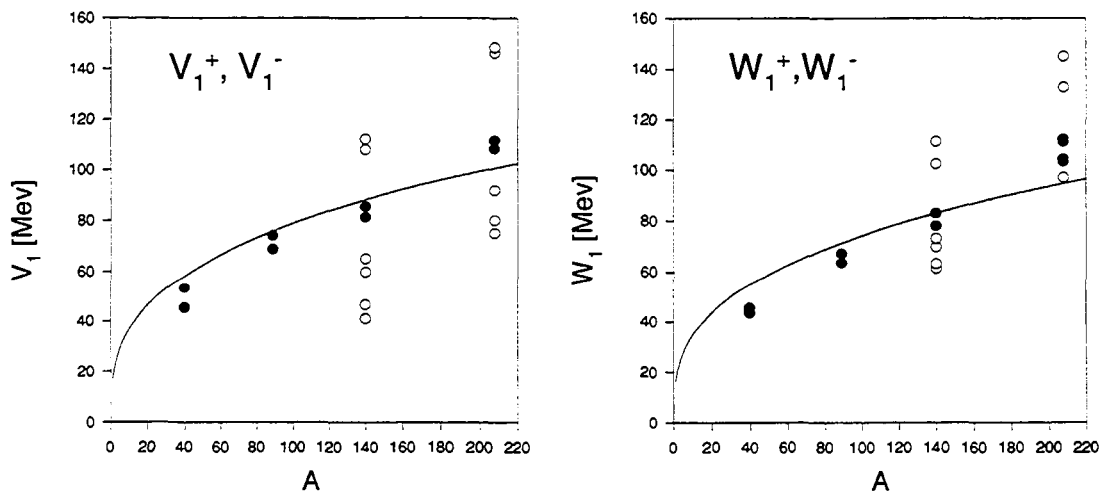


Figure 2: A-dependence of the equivalent parameters V_1 and W_1 from this analysis. All single particle states considered has been taken into account. The solid lines are the fits through the values for the ground state transitions (full circles) for the curve proportional to $A^{1/3}$.

Calculation of Photon Production in Light Nuclei

A. Mengoni*

*ENEA, Applied Physics Division,
via Don Fiammelli 2, 40129 Bologna, Italy
and*

*RIKEN, Radiation Laboratory,
2-1 Hirosawa, Wako, Saitama 351-02, Japan*

1 General considerations

Neutron capture and γ -ray production cross section calculations for light nuclei suffer from the intrinsic disadvantage of dealing with systems where statistical methods cannot be applied. In fact, unlike the case of medium-mass and heavy nuclei where in consequence of the high level density at excitation energies of the order of 5 ~ 8 MeV statistical theories (Hauser-Feshbach) can be utilized, individual resonance (not always compound!) states and the “background” direct capture process play distinct and in some case antagonistic roles in light nuclei. Physical properties of narrow, isolated resonances cannot usually be derived from theoretical methods and the resonance parameters can only be determined with the support of experimental information.

The traditional method applied in the calculation of neutron capture cross section in this situation is the direct radiative capture model of Lane and Lynn[1] occasionally coupled to the simple single-level Breit-Wigner formalism.

Recent experimental results on capture reactions in light nuclei for neutron energies ranging from thermal up to several hundred of KeV have been obtained by the groups at Karlsruhe Forschungszentrum, the Tokyo Institute of Technology, the Oak Ridge National Laboratory (ORELA facility) and the European Center for Reference Material Measurements in Geel. It is worth noting here that these four are the only remaining active facilities at least partially devoted to neutron induced reactions measurements in the range of interest for the nuclear data community.

*e-mail: mengoni@bologna.enea.it

Recently, the great progress made in producing and accelerating radioactive nuclear beams (RIBs) has made it possible to revisit the subject. In fact, it has been shown that nuclear dissociation experiments (in particular the Coulomb dissociation process) can be used to obtain the electromagnetic transition matrix elements necessary to calculate neutron capture cross sections and γ -ray production probabilities. These new developments are to be considered of extreme importance for exploring nuclear structure and reaction mechanisms in light nuclei, in particular radioactive and/or less-abundant light isotopes. We would like to mention here that in addition to the traditional applications of nuclear data in fission and fusion devices, the construction and operation of RIBs facilities requires a large amount of nuclear data for unstable nuclei and therefore nuclear data related activities are considered of high importance to this end. Finally, we would like to mention here the importance of γ -ray production data for application to basic science fields such as exotic nuclear structure properties of nuclei far from stability and nuclear astrophysics.

2 Capture Models

A particular neutron capture process, the direct radiative capture (DRC) process, has been recently investigated in connection with the observation that p -wave induced neutron capture may dominate the reaction mechanism for light nuclei in the energy region up to several hundred of KeV [2-6]. Here, the compound nucleus formation probability is hindered by the low level density around the neutron binding energy. The only way a nucleus can capture a neutron is through a direct γ -ray emitting transition leading to one of the bound orbits of the residual nucleus. Since the low-multipolarity E1 radiation is much favored in these low energy transitions, the bound orbits which can be reached by incident p -wave neutrons are s and d orbits, while those reached by incident s -wave neutrons can only be p orbits.

Because the neutron wave function for the $l = 1$ relative motion in the continuum is not significantly deformed by nuclear interaction, an important property of p -wave DRC follows: the capture cross section is not sensitive to the neutron-nucleus potential in the incident scattering channel. The capture process itself will only be sensitive to the structure properties of the bound state, thus removing the uncertainty deriving from the (optical) potential used to describe the continuum. We will give here the basic relations of a DRC model for the calculation of (n, γ) cross sections.

The direct capture process is an alternative to the compound nucleus (CN) formation mechanism. The collision matrix can be separated into two components

$$U_{c \rightarrow b} = U_{c \rightarrow b}(CN) + U_{c \rightarrow b}(DRC),$$

where all the quantum numbers necessary to define uniquely the initial and final reaction channels are grouped into the notation c and b . Here we will only consider the DRC part of the collision matrix, $U_{c \rightarrow b}(DRC)$. We give here a scheme containing

all the definitions necessary for building up a DRC model (a full description can be found in the Ref. [6]):

- Capture cross section for emission of electric dipole radiation (E1) in the transition $i \rightarrow f$

$$\sigma_{n,\gamma} = \frac{16\pi}{9\hbar} k_\gamma^3 \bar{e}^2 |Q_{c \rightarrow b}^{(1)}|^2$$

- Matrix elements for the transition

$$Q_{c \rightarrow b}^{(1)} = \langle \Psi_b | \hat{T}^{E1} | \Psi_c \rangle \equiv \sqrt{S_b} \mathcal{I}_{c,b} A_{c,b}$$

with $\hat{T}^{E1} = rY^{(1)}(\theta, \phi)$. S_b is the spectroscopic factor of the final bound state and $A_{c,b}$ a geometric factor containing only angular momentum coupling constants.

- Entrance channel wave function

$$\Psi_{lm}(\mathbf{r}) \equiv w_l(r) \frac{Y_{l,m}(\theta, \phi)}{rv^{1/2}}$$

where

$$w_l(r) = \frac{i\sqrt{\pi}}{k} \sqrt{2l+1} i^l [I_l - U_l O_l]$$

and asymptotically

$$I_l \sim \exp(-ikr + \frac{1}{2}il\pi) \quad \text{and} \quad O_l \sim \exp(+ikr - \frac{1}{2}il\pi)$$

U_l is the collision matrix for the scattering process in the entrance channel, v is the incoming neutron velocity, and k the corresponding wave number

- Radial matrix elements

$$\mathcal{I}_{l_c l_b} \equiv \int_0^\infty u_{l_b}(r) r w_{l_c}(r) dr$$

- The DRC cross section for incident neutrons with incident velocity v is given by

$$\sigma_{n,\gamma}(c \rightarrow b) = \frac{16\pi}{9\hbar v} k_\gamma^3 \bar{e}^2 S_b A_{cb}^2 |\mathcal{I}_{cb}|^2.$$

For incident p -wave neutrons this cross section is insensitive to the neutron-nucleus interaction. This is equivalent to assuming that the radial overlap $\mathcal{I}_{l_c l_b}$ with the incident part of the radial wave function is simply given by the $l = 1$ component of the partial wave decomposition of a plane wave in the incident channel

$$w_{l_c=1}(r) = \frac{(2i)\sqrt{3\pi}}{k} kr j_1(kr).$$

The final state wave function can be calculated from some model potential, *e.g.* Woods-Saxon or microscopic. The only unknown quantity to be determined is the spectroscopic factor S_b . This is usually a known quantity derived from (d, p) reactions or from full shell model calculations, which can be done for light nuclei.

Capture strength coming from neutron resonances can be included in the calculation using the single- or multi-level Breit-Wigner formalism. Interference effects between resonance and DRC give rise to terms of type

$$\sum_{\lambda} \frac{U_{\gamma}^{DRC} \Gamma_{\lambda n}^{1/2} \Gamma_{\lambda \gamma}^{1/2} (E_{\lambda} - E_n)}{(E_{\lambda} - E_n)^2 + \frac{1}{4} \Gamma_{\lambda T}^2},$$

where the sum is over resonances λ with parameters $E_{\lambda}, \Gamma_{\lambda n}, \Gamma_{\lambda \gamma}$, and U_{γ}^{DRC} is the DRC collision matrix. These interference effects have been never observed in the capture channel, although they are well known in the scattering channel. In our calculations we have omitted the interference terms as there has been no confirmation of these effects in experiments so far.

3 Neutron capture and Coulomb dissociation

The basic idea underlying Coulomb dissociation experiments is to measure the ejectiles of a binary break-up process generated by the Coulomb field of a (usually high Z) target. Together with the development and availability of radioactive ion beams, this method is becoming a key technique for investigating exotic nuclear structure properties.

Here we will only briefly describe break-up and capture mechanisms generated by the electric dipole (E1) component of the electromagnetic field. Other components may of course be important in some specific cases, but the general arguments presented here would remain valid for higher order multiplicities. Under well-defined kinematic conditions, the $B(E1)$ strength distribution for the dissociation of the incident ^{A+1}X nucleus into, say, $^A X+n$ is measured. The $B(E1)$ strength distribution is related to the matrix elements $Q_{b \rightarrow c}^{(E1)} = \langle \Psi_c | \hat{T}^{E1} | \Psi_b \rangle$ for a transition starting from a bound state Ψ_b (usually the ground state of the projectile) to the two-body continuum Ψ_c by

$$\frac{dB(E1)}{dE_x} = \frac{k_n^2}{\pi^2 \hbar v} \bar{e}^2 \frac{2J_c + 1}{2J_b + 1} |Q_{b \rightarrow c}^{(E1)}|^2.$$

Here E_x is the excitation energy (defined as the sum of the neutron-residual nucleus relative energy plus the neutron binding energy), k_n and v are the neutron wave number in the continuum and the relative velocity, respectively, J_b is the total angular momentum of the bound state, J_c is the spin of the residual nucleus in the continuum, and \bar{e} the neutron effective charge.

A first notable application of this method has been the measurement of the Coulomb dissociation of ^{11}Be [7]. This is a very well known example of a halo

nucleus. In fact, its ground state is bound by only 505 KeV and is dominated by the $|^{10}\text{Be}(0^+) \otimes (2s_{1/2})_\nu \rangle$ configuration. The $dB(E1)/dE_x$ strength distribution can be well reproduced [7] by a calculation made using the two-body continuum $\langle \psi_\nu^{l=1} \otimes ^{10}\text{Be}(0^+) |$, where $\psi_\nu^{l=1}$ represents the p -wave component of the wave function for neutron scattering off ^{10}Be . A detailed description of the methods and parameters used in the calculation can be found in the reference [8].

The $B(E1)$ strength distribution can be immediately related to the neutron capture cross section for the time-reversed transition by [6]

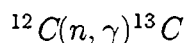
$$\frac{dB(E1)}{dE_x} = \frac{9}{16\pi^3} \frac{k_n^2}{k_\gamma^3} \frac{2J_c + 1}{2J_b + 1} \sigma_{n,\gamma},$$

where $k_\gamma = \epsilon_\gamma/\hbar c$ is the emitted γ -ray wave number.

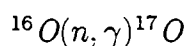
This technique is being used in several experiments using RIBs and is expected to provide extremely useful information on the structure of nuclei far from stability.

4 Examples

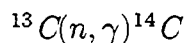
The calculations performed using the DRC and resonance formalisms have been performed so far for a number of neutron-induced reactions in light nuclei.



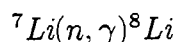
The results for this reaction have been described in [6] and in a previous CRP meeting report [9]. It is further documented in another section of this report. The experimental results for the capture process induced by incident p -wave neutrons can be reproduced by the DRC model. The results of the calculations have been included in the JENDL-3 special purpose file (Fusion File).



This cross section calculation has been reported in a previous CRP meeting [9] and will be described in another section of this report. The results of the calculations have been included in the JENDL-3 special purpose file (Fusion File).



This reaction cross section has been calculated recently and will be described in another section of this report.



This reaction cross section has been calculated recently and will be described in another section of this report.

References

- [1] A. M. Lane and J. E. Lynn, Nucl. Phys. **17**, 563 (1960); *ibid.* **17**, 686 (1960).
- [2] Y. Nagai, M. Igashira, N. Mukai, T. Ohsaki, F. Uesawa, K. Takeda, T. Ando, H. Kitazawa, S. Kubono and T. Fukuda, Ap. J. **381**, 444 (1991).
- [3] T. Ohsaki, Y. Nagai, M. Igashira, T. Shima, K. Takeda, S. Seino and T. Irie, Ap. J. **422**, 912 (1994).
- [4] M. Igashira, Y. Nagai, K. Masuda, T. Ohsaki and H. Kitazawa, Ap. J. **441**, L89 (1995).
- [5] T. Otsuka, M. Ishihara, N. Fukunishi, T. Nakamura, and M. Yokoyama, Phys. Rev. C **49** (1994) R2289 .
- [6] A. Mengoni, T. Otsuka, and M. Ishihara, Phys. Rev. C **52** (1995) R2334.
- [7] T. Nakamura *et al.*, Phys. Lett. B **331** (1994) 296.
- [8] A. Mengoni, T. Otsuka, T. Nakamura and M. Ishihara, in *Proceedings of the 9th International Conference on Capture Gamma-ray Spectroscopy*, Budapest, October 8-12, 1996, Vol. 1, G. L. Molnar, T. Belgya, Zs. Revay, Eds. (1997), p. 416.
- [9] A. Mengoni, 2nd CRP meeting, Vienna, May 1996, unpublished.

Computer Programs and Data Libraries Pertaining to Photon Production Data

John E. White, Jennifer B. Mannes Schmidt, Sheila Y. Finch, and J. Kirk Dickens

Radiation Safety Information Computational Center
Oak Ridge National Laboratory
Bldg. 6025, MS 6362
Oak Ridge, Tennessee 37831-6362 USA

1. Introduction to the compilation

A compilation of information on computer programs and data libraries relevant to photon production has been published as Oak Ridge National Laboratory document number ORNL/RSIC-57. The title and authors of this document are the same as indicated above. The document is available electronically as well as in hard copy; contact the authors for further information on availability. Herein we summarize the contents of this document and include a table of contents.

This compilation contains abstracts, or descriptions, as supplied by the respective Specialized Information Analysis Center of 54 programs (codes) and 8 photon data libraries. Code descriptions were obtained from either the Radiation Safety Information Computational Center (RSICC) at the Oak Ridge National Laboratory (USA) or from the OECD/Nuclear Energy Agency Data Bank (Paris) or both. These 54 codes are separated into four categories, namely experimental data reduction by (a) photon peak analysis, or by (b) unfolding; (c) model predictions, and (d) miscellaneous. A fifth category presents information on data libraries. There are several codes listed in each section; no recommendation is given for a preferred program in a given section because individual preferences may dictate a preferred choice for a specific user (*e.g.*, computer architecture, experimental configuration, etc.). Each program listed has been thoroughly tested and packaged by the responsible Data Center. The authors, however, did not include some older programs in these categories since they were out of date, and also did not include programs whose abstracts did not specify a relationship to photon production.

Each program listed in the compilation includes information under the following subheadings; a somewhat different set of subheadings is used for the data libraries.

1. Name and Title of the program;
2. Contributor(s), including Organization;
3. Coding Language and Computer;
4. Nature of the Problem Solved;
5. Method of Solution;
6. Restrictions and Limitations;
7. Typical Running Time;
8. Computer Hardware Requirements; and
9. References.

2. Contents of the Report ORNL/RSIC-57

ABSTRACT	1
SECTION 1	
INTRODUCTION	3
SECTION 2	
PEAK ANALYSIS CODES	5
<u>ACTIVE-PC</u>	7
<u>AMUSE</u>	9
<u>ANA</u>	11
<u>BOB-7 SERIES</u>	13
<u>CERPI-CEREL</u>	15
<u>GAMAN</u>	17
<u>GAMANAL</u>	19
<u>GAMX1</u>	27
<u>GASPAN-ZKD</u>	29
<u>GAUSS</u>	33
<u>GAUSS6</u>	35
<u>GRETEL</u>	39
<u>GRPANL</u>	41
<u>HYPERMET</u>	43
<u>JADSPE</u>	45
<u>RICKI</u>	49
<u>SAMPO-LRC</u>	55
<u>SAMPO80</u>	57
<u>SKEWGAUS</u>	59
<u>TPASS</u>	61
SECTION 3	
UNFOLDING ANALYSIS CODES	63
<u>ALPHA-M</u>	65
<u>CONFOLD</u>	67
<u>CUPED</u>	69
<u>DOMUS</u>	71
<u>FERDO/FERD</u>	73
<u>FERD-PC</u>	75
<u>NAISAP</u>	77
<u>RADAK</u>	79
<u>UNSPEC</u>	83
<u>UPEAK</u>	85
SECTION 4	
MODEL PREDICTIONS OF PHOTON YIELDS	87

<u>ALICE-91</u>	<u>89</u>
<u>CASTHY</u>	<u>93</u>
<u>EMPIRE</u>	<u>95</u>
<u>ERINNI</u>	<u>97</u>
<u>EXIFON-GAMMA</u>	<u>99</u>
<u>GNASH-FKK</u>	<u>101</u>
<u>PEGAS</u>	<u>103</u>
<u>PEQAG-2</u>	<u>105</u>
<u>TNG1</u>	<u>107</u>
SECTION 5	
<u>MISCELLANEOUS PROGRAMS</u>	<u>109</u>
<u>BOMJ</u>	<u>111</u>
<u>COINC</u>	<u>113</u>
<u>CURVE,LSFIT</u>	<u>117</u>
<u>DIMEN</u>	<u>121</u>
<u>GABAS</u>	<u>123</u>
<u>GASS</u>	<u>125</u>
<u>GRAP</u>	<u>127</u>
<u>MARTHA</u>	<u>131</u>
<u>MGA</u>	<u>135</u>
<u>PAPER 1</u>	<u>139</u>
<u>XRAY_AAC</u>	<u>141</u>
SECTION 6	
<u>DATA LIBRARIES</u>	<u>143</u>
<u>GAMDAT-78</u>	<u>145</u>
<u>GAMTAB</u>	<u>147</u>
<u>GAMTOT78</u>	<u>149</u>
<u>NFCLIST</u>	<u>151</u>
<u>NUCDECAY</u>	<u>153</u>
<u>RADDECAY 4.02</u>	<u>155</u>
<u>TPASGAM85</u>	<u>157</u>
<u>XG-IAEA</u>	<u>159</u>
ACKNOWLEDGMENTS	<u>161</u>

PRE-EQUILIBRIUM CODES FOR GAMMA EMISSION

E. Běták

Institute of Physics, Slov. Acad. Sci., 84228 Bratislava, Slovakia

Abstract

Several commonly used and easily available pre-equilibrium computer codes that can be used to calculate particle and gamma spectra and cross sections are compared. Differences in their physical assumptions and implications for the predictive ability of these codes are outlined.

1 Introduction

The spectrum of presently available pre-equilibrium codes is very rich. However, the majority of these codes does not include any possibility of pre-equilibrium γ emission and usually not even any γ emission at all. Although the inclusion of the pre-equilibrium mechanism is not essential for understanding γ emission following emission of nucleons and/or clusters in lower-energy reactions (such as reactions induced by 14 MeV neutrons), it is nevertheless welcome.

A general comparison of codes relevant to photon production is the subject of a recent ORNL report [1]. The main emphasis of [1] is on the analysis of experimental data, and only a small fraction of this effort is devoted to describing codes predicting photon yields. Here, the emphasis is on the codes able to calculate γ emission in low-energy (excitations below about 50 MeV) nuclear reactions. Obviously, there is some overlap with Ref. [1].

2 Main groups of pre-equilibrium codes with γ emission

What we shall consider to be pre-equilibrium codes with γ emission are the following:

- Published (or otherwise documented) pre-equilibrium codes with the possibility of pre-equilibrium γ emission;

- Pre-equilibrium codes with the possibility of pre-equilibrium γ emission, which have not been released in any form. Typically, they have been written just for a single purpose, and they are not intended for general use ¹;
- Pre-equilibrium codes with inclusion of γ emission, although the treatment of γ emission does not use the pre-equilibrium formalism ²;

The codes of the second group (single-purpose ones), although rather important, are beyond the scope of this comparison for obvious reasons. They have been used in preparing various papers on pre-equilibrium γ emission in the energy range considered. Examples of these are the codes of J. M. Akkermans, E. Běták, M. Blann, M. B. Chadwick, J. Dobeš, H. Gruppelaar, Zh. Kychkina, P. Obložinský, G. Reffo, B. A. Remington, and F. Zhivopistsev.

3 Pre-equilibrium codes with equilibrium γ emission

These codes have been rather successfully applied to calculating the population of discrete states in reactions of type $(n,n'\gamma)$, $(n,2n\gamma)$, $(n,p\gamma)$ etc., and (if needed) also the corresponding isomeric cross sections. They are able to produce also the continuous γ spectrum, if that is below the giant resonance region. In reactions induced by 14 MeV neutrons (as well as reactions of protons of similar energy), the emission of the first particle is at the fast (pre-equilibrium) stage of the reaction, but all the emission after that (including the γ -rays) can be reasonably approximated by that from a compound nucleus. Typically, the transitions E1, E2 and M1 are considered.

The main codes of this group are STAPRE of the late M. Uhl [2], TNG of C. Y. Fu [3], EMPIRE of the Polish group [4] (preceded by another very successful code from the same laboratory written specifically for the GIER computer), or MINGUS by A. Koning [5] ³. All of these codes incorporate the angular-momentum formalism (at least in the equilibrium, *i.e.* the compound-nucleus stage), which is necessary to handle discrete states with given spin (and parity). The treatment of spin at the pre-equilibrium stage of the reaction is done only in an approximate way, since these codes have been written prior to the proper formulation of the "spin kitchen" for pre-equilibrium decay (see [7] and the following papers).

¹If I have included a code in this group even if it has been sufficiently documented or even published, it is due to my insufficient knowledge (or unreliable memory) and does not contain any intended statement about the quality of the code and/or its write-up.

²This obviously implies that although these codes can be successfully used for population of levels after nucleon emission at excitation energies about 20 MeV, they are not suitable for calculations of the radiative capture type.

³In some respects, compound nucleus codes are also able to give reasonable results for this category of reactions. Although there are several codes of this kind, let us mention at least CASTHY by Igarashi and Fukahori [6].

4 Pre-equilibrium codes with pre-equilibrium γ emission

Pre-equilibrium γ emission was originally formulated without taking account of the spin variables [8]. Only at a later stage was spin dependence introduced in [7]. The codes that incorporate pre-equilibrium γ emission can also be grouped according to this criterion. Published or otherwise documented codes of these two groups are few in number.

4.1 Pre-equilibrium γ emission – the non-spin case

Not many codes incorporating γ emission without a treatment of spin have been released. The first of these codes is the PEQGM code [10], later modified for small PC's as PEQAG [11]. The second of these codes is an update of the well-known code GNASH [12]. Although first-chance pre-equilibrium γ emission is treated essentially in the same way within both of these codes using the formalism of Akkermans and Grupelaar [8] applied only to the continuous part of the γ emission, the PEQGM/PEQAG code remains at this level for all subsequent emissions, whereas GNASH switches to the equilibrium treatment of γ emission with all spin couplings and discrete states included afterwards. The third of the codes in this class, GRAPE [13], in many respects lies between the two others in its treatment of γ emission. A great advantage of this code is that it is the only one from this group capable of producing also the angular distributions of the γ -rays. Unfortunately, the development of this code has not continued, and it remains in its version of 1986. The code GNASH is continuously updated and growing, and currently (if one does not need angular distributions) it is very suitable for interpretation of the measured data and/or prediction of cross sections in unmeasured ranges. The only advantage of PEQAG is that it is a small, compact code that is easily used and with a small input file, and it is also somewhat faster, although (due to the use of the master equation approach) the difference in the CPU time is not essential.

The code ALICE by M. Blann has been improved in the course of time. Its 1991 version [14] includes also γ rays competing with nucleon emission. The γ emission itself is non-spin, although some attention is paid to including some aspects of the spin dependence in the equilibration process. However, the code employs γ -emission mechanisms [15] which do not correspond to the others, so that the use of ALICE for γ emission is not strongly recommended.

There is also a very special code EXIFON (H. Kalka, [9]). It includes multi-step direct as well as multi-step compound processes, and pre-equilibrium γ emission is treated in its standard E1 form, as in PEGAS, GNASH and GRAPE. The results produced by EXIFON excellently reproduce experimental data of all kinds (not limited to photon production), and these results are achieved with very modest computer requirements (memory, CPU time). However, the input data needed are not very

transparent, and to the best of our knowledge the code EXIFON has not been used outside its original laboratory.

4.2 Pre-equilibrium γ emission — the spin case

Even though spin-dependent calculations were performed first by Obložinský and by Obložinský and Chadwick [7], their code has not been made widely available. Thus, the only readily available code is the PEGAS code [16], which after several years of effort has been converted to DEGAS [17] by addition of discrete levels, the possibility of cluster emission, and also multipolarities other than E1). The results from DEGAS are comparable to those from GNASH for γ emission, although the pre-equilibrium γ emission in GNASH does not take account of the spin variables. A detailed comparison of these codes may be found in a separate section.

References

- [1] J. E. White, J. B. Manneschildt, S. Y. Finch, J. K. Dickens, Report ORNL/RSIC-57 (to be published, 1997); J. K. Dickens, in this report.
- [2] M. Uhl, Code STAPRE, (NEA code No. NEA 0461).
- [3] C. Y. Fu, Code TNG, (NEA code No. NEA 0678).
- [4] A. Herman, A. Marcinkowski, K. Stankiewicz, Code EMPIRE, Comp. Phys. Comm. 33 (1984), 373 (CPC code No. ACCQ); A. Marcinkowski, Report IAEA-NDS-95 (1988) (NEA code No. IAEA 0973) (RSICC code PSR-292).
- [5] A. J. Koning, Code MINGUS.
- [6] S. Igarashi, T. Fukahori, Code CASTHY, JAERI 1321, NEANDC(J)-156/U, INDC(JPN)-143/L (1991) (NEA code No. NEA 1395).
- [7] P. Obložinský, Phys. Rev. **C35** (1987), 407; P. Obložinský, M. B. Chadwick, Phys. Rev. **C42** (1990), 1652.
- [8] E. Běták, J. Dobeš, Phys. Lett. **84B**, 368 (1979);
J. M. Akkermans, H. Gruppelaar, Phys. Lett. **157B**, 368 (1985).
- [9] H. Kalka, Code EXIFON, (NEA code No. IAEA 1211) (RSICC code PSR-305);
H. Kalka, Report INDC(GDR)-601L (IAEA 1990); H. Kalka, TU Dresden manuscript (1990, unpublished); H. Kalka, in *Nuclear Data for Sci. Technol., Proc. Int. Conf.*, Jülich 1997. Ed. S.M. Qaim, Springer-Verlag, Berlin, 1992, p. 897.
- [10] E. Běták, J. Dobeš, Code PEQGM, Report IP EPRC SAS No. 43/1983 (Bratislava 1983).

- [11] E. Běták, Code PEQAG, Report INDC(CSR)-016/LJ (IAEA Vienna 1989) and Report FU SAV 89/5 (Bratislava 1989) (NEA code No. IAEA 1185).
- [12] P. G. Young, E. D. Arthur, M. B. Chadwick, Code GNASH, Report LA-12343-MS (UC-413) (Los Alamos 1992); updated 22 Sept., 1995; (NEA codes Nos. NESC 0757 and PSR 0125) M. B. Chadwick, P. G. Young, private communication.
- [13] H. Gruppelaar, J. M. Akkermans, Code GRAPE, Report ECN-164 (Petten 1985), plus correction (1986), (NEA code No. NEA 1043).
- [14] M. Blann, Code ALICE/85/300 LLNL Report UCID-20169 (1984); M. Blann, LLNL Report UCRL-JC-109052 (1991) (RSICC code PSR-146).
- [15] G. Reffo, M. Blann, B. A. Remington, Phys. Rev. **C38**, 1190 (1988); *ibid.* **C39**, 1188 (1989).
- [16] E. Běták, P. Obložinský, Code PEGAS, Report INDC(SLK)-001 (IAEA Vienna 1993) (NEA code No. IAEA 1261).
- [17] E. Běták, Code DEGAS, *Development of code PEGAS*, unpublished.

Direct-Semidirect (DSD) Codes

F. Cvelbar

*"J. Stefan" Institute and Faculty of Natural Sciences
and Technology, University of Ljubljana, Slovenia*

Abstract

Recent codes for direct-semidirect (DSD) model calculations in the form of answers to a detailed questionnaire are reviewed. These codes include those embodying the classical DSD approach covering only the transitions to the bound states (RAF, HIKARI, and those of the Bologna group), as well as the code CUPIDO++ that also treats transitions to unbound states.

1 Introduction

The DSD model is a widely employed semi-microscopic model for the description of radiative capture of nucleons in the region of excitation energy where the giant dipole resonance (GDR) and other multipole resonances are excited. The matrix element in the model is the sum of the direct and semidirect (two step) matrix elements describing transitions via giant dipole and/or other multipole states to the selected final state. The DSD model requires input on the properties of the resonances (energy, width) and the interaction between the nucleon and the collective multipole motion. Data on the former are taken from experiment or systematics, and the strength of the latter is usually treated as a free parameter obtained from the systematic analysis of the available experimental data. In traditional DSD calculations, the initial and final state wave functions are calculated from an optical potential and from a real potential which reproduces the binding energy of the considered state, respectively.

The DSD model provides the ability to calculate the angular distribution of the capture photons, as well as analyzing powers for polarized projectiles. The bombarding energy dependence of the corresponding Legendre coefficients is rather strongly sensitive to the interference between different multipole contributions. It is just this sensitivity which allows the study of the higher multipole resonances by observing these coefficients.

It should also be noted that F. Dietrich (code CUPIDO++) has extended the DSD model to describe also the transitions to the region of unbound final states, which are described by optical model wave functions. In this code optical model wave functions may also be used to treat the transitions to the region where the bound states cannot be treated separately.

2 Short review of the DSD codes

Classical DSD codes, allowing the calculation of the differential cross section to bound final states, presented here are the codes HIKARI (H. Kitazawa, Tokyo) and RAF (R. Martinčič and A. Likar, Ljubljana). As noted in the introduction, these codes use as free parameters the strength of the real and imaginary form factors V_1 and W_1 . The codes differ in the details of the algorithms used. The contribution of the Bologna group to the development of the DSD model should also be noted. Although no longer in general use, we have included their codes (DIRCO, SPEC, and KISS) in this report from information supplied by G. Longo. The first two of these calculate dipole capture, while the third includes quadrupole radiation as well.

The already mentioned code CUPIDO++ (F. Dietrich, Livermore) is based on an extended DSD model. Its calculated observables are similar to those from the classical DSD codes.

Recently A. Likar (Ljubljana) has introduced the so-called consistent version of the DSD model in which the imaginary coupling strength W_1 follows directly from equating the current and density expression of the multipole operator. In this approach W_1 is no longer a free parameter (A. Likar and T. Vidmar, Nucl. Phys. **A598**, (1996). The corresponding code is in the developmental stage and has not yet been disseminated.

Questionnaire Regarding Direct-Semidirect Codes

1. Name and/or designation of the program

CUPIDO++

2. Computer for which program is designed

The program was developed on a 486 66-MHz IBM-PC compatible with 20MB memory, but should run on any computer with a C++ compiler adhering to the ANSI standard.

3. Nature of physical problem solved

Implementation of the direct-semidirect (DSD) capture mechanism for spin-0 and spin-1/2 projectiles, with particular attention to unbound final states and to bound final single-particle states that damp into a dense background of compound states. The standard DSD calculation for capture to bound single-particle states is included as an option. Direct E1 through E4 radiation is treated, as well as convective-current M1 through M4. Semidirect E1, isoscalar E2, and isovector E2 radiations are included with several options for the complex form factors. The direct radiation may be calculated using either current or density forms for the operators, and with either the full Bessel forms for the operators or a long-wavelength approximation. Quantities calculated are total (angle-integrated) cross sections, gamma energy spectra, angular distributions, and (for spin-1/2 projectiles) analyzing powers.

4. Method of solution

Standard coordinate space methods are used. Initial-state wave functions are derived from an optical potential. The final-state wave functions are derived from a real potential well in the standard DSD option. Unbound final-state wave functions are derived from an optical potential, while unstable bound final-state configurations are treated via radial Green's functions using an optical potential. In the case of unbound final states, the long-range parts of the radial integrals are calculated using the Vincent-Fortune technique of integration in the complex plane.

5. Restrictions on the complexity of the problem

The program has been successfully tested up to approximately 50 MeV for nucleon capture. Extension to higher energies is possible but will require attention to the stability of the numerical techniques used to calculate the long-range part of the radial integrals in the case of capture to unbound final states.

6. Typical running time

For the most complex case so far attempted, calculation of a full gamma energy spectrum in 1-MeV steps for 34-MeV incident protons on a medium-weight nucleus with all electromagnetic operators included requires approximately 5 minutes on a

166-MHz Pentium processor. The running time for capture to a single bound state using the standard DSD model is very short.

7. Unusual features of the program

See question 3 above.

8. Related and auxiliary programs

The CUPIDO++ code system consists of a main program, CUPIDO, that calculates a Legendre polynomial decomposition of the results, and a second program, SPECTRA, that processes these Legendre coefficients into physical observables. For standard DSD calculations, bound-state wave functions may be calculated internally within CUPIDO or alternatively from a file of wave functions created by an auxiliary program, BOUND.

9. Machine requirements

The program was developed using Borland and Microsoft C++ compilers on a PC-compatible system. It should run on a 486 or higher system of this type. It should be easily adaptable to other platforms that have an ANSI-standard C++ compiler.

10. Programming language used

ANSI-standard C++. Platform- and compiler-specific extensions were avoided.

11. Operating system under which program is executed

Currently Windows 98 on a 600-MHz Pentium3 system. It was formerly run with Windows 3.1 on a 66-MHz 486 and Windows95 on a 166-MHz Pentium.

12. Other programming or operating information or restrictions

None.

13. References

A reasonably complete description of the formalism, but not the computational details, may be found in W. E. Parker *et al.*, Phys. Rev. **C52**, 252 (1995).

14. Name and establishment of author(s)

F. S. Dietrich, Lawrence Livermore National Laboratory
Mail Stop L-050, P. O. Box 808
Livermore, CA 94551, USA
E-mail address dietrich2@llnl.gov

15. Status (well documented, in progress ...)

This is a developmental program; there is no specific documentation currently available.

16. Availability of the program

The program has not been officially released but may be made available on a collaborative basis.

17. Material available (source code, sample I/O, command files ...)

Source code as well as sample input and output.

18. Keywords

radiative capture, direct-semidirect, continuum final states, damped final states, final state fluctuations

Questionnaire Regarding Direct-Semidirect Codes

1. Name and/or designation of the program

RAF

2. Computer for which program is designed

The program was developed on a VAX-4200 computer running VMS, but should run on any computer with a F77 compiler adhering to the ANSI standard.

3. Nature of physical problem solved

Implementation of the direct-semidirect (DSD) capture mechanism for neutrons and protons to bound final states. Total and differential cross sections and angular distribution coefficients are determined as a function of the projectile energy in the region of the giant multipole resonances. Isovector dipole, isovector and isoscalar resonances can be taken into account.

4. Method of solution

Standard coordinate space methods are used (Merson integration, Simpson quadrature). Initial-state wave functions are derived from an optical potential. The final-state wave functions are derived from a real potential well.

5. Restrictions on the complexity of the problem

None noted.

6. Typical running time

Up to a quarter of an hour on a VAX-4200 machine for a problem involving a few final states.

7. Unusual features of the program

See question 3 above.

8. Related and auxiliary programs

The RAF code system consists of a main program, RAF.EXE and a command file RAF.COM which assigns the appropriate fortran files and starts the execution.

9. Machine requirements

The program was developed using an F77 compiler on a VAX-4200 machine running VMS. It should be easily adaptable to other platforms that have an ANSI-standard F77 compiler.

10. Programming language used

ANSI-standard F77. Platform- and compiler-specific extensions were avoided.

11. Operating system under which program is executed

Currently VMS on a VAX-4200 machine.

12. Other programming or operating information or restrictions

None.

13. References

A reasonably complete description of the formalism, but not the computational details, may be found in the following references:

A.Likar, M. Potokar and F. Cvelbar, Nucl. Phys. **A280** (1977) 49

A.Likar and F. Sever, Nucl. Phys. **A295** (1978) 405

A.Likar and R. Martinčič, Nucl. Phys. **A321** (1979) 306

A.Likar, and R. Martinčič, Nucl. Phys. **A350** (1980) 74

14. Name and establishment of author(s)

R. Martinčič, A. Likar

J. Stefan Institute

Ljubljana, Slovenia

E-mail address: Rafael.Martincic@ijs.si, Andrej.Likar@ijs.si

15. Status (well documented, in progress ...)

This is a developmental program; there is no specific documentation currently available, but the source code is extensively commented.

16. Availability of the program

The program has been sent to the ENEA software data bank.

17. Material available (source code, sample I/O, command files ...)

Source code as well as sample input and output.

18. Keywords

radiative capture, direct-semidirect

Questionnaire Regarding Direct-Semidirect Codes

1. Name and/or designation of the program

HIKARI

2. Computer for which program is designed

Any computer on which a Fortran 77 compiler is installed.

3. Nature of physical problem solved

The computer code "HIKARI" calculates the angular distribution of cross sections and analyzing powers of gamma-rays produced by the radiative capture of polarized nucleons by unpolarized nuclei. The formalism is based on the direct-semidirect capture model and takes account of the electric dipole, quadrupole, octupole and magnetic dipole transitions. Special features include the ability to calculate transitions from the isovector (E1, E2, E3, M1) and isoscalar (E2, E3) resonances and to take the isospin splitting of the electric giant dipole state into account. The use of a complex coupling between incident nucleons and target nuclei is optional. Options are also given for the particle-vibration coupling form factor for E2 and E3 transitions and for the form of the optical potential.

4. Method of solution

Fox-Goodwin method.

5. Restrictions on the complexity of the problem

None stated.

6. Typical running time

Very short time.

7. Unusual features of the program

None.

8. Related and auxiliary programs

None.

9. Machine requirements

No special requirements.

10. Programming language used

Fortran 77.

11. Operating system under which program is executed

UNIX system (SUN OS 4.1.3).

12. Other programming or operating information or restrictions

None.

13. References

H. Kitazawa, Triangle Universities Nuclear Laboratory Annual Report TUNL-XIX (1980).

14. Name and establishment of author(s)

Hideo Kitazawa
Department of Energy Sciences
Interdisciplinary Graduate School of Science and Engineering
Tokyo Institute of Technology
4259, Nagatsuta-Cho, Midori-Ku, Yokohama 226, Japan
TEL. 045-924-5688
FAX. 045-924-5688
E-mail: kitazawa@es.titech.ac.jp

15. Status (well documented, in progress ...)

The code manual is in preparation.

16. Availability of the program

The program is not yet released, but it is available; contact the author.

17. Material available (source code, sample I/O, command files ...)

source code, sample input and output.

18. Keywords

Direct-semidirect model, polarized and unpolarized nucleon capture.

Questionnaire Regarding Direct-Semidirect Codes

1. Name and/or designation of the program

DIRCO, SPEC, and KISS

2. Further information

As noted in the introduction, these codes and the work performed with them played an important part in the development of the direct-semidirect model. They were written in FORTRAN IV and developed for an IBM 360/75 system. While these codes are now considered obsolete by their authors, information about them may possibly be obtained from the ENEA Nuclear Data Center, Bologna. DIRCO and SPEC calculated dipole capture to single bound final states and to a spectrum of bound final states, respectively, while KISS calculated quadrupole radiation as well. The codes were documented in the reports indicated below, and these may be available via the ENEA Nuclear Data Center. Inquiries may also be directed to one of the authors at the address below.

3. References

The codes were documented in the following CNEN Reports:

DIRCO: RT/FI/(71)29

SPEC: RT/FI/(71)30

KISS: RT/FI/(71)31

4. Name and establishment of author(s)

Giuseppe Longo
Department of Physics
University of Bologna
Via Irnerio 46
I-40126 Bologna Italy
e-mail: longo@bo.infn.it
Fax: 39-51-244101, 39-51-247244
<http://bohp03.bo.infn.it/tunguska96/>

5. Keywords

direct-semidirect, dipole capture, quadrupole capture

RECOMMENDED GAMMA RAY STRENGTH FUNCTIONS

J. Kopecky

ECN, P.O. Box 1, 1755 ZG Petten and JUKO Research, 1817 HX Alkmaar,
The Netherlands

1. Introduction

This work comprises results of our studies and calculations of gamma-ray strength function modelling over past 6 years [1-10] and is an extension of Ref. [10]. Almost all of the calculations were performed by the late Mario Uhl, to whom this report is dedicated.

The gamma-ray strength function for multipole type XL is defined as the average reduced partial radiation width $E_\gamma^{-(2L+1)} \langle \Gamma_{XL}(E_\gamma) \rangle$ per unit energy interval

$$f_{XL}(E_\gamma) = E_\gamma^{-(2L+1)} \langle \Gamma_{XL}(E_\gamma) \rangle / D \quad (1)$$

of resonances with average spacing D; E_γ is the transition energy. The corresponding gamma-ray transmission coefficient $T_{XL}(E_\gamma)$ is given by the relation

$$T_{XL}(E_\gamma) = 2\pi E_\gamma^{(2L+1)} f_{XL}(E_\gamma). \quad (2)$$

Therefore gamma-ray strength functions enter as important ingredients into compound nucleus model calculations of capture cross sections, gamma-ray production spectra, isomeric state populations and into the assessment of the competition between gamma-ray and particle emission. The relevant multipolarities in this context are E1, M1 and E2.

In this contribution we test strength function models by comparison to various experimental data related to neutron capture. Cross sections and spectra depend on the gamma-ray strength at all transition energies but do not differentiate between multipolarities, so they are mainly sensitive to the dominant E1 strength. Analysis of resonance transitions allows determination of the multipolarity but the resulting strength functions encompass only a narrow energy region.

2. Strength function models

The simplest model for gamma-ray strength functions is the *single-particle model* prescribing an energy independent strength [11]. We used this model for M2, E3, and M3 radiation with a strength of one Weisskopf unit per MeV.

Gamma-ray strength functions may be related to the photoabsorption cross section. If the latter is dominated by a giant resonance (GR) of Lorentzian shape Brink's hypothesis [12] leads to a strength function derived from a *standard Lorentzian* (SLO),

$$f_{XL}^{SLO}(E_\gamma) = 26 \times 10^{-8} [\text{mb}^{-1} \text{MeV}^{-2}] / (2L+1) \times \sigma_0 \Gamma E_\gamma^{(3-2L)} \Gamma_0 / (E_\gamma^2 - E_0^2)^2 + E_\gamma^2 \Gamma_0^2, \quad (3)$$

where the Lorentzian parameters (σ_0 , E_0 , Γ_0) stand for the peak cross section, energy, and width of the GR, respectively. We used this model for E1, M1 and E2 radiation. For E1 the Lorentzian parameters were taken from the analysis of the photoabsorption cross section [13] of the compound or a neighbouring nucleus. Global parameters were employed for M1 and E2 radiation:

- i) an M1 spin-flip resonance as proposed by Bohr and Mottelson [14] with $E_0 = 41A^{-1/3}$ (MeV), $\Gamma_0 = 4$ (MeV) and the peak cross section determined either from experimental data or from the systematics $f_{M1}(7\text{MeV}) = 1.88A^{1.41} \times 10^{-11} (\text{MeV}^{-3})$ [15];
- ii) an (isoscalar) quadrupole GR with $E_0 = 63A^{-1/3}$ (MeV) [16], $\Gamma_0 = (6-0.012A)$ (MeV) [17], and $\sigma_0 = 1.5 \times 10^{-4} Z^2 E_0^2 A^{-1/3} / \Gamma_0$ (mb) [17].

For the dominant E1 radiation improvements of the SLO based on microscopic theory are available. The theory of Fermi liquids [18] predicts an energy and temperature dependent width of the giant dipole resonance (GDR), $\Gamma(E_\gamma, T) = \beta(E_\gamma^2 + 4\pi^2 T^2)$, where β is a normalisation constant. The first term reflects the spreading of particle-hole states into more complex configurations while the second one accounts for collision of quasiparticles. The temperature T refers to the absorbing state and can be calculated within a level density model. Kadenskij [19] suggested choosing β so as to guarantee compatibility with photoabsorption data

$$\Gamma_K(E_\gamma, T) = \Gamma_0 / E_0^2 (E_\gamma^2 + 4\pi^2 T^2). \quad (4)$$

The *generalised Lorentzian* (GLO), as proposed by Kopecky and Chrien [20], consists of two terms: a Lorentzian with the energy dependent width according to Eq. (4) and the (non-zero) $E_\gamma \rightarrow 0$ limit of the model of Kadenskij et al. [19]:

$$f_{E1}^{GLO}(E_\gamma, T) = 8.68 \times 10^{-8} [\text{mb}^{-1} \text{MeV}^{-2}] \sigma_0 \Gamma_0 \times \{E_\gamma \Gamma_K(E_\gamma, T) / (E_\gamma^2 - E_0^2)^2 + E_\gamma^2 \Gamma_K^2(E_\gamma, T) + 0.7 \Gamma_K(E_\gamma=0, T) / E_0^3\}. \quad (5)$$

Up to an energy around the neutron binding energy the E1 strength resulting from Eq. (5) and that from the model of Kadenskij *et al.* [19] are very similar. In Ref. [1] we showed for some selected spherical nuclei that the GLO model provides a reasonable simultaneous description of average resonance capture (ARC) data, capture cross sections, and gamma-ray production spectra. To reproduce also data for strongly

deformed nuclei we proposed in Refs. [3,4,5,8] using in Eq. (5) instead of $\Gamma_k(E_\gamma, T)$ the following *empirical* generalisation of the energy dependent width

$$\Gamma_{En}(E_\gamma, T) = [k_0 + (1 - k_0)(E_\gamma - \varepsilon_0)/E_0 - \varepsilon_0] \Gamma_k(E_\gamma, T), \quad (4)$$

which is determined by two parameters (k_0, ε_0). For $k_0 > 1$ the width is enhanced compared to the result of Eq. (4). In that case the resulting El strength, obtained by replacing in Eq.(5) $\Gamma_k(E_\gamma, T)$ by $\Gamma_{En}(E_\gamma, T)$, is denoted as derived from an *enhanced generalised Lorentzian* (EGLO):

$$f_{El}^{EGLO}(E_\gamma, T) = 8.68 \times 10^{-8} [\text{mb}^{-1} \text{MeV}^{-2}] \sigma_0 \Gamma_0 \times \Gamma_{En}(E_\gamma, T) / (E_\gamma^2 - E_0^2)^2 + E_\gamma^2 \Gamma_{En}^2(E_\gamma, T) + 0.7 \Gamma_{En}(E_\gamma=0, T) / E_0^3 \}. \quad (7)$$

The enhancement k_0 can be used to reproduce the experimental El strength around the reference energy ε_0 . Note, that i) for $k_0 = 1$ the GLO model is obtained and ii) $\Gamma_{En}(E_\gamma \rightarrow E_0, T \rightarrow 0) \rightarrow \Gamma_0$: *i.e.* compatibility with photoabsorption is maintained.

For nuclei with a split GDR we used in Eqs. (3), (5) and (7) the incoherent sum of two analogous terms; the same parameters (k_0, ε_0) for each term were used in Eqs. (6) and (7). For targets with $A=175-205$ and for ^{93}Nb we included a SLO pygmy resonance with parameters determined by fitting the high-energy end of the gamma-ray production spectrum.

3. Model calculations of cross sections and spectra

For the calculation of neutron capture cross sections and the resulting gamma-ray spectra we employed the Hauser-Feshbach theory in the formulation of Moldauer [21] and an appropriate treatment of gamma-ray cascades. The calculations were performed with the code MAURINA [22].

In the mass and energy region considered ($A > 100$, $E_n < 3$ MeV) charged particle emission can be neglected. Neutron optical potentials were taken from the literature and eventually slightly modified in order to improve the reproduction of total cross sections and (neutron) strength functions. For strongly deformed nuclei the neutron transmission coefficients were generated by coupled channels calculations.

For the level density, characterising the excited states beyond the known levels, we used semi-empirical models with parameters relying on recent results for the average spacing of s-wave resonances D_0 and the number of low excited levels N_{lev} . For all nuclei calculations were performed employing the backshifted Fermi gas model (BSFG) [23] and the model by Kataria, Ramamurthy and Kapoor (KRK) [24] which accounts for shell effects in terms of the ground-state shell correction to the nuclear binding energy. The genuine KRK model is supplemented according to the Gilbert-Cameron prescription [25]:

a conventional pairing shift and a constant temperature portion at lower excitation energy where the spin distribution parameter σ^2 is linearly interpolated between the value σ_{lev}^2 , deduced from the levels and $\sigma^2(E_x)$, the value prescribed by the KRK model at the matching energy E_x . For comparisons we also used in some cases a more sophisticated level density model: the generalised superfluid model in its phenomenological version (GSFPH), which was developed by Ignatyuk and collaborators [26-28]. This model accounts for shell effects, pairing (employing the BCS approach) as well as for collective enhancement with empirical prescriptions for its damping. For each model the respective parameters are chosen so as to reproduce the same values D_0 and N_{lev} ; in the case of the GSFPH model this was achieved by an additional shift of the excitation energy as proposed in Ref. [27].

When employing a particular level density model we also used the pertinent temperature T in the expressions for the gamma-ray strength functions according to the models GLO and EGLO (see Eqs. 4-7). Under these conditions the EI strength depends on the level density model employed. In the case of the KRK model we used the genuine temperature prescription also in the constant temperature region.

4. Results of calculations

As a continuation of previous investigations in the mass regions $A < 100$ [1,2] and $A = 140-200$ [3,4,5,8,9] we include here more nuclei with $100 < A < 200$. For the targets considered, at least two pieces of the following experimental information exist: average s-wave radiation widths, capture cross section excitation functions, and gamma-ray production spectra. We evaluate EI strength function models by comparing the results of model calculations with these data. The results obtained so far can be summarised as follows:

i) In general the results of model calculations strongly depend on the level density model employed. On the other hand, a rather small dependence has been found on the optical model parameters [4]. For incident energies low enough so that only the level density of the product nucleus enters, the BSFG model produces larger cross sections and average radiation widths. This effect increases with the neutron separation energy. This is illustrated in Fig. 1 for the transitional nucleus ^{189}Os . The capture cross sections are reasonably well reproduced with an EI strength according to the GLO model and the BSFG model for the level density (Fig. 1b). With the KPK level density, however, a description of the data requires the EGLO model with parameters ($k_0 = 1.8$, $\epsilon_0 = 4.5\text{MeV}$) (Fig. 1).

ii) For transitional and spherical nuclei at the lower and the upper end of the mass region $A = 100-200$ the SLO model in general fails to reproduce the data. This is a confirmation of a longstanding result that this formulation overestimates the large body of experimental f_{E1} data both from discrete-resonance and averaged-resonance capture experiments (*e.g.* Refs. [12,20,30,31]) as well as other pertinent quantities such as $\langle \Gamma_\gamma \rangle$, σ_γ and $d\sigma_\gamma/dE$ (*e.g.* Refs. [1,2]). This overestimation is also confirmed for $\langle f_{E1} \rangle$

experimental values as demonstrated in Refs. [15,29]. The GLO model is reasonably successful but for many nuclei the EGLO model is required. The enhancement, however, is small and considerably lower than for $A=150-165$ (see further) and probably only reflects inaccuracies in different input parameters used in calculations. Further we observed that for several targets it is impossible to simultaneously reproduce the capture excitation function and the average total s-wave radiation width. This may be due to valence contributions favoured by the 4s maximum of the neutron strength function and/or inaccuracies in the average spacing D_0 determining the level density parameters.

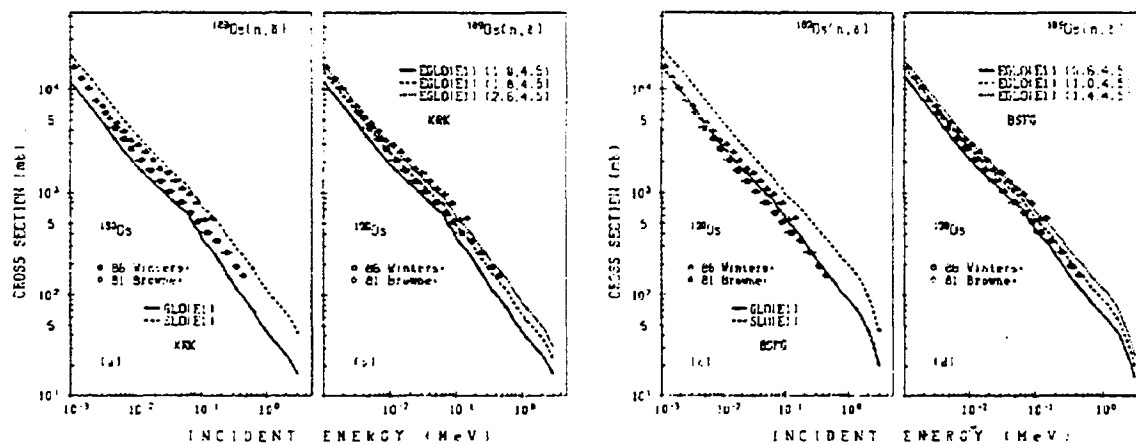


Fig. 1. The capture cross section of ^{189}Os calculated with different models for the E1 strength. The underlying level densities are calculated according to the KRK model (a,b) and the BSFG model (c,d).

iii) For strongly deformed nuclei with masses between 150 and 165 we confirmed earlier results for some Gd and Eu isotopes [3,5]. The GLO model for the E1 strength fails to reproduce the experimental data. A reasonably good description is either achieved with the SLO model or the EGLO model with an enhancement $k_0 > 1$, the actual value depending on the level density model employed. For $^{155,156,157}\text{Gd}$ these results are also directly confirmed by experimental E1 strength functions deduced from average resonance capture data [5]. As an illustration for the model calculations we display in Fig. 2 the gamma-ray production spectrum for $^{159}\text{Tb}(n,\gamma)$ at $E_n=0.5$ MeV. The enhancement parameters for the EGLO model (k_0, ϵ_0) required to reproduce the data are indicated on the plots. The failure of the GLO model does not hold to the same extent for all deformed nuclei. For some isotopes of W and Re a quite reasonable reproduction of cross sections and spectra can be achieved with this model for the E1 strength.

iv) Neither the SLO nor the GLO model can be used for model calculations in the whole mass region. The flexible EGLO model could do the job if its parameters (k_0, ϵ_0) show a sufficiently smooth behaviour, so that it can be applied for cross section predictions. For a fixed reasonable value of the reference energy, namely $\epsilon_0 = 4.5$ MeV, we therefore determined for all nuclei considered in our studies the enhancement k_0 , by simultaneously

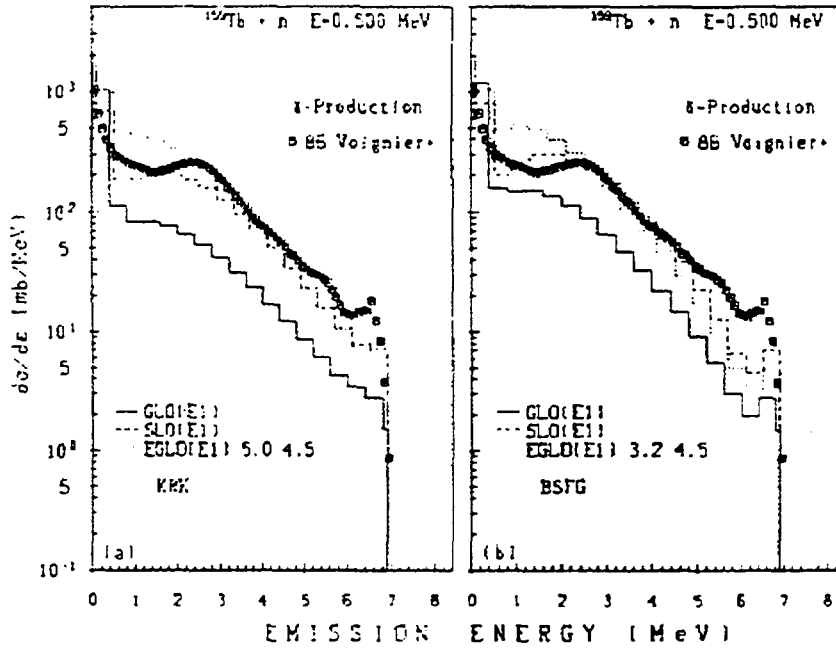


Fig. 2. The gamma-ray production spectrum for $^{159}\text{Tb}(n,\gamma)$ calculated with 3 models for the E1 strength. The level density models are KKK (a) and BSFG (b).

reproducing at least two pieces of experimental data. This was done by graphical comparisons between experimental data and the results obtained with different k_0 values as illustrated in Figs. 1b and 1c. In this context we permitted k_0 to assume values moderately smaller than 1. Because of the strong dependence of the results on the level density model we had to do this separately for the KKK and the BSFG model. The derived k_0 values only weakly depend on the reference energy ϵ_0 . Some test calculations indicated that a change of 1 MeV in ϵ_0 affects k_0 only by a few percent. The enhancements found in this way are displayed in Fig. 3 as function of the mass number of the compound nucleus. The error bars reflect uncertainties of the experimental data and the spacing D_0 as well as inconsistencies between the enhancements required for different types of data; they were found by rather rough assessments and not by detailed sensitivity studies. The trend of the enhancements can be described as a function of the mass number A by simple purely empirical expressions such as

$$k_0(x) = 1.5 \quad \text{for } A \leq 145, \quad (8a)$$

$$= 1.5 + 0.131(A-145)^2 \exp[-0.154(A-145)] \quad \text{for } A \geq 145$$

for the KKK model and

$$k_0(x) = 1.0 \quad \text{for } A \leq 148, \quad (8b)$$

$$= 1.0 + 0.09(A-148)^2 \exp[-0.180(A-148)] \quad \text{for } A \geq 148$$

for the BSFG model. The expressions are actually the same as in Ref. [9]; the constants may change when we consider more nuclei with $A < 100$. Fig. 4 displays calculated average s -wave radiation widths and the experimental value for the nuclei considered for the determination of k_0 and some additional nuclei. For the calculations we employed the EGLO model with the enhancement k_0 according to Eq. (8a) or (8b).

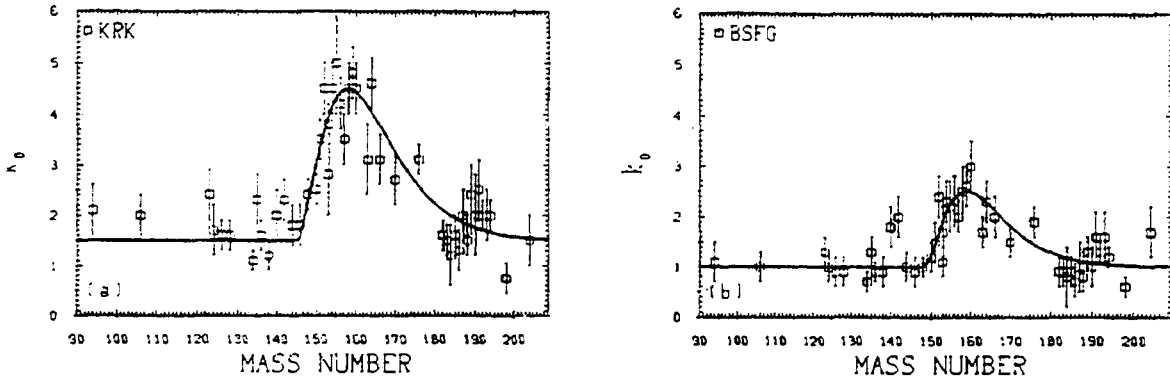


Fig. 3. The enhancements k_0 plotted against the mass number of the compound nucleus. They are extracted from calculations employing the KRK (a) and the BSFG model (b) for the level densities.

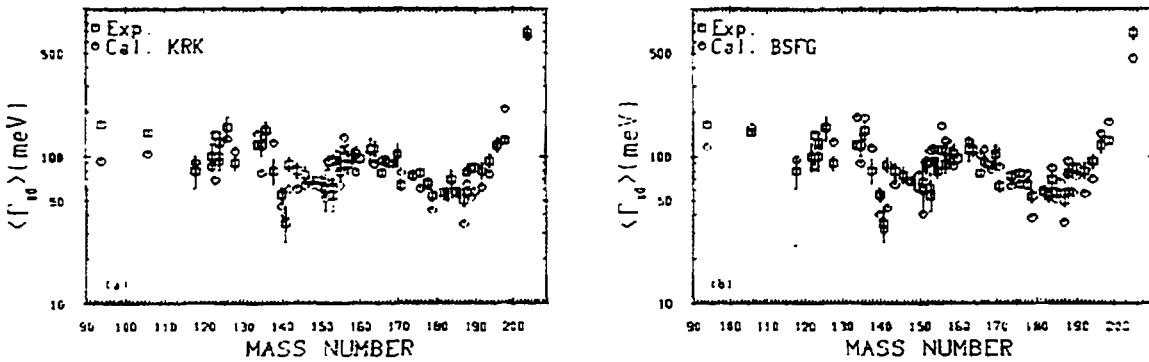


Fig.4: The calculated average s -wave radiation width and the corresponding experimental value. The calculations employ the EGLO model for the $E1$ strength with k_0 values according to Eqs. (8a) and (8b), depending on the level density models employed, *i.e.* the KRK model (a) and the BSFG model (b).

5. Discussion

The enhancements k_0 derived from the above mentioned experimental data in the framework of the EGLO model show a clear dependence on the mass number A with a peaking between $A = 150$ and 170 . Though the individual values scatter considerably we

hope that the systematics of k_0 given Fig. 3 can be used for cross section predictions. This is illustrated by the reasonable reproduction of the total average radiation width in Fig. 4 by means of the simple empirical relation Eqs. (8). Note, that each k_0 systematics is connected with a particular level density model.

5.1 The A=150-170 enhancement

A possible explanation of this enhancement for the nuclei in the rare earth deformed region is discussed here. The surprising feature is that the enhancement does not cover the whole deformed range but starts to disappear between A=170 and 180. This enhancement (about a factor of 2 to 3) remained hidden within the scatter of the present experimental averaged $\langle f_{E1} \rangle$ strength function data (see Ref. [29]). However, it seems that it is possible to detect it and explain it globally from the distribution of the total radiative widths as a function of mass (see e.g. [38]). Inspection of these data shows three distinct regions of enhanced $\langle \Gamma_\gamma \rangle$ values around a smooth trend curve, which correspond to well established non-statistical regions. Two of them are the well known double magic number regions with A=50-60 and A=200-210, corresponding to the 3s- and 4s-giant resonances in the s-wave neutron strength functions. The less distinct enhancement lies just above A=150 and is again associated with the non-statistical capture in the lower part of the double-humped 4s-giant resonance.

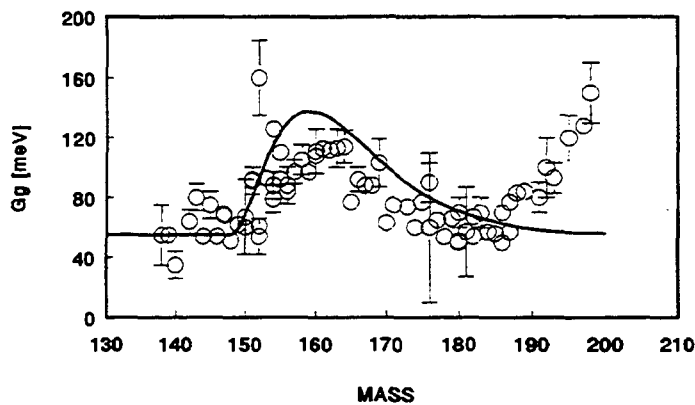


Fig. 5. The f_{E1} enhancement factor (from Eq. (8b)) plotted together with $\langle \Gamma_\gamma \rangle$ values, taken from [38], around the A = 150-170 mass region.

For a graphical comparison with our previous results on the f_{E1} enhancement, we have plotted the experimental $\langle \Gamma_\gamma \rangle$ values in the discussed mass region together with the calculated enhanced values of $\langle \Gamma_\gamma \rangle$. This calculation was based on application of the enhancement factor, as derived in Eq. (8b), on the mean value of $\langle \Gamma_\gamma \rangle = 60$ meV for nuclides with $A \leq 148$. The results displayed in Fig. 5 show very nice agreement of the enhancement factor with the experimental $\langle \Gamma_\gamma \rangle$ values, and support the explanation of this effect by a global enhancement of the total radiative width by the non-statistical reaction mechanism.

5.2 Other modes of excitation

The scatter of the individual enhancements is at least in part caused by the uncertainties of the various input data. In addition to the ingredients mentioned before, the deduced E1 enhancements also depend on the M1 strength employed. In general M1 radiation contributes only 10 to 20% to the radiative width or the capture cross section and so our often global assessments of its strength is in general of only moderate influence on the deduced trend of the enhancements.

A special caution, however, applies to strongly deformed nuclei where an isovector collective M1 excitation ("scissors mode") can be observed, *e.g.* in inelastic electron scattering or nuclear resonance fluorescence [32,33]. If Brink's hypothesis [12] holds also for the scissors mode it is conceivable that it apparently contributes to the enhancement of the E1 strength deduced for deformed nuclei from cross sections and related quantities. But we emphasise that for the targets $^{155,157,158}\text{Gd}$ the E1 enhancement is confirmed by average resonance capture data [5] for which, in contrast to cross sections and spectra, the E1 and M1 contributions can be separated. Moreover, a SLO scissors mode contribution to the M1 strength with parameters based on a theoretical assessment should lead for the target ^{155}Gd to a low energy peak around an emission energy of 3 MeV [5] in the gamma-ray spectra which is not confirmed by experimental data. On the other hand, recently the group in Prague [34] found preliminary evidence for a scissors mode in the analysis of two-step gamma-ray cascades following thermal neutron capture in ^{162}Dy . As these data are more sensitive than the total gamma-ray spectra the problem of a possible M1 scissors mode contribution to our observed E1-strength enhancements should be kept in mind. Furthermore, evidence has been very recently found for E1-enhanced gamma strength concentrated also around 3 MeV by the group in Oslo [35]. More information on these low energy excitations is definitely needed.

5.3 Influence of level density models

The strong dependence of the extracted E1 enhancement parameter k_0 on the level density model employed is not very satisfying. It probably represents the price for using oversimplified formulas that may fail to describe the energy dependence of the level density. We therefore compare for some representative cases the results obtained with KRK and BSFG level densities to those employing the more advanced GSFPH model. The dependence of the cross sections on the level density model stems from two sources: i) the temperature entering into the E1 strength functions, and ii) the level density itself determining the number of final states in the Hauser-Feshbach formula. In Fig. 6 we compare for ^{106}Pd , ^{158}Gd and ^{198}Au the E1 strength functions according to the EGLO model with an enhancement k_0 that is a compromise between the requirements of the KRK and the BSFG models, as well as the level densities summed over those spin values populated by s-wave capture assuming dipole radiation only. Figs. 7a-c show that due to the different temperatures at a given excitation energy the EGLO strength for the BSFG

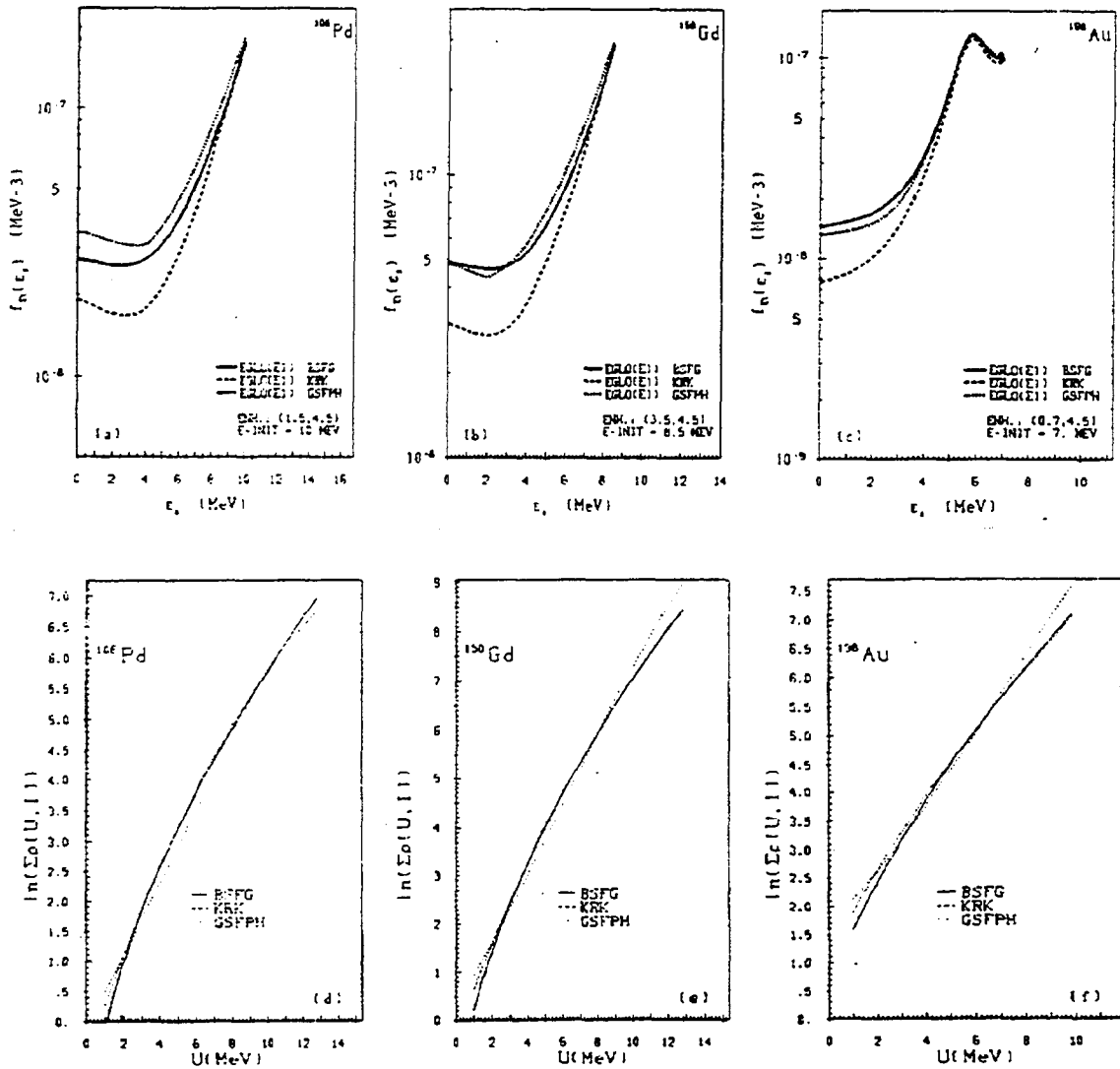


Fig. 6. The E1 strength functions (a-c) for a given initial energy E-INIT and level densities (d-f) for ^{106}Pd , ^{158}Gd and ^{198}Au , respectively, calculated with three level density models (see text).

model is considerably larger than for the KRK, and comparable to that resulting from the GSFPH model; for ^{198}Au the effect of the pygmy resonance is visible. The summed level densities for ^{106}Pd and ^{158}Gd (Figs. 7d and e) show that in the excitation energy region relevant for the capture cross sections considered here, BSFG results in larger values than KRK (actually its constant temperature region). These results, which are typical for many targets, are less pronounced for ^{198}Au (Fig. 7f). For ^{106}Pd and ^{159}Gd and to a lesser extent for ^{198}Au the more sophisticated GSFPH model supports the energy dependence of the level density resulting from the BSFG model. The somewhat deviating behaviour of ^{198}Au may be related to the large negative shell correction energy due to the nearby major ($Z=82$, $N=126$) shell closure.

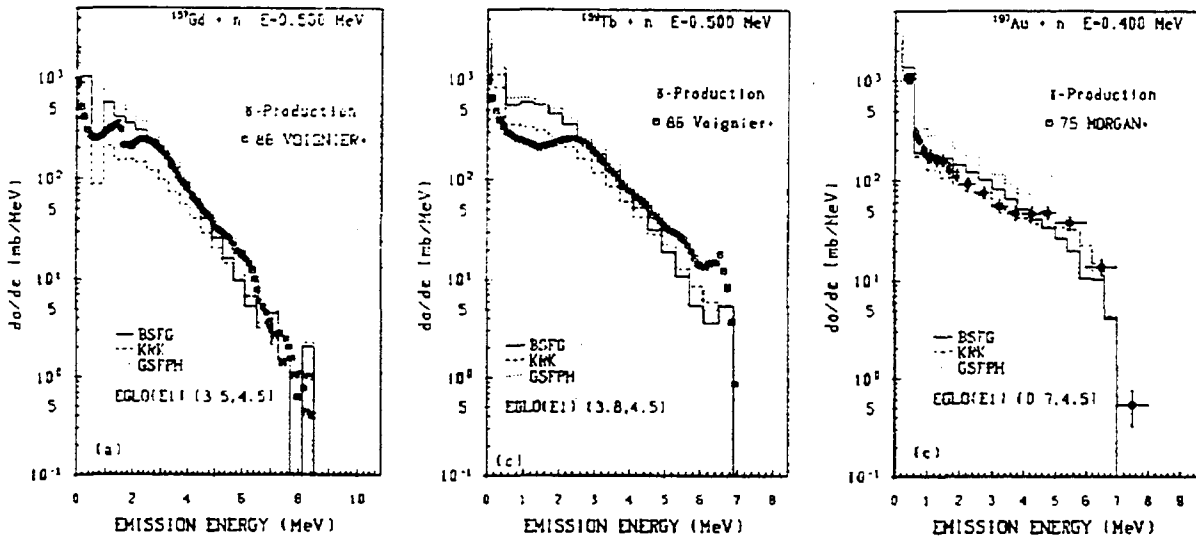


Fig. 7. : The neutron capture cross sections for ^{105}Pd (a), ^{157}Gd (b), and ^{197}Au (c) calculated with three models for the level densities (see text).

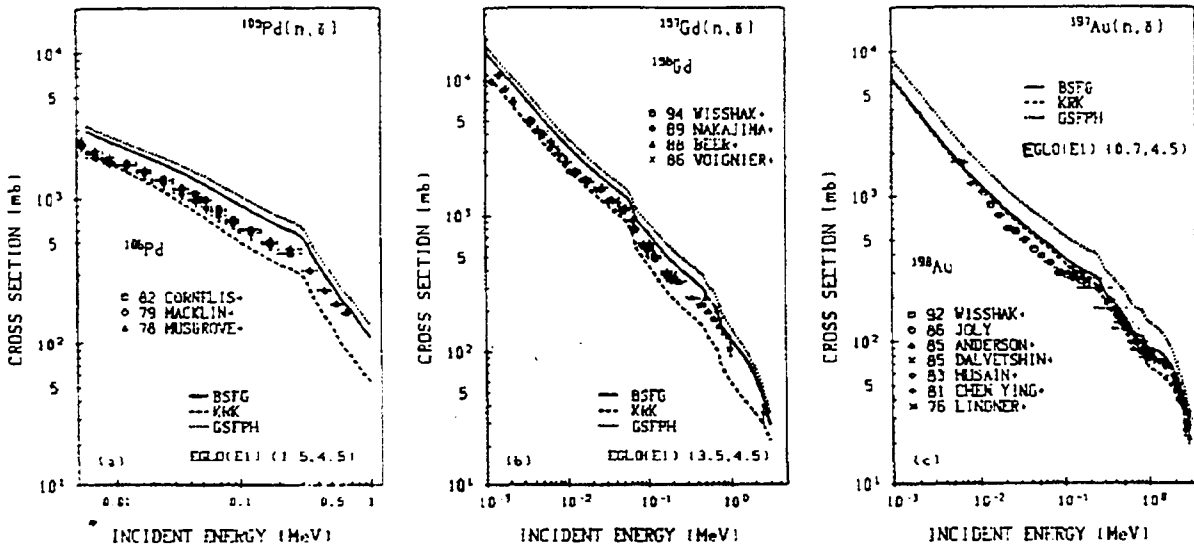


Fig. 8. The gamma-ray production spectrum resulting from neutron capture in ^{157}Gd (a), ^{159}Tb (b), and ^{197}Au (c), calculated with three models for the level density (see text).

Fig. 7 displays the neutron capture excitation functions for ^{105}Pd , ^{157}Gd and ^{197}Au calculated with the EGLO model for the E1 strength and the enhancements indicated in Figs. 7a-c. The underlying level densities result from employing the BSGF, KRK, and GSFPH models. The shape of the excitation functions only weakly depends on the level

density model employed. The difference in magnitude of the cross sections represents the combined effect of the temperature dependence of the E1 strength according to the EGLO model and the level density itself as illustrated in Fig. 7. These examples also illustrate why in general the enhancements k_0 required to reproduce the data are considerably larger for the KRK than for the BSFG model. The results obtained with the GSFPH model are closer to those with the BSFG model; for ^{105}Pd and ^{157}Gd the difference in the cross sections is quite small.

A comparison of the gamma-ray spectra for ^{157}Gd , ^{159}Tb and ^{197}Au obtained under the same conditions as the aforementioned excitation functions is displayed in Fig. 8. Note that the experimental data for ^{157}Gd and ^{159}Tb by Voignier et al. [37] begin at an emission energy of 1.5 MeV; below that energy the authors extrapolated by a model calculation. The spectra of ^{157}Gd and ^{159}Tb (Figs. 8a-b) are quite representative; their shape only weakly depends on the level density model chosen. The slope in the central region of emission energies is slightly better reproduced by the KRK model, but the effect is marginal. The GSFPH and the BSFG results are very close. For ^{197}Au (Fig. 7c) the best reproduction of the experimental data is achieved with the KRK model; the worst with the BSFG model. However, because of the large negative shell correction energy and the presence of a pygmy resonance, ^{197}Au is perhaps not very typical. In general neither the shape of excitation functions nor that of the gamma-ray spectra critically depend on the underlying level density model.

These preliminary comparisons seem to indicate that the results obtained with the simple BSFG model are closer to those obtained by using the more realistic GSFPH model. However, before concluding that among the two simple models BSFG should be preferred for most nuclei, comparisons such as those described before must be performed for a much larger sample of nuclei.

5.4 Low-multiplicity cascade spectra

In the calculation of the type of data considered here the product of level densities and gamma-ray strength functions always enters. Hence the purely empirical expression Eq. (4) for the enhancement may also affect conclusions concerning the level density. Therefore the analysis of additional experimental data which depend more critically on the level density model than excitation functions and spectra may prove useful. This has been demonstrated for thermal capture by Becvar et al. (see e.g. Ref. [32]) in the two-step cascade method. Preliminary calculations show that the energy distribution of gamma-ray cascades with fixed low multiplicity resulting from neutron capture in the keV region have also this property. This is illustrated in Fig. 9 by the spectra of multiplicity-two cascades for the targets ^{150}Sm , ^{157}Gd , and ^{197}Au . For each level density model the E1 strength is calculated according to the EGLO model with enhancements chosen to reproduce the capture cross section at an incident energy of 100 keV. The strong dependence of the shape and the intensity (that is, the multiplicity distribution) of the spectra is evident. Preliminary experimental data by the Karlsruhe group [37] concerning

relative spectra with fixed multiplicities support shapes of the spectra for ^{150}Sm between those obtained with the GSFPH and the BSFG model. In the case of ^{197}Au the experimental spectra favour shapes between those resulting from the GSFPH and the KRK model. As the multiplicity 2 spectra also depend on the E1 strength function model (but hopefully to a lesser extent) one should aim at a simultaneous reproduction of as many different experimental data as possible.

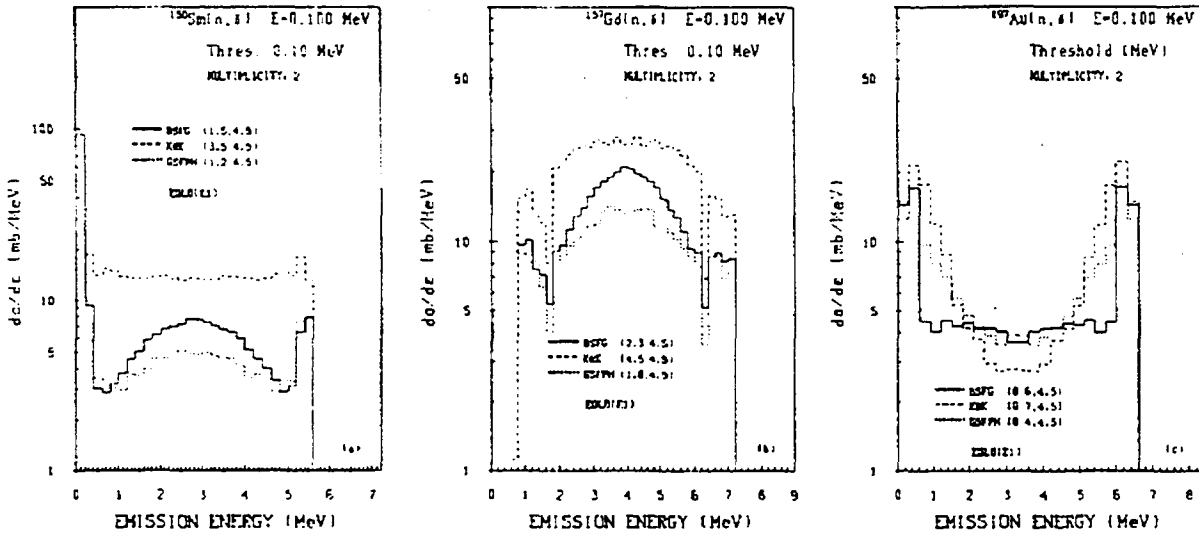


Fig. 9. The spectra of gamma-ray cascades with multiplicity 2 resulting from the capture of 100 keV neutrons in ^{150}Sm (a), ^{157}Gd (b), and ^{197}Au (c). (see text).

5.5 Summary

Summarising, we may state that the flexible enhanced generalised Lorentzian model (EGLO) for the E1 strength function is useful for the calculation of capture cross sections and related quantities since its parameters exhibit a reasonably smooth behaviour. The required enhancement depends on the level density model employed. Therefore a realistic level density model should be used. It seems at present that the BSFG model is the best solution for practical applications. This results also in the applicability of the enhanced generalised Lorentzian (EGLO) for nuclei outside the $A=150-170$ range, because $k_0=1$ in Eq. (8b) and EGLO is identical to GLO. In view of our empirical formulation of the enhancement of the width of the generalised Lorentzian, a better understanding of the effect and a subsequent theoretical description would be very helpful.

Very recently Plujko has presented a new model [40] for the f_{E1} radiative strength function, based on a microcanonical ensemble of initial states. The resulting formula has the same features as the Kadenskij *et al.* approach [19], namely the energy and temperature dependence of the GDR width and the non-zero limit for $E_\gamma \rightarrow 0$. This work provides independent theoretical support for the GLO formalism.

References

- [1] J. Kopecky and M. Uhl, Phys. Rev. **C41**, 1941 (1990).
- [2] M. Uhl and J. Kopecky, "Calculations of Capture Cross Sections and Gamma-Ray Spectra as a Tool for Testing Strength Function Models", INDC(NDS)-238 (1990). p.113.
- [3] J. Kopecky, Proc. VII. Int. Symposium on Capture Gamma-ray Spectroscopy and Related Topics (AIP Conf. Proc. No. 238, AIP, New York, 1991), p. 607.
- [4] M. Uhl and J. Kopecky, Proc. Int. Conf. Nuclear Data for Science and Technology, Juelich, 1991 (Springer-Verlag, Berlin/Heidelberg, 1992), p. 977.
- [5] J. Kopecky, M. Uhl and R.E. Chrien, "Distribution of Radiative Strength in Gd-156, 157 and 158 Nuclei, ECN-RX-92-011 (April 1992).
- [6] J. Kopecky and M. Uhl, Proc. Int. Symposium on Nuclear Data Evaluation Methodology, Brookhaven, 1992 (World Scientific, Singapore, 1993), p.381.
- [7] M. Uhl and J. Kopecky, Proc. Int. Symp. on Nuclear Astrophysics, Karlsruhe, 1992 (IOP Publishing Company Ltd., 1993), p. 259.
- [8] J. Kopecky, M. Uhl and R.E. Chrien, Phys. Rev. **C47**, 312 (1993).
- [9] M. Uhl and J. Kopecky, Proc.Int.Conf. Nuclear Data for Science and Technology, Gatlinburg, 1994 (American Nuclear Soc., La Grange Park, 1994), p. 438.
- [10] M. Uhl and J. Kopecky, "Gamma-ray Strength Function Models and their Parameterization", INDC(NDS)-335 (May 1995), p. 157.
- [11] M. Blatt and V.F. Weisskopf. Theoretical Nuclear Physics, p. 647, Wiley, New York, (1952).
- [12] D.M. Brink, Ph. D. Thesis, Oxford University, (1955).
- [13] S.S. Dietrich and B.L. Berman, At. Nucl. Data Tables **38**, 199 (1988).
- [14] A.G. Bohr and B.R. Mottelson, Nuclear Structure, Vol.II, p. 636, Benjamin, London, (1975).
- [15] J. Kopecky and M. Uhl, Proc. IAEA Specialists' Meeting on the Measurement, Calculation and Evaluation of Photon Production Cross Sections, Feb. 5-7, 1990. Smolenice, (CSFR), p. 103, INDC(NDS)- 238(1990).
- [16] J. Speth and A. van der Woude, Rep. Progr. Phys. **44**, 719 (1981).
- [17] W. V. Prestwich, M. A. Islam, and T. J. Kennet, Z. Phys. **A315**, 103 (1984).
- [18] D. Pines and D. Nozier, The Theory of Quantum Liquids, Benjamin, New York (1966).
- [19] S.G. Kadenskij, V.P. Markushev, and V.L. Furman, Sov. J. Nucl. Phys. **37**, 165 (1983).
- [20] J. Kopecky and R.E. Chrien, Nucl. Phys. **A468**, 285 (1987).
- [21] P. A. Moldauer, Nucl.Phys. **A344**, 185 (1980).
- [22] M. Uhl (unpublished).
- [23] W. Dilg, W. Schantl, H. Vonach and M. Uhl, Nucl.Phys. **A217**, 269 (1973).
- [24] S.K. Kataria, V.S. Ramamurthy, and S.S. Kapoor, Phys.Rev. **C18**, 549 (1978).
- [25] A. Gilbert and A.G.W. Cameron, Can. J. Phys. **43**, 1446 (1965).

- [26] A.V. Ignatyuk, K.K. Istekov, and G.N. Smirenkin, *Sov. J. Nucl. Phys.* **29**, 450 (1979).
- [27] O.T. Grudzevich, A.V. Ignatyuk, V.L. Plyaskin, and A.V. Zelenetsky, *Proc. Int. Conf. Nuclear Data for Science and Technology*, May 30 - June 3, 1988, Mito, Japan, edited by S. Igarasi, p. 187, Saikon, Japan (1988).
- [28] A.V. Ignatyuk, *Proc.Int.Symposium on Nuclear Data Evaluation Methodology*, 12-16 Oct, 1992, Brookhaven National Laboratory, Upton, New York, p. 411, World Scientific, Singapore (1993).
- [29] J. Kopecky and M. Uhl, "Present Status of Experimental Gamma Ray Strength Functions", *ENEA/NSC/Doc (95) 1*, 119 and *ECN-RX-94-103*.
- [30] S.Raman, in *Neutron-Capture gamma Ray Spectroscopy and related Topics 1981*, (The Institute of Physics, Bristol and London, 1982), p.357.
- [31] F. Becvar *et al.*, in *Capture Gamma Ray Spectroscopy 1987*, (Institute of Physics Series 88), p.649, and private communication.
- [32] D. Zavischa, M. Macfarlane, and J. Speth, *Phys. Rev.* **C42**, 1461 (1990).
- [33] A. Richter, *Nucl.Phys.* **A522**, 139 (1991).
- [34] F. Becvar, P. Cejnar, J. Honzatko, K. Konecny, I. Tomandl and R.E. Chrien, *Phys. Rev.* **C52**, 1278 (1995).
- [35] T.S. Tveter, L. Bergholt, M. Guttormsen and J. Rekstad, *Phys. Rev. Letters* **77**, 2404 (1996).
- [36] J. Voignier, S. Joly, and G. Grenier, *Nucl. Sci. Eng.* **93**, 43 (1986); **96**, 343 (1987).
- [37] K. Wisshak, private communication (1992).
- [38] S.F. Mughabghab, M. Divadeenam, and N.E. Holden, *Neutron Cross Sections* (Academic, New York), Vol. 1, Part A and B.
- [39] Huang Zhongfu, *Com. of Nuclear Data Progress*, No 9, 60 (1993).
- [40] V.A. Plujko, "Radiative Strength Functions as a Tool in Studying of Mechanisms of the Nuclear Dissipation", *Contribution to Int.Conf. Nuclear Data for Science and Technology*, Trieste, May 1997, to be published.

RECOMMENDATIONS FOR PRE-EQUILIBRIUM CALCULATIONS

E. Běták

Institute of Physics, Slov. Acad. Sci., 84228 Bratislava, Slovakia

Abstract

Usually, one employs in pre-equilibrium calculations the the same values of input parameters as are used in compound nucleus calculations. However, as the compound-nucleus values already contain some averaging over all possible reaction mechanisms, the preferred way should be do decompose them back into contributions from the various mechanisms. Technically this is not easily done, but some departure of the pre-equilibrium parameters from their compound-nucleus values can effectively compensate this averaging.

1 Introduction

Pre-equilibrium calculations depend on a wide set of parameters of different types. Some of these are common to other types of reaction formalisms, while some are specific for the pre-equilibrium stage of the reaction. In the following, we will review some of the parameters used specifically in the pre-equilibrium models, and also some of those which, although used also in equilibrium (compound nucleus) calculations, have somewhat different forms when used in the pre-equilibrium stage. One should refer also to the recent IAEA CRP meeting on the Reference Input Parameter Library [1], in which a great deal of relevant information can be found.

2 Basic pre-equilibrium parameters

Apart from general reaction parameters, such as binding energies, transmission coefficients (and/or inverse reaction cross sections), spins (and parities) of the participating nuclei, etc., pre-equilibrium calculations strongly depend on the initial exciton number, transition matrix element (or other parameter which determines the "strength" or fraction of pre-equilibrium decay), and charge factor (as an alternative to the two-component treatment for the target nucleons). Additionally, as the pre-equilibrium emission rates are proportional not to the exponential of energy, as the equilibrium

(compound nucleus) calculations are, but rather to a polynomial in energy, their dependence on relatively well known quantities (such as the level densities and their parameters) may be differently sensitive to the details than the equilibrium calculations are. An additional potential source of ambiguities is hidden in the gluing together of the pre-equilibrium and the equilibrium parts of the calculation (if one does not use a unique formalism throughout all stages of the reaction).

3 Initial exciton number

One of the most important quantities or parameters in pre-equilibrium models is the initial exciton number. Although originally treated simply as a free parameter, in later years values used for this quantity have achieved some (not very firm) validity. Analyses of the nucleon spectra from nucleon-induced reactions usually lead to the value of $n_0 = 3$ and to $n_0 = 4 - 6$ in the case of reactions induced by α particles¹. A general philosophy would yield $n_0 = A_{proj}$, at least insofar as we can ignore the mutual interaction of the Coulomb fields of the target and projectile and if we can ignore fine details of the structure (or statistics) of nuclei. It is important to note that (up to a tiny fraction of the cross section due to radiative capture, which is typically between 10^{-4} to 10^{-3} of the reaction cross section at typical incident energies) the value of $n_0 = 1$ yields indistinguishable results from those with $n_0 = 3$, so that the general philosophy does not contradict the results of systematic analysis.

We recommend the adoption of this philosophy as a starting point for blind calculations. If sufficient data of reasonable quality is available, more detailed even-odd effects (or so-called active and passive particles/holes) may enter the calculations.

4 Charge factor

The charge factor has been introduced into pre-equilibrium decay as a compensation for replacing its two-component (proton-neutron) nature with a one-component formalism [2]. There is a plentiful variety of approaches to this problem. Three of these have become widely used, namely: *i*) no charge factor at all; *ii*) R -charge factor of Kalbach [2] with equilibrium limit (for nucleons) $\approx \frac{1}{2}$; and *iii*) Q -charge factor (again of Kalbach [3]), with the nucleon equilibrium limit of ≈ 1 . The first case clearly is not suitable for pre-equilibrium reactions, as it does not reflect in any way the charge composition of the freshly created composite system at the early stage of a reaction. Apart from some small deviations for nuclei with $N \neq Z$, the two other factors differ just by a factor of 2, which is compensated by adjusting another parameter, namely $|M|^2$. Thus, in practical applications, both the factors R and Q yield very similar

¹The data on reactions induced by deuterons, helions and tritons have not been analyzed sufficiently systematically. Reactions of heavy ions are so specific that we cannot include them in this short report.

results (some deviations may be found for heavier nuclei and/or far off the line of the β -stability, where $N \neq Z$, but generally they are not significant) and the main controversy is in the theoretical justification of the charge factors, not so much in their predictions.

5 Intranuclear transition matrix element

While the emission rates can be expressed in an unique way, the strength of the equilibration process, which competes with the emission, is not so straightforwardly determined. Very often a value corresponding to the average transition matrix element of the residual interaction is employed as a parameter, or some other value of similar effect (as *e.g.* the "multiplication factor" k in the hybrid model). In principle, some functional dependence of such a parameter can be derived, and only the proportionality constant remains as a free parameter, which is obtained from systematics. As slight variations among different formulae yield similar behaviour of the squared matrix element (a decreasing function of both the excitation energy of a composite system and of its mass number), these slight differences among various functional dependences are in practice compensated by altering the value of the corresponding proportionality constant. Therefore, the exact form of the dependence is usually not essential for calculations of a specific reaction (but may be seen when one ranges over all possible masses of the nuclei and/or energies).

Codes that incorporate the exciton model most often use the matrix element in the form suggested by Kalbach, *i.e.* either $|M|^2 = KA^{-3}E^{-1}$, or in a somewhat more sophisticated form dependent on the per-exciton energy, which for the per-exciton excitation energy e ($e = E/n$) between 7 and 15 MeV takes formally the same form, $|M|^2 = K'A^{-3}e^{-1}$ and is more complicated outside the interval quoted [4]. The exact value of the matrix element constant K' is (to some extent) dependent also on other details of the calculation. Thus, PEQAG [5] gives best overall results with $K' = 100 - 110 \text{ MeV}^3$, and GNASH [6] with a somewhat higher value of 130-160 MeV^3 . The slight difference may be caused by different charge factors used, and also by possible inclusion of direct reactions in GNASH.

However, especially near the closed shells, significant departures from the generally accepted value may be observed. And when used together with so-called realistic densities, there is no reasonable guidance up to the present time.

6 Level densities

The level densities have been addressed already in the RIPL (Reference Input Parameter Library) meeting for the general case of nuclear reactions [1]. The recommendations there are, nevertheless, more general, as they apply as well to all types of reaction calculations. Pre-equilibrium calculations of γ emission are in some sense a

specific case, and we therefore include additional details here. According to calculations performed at Bratislava, it is advisable to use proper (*i.e.* individual for each nucleus) level density parameters (g or a plus pairing; *e.g.* of the Gilbert-Cameron type, though in some more updated form (see, *e.g.*, [7, 8, 9, 10, 11, 12])), at least if the equidistant-spacing scheme is used consistently for the pre-equilibrium stage, at least for the case when the approximation of the equidistant scheme of levels is used for a complete calculation.

This conclusion is not so unique for calculations combined with discrete levels, especially if they extend sufficiently high in energy. Calculations performed at Bratislava indicate that probably an "overall" value of g without any pairing-energy corrections would be a reasonable solution for such a case. This value should not strongly fluctuate from one nucleus to another, but should allow for significant deviation from the "straight-line trend" of $g = A/13$, particularly for cases close to ^{208}Pb . This conclusion is of preliminary nature at present.

As for the details of pairing, the situation is not very clear, although there are some indications that a sophisticated treatment of pairing dependent on the excitation number (as originally suggested by Ignatyuk and put into a more friendly form by Fu) does a better job than the classical one, in which pairing is treated the same way for all the exciton states.

There is also an important question of parity in the pre-equilibrium calculations, especially for γ emission. It has been addressed partially by Antalík [13] and studied in more detail by Obložinský [14]. The parity effect is smeared out if both parities are equally populated in the reaction, but may be of some importance where one of the parities prevails, which is a rather frequent situation at low excitations (say, below the nucleon binding energy).

7 Parameters specific to γ emission

Here, in practice, the only really specific quantity which enters γ emission calculations (at excitation energies of several tens of MeV) is the form of the photoabsorption cross section, usually taken as the Lorentzian form of the GDR. Though clearly the experimental cross sections are preferred, tabulated values (if available) of the GDR (double-peaked for deformed nuclei) give a reasonable fit to the data. Additionally, there is some indication that one should prefer a generalized Lorentzian (with energy-dependent width) to the standard one [15].

References

- [1] IAEA Final Report from the CRP Meeting on Reference Input Parameter Library (Trieste, May 1997) (*preliminary draft obtainable via ftp from IAEA*).

- [2] C. K. Cline, Nucl. Phys. **A193**, 417 (1972).
- [3] C. Kalbach, Z. Phys. **A283**, 401 (1977).
- [4] C. Kalbach, Z. Phys. **A287**, 319 (1978).
- [5] E. Běták, Report INDC(CSR)-016/LJ (IAEA Vienna 1989).
- [6] P. G. Young, E. D. Arthur, M. B. Chadwick, Report LA-12343-MS (UC-413) (Los Alamos 1992); updated 22 Sept., 1995; M. B. Chadwick, P. G. Young, private communication.
- [7] A. Gilbert, A. G. W. Cameron, Can. J. Phys. **43**, 1446 (1965).
- [8] U. Facchini, E. Saetta-Menichella, Energ. Nucl. **15**, 54 (1968).
- [9] W. Dilg, W. Schantl, H. Vonach, Nucl. Phys. **A217**, 269 (1973).
- [10] G. Rohr, Z. Phys. **A318**, 299 (1984).
- [11] A. S. Iljinov, M. V. Mebel, N. Bianchi, S. E. De Sancti, V. Lucheroni, W. Mucifora, E. Polli, A. R. Reolin, P. Rossi, Nucl. Phys. **A543**, 517 (1992).
- [12] A. Mengoni, Y. Nakajima, J. Nucl. Sci. Technol. **3**, 535 (1994).
- [13] R. Antalík, in *Neutron Induced Reactions, Proc. Europhys. Top. Conf.*, June 21-25, 1982, Smolenice, Ed. P. Obložinský (Inst. Phys. SAS, Bratislava 1982), p. 357.
- [14] P. Obložinský, Phys. Rev. **C41**, 401 (1990).
- [15] E. Běták, J. Kopecky, F. Cvelbar, Phys. Rev. **C46**, 945 (1992);
E. Běták, F. Cvelbar, A. Likar, in *Int. Conf. Nucl. React. Mech.*, Varenna 1997.

Recommendations for DSD Model Calculations

F. Cvelbar

*"J. Stefan" Institute and Faculty of Mathematics and Physics,
University of Ljubljana, Slovenia*

Abstract

The latest achievements of the DSD (direct-semidirect) capture model, such as the extension to unbound final states or to densely distributed bound states, and the introduction of the consistent DSD model are reviewed. Recommendations for the future use of the model are presented.

1 General

The DSD model([1],[2]) is the best available model for the calculation of radiative capture of polarised and unpolarised nucleons in the region of the GDR and also of the isoscalar and isovector quadrupole GR ([3]). It has proved successful in reproducing differential cross sections for nucleon capture to the well defined single particle states of not too high spin. On the basis of this model one can therefore calculate the γ -ray spectra and energy integrated capture cross sections in the region near closed shell nuclei for applications such as reactions involving 14 MeV neutrons from fusion reactors.

In the present CRP attention has been paid to the general behaviour of the model (such as the mass dependence of 14 MeV neutron capture results) and to some its fundamental questions (radiative capture to unbound states, particle - collective vibration coupling (PVC)).

The classical DSD model had been formulated to describe only the transitions to the bound states. Recently (partly also in the framework of the present CRP) Dietrich, Chadwick and Kermann ([4], see also [5], [6]) have reformulated the model to cover also the transitions to the unbound states. The authors call this version of the model the **Extended DSD** (EDSD) model.

On the other hand Likar and Vidmar (also partly supported by the present CRP) eliminated the need for the imaginary part (W_1) of the PVC to be considered a free parameter by equating the current and density form of the effective (dressed) electric

multipole operator (see *e.g.*[3]). As this procedure requires consistent treatment of the equation of continuity, the authors name this approach to the DSD model the **Consistent DSD (CDS D)** model.

2 Recommendations

2.1 "Extended DSD" (EDSD) model

1. Using the EDSD model, for the first time in the history of the DSD model one is able to calculate the spectrum of γ -rays corresponding to capture of nucleons to unbound states. The population of these states and also of bound states close to the nucleon binding energy has been in the past experimentally rather uncertain. New calculations using EDSD should stimulate interest in reexamining experimentally the corresponding part of the γ -ray spectra.

2. The use of the optical model to describe unbound final states has been in [6] extended also to the region of dense bound states just below the threshold for particle emission. This method should deserve more attention in the future. It could prove useful for the calculation of the complete radiative capture γ -ray spectra including the energy region where single particle structure is not evident. The challenge here is that the imaginary part of the potential suitable for the bound state region has not yet been studied intensively enough.

2.2 "Consistent DSD" (CDS D) model

1. The form of the effective electric dipole (multipole) operator has been in the CDS D model obtained phenomenologically just by multiplying its current and density expressions by a factor $(1+F(r))$ and equating them [3]. It remains now to understand the microscopic background of this successful procedure.

2. The CDS D model has not yet been applied to the capture of polarised nucleons.

3. In the near future the consistent approach should be introduced also in the extended DSD model.

2.3 DSD model in general

The DSD model can be considered as a semimicroscopic one. Only its fundamental "ansatz" is microscopic. In the final development of the formulas, besides the strengths of the particle-vibration coupling mentioned above, experimental or classical parameters describing the giant dipole (multipole) resonances (Energy E_R and width Γ) are introduced. The exhausted part of the sum rule f_s , which also appears in the final expression for the cross section, may be extracted only from the experimental data. If the aim of the calculation is to follow the general trend of the cross

sections, classical parameters (see *e.g.* [9]) serve reasonably well. For the comparison of the calculated and experimental cross sections, experimental giant resonance parameters should be used. One can find an extensive collection of these data in [8]. Sometimes one can profit from evaluated and graphically presented mass dependences of the parameters in question, as *e.g.* in Ref. [9].

As mentioned above, the DSD model has failed to describe the angular distribution of γ -rays from radiative capture of nucleons to high spin states (*e.g.* $2g_{9/2}$ and $1i_{11/2}$ in Pb^{209} [7]). To study in detail this drawback theoretically and experimentally remains a task for future research in this field.

References

- [1] C. L. Clement, A. M. Lane and J. A. Rook, Nucl. Phys. **66**, 273,293 (1965).
- [2] M. Potokar, Phys. Lett. **B46**, 346 (1973).
- [3] A. Likar and T. Vidmar, Nucl. Phys. **A591**, 458 (1996).
- [4] W. E. Parker *et al.*, Phys. Rev. **C52**, 252 (1995).
- [5] F. S. Dietrich, in *Capture Gamma-Ray Spectroscopy and Related Topics*, Ed. S.Raman, AIP conf. Ser. No 125, 1984.
- [6] F. S. Dietrich, M. B. Chadwick and A. K. Kerman, in INDC(NDS)-357 (1996).
- [7] S. E. King, M. Potokar, N. R. Robertson, H. R. Weller and D. R. Tilley, Nucl. Phys. **A384**, 129 (1982).
- [8] E. G. Fuller, H. M. Gerstenberg, H. Van der Molen, and T. C. Dunn, *Photonuclear Reaction Data*, NBS, Washington, 1973.
- [9] J. Speth and A. Van der Woude, Rept. Prog. Phys. **44**, 719 (1981).

4 Compilations and Evaluations

Several contributions of this Chapter concern critical tests of evaluations available in the various data files. In particular, a report on the status of experimental and evaluated data availability for discrete γ -ray produced by 14.5 MeV neutrons is included here. The effort of producing an *Atlas of Neutron Capture Cross Section* was initiated by the CRP and is documented here with a data-base of more than 737 target nuclei. This Atlas has been made available on the network at the Internet address of the Web server of the IAEA Nuclear Data Section <http://iaeaand.iaea.or.at/ngatlas>. An updated compilation of γ -ray strength functions in extensive nuclear mass ranges show the considerable amount of data accumulated and critically analyzed in the course of the CRP work.

New evaluations of the neutron capture cross sections for some light nuclei (some Li, C and O isotopes) are reported here. Evaluations of photon production rates by the most studied structural materials, Fe and Ni, together with a critical analysis of the available evaluations of photon production data for ${}^7\text{Li}$ and ${}^{52}\text{Cr}$ have been also made part of the CRP successful tasks.

The present Chapter includes 7 papers to be found in the following pages.

STATUS OF EXPERIMENTAL AND EVALUATED DATA FOR DISCRETE GAMMA-RAY PRODUCTION AT 14.5 MeV NEUTRON INCIDENT ENERGY

S. P. Simakov¹, A. Pavlik², H. Vonach², S. Hlavac³

¹Institute of Physics and Power Engineering, Obninsk, Russia

²Institut fuer Radiumforschung und Kernphysik, University of Vienna, Vienna, Austria

³Institute of Physics SAS, Bratislava, Slovakia

The experimental data on discrete γ -ray production cross-sections from (n,x γ) reactions at 14 MeV neutron energy, measured in different laboratories beginning from 1960 up to today, are reviewed and compiled. In all, a total 36 elements plus 8 enriched isotopes from Li to Bi, those which are requested in WREND A 93/94 [1] and/or included in the general purpose FENDL-1 [2] library, were selected for compilation. For every nucleus all γ -ray transitions, confirmed by at least two experiments or included an adopted excited level scheme, were incorporated (about 1050 experimental points were considered).

The following information about every experiment was collected: incident neutron energy; the material, sizes and weight of the sample; detector type; angles at which γ -rays were detected; whether the prompt part or the total γ -production were measured; whether the measured cross sections were corrected for attenuation of neutron and γ -ray fluxes and multiple neutron scattering in the sample; and the method of absolute normalization and use of reference cross sections. This information was derived from original publications, EXFOR libraries, or from private communications with authors.

Then this data base was critically analyzed: all cross sections were interpolated to 14.5 MeV incident neutron energy (the gradients of γ -ray production of specific energy were derived from experimental or ENDF/B6 data). Some measured cross sections were renormalized taking into account modern reference cross sections. The data measured at angles different from 55 or 125 degrees were corrected for angular dependence of the γ -yield, where such information was available from experiment or ENDF/B6 evaluation, or else uncertainties were increased in other cases. Uncertainties less than 6% were increased up to this level. The unresolved transitions and obviously erroneous experimental results (those that differ from the mean by factor more than 3-4) were skipped.

Finally estimated cross sections for each γ -ray transition were obtained by weighting the individual experimental data $\sigma_i(E_\gamma)$, taking into account the relative uncertainties $\Delta\sigma_i(E_\gamma)/\sigma_i(E_\gamma)$:

$$\sigma(E_\gamma) = \frac{\sum_{i=1}^n \sigma_i(E_\gamma) / (\Delta\sigma_i(E_\gamma) / \sigma_i(E_\gamma))^2}{\sum_{i=1}^n 1 / (\Delta\sigma_i(E_\gamma) / \sigma_i(E_\gamma))^2}$$

The uncertainty of the cross section for each transition was estimated as the maximum of the internal (the weighted quadratic sum of the original experiments' uncertainties) and the external (the weighted quadratic sum of the deviations from average) ones:

$$\Delta\sigma^{\text{int}}(E_\gamma) = \frac{\sqrt{\sum_{i=1}^n \Delta\sigma_i^2(E_\gamma) / (\Delta\sigma_i(E_\gamma) / \sigma_i(E_\gamma))^4}}{\sum_{i=1}^n 1 / (\Delta\sigma_i(E_\gamma) / \sigma_i(E_\gamma))^2}, \text{ and}$$

$$\Delta\sigma^{\text{ext}}(E_\gamma) = \sqrt{\frac{\sum_{i=1}^n (\sigma_i(E_\gamma) - \sigma(E_\gamma))^2 \times 1 / (\Delta\sigma_i(E_\gamma) / \sigma_i(E_\gamma))^2}{(n-1) \times \sum_{i=1}^n 1 / (\Delta\sigma_i(E_\gamma) / \sigma_i(E_\gamma))^2}}$$

Typically the external uncertainties are larger, except for cases in which the differences between the cross sections, measured in two or three laboratories, are less than reported errors.

Table 1 lists the WREND A requests, which are usually formulated as requirements for total and energy-angular differential cross sections. For quantitative comparison with practical demands and estimation of the status of experimental and evaluated data, the relative uncertainty of the total (sum of N_γ) discrete production cross sections σ and the uncertainty of energy-differential (averaged over available discrete transitions) spectra S were calculated:

$$\Delta\sigma / \sigma = \frac{\sqrt{\sum_{E_\gamma} (\Delta\sigma(E_\gamma))^2}}{\sum_{E_\gamma} \sigma(E_\gamma)}; \quad \Delta S / S = \frac{\sum_{E_\gamma} (\sigma(E_\gamma) \times (\Delta\sigma(E_\gamma) / \sigma(E_\gamma)))}{\sum_{E_\gamma} \sigma(E_\gamma)}$$

The estimated experimental uncertainties, obtained in the present work, are listed in Table 1. From the comparison with WREND A requests, the status of the experimental data is indicated. A request is regarded as satisfied (Y) if the uncertainties of both total and differential cross sections are less than the requested one, as unsatisfied (N) if greater, and intermediate (YN) if the total cross section meets the request and the differential one does not. The symbol Y(?) denotes that although the experimental data satisfy the requirements, they were measured in only one experiment.

The evaluated data libraries usually contain the cross-sections for γ -ray transitions between excited levels of residual nuclei (files 12, 13) and continuous photon energy spectra (Files 6, 15), which may show sharp peaks. The sums of these contributions (inter-level cascades and discrete intensities from continuous energy distributions) were regarded as evaluated discrete γ -ray production cross sections. The status (quality Q) of evaluated

data libraries (FENDL-1 [2], BROND-2 [3], ENDF/B6 [4]) was estimated by comparison with experimental data for the total Q_{tot} and averaged over evaluated energy differential Q_{dif} discrete production cross sections as follows:

$$Q_{tot} = (\sigma^{eval} - \sigma^{exp}) / \Delta\sigma^{exp}; \quad Q_{dif} = \frac{\sum_{E_\gamma} \sigma^{eval}(E_\gamma) \times |\sigma^{eval}(E_\gamma) - \sigma^{exp}(E_\gamma)| / \Delta\sigma^{exp}(E_\gamma)}{\sum_{E_\gamma} \sigma^{eval}(E_\gamma)}$$

These criteria indicated the quality of the comparison between the experimental and evaluated data, taking account of the experimental uncertainties. Thus when $-1 \leq Q \leq 1$, the status of the evaluated library was regarded as satisfactory (Y), otherwise unsatisfactory (N).

Detailed information is included in Table 1, Figure 1, and Reference [5]. The general conclusions are the following:

Experimental data:

- nuclei for which discrete γ -ray production cross sections have not yet been measured, and which may be regarded as first candidates for experimental investigation are Zr, Sn, Cs, Ba, Ta, and W;
- there are few measurements for separated isotopes;
- nuclei for which discrete γ -ray production cross sections have been measured in only one experiment, and thus should be checked by other independent experiments are ${}^6\text{Li}$, ${}^{52}\text{Cr}$, ${}^{56}\text{Fe}$, Ge, Nb, Mo, and I;
- nuclei for which the accuracy of experimental discrete γ -ray production cross sections satisfy the practical requests are Li, C, Si, and V;
- for other nuclei the measured total discrete production cross sections, as a rule, satisfy the requirements declared in the WRENDA list, except for ${}^6\text{Li}$, Be, and Ge, whereas the energy differential uncertainties do not satisfy the requests for F, Cl, K, Ca, Ge, Pb, and Bi;
- the following γ -ray transitions and cross sections at 14.5 MeV incident energy may be recommended as a reference cross-sections for the research in which an accuracy of 5-10% is acceptable: 4439 keV from $\text{C}(n,n')^{12}\text{C}$; 3004 keV and 2211 keV from $\text{Al}(n,n')^{27}\text{Al}$; 2211 keV from $\text{Al}(n,n')^{27}\text{Al}$; and 847 keV from $\text{Fe}(n,n')^{56}\text{Fe}$.

Evaluated data libraries:

- there do not exist evaluations of γ -ray yields for Ge, Sn, and Cs;
- elements for which evaluated γ -production cross sections are presented only as a discrete transitions are ${}^6\text{Li}$, ${}^7\text{Li}$, ${}^9\text{Be}$, ${}^{10}\text{B}$, ${}^{11}\text{B}$, ${}^{12}\text{C}$, ${}^{14}\text{N}$, ${}^{16}\text{O}$, and ${}^{19}\text{F}$;
- elements for which evaluated discrete γ -production cross sections agree with measured data within experimental uncertainties are ${}^6\text{Li}$, ${}^9\text{Be}$, ${}^{10}\text{B}$, and ${}^{12}\text{C}$;
- for all elements heavier than F, the evaluated cross sections are presented as a sum of discrete transitions and continuous energy distributions. For all of these nuclei the evaluated data (including discrete intensities from continuous distributions) seriously

underestimate the experimental cross sections. The differences usually exceed the experimental uncertainties by a few times. Thus it should be recommended that available experimental information on discrete γ -ray production cross sections should be included in evaluated data libraries.

References:

1. N. Kocherov, P. K. McLaughlin (Eds), "WRENDA 93/94", Report INDC(SEC)-104, Vienna, 1993.
2. A. B. Pashchenko, H. Wienke, S. Ganesan and P. K. McLaughlin, "FENDL/E, Evaluated Nuclear Data Library of Neutron Interaction Cross Sections, Photon Production Cross Sections and Photon-Atom Interaction Cross Sections for Fusion Applications, version 1.1 of November 1994". Report IAEA(NDS)-128, 1996.
3. V. N. Manokhin *et. al.*, "BROND-2.2 Russian Evaluated Neutron Reaction Data Library", Report IAEA(NDS)-90, 1994.
4. P. F. Rose (Ed.), "ENDF-6. The U.S. Evaluated Nuclear data Library for Neutron Reaction data by the US National Nuclear Data Center-Including Revisions up to June 1993", Report IAEA(NDS)-100, 1993.
5. S. P. Simakov, A. Pavlik, H. Vonach, S. Hlavac, to be published.

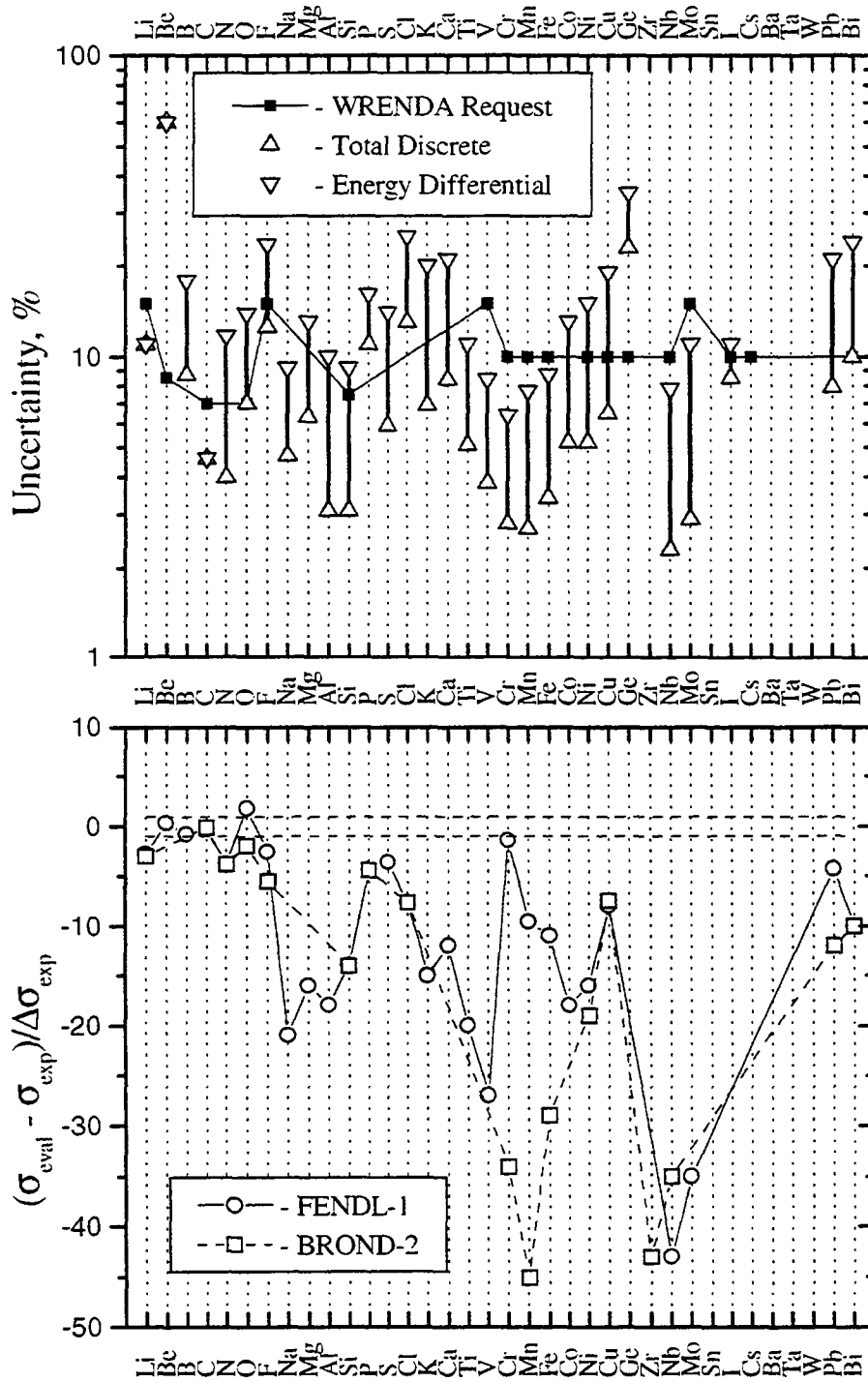


Fig. 1. Status of experimental data against WRENDA request (top) and evaluated data against experimental data (bottom)

Table 1. List of WRENDA requests, status of experimental and evaluated (FENDL-1, ENDF/B6, BROND-2) data for discrete γ -ray production cross sections.

N	Element	WRENDA Request (Priority)	Estimated Experiment					FENDL-1/E					ENDF/B6					BROND-2				
			N γ	$\sigma \pm \Delta\sigma$ (mb)	$\Delta\sigma/\sigma$	$\Delta S/S$	Status	N γ	σ (mb)	Qtot	Qdif	Status	N γ	σ (mb)	Qtot	Qdif	Status	N γ	σ (mb)	Qtot	Qdif	Status
1	Li	15%(2)	2	96 \pm 11	11%	11%	Y	2	59	-2.8	2.8	N	2	59	-2.8	2.8	N	1	57	-3.0	3.0	N
	⁶ Li		1	1.3 \pm 0.5	36%	36%	N	1	1.5	+0.4	0.4	Y	1	1.5	+0.4	0.4	Y			NE		
	⁷ Li		1	104 \pm 11	11%	11%	Y	1	64.1	-2.9	2.9	N	1	64.1	-2.9	2.9	N	1	62.0	-3.8	3.8	N
2	Be	4-15%(2)	1	4.8 \pm 2.9	60%	60%	N	1	6.0	+0.3	0.3	Y	1	6.0	+0.3	0.3	Y			NE		
3	B		6	265 \pm 23	8.7%	17.8%		6	239	-0.8	2.7	N	6	239	-0.8	2.7	N			NE		
	¹⁰ B		5	103 \pm 5.7	5.6%	11.0%		5	99	-0.7	0.8	Y	5	99	-0.7	0.8	Y			NE		
	¹¹ B		5	288 \pm 19	6.4%	12.1%		5	285	-0.2	2.8	YN	5	285	-0.2	2.8	YN			NE		
4	C	4-10%(2)	1	184.4 \pm 7.0	3.8%	3.8%	Y	1	184	-0.1	0.1	Y	1	184	-0.1	0.1	Y	1	184	-0.1	0.1	Y
5	N		9	286 \pm 12	4.0%	11.7%		9	242	-3.8	4.0	N	9	255	-2.6	1.7	N	9	242	-3.8	4.0	N
6	O	4-10%(2)	12	471 \pm 33	7.0%	13.8%	YN	11	531	+1.8	3.1	N	11	531	+1.8	3.1	N	11	406	-1.9	1.5	N
7	F	15%(2)	7	497 \pm 62	12.5%	23.5%	YN	6	337	-2.6	1.6	N	6	337	-2.6	1.6	N	6	154	-5.5	5.3	N
8	Na		7	1132 \pm 54	4.7%	9.2%		3	0	-21	21	N	2	495		2.6				NE		
9	Mg		7	806 \pm 51	6.3%	13%		0	0	-16	16	N	1	285						NE		
10	Al		13	887 \pm 27	3.1%	10%		7	403	-18	3.9	N	6	546		1.7				NE		
11	Si	5-10%(2)	14	967 \pm 30	3.1%	9.2%	Y	4	549	-14	2.1	N	4	786		9.2		4	549	-14	2.1	N
12	P		3	553 \pm 59	11%	16%		2	292	-4.4	2.2	N	2	292	-4.4	2.2	N	2	292	-4.4	2.2	N
13	S		6	845 \pm 50	5.9%	14%		2	664	-3.6	10	N	2	664	-3.6	10	N			NE		
14	Cl		6	844 \pm 109	13%	25%		1	0	-7.7	3.2	N	1	0	-7.7	3.2	N	5	0	-7.7	4.0	N
15	K		11	673 \pm 46	6.9%	20%		1	0	-15	9.6	N	1	0	-15	9.6	N			NE		
16	Ca		7	405 \pm 34	8.4%	21%		0	0	-12	12	N	1	12	-12	7.0	N			NE		
17	Ti		10	1607 \pm 82	5.1%	11%		0	0	-20	20	N	3	0	-20	20	N			NE		
18	V	15%(1)	18	1389 \pm 52	3.8%	8.4%	Y	6	6.8	-27	21	N	6	6.8	-27	21	N			NE		
19	Cr	10%(1)	13	1476 \pm 41	2.8%	6.4%	Y	13	1417	-1.4	3.4	YN	13	1417	-1.4	3.4	YN	7	88	-34	17	N
	⁵² Cr		11	1591 \pm 34	2.1%	4.7%	Y(?)	11	1488	-3.0	2.5	N	11	1488	-3.0	2.5	N	5	78	-45	24	N
20	Mn	10%(1)	15	1988 \pm 55	2.7%	7.7%	Y	13	1459	-9.6	2.0	N	13	1459	-9.6	2.0	N			NG		
21	Fe	10%(1)	14	1848 \pm 68	3.4%	8.7%	Y	14	1233	-9.0	4.7	N	14	1233	-9.0	4.7	N	0	0	-29	29	N
	⁵⁶ Fe		16	1423 \pm 37	2.6%	7.1%	Y(?)	13	1373	-1.4	1.8	YN	13	1373	-1.4	1.8	YN	0	0	-38	38	N

N	Element	WREND A Request (Priority)	Estimated Experiment					FENDL-1/E					ENDF/B6					BROND-2				
			N γ	$\sigma \pm \Delta\sigma$ (mb)	$\Delta\sigma/\sigma$	$\Delta S/S$	Status	N γ	σ (mb)	Q _{tot}	Q _{dif}	Status	N γ	σ (mb)	Q _{tot}	Q _{dif}	Status	N γ	σ (mb)	Q _{tot}	Q _{dif}	Status
	⁵⁷ Fe		4	212±24	12%	24%																
22	Co		12	877±45	5.2%	13%		6	69	-18	6.4	N	6	69	-18	6.4	N			NE		
23	Ni	10%(1)	11	937±49	5.2%	15%	YN	9	143	-16	2.5	N	9	143	-16	2.5	N	0	0	-19	19	N
24	Cu	10%(1)	11	853±55	6.5%	19%	YN	11	411	-8	4.1	N	11	411	-8	4.1	N	4	443	-7.5	0.7	N
25	Ge	10%(2)	4	185±42	23%	35%	N		NE					NGE						NE		
26	Zr		0	No Exp										NGE				0	0	-43	43	N
27	Nb	10%(1)	15	1825±42	2.3%	7.8%	Y(?)	0	0	-43	43	N	0	0	-43	43	N	0	0	-35	35	N
28	Mo	15%(1)	24	1634±47	2.9%	11%	Y(?)	0	0	-35	35	N	0	0	-35	35	N			NGE		
29	Sn		0	No Exp	-	-			NGE					NGE						NGE		
30	I	10%(1)	2	333±28	8.5%	11%	Y(?)		NE				0	0	-12	12	N			NGE		
31	Cs	10%(2)	0	No Exp					NE					NGE						NE		
32	Ba		0	No Exp				0	0				0	0								
33	Ta		0	No Exp																		
34	W		0	No Exp																		
35	Pb		12	3138±248	7.9%	21%		10	2063	-4.3	1.4	N	10	2063	-4.3	1.4	N	9	275	-12	4.5	N
	²⁰⁸ Pb		14	2159±65	3.0%	8.7%		6	2603	+6.8	14	N	6	2603	+6.8	14	N	5	305	-29	2.0	N
36	Bi	10%(1)	9	1489±147	10%	24%	YN	0	0	-10	10	N	5	40	-10	10	N	6	71	-10	1.7	N

Comments for Table 1:

No Exp - No available Experimental data

NGE - No Gamma-rays production cross section Evaluation in this library

NE - No Evaluation for this element at all in this library

ATLAS OF NEUTRON CAPTURE CROSS SECTIONS (NGATLAS)

J. Kopecky

ECN, P.O. Box 1, 1755 ZG Petten and JUKO Research, 1817 HX Alkmaar,
The Netherlands

1. Introduction

This work in assembling the NGATLAS data base has been initiated by recognizing the high practical value of a comprehensive compilation of (n,γ) cross sections for a complete set of targets in the whole energy range (10^{-5} eV - 20 MeV). The best sources of such data can be found among recent activation libraries for fusion applications, such as ADL-3, EAF-4.1, JENDL/A-96 and FENDL/A-2, because they contain the largest number of target materials. The recently released European Activation File, EAF-4.1 [1], has been chosen as the main source of data. Further, some improved and newly evaluated data have been included.

2. NGATLAS contents

The Atlas of Neutron Capture Cross Sections (NGATLAS) contains cross section data for targets from H up to, and including, curium ($Z=96$). It comprises 739 target isotopes with half-lives above 0.5 day. Cross sections to ground, first, and second isomers are listed separately. If isomers have a half-life longer than 0.5 day they are also included as targets. This gives a total of 972 reaction channels, with data in pointwise format in the range 10^{-5} eV to 20 MeV. Energy dependent isomeric branching ratios are based on a combination of experimental information and data based on empirical systematics at thermal and 14.5 MeV energies.

The detailed description of the data base for neutron capture cross sections at incident energies in the 10^{-5} eV -20 MeV range is given in the INDC Report [2]. There, an index of 972 included reactions and their data origin is provided. In addition, plots of the pointwise data are shown and comparisons are made with the available experimental values at 0.0253 eV, 30 keV and 14.5 MeV. All procedures for data selections, evaluations and renormalizations are described in Refs. [2,3,4,5].

3. Data availability

Cross section data in pointwise ENDF-5 format, with EAF extensions (see Refs. [1,2]), are available from the IAEA Nuclear Data Section. The data can be retrieved online through the World Wide Web using <http://www-nds.iaea.or.at/ngatlas.main.htm>.

4. Formats of NGATLAS data

The format of the NGATLAS file is essentially that of the MF=3 file of ENDF5 format with the following deviations (the resulting format is usually referred to as the EAF format; see EAF-4 final document [1]).

1. Two comment lines were added in an earlier stage. Only one is now used, stating the origin of data and the EAF revisions. The second one was used earlier to store more detailed information about renormalizations and is now empty.
2. The material number MAT consists of Z and two last digits of A. To describe metastable targets, A has been increased by 50 or 70 (m1 or m2, respectively). Consequently, the order of the cross sections (according to increasing MAT numbers) is not always in accordance with increasing Z and A.
3. The identifiers LIS and LFS are used to indicate the (isomeric) states of the target and final nucleus, respectively. Here we have adopted the convention that LFS = 99 means total production cross section; LFS = i means production of the ground state (i = 0), m1 (i = 1), and m2 (i = 2), respectively. The reaction nomenclature is that of ENDF format, except that reaction numbers leading to metastable states have been increased by 300 or 600 (for m1 and m2, respectively). The cross sections for one material number are ordered according to increasing MT numbers, except that cross sections leading to metastable states follow immediately after the cross section leading to the ground state.

In some adopted data, a condensation to 1282 point-structure was applied, if the number of data points in the original source exceeded 10,000 energy points.

In the pointwise file the reaction to the ground state is given first, followed by reactions to the metastable states (if any). Example of MT numbers are listed below:

MT	Reaction	MT	Reaction channel
102	(n,g)	102	ground state production
	(n,g)*	402	1st isomer production
	(n,g)#	702	2nd isomer production

In order to fully enable automatic retrieval of the history of the previous renormalization procedures and execution of the new renormalization, the composition of the comment line has been recently simplified and only two major items of information are stored:

1. The source of the data adopted in MDF is quoted in a format FACTOR*SOURCE (e.g. 1.0000+00*JEF-2.2 means that the data are taken from JEF-2.2 with no renormalization; 8.2500-01*ENDF/B-VI indicates that the excitation curve has been renormalized to 82.5% of its original value).
2. The flag RN displays the information for experimental or systematic renormalizations, respectively, formatted as RN - XXX/YYYY. The first item stands for the total cross section at 14.5 MeV, while the second refers to the isomeric branching (e.g., RN - EXP/SYS means that $\sigma(\text{tot})$ has been renormalized to the experiment, while the $\sigma(\text{gs})$ and $\sigma(\text{m1})$ values have been generated by applying the branching systematics).

References

1. J. Kopecky and D. Nierop, The European Activation File EAF-4 – Summary Documentation – ECN-C-95-075, (ECN Report, Petten, The Netherlands, December 1995).
2. J. Kopecky, J-ch. Sublet, J.A. Simpson, R.A. Forrest and D. Nierop, Atlas of Neutron Capture Cross Sections, INDC(NDS)-362 (IAEA Report, Vienna, April 1997).
3. J. Kopecky, M.G. Delfini, H.A.J. van der Kamp and D. Nierop, Revisions and Extensions of Neutron Capture Cross Sections in the European Activation File EAF-3, ECN-C-92-051, (EC Report, Petten, The Netherlands, July 1992).
4. J. Kopecky, Experimental Data Base compiled for Renormalisation and Validation of EAF-4.1 Cross Sections, EAF-DOC-008, January 1996, (available upon request from the author).
5. J.A. Simpson, J.-Ch. Sublet and D. Nierop, SYMPAL User Guide, UKAEA FUS 356, (UKAEA Report, Culham, United Kingdom. 1997).

Review of Experimental Capture Gamma Spectra for Neutrons above 10 MeV

Frank S. Dietrich
Lawrence Livermore National Laboratory
Livermore, CA 94551 USA

1 Introduction

In this section we review the available data on gamma spectra following radiative capture of neutrons above 10 MeV. A few measurements below that energy are included. An important source for references to this topic is the CINDA compilation maintained by the IAEA in cooperation with three other major data centers. An additional useful source is the review article by Weller and Roberson [1], which treats capture reactions with neutrons, protons, and alpha particles. The following discussion refers only to data that are easily accessible through readily-available journals, reports, or the EXFOR database.

Most of the reported measurements were made for the purpose of determining cross sections for discrete states at the high energy end of the gamma spectra which are resolvable or nearly so. In only a few cases have cross sections been measured over a wide range of gamma energies. These measurements are first reviewed below, followed by a review of more detailed measurements such as angular distributions and analyzing powers. Neutron capture on hydrogen isotopes have not been included with the exception of a fairly recent measurement on deuterium [3]; see CINDA [2] for references to this specialized topic.

2 Absolute cross sections for gamma spectra induced by 14 MeV neutrons

We focus on three sets of measurements that have been carried out to measure absolute cross sections of the gamma spectra for neutrons in the neighborhood of 14 MeV. These spectra extend from the 12–14 MeV gamma region to the endpoint of the spectrum. Two of these sets measured the spectrum with a pair spectrometer, which

is relatively insensitive to neutrons: these are the measurements of Stamatelatos *et al.* [4] and of the Ljubljana group [5, 6, 7, 8, 9, 10, 11]. The third data set, Rigaud *et al.* [12, 13, 14], used a NaI spectrometer. The pair spectrometer experiments used large targets surrounding the neutron source, leading to results that are very close to total (angle-integrated) cross sections. On the other hand, in the measurements of Rigaud *et al.*, the NaI measured gammas emerging perpendicular to the neutron beam, with the consequence that the measurements reported are actually 4π times the 90° differential cross section. The targets included in each of these data sets are indicated in the following list:

- Pair spectrometer (Stamatelatos *et al.*): Cu, Zr, Sb
- Pair spectrometer (Ljubljana): Mg, ^{27}Al , Si, ^{31}P , S, Ca, ^{45}Sc , ^{51}V , Cr, ^{55}Mn , Fe, ^{59}Co , Cu, Se, Br, Sr, ^{89}Y , In, Sb, ^{127}I , Ba, ^{141}Pr , ^{165}Ho , ^{181}Ta , W, Tl, Pb, ^{209}Bi
- NaI spectrometer (Rigaud *et al.*): Si, ^{59}Co , Rb, Sr, Y, ^{93}Nb , ^{103}Rh , ^{133}Cs , ^{139}La , Ce, ^{159}Tb

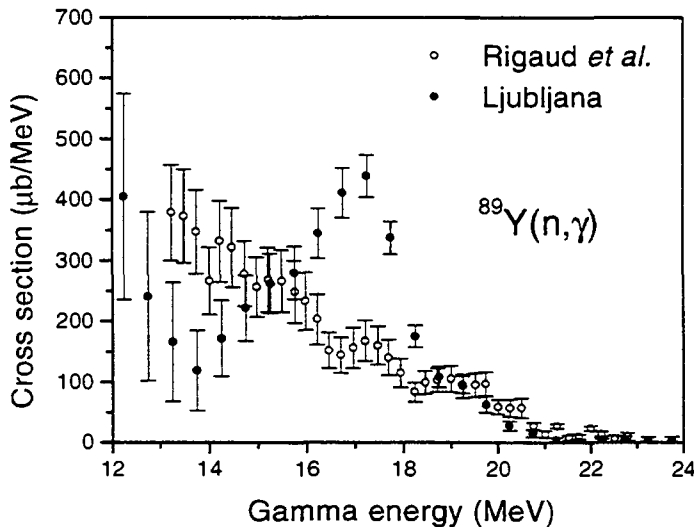


Figure 1: Gamma spectra from 14-MeV neutrons incident on ^{89}Y as measured by a pair spectrometer (Ljubljana) and a NaI spectrometer (Rigaud *et al.*).

We also note another measurement using NaI on ^{27}Al and ^{127}I targets [15]. However, the statistical accuracy is significantly poorer than that of the other NaI measurements.

Additional spectral measurements using a NaI spectrometer have been made at Los Alamos on targets of Gd, Ho, Ta, Au, ^{208}Pb , and ^{238}U [16]. These measurements

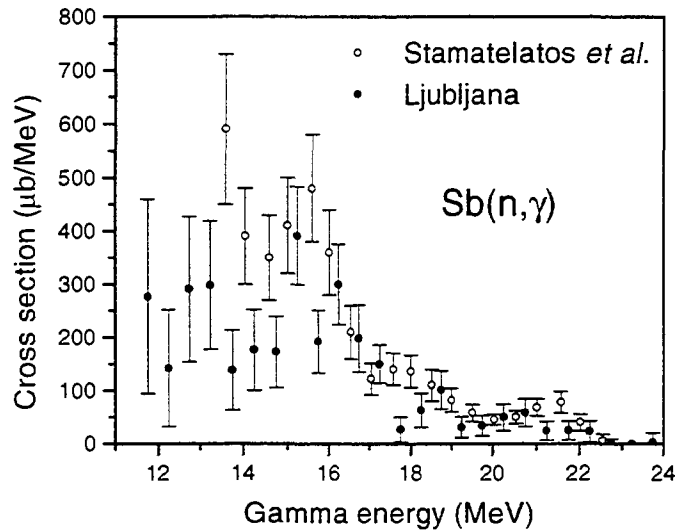


Figure 2: Gamma spectra from 14-MeV neutrons incident on Sb as measured in two pair spectrometer experiments.

were important in showing that the energy-integrated cross section from 14 MeV to the endpoint is approximately 1 mb over a wide mass range (approximately 40 to 240). This work eventually led to the conclusion that activation measurements of this same quantity, which in some cases were an order of magnitude larger, were faulty because of contamination by lower-energy neutrons. Although spectra with an absolute cross section normalization have not been made available, the unnormalized spectra for Ho, ^{208}Pb , and ^{238}U shown in Ref. [16] may be used with the integrated values of the spectra above 14 MeV to obtain an absolute normalization.

There are important discrepancies among the three principal data sets listed above. Examples of these discrepancies are shown in Figs. 1 and 2. In Fig. 1 the comparison of pair spectrometer (Ljubljana) and NaI (Rigaud *et al.*) measurements on ^{89}Y show the significantly lower values of the pair spectrometer measurements in the 14-MeV gamma energy region compared to the NaI results. This appears to be a systematic difference between these two data sets. Results for Sb of the two pair spectrometer measurements are shown in Fig. 2. The Ljubljana measurements appear to be lower than those of Stamatelatos *et al.* below 15 MeV. There is rather better agreement among the various data sets for the gammas within a few MeV of the endpoint of the spectrum. While the discrepancies among these data sets are not understood, it may be useful to note that neutrons interacting in the spectrometer are a potential problem in all of these measurements. Such backgrounds, if present in spite of measures taken to reduce them, are more likely to be a problem in the low-energy part of the spectrum than near the endpoint.

Spectral Shape Measurements		
Target	Reference	Neutron Energies (MeV)
S	[17]	6.8, 10.9, 15
⁴⁰ Ca	[18]	10.2, 11.2, 12.2, 13.2, 14.2, 15.2
⁸⁹ Y	[19]	7.2, 8.9, 10.7, 10.9, 12.9, 15.6
¹⁴⁰ Ce	[19]	7.2, 8.9, 10.7, 10.9, 12.9, 15.6
¹⁶⁵ Ho	[20]	10.7
²⁰⁸ Pb	[21],[22]	9.2, 10.2, 11.2, 12.2, 13.2, 14.7
²³⁸ U	[20]	10.7

Table 1: Spectral shape measurements taken with NaI at indicated energies. All measurements were made with a NaI spectrometer.

90° Differential Cross Section Measurements (also see references in Table 1)		
Target	Reference	Neutron Energies (MeV)
³ He	[23]	6–17
⁴⁰ Ca	[24]	0.5–11
⁵⁸ Ni	[25]	0.9–8.3
⁵⁸ Ni	[24]	0.5–11
⁸⁹ Y	[24]	0.5–11
²⁰⁶ Pb	[26]	1.5–8.5
²⁰⁸ Pb	[24]	0.5–11
²⁰⁹ Bi	[25]	4.7–8.3

Table 2: Measurements of 90° differential cross sections taken with NaI spectrometers

3 Variation of the spectral shape with neutron energy

A number of the papers reporting excitation functions of the discrete gammas at the high end of the spectrum have also shown unnormalized spectra at selected energies. These spectra were measured at 90° with NaI spectrometers. The experimental resolution has not been unfolded from the spectra, although usually the energy variation of the efficiency has been corrected for. In most cases an absolute cross section can be guessed (though with limited accuracy) by noting the absolute cross sections for the discrete transitions reported in these papers. These results are shown in Table 1.

Angular Distributions with Unpolarized Neutrons						
Tgt	Final States	Ref.	Neutron Energies (MeV)	Angles (degrees)	Absolute Cross Sections	Comments
^2H	0	[3]	9,10,8,14	various	yes	
^3He	0	[23]	9	various	yes	
^{10}B	0	[27]	14	55,90,125	no	
^{12}C	0	[27]	14	55,90,125	no	
^{28}Si	1	[27]	14	55,90,125	no	
^{40}Ca	0	[27]	14	55,90,125	no	
^{40}Ca	0	[28]	8, 12	several	no	
^{40}Ca	0	[29]	6-13	several	yes	
^{40}Ca	0	[30]	20-28	55,90,125	yes	
^{40}Ca	0	[31]	8-44	55,90,125	yes	BGO crystal spectrometer
^{88}Sr	—	[32]	7-11	55,90,125	no	two s.p. final configurations
^{89}Y	—	[32]	7-11	55,90,125	no	two s.p. final configurations
^{89}Y	—	[33]	12-27	55,90,125	no	several s.p. final configurations
^{208}Pb	0	[34]	7-20	55,125	no	
^{208}Pb	—	[34]	20	55,125	no	γ spectrum measured
^{208}Pb	0	[35]	0.8-7.7	?	?	
^{208}Pb	0,1	[36]	7-13	several	yes	
^{209}Bi	0-5	[37]	17.7-22	55,125	no	some final states unresolved

Table 3: Angular distribution measurements taken with NaI spectrometers unless otherwise indicated.

4 90° differential cross section, angular distribution, and analyzing power measurements

Absolutely-normalized measurements of excitation functions of 90° differential cross sections to low-lying states or groups of states in the final nucleus have been important in the establishment of the direct-semidirect capture model. Most of the references in Table 1 contain data of this type. Additional measurements are noted in Table 2.

There has been a large number of angular distribution measurements to discrete final states. The majority of these have been measured at only two or three angles, either 55° and 125°, or 55°, 90°, and 125°. These measurements of the fore-aft asymmetry in the cross sections have been important in elucidating the properties of collective E2 radiation, since direct E2 is highly suppressed by an effective charge factor. Most of the results of the experiments indicated in Table 3 have reported the results in the form of Legendre coefficients, although in a few cases the angular distributions themselves are shown. In the column indicating final states, 0 is the ground state, 1 is the first excited state, and so on. When the final states are not specified, the final states are unresolved and the spectrum is assumed to be dominated by one or more single-particle final state configurations that produce the observed structure.

Observation of analyzing powers in measurements with polarized beams provides extra information and constraints on the multipolarities and amplitudes contributing to the reactions. These measurements are indicated in Table 4. In all cases the transition to the ground state of the residual nucleus was measured.

Measurements with Polarized Neutrons				
Target	Reference	Neutron Energies (MeV)	Angles (degrees)	Absolute Cross Sections
² H	[3]	9	various	yes
¹² C	[38]	20–35	55,90,125	no
¹² C	[39]	16–22.3	various	no
¹³ C	[40]	5.6–17	various	no
⁴⁰ Ca	[41]	10	various	no

Table 4: Measurements of analyzing powers taken with NaI spectrometers.

5 Isospin tests

A few measurements in light nuclei have been carried out to test isospin conservation by comparison with proton capture reactions. For a ¹²C target, the excitation function of the ¹²C(n,γ₀) reaction at 90° at neutron energies 7–19.5 MeV [42] and 5.6–13 MeV

[43] has been compared with the $^{12}\text{C}(p,\gamma_0)$ reaction. The 90° excitation function of the $^{14}\text{N}(n,\gamma_0)$ reaction in the 5.6–13 MeV neutron energy range has been measured in [44] and compared with the $^{14}\text{C}(p,\gamma_0)$ and $^{14}\text{N}(p,\gamma_0)$ reactions. Angular distributions at seven energies were also measured in [44].

6 Conclusions

The measurements compiled above show that the behavior of the capture reaction for gammas near the high energy end of the gamma spectrum is reasonably well characterized up to 20 to 30 MeV, although the choice of targets is rather limited. These results have been useful in the development of direct-reaction models (such as direct-semidirect) for capture, since there is little competition from statistical reaction mechanisms. Angular distribution and analyzing power measurements in this part of the spectrum have also been important in elucidating the properties of E2 radiation in neutron capture.

On the other hand, spectral measurements over a wide energy range are in a much less satisfactory state, since there are discrepancies between the various measurements of absolute cross sections at 14 MeV, and measurements at other energies have been reported without an absolute energy scale. New measurements would be desirable to provide an adequate data base for the testing of models that include statistical reactions or direct reactions to highly excited states (see, *e.g.*, the discussion of extensions to the DSD model earlier in this report).

This work was performed under the auspices of the U. S. Department of Energy under contract No. W-7405-ENG-48 (Lawrence Livermore National Laboratory).

References

- [1] H. Weller and N. Roberson, *Rev. Mod. Phys.* **52**, 699 (1980).
- [2] CINDA database, accessible via Brookhaven National Nuclear Data Center web site and mirror sites including that of the IAEA Nuclear Data Section.
- [3] G. Mitev *et al.*, *Phys. Rev.* **C34**, 389 (1986).
- [4] M. Stamatelatos, B. Lawergren, and L. Lidofsky, *Nucl. Sci. and Eng.* **51**, 113 (1973).
- [5] F. Cvelbar *et al.*, *Nucl. Inst. and Meth.* **44**, 292 (1966).
- [6] F. Cvelbar *et al.*, *Nucl. Phys.* **A130**, 401 (1969).
- [7] F. Cvelbar *et al.*, *Nucl. Phys.* **A130**, 413 (1969).

- [8] F. Cvelbar *et al.*, Nucl. Phys. **A138**, 412 (1969).
- [9] F. Cvelbar *et al.*, Nucl. Phys. **A159**, 555 (1970).
- [10] M. Potokar *et al.*, Nucl. Phys. **A213**, 525 (1973).
- [11] A complete and updated data set is available in M. Budnar *et al.*, IAEA report INDC(YUG)-6 (1979). This data set is available in electronic form as EXFOR 30532.
- [12] F. Rigaud *et al.*, Nucl. Phys. **A154**, 243 (1970).
- [13] F. Rigaud *et al.*, Nucl. Phys. **A173**, 551 (1971).
- [14] F. Rigaud *et al.*, Nucl. Phys. **A176**, 545 (1971).
- [15] H. Dinter, Nucl. Phys. **A111**, 360 (1968).
- [16] D. Drake, I. Bergqvist, and D. McDaniels, Phys. Lett. **36B**, 557 (1971).
- [17] A. Lindholm *et al.*, Nucl. Phys. **A279**, 445 (1977).
- [18] I. Bergqvist, D. Drake, and D. McDaniels, Nucl. Phys. **A231**, 29 (1974).
- [19] I. Bergqvist *et al.*, Nucl. Phys. **A295**, 256 (1978).
- [20] D. McDaniels *et al.*, Nucl. Phys. **A384**, 88 (1982).
- [21] I. Bergqvist, D. Drake, and D. McDaniels, Nucl. Phys. **A191**, 641 (1972).
- [22] I. Bergqvist, D. Drake, and D. McDaniels, Phys. Rev. Lett. **27**, 269 (1971).
- [23] L. Ward *et al.*, Phys. Rev. **C24**, 317 (1981).
- [24] A. Lindholm *et al.*, Nucl. Phys. **A339**, 205 (1980).
- [25] I. Bergqvist *et al.*, Nucl. Phys. **A120**, 161 (1968).
- [26] I. Bergqvist, B. Lundberg, and L. Nilsson, Nucl. Phys. **A153**, 553 (1970).
- [27] E. Arthur, D. Drake, and I. Halpern, Phys. Rev. Lett. **35**, 914 (1975).
- [28] H. Weller *et al.*, Phys. Rev. **C17**, 1260 (1978).
- [29] S. Wender *et al.*, Phys. Rev. Lett. **41**, 1217 (1978).
- [30] I. Bergqvist *et al.*, Nucl. Phys. **A419**, 509 (1984).
- [31] C. Laymon *et al.*, Phys. Rev. **C46**, 1880 (1992).

- [32] A. Likar *et al.*, Nucl. Phys. **A298**, 217 (1978).
- [33] R. Zorro *et al.*, Nucl. Phys. **A472**, 125 (1987).
- [34] D. Drake *et al.*, Phys. Rev. Lett. **47**, 1581 (1981).
- [35] S. Joly *et al.*, Nucl. Phys. **A382**, 71 (1982).
- [36] S. King *et al.*, Nucl. Phys. **A384**, 129 (1982).
- [37] A. Håkansson *et al.*, Nucl. Phys. **A512**, 399 (1990).
- [38] G.-D. Wicke *et al.*, Z. Phys. **A341**, 453 (1992).
- [39] J. Woodworth *et al.*, Phys. Rev. **C29**, 1186 (1984).
- [40] M. Wright *et al.*, Phys. Rev. **C31**, 1125 (1985).
- [41] M. Jensen *et al.*, Phys. Rev. Lett. **43**, 609 (1979).
- [42] I. Bergqvist *et al.*, Nucl. Phys. **A456**, 426 (1986).
- [43] R. August *et al.*, Phys. Rev. **C35**, 393 (1987).
- [44] S. Wender *et al.*, Phys. Rev. **C25**, 89 (1982).

EXPERIMENTAL DATA BASE FOR GAMMA-RAY STRENGTH FUNCTIONS

J. Kopecky

ECN, P.O. Box 1, 1755 ZG Petten and JUKO Research, 1817 HX Alkmaar,
The Netherlands

1. Introduction

The compound nucleus mechanism is dominant for the neutron capture process up to several MeV incident neutron energy. Therefore, the statistical model is generally used to describe and calculate the (n,γ) cross sections and spectra for these energies. An exception to this can occur in thermal and resonance regions (thus at low neutron energies) in mass regions, where nonstatistical processes (potential and valence capture) may become important.

The γ -ray transmission coefficient T_{XL} , usually used in the model calculations, is related to the γ -ray strength function f_{XL} as

$$T_{\text{XL}}(E_\gamma) = 2\pi E_\gamma^{2L+1} f_{\text{XL}}(E_\gamma), \quad (1)$$

where E_γ is the γ -ray energy and L indicates the multipolarity of the radiation. Therefore, both theoretical and experimental knowledge of γ -ray strength functions is a very important ingredient for description and calculation of photon production data in all reaction channels, not only for the (n,γ) reaction. The impact of different theoretical formulations of E1, M1 and E2 gamma-ray strength functions on the statistical model calculations have been recently studied in several publications [1-8].

In this study we concentrate on experimental γ -ray strength functions, collected over a period of about 40 years and based on measurements of partial radiative widths $\Gamma_{\gamma i}$. Such data originate from three different types of experiments. Most of the data are derived from discrete-resonance capture experiments using the method of slow neutron time-of-flight spectrometry. In some cases, the thermal neutron capture data can be used, however, with some restrictions. The last source of data is set of the photonuclear data. Common in the analysis of all these experiments is a need to average over Porter-Thomas fluctuations, which govern the distribution of partial radiative widths.

The first compilation of McCullagh et al. [9] included about 50 nuclides with absolute partial widths originating from (n_{res},γ) and (γ,n) reactions, selected from data published before 1980 and averaged over the observed resonances. These data were analysed in the framework of model dependent (single-particle model and Brink-Axel approximation) strength functions for E1 and M1 radiation. The mean energy for this data set was about 7 MeV. From fits to these

data Kopecky [10] derived global formulae for the additional dependence of f_{E1} and f_{M1} on the mass A compared to the above models. We prefer the model independent definition of strength functions for dipole radiation, written as

$$f_L(E_\gamma) = \langle \Gamma_\gamma / E_\gamma^3 \rangle \times 1/D_0. \quad (2)$$

A first update of this data set was made by Kopecky and Uhl [11] in 1990. In their study a few new data have been added and the general reliability of the data was addressed. It has been noticed that for a meaningful application of the experimental $f_L(E_\gamma)$ values in the statistical-model calculations it is necessary to check (and correct) the data for the presence of a non-statistical component in the total or partial radiative widths. Such corrections have not been applied yet and the use of data, if a non-statistical mechanism is strongly present in the resonance region, may lead to a significant overestimation of normalization in the calculation. The aim of this paper is to develop the γ -ray strength function systematics, based on the recently updated set of experimental data. A further objective of this work is to address the accuracy and reliability of f_{XL} data in general in view of all possible sources of uncertainties.

2. Update, accuracy and revision of selected data

2.1 Data additions

The original set of data [9] has been extended with data published between 1981 and 1995 with, however, no claim to completeness. The preliminary results have been published in Ref. [12] and the present compilation is a slightly extended and updated version. The extensions include resolved-resonance measurements [13-21], thermal-capture measurements [22-24] and photonuclear data [25-27].

Two comments should be made concerning the interpretation of thermal capture data in terms of strength functions. Firstly, Bollinger [28] has demonstrated that the distribution of γ -ray intensities following thermal capture follows only approximately the Porter-Thomas distribution, and in cases that both spin components contribute in thermal region, the distribution should be intermediate between χ^2 distributions with one and two degrees of freedom. Secondly, the conversion of thermal γ -ray intensities into partial radiative widths is based on the average value of the total radiative width, as derived from all measured resonances. This quantity, especially if resonances in a wide energy region are considered, may not be a good representation of the radiative width for the thermal region. Three such measurements have been included in our data set; we have selected only those where the authors derived the $f_{E1,M1}$ values by themselves [22-24]. However, it should be mentioned that a huge wealth of thermal capture data is available and it would certainly be worthwhile to consider making the effort to convert well-selected data into the γ -ray strength functions.

The final data sets of f_{E1} and f_{M1} values are listed in Table 1. Only a small number of minor corrections to the original data [9] have been made; most of the data have been adopted

without changes. Values for two different resonance spins, treated separately in Ref. [9], have been combined. The indicated errors include statistical, normalization (assumed 20%) and Porter-Thomas uncertainties. Data posterior to Ref. [9] have been adopted without changes and their origin is quoted in Table 1 by their references. Further, the number of resonances and γ -rays used in evaluation of $f_{E1,M1}$ values is quoted, just to indicate the quality of averaging.

Another assessment concerned the mean energy E_γ at which $f_{E1,M1}$ values have been derived. Following Eq. (1) only the partial E_γ^3 reduction factor has been applied and no additional energy dependence was assumed. This is reasonable if the energy region is narrow and the additional energy dependence which comes from the E1(M1) giant-resonance model is negligible. The quoted $f_{E1,M1}$ value is thus the mean value over all partial $f_{E1,M1}(E_\gamma)$ entries considered, which is assumed to correspond approximately to the mean value $\langle E_\gamma \rangle$. This energy is quoted in Table 1 in a comment line. An inspection of these values shows that the majority of data do not deviate significantly from earlier quoted $\langle E_\gamma \rangle \cong 6 - 7$ MeV. A fraction of the $f_{E1,M1}$ scatter may, however, stem from internal differences in distributions of partial data within the $\langle E_\gamma \rangle$ range. The only data outside 6 - 7 MeV to be considered are the actinide data with $\langle E_\gamma \rangle \cong 4.2$ MeV. The energy correction due to additional energy dependence (e.g. assumed E_γ^2 for E1 radiation) increases f_{E1} values by factor of 2.5. The global trend of $f_{E1,M1}$ data is, however, not significantly influenced due to a relatively small number of such data points, as was shown in Ref. [10].

2.2 Additional uncertainties in f_{E1} and f_{M1} values

In order to get a feeling for additional uncertainties, two of their main sources are discussed now in detail.

Firstly we review uncertainties in $f_{E1,M1}$ coming from the s-wave resonance spacing D_0 . This quantity may severely influence the "experimental" $f_L(E_\gamma)$ values. Recent evaluations of D_0 values at ENEA Bologna, IPPE Obninsk and CNDC Beijing published in Refs. [29-31] within the IAEA Co-ordinated Research Programme on the Reference Input Parameter Library, compared to the original BNL evaluation [32], showed in several cases significant disagreements, despite the fact that a similar methodology (corrections for missed or wrongly assigned resonances), was applied. All D_0 evaluations [29-32] are quoted in columns 2 and 3 of Table 1 together with the value used in the original reference. This enables the reader to make a judgement of the D_0 uncertainty and eventually to re-evaluate the value of $f_L(E_\gamma)$ with another D_0 .

It turned out that in some cases an incorrect D_0 value was applied in the derivation of $f_{E1,M1}$ values and a correction is proposed here. A general word of caution, however, has to be given here. As an example of such significant differences the $^{93}\text{Nb}(n,\gamma)$ reaction can be mentioned. While values of $D_0 = 37.8$ eV, 44 eV and 45 eV have been deduced in Refs. [9,29,32], respectively, the evaluations [30,31] resulted in 90 eV and 105 eV. Additionally Vertes and Grigoriew [33] quoted the value of 67 eV. Thus the data differ by more than a factor of two.

The $f_{E1,M1}$ data may therefore be categorised into two groups, those with no significant differences among the derived D_0 values and consequently with a small uncertainty due to resonance spacing, and those where significant disagreement among D_0 values occurs. For the last group the additional uncertainty has to be considered and those data are labelled with "D₀" warning in Table 1 or a correction is proposed.

Special attention has to be paid also to the absolute calibration of the radiative width and its accuracy. Several approaches have been applied in the experiments considered, such as internal normalization to a strong secondary transition in the spectrum studied or to well known values of the radiative width for individual resonances. As an external normalization, either measurements relative to the Au standard (4.9 eV resonance) have been used, or measurements relative to well established thermal capture standards, such as Cl. Recently, Becvar et al. [13] developed a method of calibration relative to the 477 keV γ -line from the $^{10}\text{B}(n,\alpha)$ reaction by a simultaneous time-of-flight measurement of the target material with a thin layer of boron. Close inspection of available data, however, raised a suspicion that in many cases the accuracy associated with the normalization procedure is underestimated, with possible consequences for the derived $f_{E1,M1}$ values.

As an example the $^{150}\text{Sm}(n,\gamma)$ reaction can be mentioned. The γ -ray intensities, based on the experiment carried out at the BNL fast chopper, were calibrated by two different methods. In the original study [34] the absolute normalization against a secondary transition in the $^{150}\text{Sm}(n,\gamma)$ spectrum resulted in a value of $f_{E1} = 4.46(110) 10^{-8} \text{ MeV}^{-3}$, while later a new calibration [18] using the boron 477 keV line, gave a value of $f_{E1} = 7.83(157) 10^{-8} \text{ MeV}^{-3}$. Their difference lies outside the quoted errors. However, it has to be remembered that it is very difficult to judge the quality of internal calibration without reviewing the original experimental data and the corresponding calibration runs in detail. It seems that an error factor of $f=1.5$ is a reasonable estimate of the additional global calibration uncertainty.

2.3 Comments on non-statistical capture mechanism

Another inspection was made for nuclides that can be influenced by a strong E1 nonstatistical component present in the resonance region. This effect may explain some of the experimental f_{E1} values that significantly exceed values based on pure statistical contributions. Further it is of relevance how large their influence is on the global systematics of f_{E1} as a function of mass. In some data the size of the valence contribution has been discussed and estimated already by the authors as referenced. Here we can list the following reactions: $^{91}\text{Zr}(\gamma,n)$, $^{92}\text{Mo}(n,\gamma)$, $^{101}\text{Ru}(n,\gamma)$, $^{198}\text{Hg}(n,\gamma)$ and $^{207}\text{Pb}(\gamma,n)$. For the mass region of the 3s-wave giant resonance, $40 < A < 60$, an estimate of approximately 50% valence contribution to the total radiative width can be quoted. This seems to be a reasonable guess based, for example, on calculations of Allen and Musgrove [35] and comparisons between $\Gamma_\gamma(s\text{-wave})$ and $\Gamma_\gamma(p\text{-wave})$ values in the above mass region, where the latter is assumed to have a pure statistical nature. Similar

enhancements of E1 radiation may be expected in the 3p-(4s-) giant resonance regions ($90 < A < 110$ and $140 < A < 200$).

For nuclides with very limited number (≤ 3) of primary transitions (e.g. ground-state transitions), the value of the derived strength function may not be reliable and not representative for the statistical capture, even if a relatively sufficient number of resonances was used for averaging. These transitions may still carry the simple (single-particle) structure through several resonances.

For M1 radiation the situation is more complicated. There is no general theoretical explanation of the non-statistical mechanism, despite the fact that these effects have been experimentally observed (see e.g. [36,37]).

3. Discussion of data

3.1 E1 radiation

All surveyed data with their original values, denoted according to their experimental origin, are displayed in Fig. 1 together with a least-squares fit of a power dependence on mass number A (solid curve). Data follow the expected smooth global trend reasonably well with two exceptions, where some deviations above the general scatter of data may be considered. These large deviations belong to data in mass regions with $A < 40$ and $170 < A < 210$. There is no difference detected in the trend of the data among the three experimental methods applied. For an indication of how the extension and revisions of the data set have influenced the general trend in f_{E1} data, the fitted curve from 1981 [10] is plotted in Fig. 1 for comparison.

Reasons for a large scatter of the low-mass data ($A < 40$) can surely be attributed to insufficient averaging together with a pronounced single-particle character of many transitions. However, it seems that their mean value reasonably represents the general trend, as expected from the other data. The situation in the mass region with $170 < A < 210$ is more complex. Several strongly enhanced data points can be explained by the presence of a non-statistical mechanism, in particular those around the double-closed shell region. However, this enhancement is not a general feature of all data, since some values seem to follow the general trend, as determined by data from the mass region with $100 < A < 170$. It can be noticed that the general behavior of the scatter in the data around the trend curve in Fig. 1 can be characterised by an uncertainty factor of $k=2$, which leaves about 10% of data points outside the uncertainty band (see Fig. 1).

This data scatter probably masks the expected enhancement of f_{E1} values in other mass regions (see Sect. 2.3). This is demonstrated in Fig. 2, where data with well established nonstatistical contributions have a tendency to lie in the upper half of the data band. It turns out, however, that these nonstatistical data have very little influence on the overall trend and fit to the f_{E1} values. This can be seen in Fig. 2, where the fit to data without those labelled as "nonstat" is drawn and differs negligibly from the fit to all data.

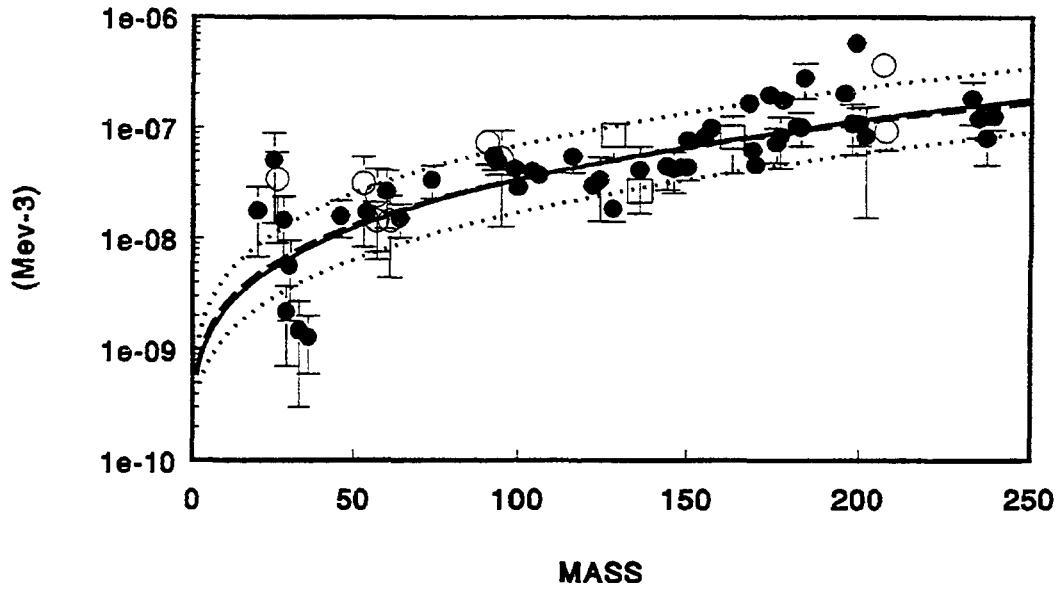


Fig. 1. Plot of f_{E1} values [full circles (n_{res}, γ), open circles (γ, n), and squares (n_{th}, γ)] against the mass number. The full curve represent a least-squares fit to recent data; the fit from 1981 [10] is denoted by the dashed curve. Dotted curves display an uncertainty band with $k=2$ (see Eq. (4)).

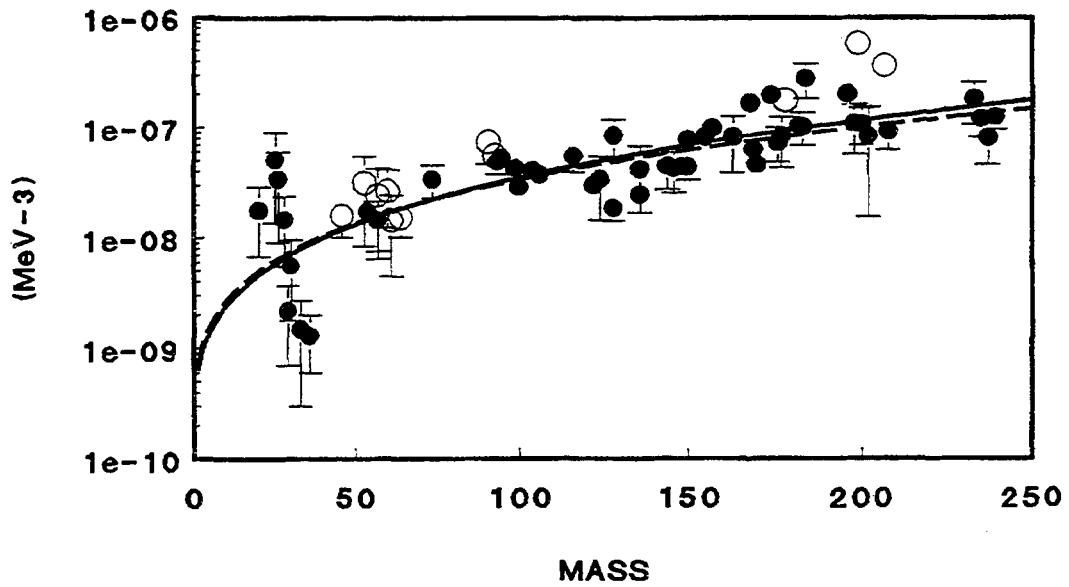


Fig. 2. The same as Fig.1: the open circles denote entries with nonstatistical contributions. The dotted curve results from a LSQ fit to only statistical data (full circles), while the full curve stems from Fig. 1.

A substantial fraction of this scatter can be certainly attributed to uncertainties (see Section 2.2) and to insufficient averaging of Porter-Thomas fluctuations. All facts discussed above suggest that extensions and changes in basic data including recent revisions (D_0 revisions; see comments in Table 1) have very small influence on the global behavior of f_{E1} values and their fit.

3.2 M1 radiation

For M1 radiation, the situation is more complicated for several reasons. The systematic behavior of the M1 strength function (see Fig.3) shows a mass dependence similar to E1 radiation. These data, however, are scarce and statistically less accurate, often based on inadequate averaging. The uncertainty representing data scatter, determined in a similar way as for E1 radiation with about 10% data points outside, amounts to a factor of three (see Fig.3). The curve fitted to data available in 1981 (Ref. [10]) differs very little from the present fit.

There is no well-established general theoretical expression for f_{M1} . The frequently used single-particle estimate is at variance with a finite energy-weighted sum rule and is also ruled out by the observed mass dependence. The recently proposed giant resonance model [38], based on the Brink hypothesis [39] and the spin-flip M1 resonance, lacks a global description of the sum rule. The data display also some effects that may be attributed to a nonstatistical origin. Some of the enhanced data seem to cluster in a gross structure but a clear identification is difficult. However, their influence on the general trend is marginal, as can be seen in Fig. 4. Only in two original references was the nonstatistical origin of the data identified.

4. Recommended systematics

It has been shown that there is no significant influence on the global trend of the fitted strength functions as a function of mass as a result of updating the basis data set since 1981. It has been shown further that this global trend is also not influenced by data enhanced by nonstatistical effects. The general reason for this is that the associated individual errors, dominated by Porter-Thomas uncertainties, are sometimes comparable to these effects and that the number of nonstatistical entries is relatively small. Therefore, we have decided to apply only corrections to those D_0 values in the original entries that were obviously wrong. These changes are documented in Table 1. The least-square fit to these data have resulted in a recommended experimental (trend) systematics, which is

$$\begin{aligned} f_{E1}(\text{exp}) &= 9.23 \times 10^{-11} A^{1.34 \pm 0.14}, \\ f_{M1}(\text{exp}) &= 1.58 \times 10^{-9} A^{0.47 \pm 0.21}. \end{aligned} \tag{3}$$

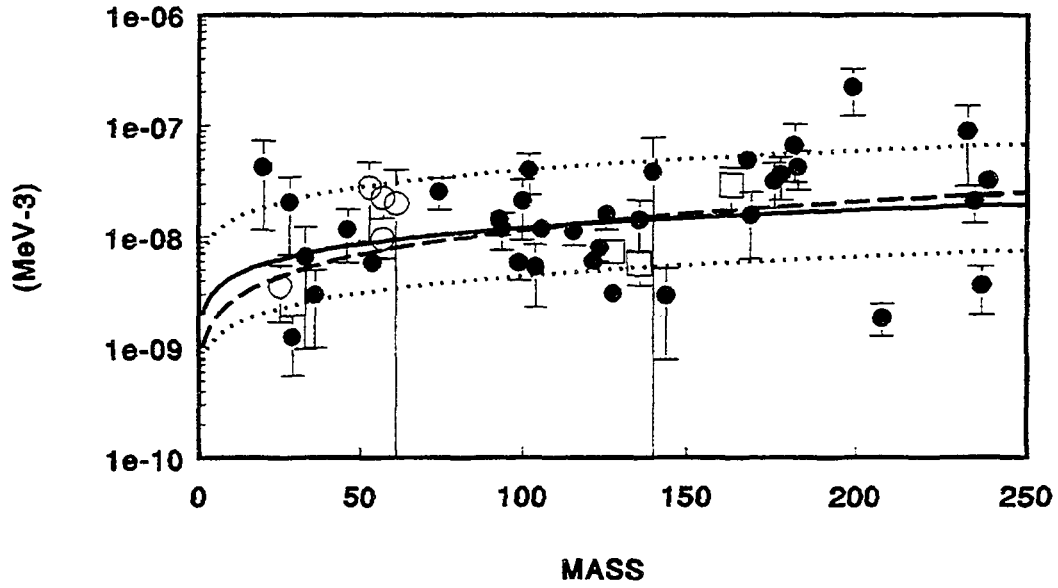


Fig. 3. Plot of f_{M1} values. The uncertainty band has a value of $k=3$ (symbols are the same as used in Fig.1).

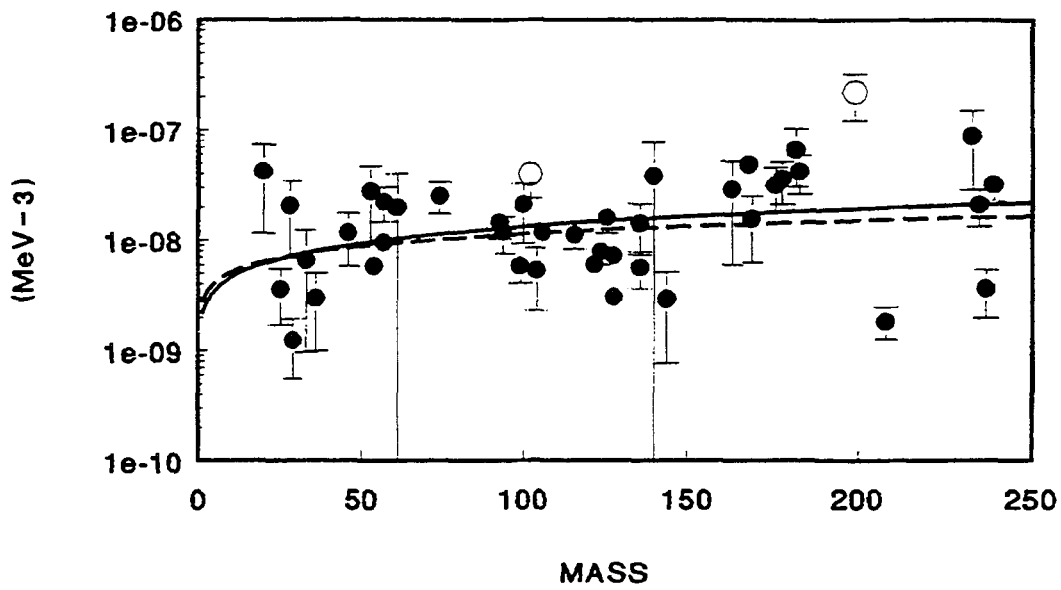


Fig. 4. Non-statistical f_{M1} data. Symbols are as used in Fig. 2.

These expressions are recommended for estimates of $f_{E1,M1}$ values in calculation normalizations if the neutron binding energy is not too much different from a value of 6 to 7 MeV. The associated uncertainty factor k , defined as

$$f_{E1,M1}/k < f_{E1,M1} < kf_{E1,M1}, \quad (4)$$

has been proposed elsewhere and amounts to $k = 2(3)$ for E1(M1) radiation, respectively. These uncertainty factors, to some extent arbitrarily chosen, agree reasonably well with associated errors of the A power as derived from the least-squares fit, resulting in k values 2.1 and 2.9.

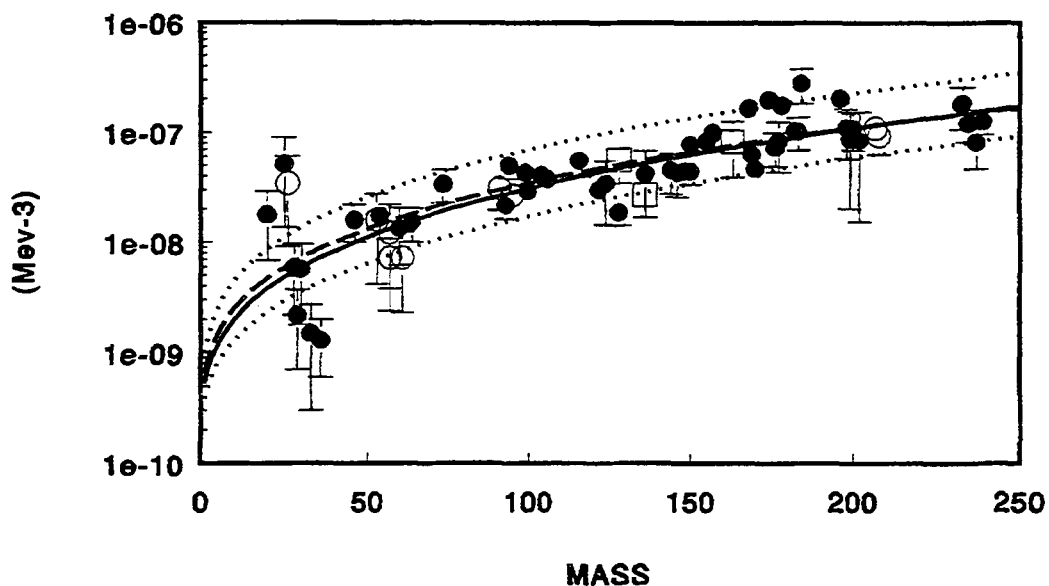


Fig. 5. The f_{E1} data corrected for non-statistical contributions (see Table 1). The fit to these data is denoted by the dashed curve; the other symbols are as in Fig. 1.

In the second phase we made an attempt, only for f_{E1} , to produce a set of data representing pure E1 statistical components. Corrections applied for nonstatistical contributions have in many cases a rather subjective character based on an educated guess, and should not be taken as a proper quantitative treatment. This exercise resulted in smoother data but with little influence on the global trend. The corrected data are again documented in Table 1 and are displayed in Fig. 5.

5. Conclusions

1. The original experimental data set for E1 and M1 gamma-ray strength functions [9] has been reviewed and extended by recent data covering the period up to 1996. The results are

compiled in Table 1. The resulting f_{E1} and f_{M1} values show a smoothly increasing dependence on mass A , different from that expected from the single-particle model. Together with an additional energy dependence above the E^3 phase-shift factor (as detected in many average-resonance capture experiments), it may be concluded that the use of the single-particle model should be disregarded for both E1 and M1 radiation.

2. The data fluctuations around the fitted systematics are dominated by the combined effects of experimental uncertainties (including the averaging properties) and uncertainties in D_0 values. Possible corrections are discussed and in several cases applied. In order to cover the uncertainty in D_0 determinations, all previous and recent D_0 evaluations are included in Table 1. The size of these fluctuations complicates the interpretation of individual data in terms of statistical and nonstatistical components; however, a global trend in the data is detected.

3. The resulting set of f_{E1} values generally underestimates the predictions of the standard Lorentzian, as expected from previous studies. This behavior constitutes a global argument for the use of the generalised Lorentzian with an energy dependent width [1,38]. The enhancements of E1 radiation above this model in mass regions $50 < A < 60$ and $150 < A < 170$, which influences all quantities such as f_{E1} , $\langle \Gamma_\gamma \rangle$, σ_γ and $d\sigma_\gamma/dE_n$, may be attributed to global nonstatistical effects. However, it is not excluded that some of the $\langle \Gamma_\gamma \rangle$ enhancements are due to experimental effects.

4. For practical applications in statistical model calculations, the experimental ratio of $\langle \Gamma_\gamma \rangle / D_0$ is probably the best normalization check. The derived systematics of f_{E1} and f_{M1} , if necessary combined with the trend in E1/M1 ratios, can be used as a reasonable approximation for the strength functions in model calculations, if experimental values are not available.

References

1. J. Kopecky and M. Uhl, Phys. Rev. C41, 1941 (1990).
2. M. Uhl and J. Kopecky, Proc. IAEA Specialists' Meeting on the Measurement, Calculation and Evaluation of Photon Production Cross Sections, February 5-7, 1990, Smolenice (Czechoslovakia), INDC(NDS)-238 (1990) p. 113.
3. J. Kopecky and M. Uhl, Proc. 7th Int. Symposium on Capture Gamma-Ray Spectroscopy and Related Topics, Asilomar 1990, (AIP New York 1991) AIP Conf.Proc. No. 238, p.607.
4. M. Uhl and J. Kopecky, Proc. Int. Conf. Nuclear Data for Science and Technology, Jülich 1991, (Springer Verlag, Berlin/Heidelberg, 1992), p. 977.
5. J. Kopecky and M. Uhl, Proc. Int. Symposium on Nuclear Data Evaluation Methodology, Brookhaven 1992, (World Scientific, Singapore, 1993), p.381.
6. J. Kopecky, M. Uhl and R.E. Chrien, Phys. Rev. C47, 312 (1993).
7. M. Uhl and J. Kopecky, Proc. Int. Conf. Nuclear Data for Science and Technology, Gatlinburg 1994, to be published.
8. M. Uhl and J. Kopecky, INDC(NDS)-335 (May 1995) p.157.

9. C.M. McCullagh, M. Stelts and R.E. Chrien, *Phys. Rev.* 23, 1394 (1981).
10. J. Kopecky, *Neutron-Capture Gamma Ray Spectroscopy and Related Topics 1981*, (The Institute of Physics, Bristol and London, 1982), p. 423.
11. J. Kopecky and M. Uhl, *Proc. IAEA Specialists' Meeting on the Measurement, Calculation and Evaluation of Photon Production Cross Sections*, February 5-7, 1990, Smolenice (Czechoslovakia), INDC(NDS)-238 (1990) p. 103.
12. J. Kopecky and M. Uhl, *NEA/NSC/DOC(95)1*, p.119 and INDC(NDS)-334 (May 1995) p.103.
13. F. Becvar et al., *Journal of Nuclear Physics (Russian)*, 44, 3 (1986).
14. O. Shahal, S. Raman, G.G. Slaughter, C. Coceva and M. Stefanon, *Phys. Rev.* C25, 1283 (1982).
15. S. Kahane, S. Raman, G.G. Slaughter, C. Coceva and M. Stefanon, *Phys. Rev.* C30, 807 (1984).
16. C. Coceva, M1 transitions from p-wave neutron resonances of ^{53}Cr , *Contr. to the 8th International Symposium on Capture Gamma-ray Spectroscopy and Related Topics*, Fribourg (Switzerland), September 20-24, 1994.
17. C. Coceva, Radiative transitions from neutron capture in ^{53}Cr resonances, to be published and private communication.
18. F. Becvar et al., *Journal of Nuclear Physics (Russian)*, 46, 3 (1987).
19. F. Becvar, *Capture Gamma Ray Spectroscopy 1987*, (Institute of Physics Conference Series 88, Institute of Physics, Bristol, 1988) p.649 and private communication.
20. F. Becvar et al., *Proc. of the Int. Conference on Neutron Physics*, Kiev (USSR), 2-6 October, 1983, p.8.
21. S Pospisil et al., *Annual Report 1995*, Frank Laboratory of Neutron Physics JINR Dubna, p. 84.
22. M.A. Islam, T.J. Kennett and W.V. Prestwich, *Z. Physik*, A 335, 173 (1990).
23. M.A. Islam, T.J. Kennett and W.V. Prestwich, *Phys. Rev.*, C42, 207 (1990).
24. H.H. Schmidt et al., *Nucl. Phys. A* 504, 1 (1989) and F. Becvar, private communication.
25. C. Coceva, Y.K. Ho, M. Magnani, A. Mauri and P. Bartolomei, *Capture Gamma Ray Spectroscopy 1987*, (Institute of Physics Conference Series 88, Institute of Physics, Bristol, 1988) p.676.
26. C. Coceva, Y.K. Ho, M. Magnani, A. Mauri and P. Bartolomei, *idem.*, p.679.
27. C. Coceva, private communication.
28. L.M. Bollinger, *Phys. Rev.* C3, 2071 (1971).
29. Huang Zhongfu, Zhao Zhixiang and Zhou Delin, *Com. of Nuclear Data Progress*, No 9, 60 (1993).
30. A.V. Ignatyuk et al., INDC(CCP)-320 (1990) 25, and private communication.
31. G. Reffo, ENEA Bologna, private communication.
32. S.F. Mughabghab, M. Divadeenam and N.E. Holden, *Neutron Cross Sections*, (Academic Press, New York, 1981 and 1984), Volume 1. Part A and B.
33. P. Vertes and Y.V. Grigoriew, *Proc. Int. Conference on Nuclear Data for Science and Technology*, Mito, Japan, 1988 (Saikon Publ. Co., Tokyo 1988) p. 623.
34. F. Becvar, R.E. Chrien and O.A. Wasson, *Nucl. Phys.* A236, 198 (1974).

35. B.J. Allen and A.R. Musgrove, *Adv. Nucl. Phys.*, Vol. 10 (Plenum, New York 1978) p. 129.
36. C.F. Clement, A.M. Lane and J. Kopecky, *Phys. Lett.* 71B, 10 (1977).
37. R.E. Chrien and J. Kopecky, *Phys. Rev. Lett.* 39, 911 (1977).
38. J. Kopecky and R.E. Chrien, *Nucl. Phys.* A468, 285 (1987).
39. D.M. Brink, Ph.D. Thesis, Oxford University, (1955).

Table 1: Compilation and revisions of experimental values for gamma-ray strength functions f_{E1} and f_{M1} in units of 10^{-8} MeV^{-3} based on s-(p-) wave neutron capture and photonuclear data.

Format of entries (see remarks at end of table for interpretation):

A_Z	[Ref.], Reac., #res/E1/M1, $\langle E_{\gamma E1}/E_{\gamma M1} \rangle$, D_0 [eV] from [32,29,30,31]
	D_0 [eV] f_{E1} f_{M1}
	Comments and revised values, if any

Table of gamma-ray strength functions:

${}^{20}\text{F}$	[9], (n, γ), 2/5/3, $\langle 4.4/4.4 \rangle$, -, 200000, -, -
	33200 1.80(112) 4.26(310)
	D_0 uncertainty
${}^{25}\text{Mg}$	[25], (γ ,n), 14/1, $\langle 8.5 \rangle$, 143500, 234000, 120000, -
	- 0.36(19)
${}^{25}\text{Mg}$	[9], (n, γ), 1/4, $\langle 6.0 \rangle$, 143500, 234000, 120000, -
	143000 5.17(380) -
${}^{26}\text{Mg}$	[9], (γ ,n), 6/1, $\langle 11.1 \rangle$, -, 193000, 14000, -
	3.46(255) -
${}^{28}\text{Al}$	[9], (n, γ), 2/5/2, $\langle 6.6/6.9 \rangle$, -, 58000, 32000, 64300
	19970 1.48(92) 2.08(139)
	$D_0 = \langle 50000 \rangle$ 0.40 0.59(37) 0.83(66)

^{29}Si	[9], (n, γ), 2/5/2, <6.0/5.4>, -, 176000, -, -		
	40000	0.22(15)	0.125(70)
	D ₀ uncertainty		
^{30}Si	[9], (n, γ), 1/2, <6.9/>, -, -, -, -		
	100000	0.57(39)	-
	D ₀ uncertainty		
^{33}S	[9], (n, γ), 1/4/3, <7.5/7.5>, 17000, 28000, 17000, -		
	203000	0.15(12)	0.66(57)
	D ₀ = 17000	11.9	1.79(143)
^{36}Cl	[9], (n, γ), 1/9/5, <7.2/5.4>, 21000, 14500, 28000, 8428		
	24500	0.13(7)	0.30(20)
	D ₀ uncertainty		
^{46}Sc	[9], (n, γ), 2/13/9, <7.0/7.2>, 1300, 1330, 1300, 1450		
	1300	1.61(59)	1.17(59)
	D ₀ uncertainty		
^{53}Cr	[9], (γ ,n), 21/1/1, <7.9/7.9>, 42000, 35600, 45000, -		
		3.19(235)	2.80(188)
	Nonst. effects	0.5	1.60(118)
^{54}Cr	[17], (n, γ), 23/33/31, <6.7/6.7>, 7100, 6310, 7100, 6550		
	7100	1.74(20)	0.59(6)
	Nonst. effects/Averaging		

^{57}Fe	[9].	(γ,n),	15/1/1,	<7.7/7.7>, 17000, 22000, 25000, -	
					2.46(181) 2.25(78)
	Nonst. effects		0.5	1.23(99)	
^{57}Fe	[26].	(γ,n),	32/1/1,	<7.8/7.8>, 17000, 22000, 25000, -	
					1.46(70) 0.96(33)
	Nonst. effects/Averaging				
^{60}Co	[9].	(n,γ),	1/8,	<7.0/>, 1100, 1170, 1100, 1340	
					1060 2.70(146) -
	Nonst. effects		0.5	1.35(73)	
^{61}Ni	[9].	(γ,n),	23/1/1,	<7.8/7.8>, 16000, 14100, 16000, 14935	
					1.46(101) 2.00(108)
	Nonst. effects		0.5	0.73(50)	
^{64}Cu	[9].	(n,γ),	3/9.	<7.5/>, 320, 895, 1040, 1452	
					629 1.53(52) -
^{74}Ge	[9].	(n,γ),	5/7/7,	<7.1/7.9>, 82, 102, 82, 165	
					76 3.44(115) 2.57(82)
^{91}Zr	[9].	(γ,n),	32/1.	<7.2/>, 6400, 7670, 8600, 10500	
					7.48(281) -
	Nonst. effects		0.42	3.14(118)	

⁹⁴ Nb	[9]. (n,γ).	7/15/16,	<6.5/6.5>, 44, 59, 90, 105	
		37.8		5.04(124) 1.20(44)
	D ₀ = 67 eV	0.5	2.84(70)	0.68(25)
⁹³ Mo	[9], (n,γ),	8/10/9,	<6.6/6.2>, 2100, 2170, 3600, 3000	
		1000		5.67(147) 1.46(42)
	Nonst. effects D ₀ = <2580>	0.20	1.13(29)	
⁹⁵ Mo	[27], (γ,n),	NA/1,	<7.3/>, 975, 1150, 1150, 2265	
				5.38(41) -
	Nonst. effects	0.50	2.69(20)	
⁹⁹ Mo	[9], (n,γ).	17/7/8,	<5.5/5.5>, 970, 941, 970, -	
		429		4.32(81) 0.59(18)
¹⁰⁰ Ru	[9]. (n,γ),	4/5/10,	<6.9/7.4>, 25, 26, 25, 26	
		31.4		2.97(41) 2.12(118)
¹⁰² Ru	[9], (n,γ),	6/5,	<7.8>, 16, 29, 18, 94	
		24.6		- 4.00(160)
	Enhanced trans.	0.62		2.46(98)
¹⁰⁴ Rh	[9]. (n,γ).	6/4/2,	<6.9/6.9>, 16, 22.8, 31, -	
		23.2		4.13(33) 0.54(31)

^{106}Pd	[9], (n, γ),	8/10/12,	<7.9/7.9>, 10, 9.8, 10.3, 13
	11.9		3.79(87) 1.19(27)
^{116}In	[9], (n, γ),	31/12/12,	<5.9/6.1>, 9.4, 9.5, 9.4, 9.3
	9.5		5.56(159) 1.13(30)
^{122}Sb	[9], (n, γ),	12/9/9,	<6.1/5.9>, 18, 16.5, 18, 18.5
	13.5		3.05(61) 0.61(12)
^{124}Sb	[9], (n, γ),	4/11/13,	<5.6/5.8>, 38, 28, 38, 42
	20.7		3.48(203) 0.79(20)
^{126}Te	[9], (n, γ),	6/10,	<7.7>, 38, 47, 48, 56.25
	38		- 1.60(44)
^{128}I	[9], (n, γ),	8/7/12	<6.5/6.5>, 9.7, 12.9, 14.5, 15
	13.3		1.88(46) 0.31(5)
^{128}I	[22], (n, γ)th,	0/11/20,	<6.5/6.5>, 9.7, 12.9, 14.5, 15
	9.7		8.64(329) 0.73(13)
	$D_0 = <15>$	0.65	5.59(213) 0.47(9)
^{136}Ba	[9], (n, γ),	6/1/4,	<6.6/7.9>, 40, 57.6, 40, -
	47.6		4.23(254) 1.40(70)
^{136}Ba	[23], (n, γ)th,	0/16/16,	<6.5/6.5>, 40, 57.6, 40, -
	40		2.7(7) 0.57(21)

^{144}Nd	[9], (n, γ),	10/3/1,	<6.6/6.3>, 45, 43, 36.5, 40
		44.6	4.59(181) 0.30(22)
^{146}Nd	[9], (n, γ),	10/2,	<6.7/>, 22, 20.2, 17, 20
		18.7	4.31(171) -
^{148}Sm	[18], (n, γ),	12/16.	<6.6/>, 5.7, 5.9, 4.7, 6.8
		5.7	4.5(9) -
^{150}Sm	[9], (n, γ),	3/31,	<6.3/>, 2.2, 2.65, 1.9, 2.45
		2.3	4.46(110) -
^{150}Sm	[19], (n, γ),	7/13.	<6.5/>, 2.2, 2.65, 1.9, 2.45
		2.2	7.83(157) -
^{155}Gd	[20], (n, γ),	15/8,	<5.9/>, 14.5, 14.1, 14.5, -
		14.5	8.3(17) -
^{157}Gd	[19], (n, γ),	NA/5,	<6.0/>, 37.8, 37.6, 38.0, -
		37.8	10.0(18) -
^{159}Gd	[21], (n, γ),	12/8/9,	<5.3/5.1>, 85.0, 91.9, 85.0, -
		85.0	9.0(3) 1.5(3)
^{168}Er	[15], (n, γ),	45/6/4.	<6.4/6.4>, 4.0, 4.44, 4.6, 4.6
		3.8	16.7(152) 4.9(5)

^{169}Er	[9], (n, γ),	7/26/9,	<4.9/5.2>, 94, 94.1, 100, 98.5
	94		6.39(147) 1.57(95)
^{163}Dy	[24], (n, γ)th,	0/9/7,	<5.7/5.3>, 64, 61, 64.6, 82
	55		8.3(4.4) 2.9(1.3)
^{170}Tm	[9], (n, γ),	9/16,	<5.9/>, 7.3, 10.3, 7.3, 16.5
	7.3		4.72(101) -
^{176}Lu	[9], (n, γ),	11/8/2,	<5.8/5.8>, 3.45, 6.05, 3.6, -
	3.47		7.41(251) 3.19(139)
^{177}Lu	[19], (n, γ),	6/15,	<5.9/>, 1.7, 2.75, 1.7, 2.3
	1.7		8.46(410) -
^{174}Yb	[19], (n, γ),	22/5/5,	<6.3/>, 7.8, 7.37, 7.8, 9.5
	7.8		20.0(33) -
^{178}Hf	[9], (n, γ),	37/18/3,	<6.5/6.2>, 2.4, 2.3, 2.4, 2.9
	2.5		17.77(335) 3.65(152)
	Abs. cal. uncert.	0.5	8.89(168)
^{182}Ta	[9], (n, γ),	19/66/1,	<5.2/4.3>, 4.17, 4.4, 4.4, 4.0
	4.5		10.47(157) 6.64(356)
^{183}W	[9], (n, γ),	7/15/5,	<5.2/4.7>, 66, 65.5, 66, 66.8
	66		10.25(338) 4.25(183)

^{184}W	[9], (n, γ), 6/13, <6.3/>, 12, 13.2, 13, 24		
	12	28.14(970)	-
	D ₀ uncertainty		
^{196}Pt	[9], (n, γ), 22/9, <7.0/>, 18, 15.7, 18, 15.4		
	16.3	20.31(257)	-
^{198}Au	[9], (n, γ), 4/5, <6.4/>, 16.5, 15.6, 16.5, 16.75		
	16.2	11.00(530)	-
^{199}Hg	[9], (n, γ), 2/3/41, <6.5/5.2>, 105, 155, 105, 93.65		
	83	58.08(445)	22.1(155)
	3 enh. trans.	0.15	8.71(67)
^{200}Hg	[9], (n, γ), 3/9, <7.2/>, 100, 62, 100, 88.3		
	88.1	10.91(404)	-
^{202}Hg	[9], (n, γ), 3/3, <7.2/>, 98, 90.8, -, 97.8		
	100.5	8.47(693)	-
^{207}Pb	[9], (γ ,n), 11/1, <7.1/>, 35700, 29600, 37100, -		
		36.61(261)	-
	Nonst. effects	0.3	10.98(78)
^{208}Pb	[9], (γ ,n), 10/1/1, <7.5/7.6>, 37500, 38200, 36000, -		
		9.37(800)	0.185(60)
	Nonst. Effects		

^{233}Th	[9].	(n, γ).	5/3/1,	<4.2/4.5>, 16.8, 16.4, 16.8, 16.55
			18.2	18.30(766) 8.88(602)
^{235}U	[9].	(n, γ).	4/53/19,	<3.90/4.4>, 10.6, 12.5, 10.6, 12.15
			12.3	12.14(392) 2.11(78)
^{237}U	[9].	(n, γ).	7/2/3,	<4.6/4.8>, 14.7, 15.8, 15, 16.45
			15.4	8.16(352) 0.37(17)
^{239}U	[9].	(n, γ).	23/9/5,	<4.1/4.2>, 20.9, 21.0, 21.7, 22.3
			16.4	12.74(314) 3.22(96)

The following quantities are quoted in the first line of each section:

^ZA – final nucleus

[Ref.] -- the origin of the data by its reference.

Reac. -- type of data (*e.g.* (n, γ)).

#res/E1/M1 - the number of resonances considered and number of E1 and M1 transitions.

< $E_{\gamma\text{E1}} / E_{\gamma\text{M1}}$ > -- mean energies of E1 and M1 transitions.

D_0 values in eV, quoted in the order of compilations from BNL (Brookhaven), CNDC (Beijing), IPPE (Obninsk), and ENEA (Bologna), published in Refs. [32,29,30,31], respectively.

In the second line, the values from the quoted references are given, together with the applied value of D_0 . The errors, indicated in parentheses, are the following, added in quadrature: statistical, normalization (20%), and Porter-Thomas uncertainty.

In a third line in many of the sections, a comment is given on the quality of data treatment in the original references (if doubts exist). If a revision has been carried out (based on strong arguments), the correction factor and the revised $f(\text{E1})$ and $f(\text{M1})$ values are presented.

Evaluations of Radiative Capture on C, O, and Li

A. Mengoni*

*ENEA, Applied Physics Division,
Via Don Fiammelli 2, 40129 Bologna, Italy,
and*

*RIKEN, Radiation Laboratory,
2-1 Hirosawa, Wako, Saitama 351-02, Japan*

K. Shibata[†]

*JAERI, Nuclear Data Center,
Tokai-mura, Naka-gun, Ibaraki-ken 319-1195, Japan
and*

J. Kopecky[‡]

JUKO Research, Kalmanstraat 4, 1817 HX Alkmaar - The Netherlands

1 Introduction

The methods and models used in the evaluations of ^{12}C , ^{13}C , ^{16}O and ^7Li are described in a previous section of the present report. As mentioned in that section, the evaluations for ^{12}C and ^{16}O have been included in the JENDL-3 special purpose file (Fusion File). Here we will only briefly summarize the points of interest for the evaluation.

1.1 $^{12}\text{C}(n, \gamma)$

The DRC model description and the parameters used for the calculation of $n+^{12}\text{C}$ are given elsewhere [1]. Here we show the results for capture leading to the four bound levels of ^{13}C . These four states are bound by 4.946 ($1/2^-$), 1.857 ($1/2^+$), 1.262 ($3/2^-$),

*e-mail: mengoni@bologna.enea.it

†e-mail: shibata@cracker.tokai.jaeri.go.jp

‡e-mail: juko@wxs.nl

and 1.093 ($5/2^+$) MeV (total angular momentum and parity are indicated between brackets). The results are shown in Figs. 1 to 4, respectively.

In comparison with the calculations provided in the Ref. [1], we have extended the incident neutron energy range up to 800 KeV. A new experimental result at $E_n = 550$ KeV has been made available recently [2] and the respective values are shown in the figures. These new experimental values agree well with the model predictions. In particular, from Figs. 1 and 3 it is possible to notice the onset of d -wave capture. Overall, the DRC model calculations reproduce well the experimental results. As is shown in the figure, a value of 0.84 has to be assumed for the spectroscopic factor of the first excited state in ^{13}C , in comparison with an experimental value of $S_b = 0.65$ derived from the (d, p) reaction. This calculation shows that an important nuclear structure property can be derived from a measurement of the neutron capture cross section, whenever the conditions for a DRC model to be applicable are satisfied.

1.2 $^{13}\text{C}(n, \gamma)$

The calculation of the neutron capture reaction on ^{13}C has been performed. This is a first report on these calculations and it will be described here in some detail.

The wave functions of the bound states of ^{14}C have been calculated using a Woods-Saxon potential model with $r_0 = 1.236$ fm, $d = 0.62$ fm and a spin-orbit interaction strength $V_{ls} = 7.0$ MeV. The depth of the Woods-Saxon potential needed to reproduce the experimental binding energy of each state is given in the table below, together with the most important parameters used for the DRC calculation of the $^{13}\text{C}(n, \gamma)$ cross section.

E_x (MeV)	n l j	V_0 (MeV)	J^π	S_b
0.0	$1p_{1/2}$	49.75	0^+	1.0
7.01	$1p_{3/2}$	26.84	2^+	0.065
6.094	$2s_{1/2}$	57.31	1^-	0.75
6.728	$1d_{5/2}$	54.18	3^-	0.65
6.902	$2s_{1/2}$	54.27	0^-	1.02
7.341	$1d_{5/2}$	52.60	2^-	0.72

There are two sets of states. The positive-parity states can be reached by s - and at high energy by d -wave neutrons. These are dominated by the $^{13}\text{C}(1/2^-) \otimes (1p_{3/2})_\nu >$ or $^{13}\text{C}(1/2^-) \otimes (1p_{1/2})_\nu >$ configurations (p orbits). The negative parity states can only be reached (through a E1 transition) by p -wave neutrons, and their dominant single-particle configurations are

$$^{13}\text{C}(1/2^-) \otimes (2s_{1/2})_\nu > \quad \text{or} \quad ^{13}\text{C}(1/2^-) \otimes (1d_{5/2})_\nu >.$$

The DRC capture cross section leading to these four states is therefore increasing with incident neutron energy. p -wave DRC starts to dominate the capture cross section at $E_n \sim 1$ KeV. At $E_n = 152.9$ KeV there is a p -wave ($J = 2$) resonance with

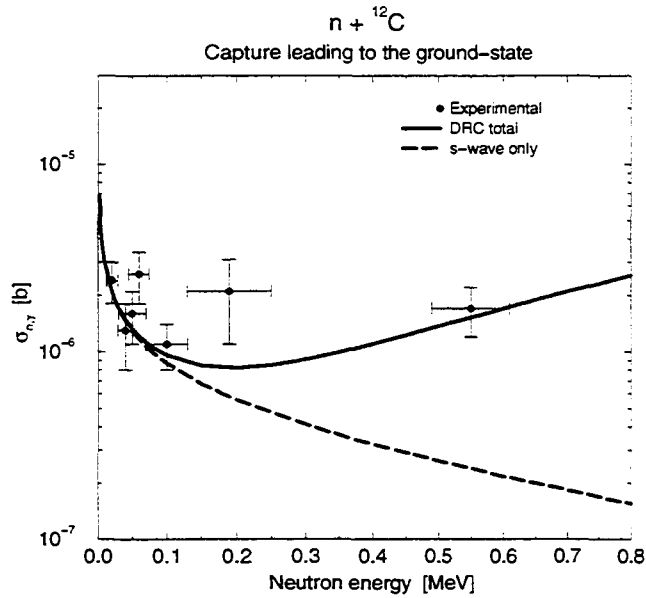


Figure 1: Neutron capture cross section of ${}^{12}\text{C}$ leading to the first excited state of ${}^{13}\text{C}$ ($J^\pi = 1/2^+$). The experimental values are from [8, 2].

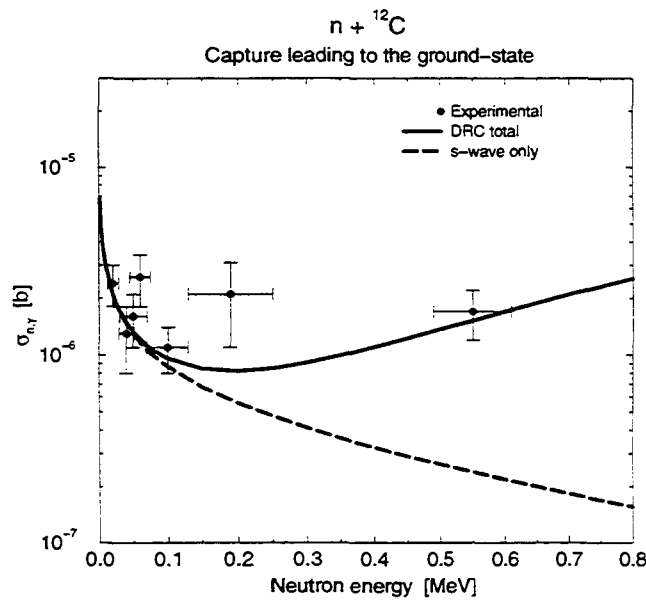


Figure 2: Neutron capture cross section of ${}^{12}\text{C}$ leading to the ground state of ${}^{13}\text{C}$ ($J^\pi = 1/2^-$). The experimental values are from [8, 2].

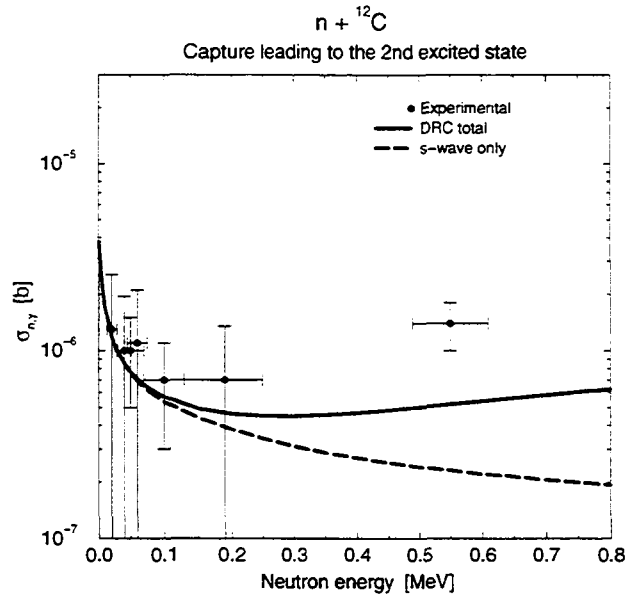


Figure 3: Neutron capture cross section of ${}^{12}\text{C}$ leading to the second excited state of ${}^{13}\text{C}$ ($J^\pi = 3/2^-$). The experimental values are from [8, 2].

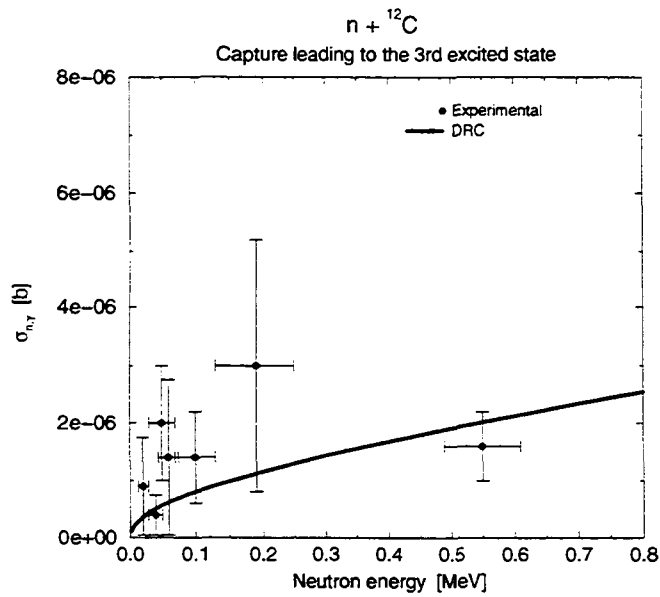


Figure 4: Neutron capture cross section of ${}^{12}\text{C}$ leading to the third excited state of ${}^{13}\text{C}$ ($J^\pi = 5/2^+$). The experimental values are from [8, 2].

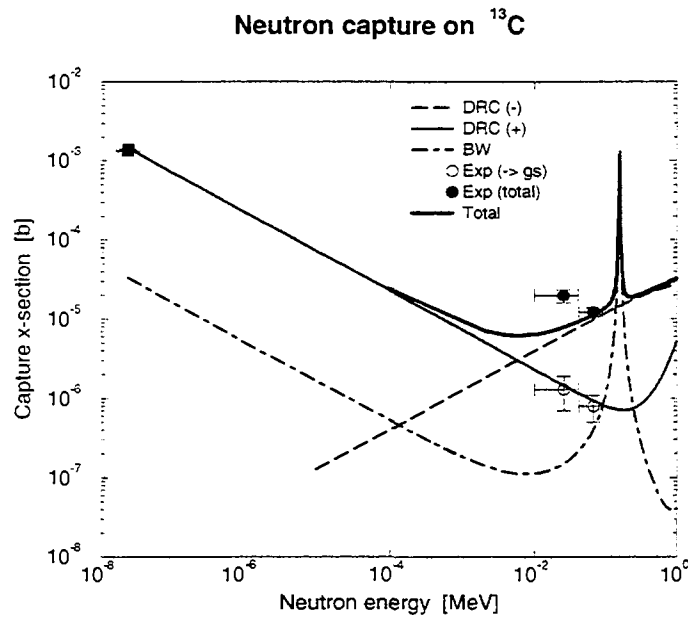


Figure 5: Neutron capture cross section of ^{13}C . The various contribution shown have been calculated as described in the text. The experimental values are from [2].

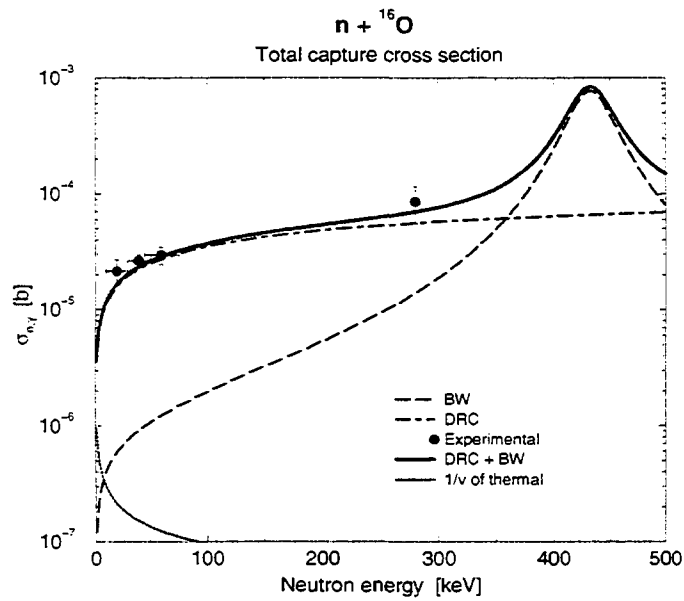


Figure 6: Neutron capture cross section of ^{16}O . The various contribution shown have been calculated as described in the text. The experimental values are from [5].

parameters $\Gamma_n = 3.7 \pm 0.7$ KeV and $\Gamma_\gamma = 0.215$ eV. These parameters are from [3] and must be considered an update of the BNL-Mughabghab (1981) compilation [4] values.

The results of the calculations done including the DRC and single-level Breit-Wigner formula (without interference) are shown in the figure. The calculated thermal capture cross section is $\sigma_{n,\gamma}^{th} = 1.49$ mb, to be compared with the experimental value $\sigma_{n,\gamma}^{exp} = 1.37 \pm 0.04$ mb [4]. The experimental values in the KeV incident neutron energy range are from [2]. The agreement is reasonable for both the transition leading to the ground state as well as for the total capture.

1.3 $^{16}\text{O}(n, \gamma)$

The calculation for $n + ^{16}\text{O}$ has been done following the technique used in the carbon case. Here, the contribution of incident p -waves shows up in the capture leading to the ground and to the first excited state of ^{17}O . These two levels are bound by 4.145 ($5/2^+$) and 3.273 ($1/2^+$) MeV, respectively. They both have strong single-particle character (a spectroscopic factor ≈ 1 can be assumed for both levels), making the DRC model assumptions particularly reliable in the present case.

The cross sections for the transitions leading to the two negative-parity states, bound by 1.088 ($1/2^-$) and 0.303 ($5/2^-$) MeV, are essentially due to incident s -wave neutrons. This contribution can be derived from ^{16}O thermal neutron capture, $\sigma_\gamma = 202 \pm 28$ μb . A $1/v$ approximation can be adopted to evaluate this contribution at higher energies. The contribution of the capture leading to the two negative-parity levels is negligible compared to the contribution coming from incident p -wave neutrons.

The results of our calculation are shown in Fig. 5. Here we show the DRC calculation as the sum of the neutron capture cross section leading to the ground ($5/2^+$) and first excited state ($1/2^+$) of ^{17}O . The contribution due to incident s -wave neutrons is shown as a $1/v$ extension of the thermal neutron capture.

In the $^{16}\text{O}(n, \gamma)$ case, there is a p -wave ($J=3/2$) resonance state at 434 KeV. The neutron and gamma widths of this resonance are respectively $\Gamma_n = 45 \pm 5$ KeV and $\Gamma_\gamma = 2.7 \pm 0.5$ eV. The single-level Bright-Wigner formalism has been applied to evaluate the contribution coming from this resonance state. No interference contribution was included in the present calculation.

The results of Fig. 5 show good agreement with the experimental values of Igashira *et al.* [5].

1.4 $^7\text{Li}(n, \gamma)$

This reaction is important for fusion applications as well as for basic applications (nuclear astrophysics). We report here a first evaluation for this reaction.

${}^8\text{Li}$ has only two bound states, the ground-state with $J^\pi = 2^+$ and an excited state at 0.981 MeV. The single-particle structure of the ground-state is supposed to be

$$|{}^7\text{Li}(3/2^-) \otimes (1p_{3/2})_\nu \rangle \quad \text{or} \quad |{}^7\text{Li}(3/2^-) \otimes (1p_{1/2})_\nu \rangle.$$

Assuming the first of these configurations for the ground state and the second for the 1^+ state at 0.981 MeV, we have calculated the bound-state wave-functions using a Woods-Saxon potential with parameters $r_0 = 1.307$ fm, $d = 0.5$ fm and a spin-orbit interaction strength $V_{is} = 13.0$ MeV. These are the same geometrical parameters required to reproduce the thermal scattering length for the $J = 2$ spin channel ($a_+ = -3.63 \pm 0.05$ fm). The same parameters (with the spin-orbit potential slightly modified: $V_{is} = 10.9$ MeV) are used to reproduce the thermal scattering length for the $J = 1$ spin channel ($a_- = +0.87 \pm 0.07$ fm). The potential well-depths necessary to reproduce the thermal scattering properties are $V_0 = 60.3$ MeV for the $J = 2$ and $V_0 = 50.5$ MeV for the $J = 1$ spin channel, respectively. The well depths required to reproduce the correct binding energy of the ground state (2.033 MeV) and of the first excited state are $V_0 = 36.14$ MeV and $V_0 = 33.44$ MeV, respectively. These last two values are for p -orbits while the values quoted for the scattering channel refer to s -wave scattering.

The thermal cross section has been reported by Lynn *et al.* [6] to be $\sigma_{n,\gamma}^{exp} = 45.4 \pm 3.0$ mb. Our calculation produces $\sigma_{n,\gamma}^{th} = 44.56$ mb with partial cross sections leading to the ground-state and to the first excited state equal to $\sigma_{n,\gamma_0}^{th} = 40.61$ mb and $\sigma_{n,\gamma_1}^{th} = 3.95$ mb, respectively. The agreement is remarkable for these transitions.

The capture cross section leading to the ground state has been recently reported by Blackmon *et al.* [7] for incident neutron energies between 1.5 and 1340 eV. The results of our calculations extend well into this region and the agreement with the experimental values is quite good in this region also.

Some new experimental values have been obtained by the group of Nagai at the Tokyo Institute of Technology [8]. Their experimental values are reported at $E_n = 20.6$, 37.8, and 58.1 KeV. The results of our calculations are in good agreement in this incident energy region as well.

Finally, in the ${}^7\text{Li}(n, \gamma)$ reaction there appears a resonance at $E_n = 254.0$ KeV, with parameters $\Gamma_n = 35.0$ KeV and $\Gamma_\gamma = 0.07$ eV. The Breit-Wigner formalism was applied to include this resonance.

The results of our calculations are shown in Figs. 7-9, in the full energy range. The result of an additional measurement in the KeV energy region including the results of the present calculation has been recently reported by Heil *et al.* [9]. See this reference for further details.

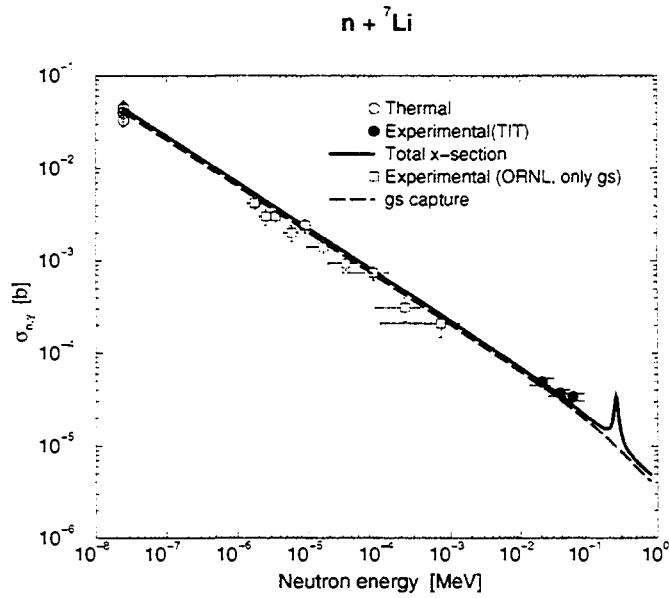


Figure 7: Neutron capture cross section of ${}^7\text{Li}$. The various contribution shown have been calculated as described in the text. The experimental values are from [7] and [5].

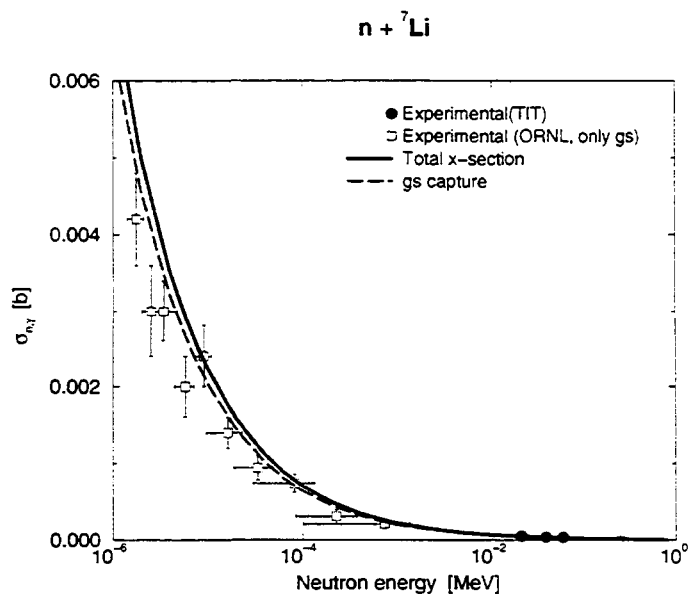


Figure 8: Neutron capture cross section of ${}^7\text{Li}$. The various contribution shown have been calculated as described in the text. The experimental values are from [7] and [5].

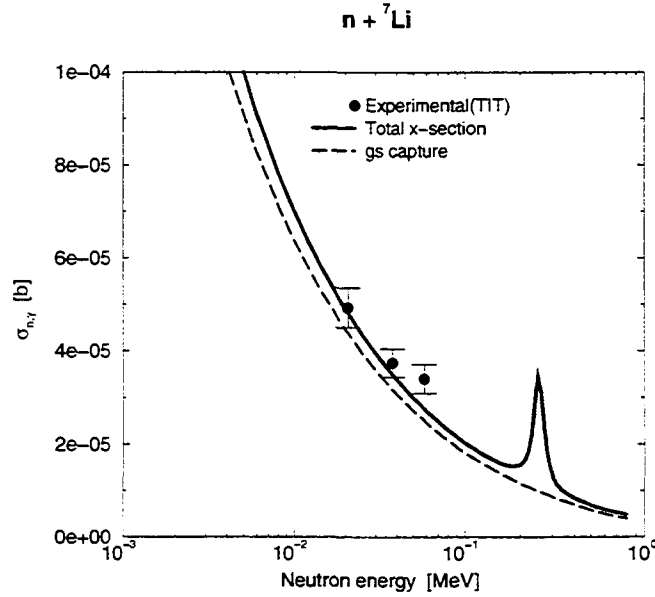


Figure 9: Neutron capture cross section of ${}^7\text{Li}$. The various contribution shown have been calculated as described in the text. The experimental values are from [7] and [5].

2 Recommendations

A recent effort in measuring the extremely small capture cross sections of light nuclei by the experimental groups at the Tokyo Institute of Technology (Y. Nagai group), at the GELINA facility (F. Corvi group), and at the Karlsruhe Forschungszentrum (F. Käppeler and H. Beer group) prompted a re-investigation of the direct radiative capture (DRC) mechanism in light nuclei. As already repeatedly stressed, this capture mechanism is responsible for a large portion of the γ -ray emission strength for incident neutron energies up to the MeV range. The new measurements have provided a set of experimental data that has been used to perform extensive DRC calculations that, in turn, have helped the evaluators in choosing a common strategy.

The parameters required in DRC calculations are commonly derived following this scheme:

- the wave functions of the bound states are calculated using a model potential with the parameters fixed to reproduce the binding energy of the capturing states.
- In the case of incident s -wave neutrons, the potential parameters used in the evaluation of the wave function for the initial states must reproduce the scattering lengths measured at thermal energies, which are usually available for stable targets. In the case of p -wave and higher partial waves, the electromagnetic

transition matrix elements are not sensitive to the potential parameters chosen. In this case, therefore, even a plane-wave approximation to the scattering wave function may be sufficient. Normally, however, the same potential used to calculate bound-state wave functions is adopted also for the continuum $l > 0$ states.

- A slightly different approach to this has been adopted by the group of H. Oberhummer (Technische Universität Wien; see for example [10]). In this case, a (single) folding potential of type

$$V(r) = \lambda \int \rho_A(\mathbf{r}) v_{eff}(E, \rho_A, |\mathbf{R} - \mathbf{r}|) d\mathbf{r}$$

is adopted. Here \mathbf{R} is the relative distance between the target A and the incident neutron, v_{eff} is the effective nucleon-nucleon potential as for example given by the density-dependent M3Y parameterization [11], and ρ_A the nuclear density distribution in the target. The strength λ is fixed in order to reproduce scattering properties. This procedure is altogether equivalent to the potential model approach described in the previous point.

- The DRC component of the capture cross section is calculated using the matrix elements evaluated as just described.
- The resonance contribution can be evaluated separately, since no indication of interference effects between the DRC and resonant components has emerged so far. Experimental resonance energies and widths must be used. We notice here that, unlike the case of medium-mass and heavy nuclei where the resonance states are usually fully developed compound states, in light nuclei many resonance states possess in fact relatively simple configurations. In some cases these states may have a width very close to the Wigner limit (pure single-particle configuration). Some simple nuclear structure model can then be employed to evaluate the widths. Due to statistical properties of compound states, this procedure would be completely unjustified in medium-mass and heavy nuclei.

In summary, the parameterization of the potential models used in DRC cross section calculations can easily be performed for each individual reaction following the recipes given above. A global description of the systematics of the parameters has not yet been produced and could, in principle, be one of the objectives of a new international evaluation cooperation effort.

References

- [1] A. Mengoni, T. Otsuka, and M. Ishihara, Phys. Rev. C **52** (1995) R2334.

- [2] Y. Nagai and T. Shima, private communication (1995, 1996).
- [3] S. Raman *et al.*, Phys. Rev. C **41** (1990) 458.
- [4] S. F. Mughabghab, M. Divadeenam, and N. E. Holden, Neutron Cross Sections (Academic, New York, 1981), Vol. 1.
- [5] M. Igashira, Y. Nagai, K. Masuda, T. Ohsaki and H. Kitazawa, Ap. J. **441**, L89 (1995).
- [6] J. E. Lynn, E. T. Journey, and S. Raman, Phys. Rev. C **44** (1991) 764.
- [7] J. C. Blackmon *et al.*, Phys. Rev. C **54** (1996) 383.
- [8] T. Ohsaki, Y. Nagai, M. Igashira, T. Shima, K. Takeda, S. Seino and T. Irie, Ap. J. **422**, 912 (1994).
- [9] M. Heil, F. Käppeler, M. Wiescher, and A. Mengoni, Ap. J. **507**, 997 (1994).
- [10] E. Krausmann, W. Balogh, H. Oberhummer, T. Rauscher, K. -L. Kratz and W. Ziegert, Phys. Rev. C **53** (1996) 274 and references therein.
- [11] A. M. Kobos, B. A. Brown, R. Lindsay and G. R. Satchler, Nucl. Phys. A **425** (1984) 495.

Evaluation of Photon Production Data for Fe and Ni

Keiichi Shibata

Nuclear Data Center
Japan Atomic Energy Research Institute
Tokai-mura, Ibaraki-ken 319-11, JAPAN

1. Introduction

The third version of the Japanese Evaluated Nuclear Data Library (JENDL-3)¹⁾, which was released in 1989, contained gamma-ray production cross sections and spectra for 59 nuclides. After a slight data modification and an addition of FP nuclide data, the first revision of JENDL-3 (JENDL-3.1) was issued in 1990, gamma-ray production data remaining unchanged. However, some drawbacks were found in photon production data in JENDL. The present work has been performed to improve the evaluated photon production data.

2. Capture gamma-ray spectrum

The evaluations of the photon production data were mainly based on statistical-model calculations except for light nuclides, but some spectral data were replaced with measurements by following the results of benchmark analysis by Cai et al.²⁾ Figure 1 shows the evaluated gamma-ray spectra of ⁵⁸Ni, ⁶⁰Ni, and elemental nickel at thermal energy. The data for the isotopes were based on model calculations, whereas those of the natural element were replaced with the measured data from ORNL. Therefore, there is numerical inconsistency between natural and isotopic data. In addition, the energy balance is not necessarily preserved for the spectra based on measurements.

To solve the problem mentioned above, gamma-ray spectra were recalculated by using a statistical model code CASTHY³⁾ in the energy region from 10⁻⁵ eV to 10 keV, where nonstatistical effects are significant. Special care was taken to consider the non-statistical effects: some branching ratios for primary E1 transitions from a capturing state to discrete levels of the compound nucleus were adjusted so as to reproduce measured spectra at thermal energy. The rest of the branching ratios were estimated with ENSDF⁴⁾ and the giant dipole model. Figure 2 shows thermal neutron capture gamma-ray spectra for

elemental iron and nickel. The re-calculated data almost reproduce the JENDL-3.1 data, which are based on measurements. It should be noted, however, that the calculated elemental data are consistent with the isotopic ones, and that the energy balance is automatically preserved. These revised data were compiled into JENDL-3.2⁵⁾ and the JENDL Fusion File⁶⁾.

3. Total photon production cross section

Total photon production cross sections of Fe and Ni are compared with experimental data in Fig. 3(a)(b). In this figure, the experimental data were obtained by multiplying the spectral measurements by 4π after being integrated over gamma-ray energy, while the evaluated data were corrected for the experimental cut-off energy of the gamma rays. The evaluated data of JENDL-3.2 are considerably larger than those in other libraries, but are consistent with the measured data. As a matter of fact, the iron and nickel data of JENDL-3.2 were obtained by renormalizing statistical-model calculations to the measurements. According to a result from benchmark tests⁷⁾, however, gamma-ray heating in iron was overestimated by the JENDL-3.2 data. Therefore it was decided to adopt the original model calculations for iron and nickel in the JENDL Fusion File without renormalization. It is found from Fig. 3 that the data in the JENDL Fusion File are almost consistent with those in ENDF/B-VI and JFE-2.2.

It should be noted that it is sometimes risky to normalize model calculations to a set of measurements without careful consideration. The particular case of iron mentioned above indicates that feedback from benchmark experiments is important to verify evaluated cross sections. It is recommended that evaluators examine measurements carefully by considering their uncertainties.

References

- 1) Shibata, K. *et al.*, "Japanese Evaluated Nuclear Data Library, Version-3 – JENDL-3", JAERI-1319 (1990).
- 2) Cai, S. *et al.*, *J. Nucl. Sci. Technol.*, **27**, 844 (1990).
- 3) Igarasi, S. and Fukahori, T., "Program CASTHY – Statistical Model Calculation for Neutron Cross Sections and Gamma Ray Spectrum", JAERI-1321 (1991).
- 4) National Nuclear Data Center (BNL), "Evaluated Nuclear Structure Data File (ENSDF).
- 5) Nakagawa, T. *et al.*, *J. Nucl. Sci. Technol.*, **32**, 1259 (1995).

- 6) Shibata, K., "Evaluation of Light-Nuclei and Gamma-ray Production Data", Proc. The Third Specialists' Meeting on Nuclear Data for Fusion Reactors, Tokai 1995, JAERI-Conf 96-005, p.34 (1996).
- 7) Maekawa, F. and Oyama, Y., Proc First Research Coordination Meeting on Measurement, Calculation and Evaluation of Photon Production Data, Bologna 1994, INDC(NDS)-334, p.139 (1995).

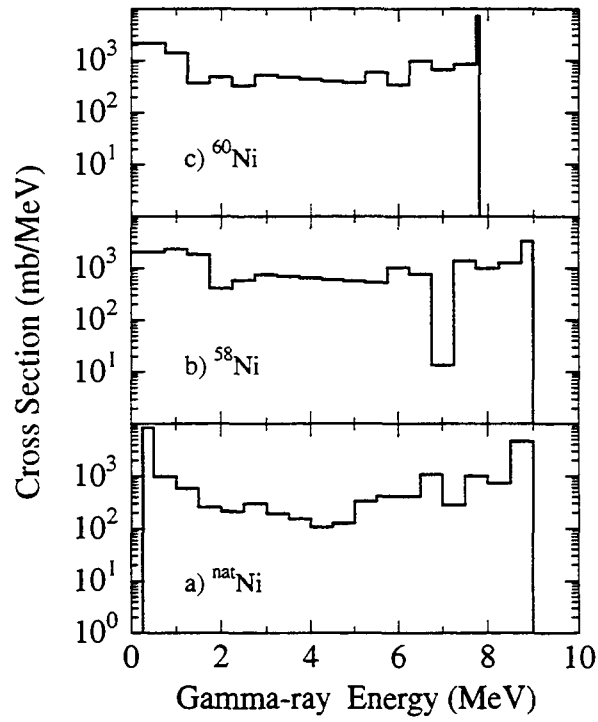


Fig. 1 Thermal capture γ -ray spectra for $^{58,60}\text{Ni}$ and elemental nickel reproduced from JENDL-3.1

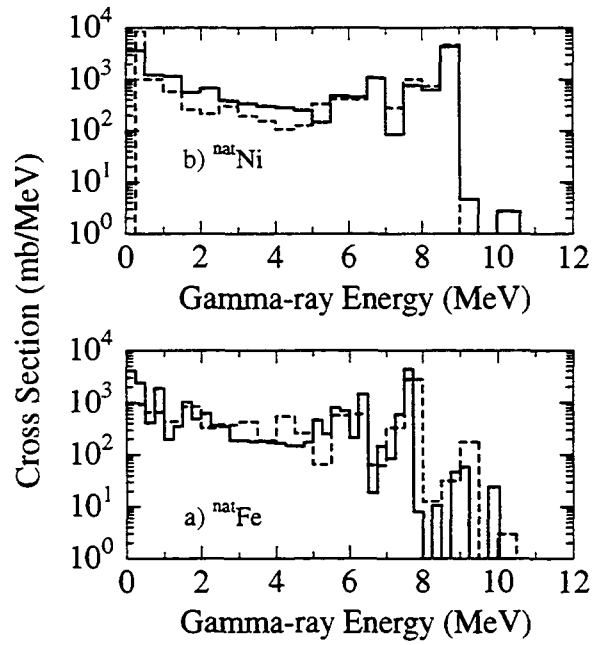


Fig. 2 Thermal capture γ -ray spectra for elemental iron and nickel. The solid lines stands for JENDL-3.2, and the dashed ones for JENDL-3.1.

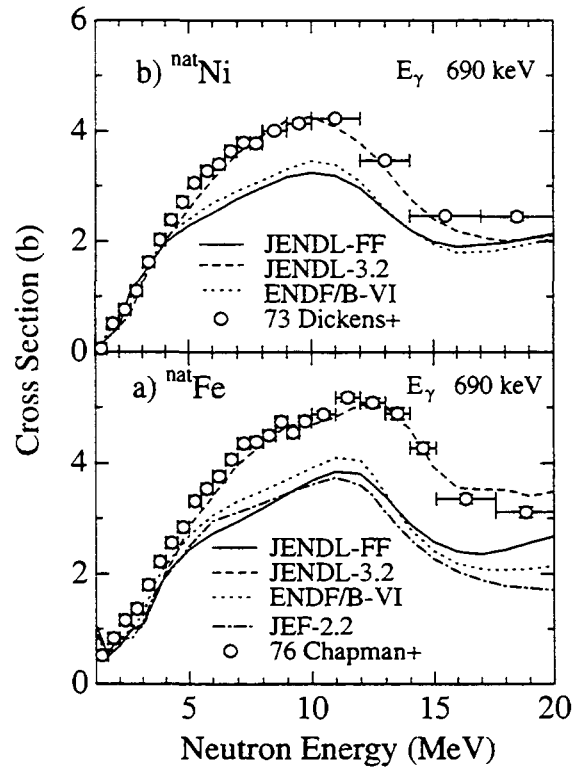


Fig. 3 Total γ -ray production cross section

Review of Evaluations of Photon Production for ${}^7\text{Li}$ and ${}^{52}\text{Cr}$

J. K. Dickens

Joint Institute for Heavy Ion Research
Oak Ridge, Tennessee 37830-6374 USA

1. Evaluations for ${}^7\text{Li}$

Lithium-7 is an important nucleus for the fusion reactor program. At present this isotope is the only convenient one for tritium production, as a world economy supported by fusion reactor power would soon exhaust naturally occurring supplies of tritium. In addition, the "blanket" surrounding the reactor vessel that will be used to convert the outgoing neutron energy into heat is expected to be based on elemental Li. Although tritium production cross sections for $\text{Li} + n$ are paramount, the accuracy of fusion-reactor neutronics calculations depends upon the complete evaluation, including the γ -ray production cross sections.

The reaction ${}^7\text{Li}(n,n'\gamma)$ results in a single gamma ray, $E_\gamma = 478$ keV. Therefore, the gamma-ray production cross section is also the 478-keV level excitation cross section, and this cross section is given in three primary evaluations, namely BROND-2, ENDF/B-VI, and JENDL-3.2. A comparison of these three evaluations is shown in Figure 1 for incident neutron energies up to 13 MeV.

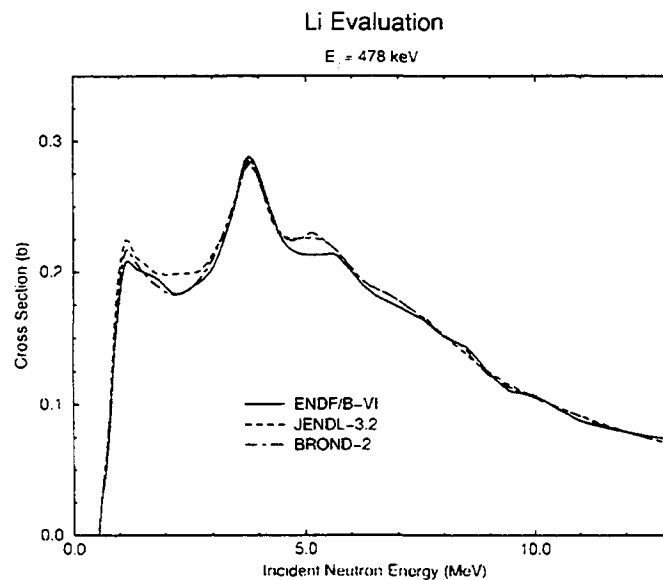


Fig. 1. Evaluated isotopic cross sections for the production of the 478-keV gamma ray following neutron inelastic scattering with ${}^7\text{Li}$.

In this figure, one will note discrepancies among the three evaluations in the regions near neutron energies of 2 and 5 MeV. A review of file 451 for the three evaluations gives an indication of the source these differences.

- 1) The BROND-2 evaluation relied on the data of Bondarenko and Petrov¹.
- 2) The ENDF/B-VI evaluation involved variance-covariance (VC) analyses of data given in 14 experimental reports, but not including the Bondarenko and Petrov experiment cited above.
- 3) The JENDL-3.2 evaluation was based on the measurements of Morgan², experimental data which were included in the ENDF/B-VI analysis.

Evidently the different choices of evaluation methods produced differences for portions of the ${}^7\text{Li}(n,n'\gamma)$ evaluation; however, there appears to be quite good agreement for the main peak for $E_n \approx 4$ MeV as well as for $E_n > 7.5$ MeV. Although it might be assumed that the VC method of evaluation, while requiring more effort, might be the method of choice, it should be noted that the discrepancy for $E_n \approx 5$ MeV is due to the ENDF/B-VI; the other two evaluations agree for this E_n .

2. Evaluations for ${}^{52}\text{Cr}$

Chromium-52 makes up 83.8% of natural Cr, which is an important constituent of stainless steel found in all reactor environments. The dominant gamma ray observed in photon-production spectral measurements³⁻⁶ is the 1.434-MeV photon representing the transition in ${}^{52}\text{Cr}$ between the first-excited state and the ground state. For E_n between threshold and 3.2 MeV the total inelastic scattering cross section is given exactly by the photon production cross section for the 1.434-MeV γ ray. For $E_n > 3.2$ MeV, additional, generally weak, more-energetic γ rays representing direct excited-state- to ground-state transitions are observed; however, the difference between the total inelastic-scattering cross section and the 1.434-MeV photon production cross section is estimated to be no more than 5-7% (refs. 3 and 7) for all E_n . The total inelastic scattering cross section is readily obtained from all evaluations, being given in File 4. Results of five different evaluations are exhibited in Figure 2, and one may note substantial differences among all of the evaluations for the whole range of E_n shown.

Existing data for production cross sections for neutron interactions are for E_n between threshold and ~ 7 MeV, and for $E_n \sim 14.5$ MeV. The latter are well represented in another paper in the present document. There is one data set³ for E_n between threshold and 45 MeV, a portion of which is shown in Figure 3, along with three other data sets,⁴⁻⁶ and an expanded portion of Figure 2. In Figure 3, uncertainties for the Lowell⁴ and Bartol⁵ data sets are total including overall absolute normalization; for the Bettis⁶ data set the quoted 15% uncertainties

in absolute normalization have been quadratically removed for clarity in Figure 3. For the ORNL³ data set, only the statistical uncertainties are available and they are the ones shown in Figure 3. For $E_n < 3$ MeV, the JENDL-3.2 evaluation follows the Lowell data. Other than that observed agreement, the relationships, if any, of any evaluated values to experimental data shown in this figure are not obvious.

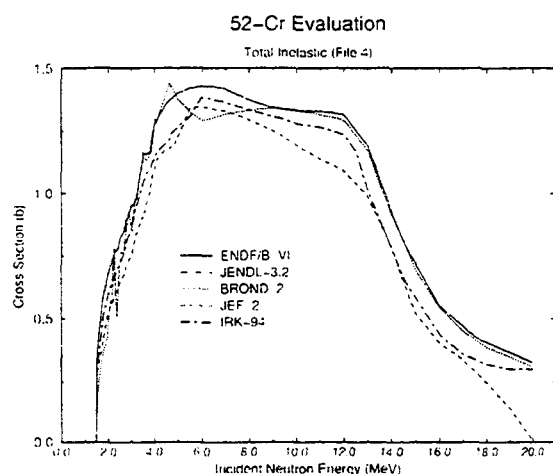


Fig. 2. Evaluated isotopic cross sections for the total inelastic scattering of neutrons from ⁵²Cr for five different major evaluations.

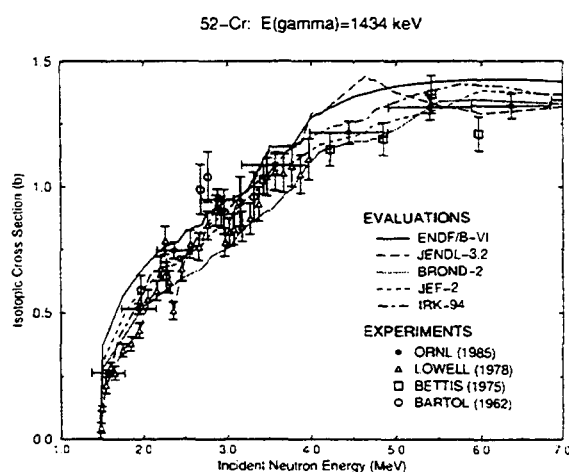


Fig. 3. Evaluated data for ⁵²Cr exhibited in Fig. 2 for E_n between 1 and 7 MeV, along with photon production data for $E_\gamma = 1.434$ MeV from four experiments (Refs. 3 to 6).

3. Conclusions and Recommendations

What is apparent in Figure 3, and to some degree in Figure 1, is that the spread in the evaluations follows the same spread exhibited in the experimental data. The experimental data may be exhibiting some real resonance-like structure; however, most of the ^{52}Cr data appear to resemble a statistical ensemble of elements having the uncertainties as shown, namely in the range 7 - 10% (and larger). (Similar 7-15% differences in evaluations of the 0.847-MeV photon cross sections in ^{56}Fe and the 1.454-MeV photon cross sections in ^{58}Ni appear to reflect the same magnitude as discussed for ^{52}Cr ; experimental data for these two gamma rays have also about the same magnitude of uncertainties assigned by experimenters to their data as shown in Figure 3 for ^{52}Cr .)

If the apparent correlation of the experimental uncertainties to the spread in the resulting evaluations is reasonably valid, then there is no advantage in obtaining additional data having the same approximate uncertainties. Only an experiment with demonstrably (hence believable) much smaller total absolute uncertainties (< 4%, say) would lead to an improvement among different evaluated data sets irrespective of the choice of evaluation methods posited by the individual evaluators.

Alternatively, one may ask, why shouldn't an additional set of data having comparable uncertainties improve the knowledge of the cross section? Bayes' theorem dictates an improvement, however slight. Here it is suggested that for a specific set of evaluation criteria, a reevaluation including an added experimental data set may result in an improved evaluated data set depending upon the criteria used. Since different criteria are being used by different evaluators (most easily observed in the ^7Li case), additional data may have little or no effect on the differences among evaluations. Whether or not such added experimental data *should* result in better agreement among the different evaluations would seem to be a question that should be addressed by evaluators.

4. Acknowledgment

The Joint Institute for Heavy Ion Research has as member institutions the University of Tennessee, Vanderbilt University, and the Oak Ridge National Laboratory; it is supported by the members and by the Department of Energy through Contract Number DE-FG05-87ER40361.

References

1. I. M. Bondarenko and E. E. Petrov, Voprosy Atom. Nauki I Tekniki ser. Yadernya Konstanty, **3** (1984) 44.
2. G. L. Morgan, "Cross Sections for the $^7\text{Li}(n,xn)$ and $^7\text{Li}(n,n'\gamma)$ Reactions Between 1 and 20 MeV," ORNL/TM-6247 (1978).

3. D. C. Larson, "High-Resolution Structural Material (n,x γ) Production Cross Sections for $0.2 < E_n \leq 40$ MeV," in *Nucl. Data for Basic and Applied Science, Proc. of the International Conf., Santa Fe, NM 13-17 May 1985* (Gordon and Breach, New York 1986), p. 71.
4. P. T. Karatzas, G. P. Couchell, B. K. Barnes, L. E. Beghian, P. Harihar, A. Mittler, D. Pullen, E. Sheldon and N. B. Sullivan, *Nucl. Sci. Engr.* **67** (1978) 34.
5. D. M. Van Patter, N. Nath, S. M. Shafroth, S. S. Malik and M. A. Rothman, *Phys. Rev.* **128** (1962) 1246.
6. G. Tessler and S. Glickstein, " γ -ray Production Cross Sections for Neutron Inelastic Scattering from Cr, Ni, ^{92}Zr and ^{94}Zr from 3 to 6 MeV," in *Nucl. Cross Sections and Technology, Proc. Conf., National Bureau of Standards, Spec. Publ. 425* (U.S. Government Printing Office, Washington 1975), Vol 2, p. 916.
7. V. Pronyaev, S. Tagesan, H. Vonach and S. Badikov, "Evaluations of the fast neutron cross sections of ^{52}Cr and ^{56}Fe including complete covariance information," *Physik Daten (Physics Data)*, no. 13-8 1995 (Fachinformationszentrum Karlsruhe, Germany, 1995).

List of Publications produced by the CRP

Given below is a list of 82 technical and scientific papers and reports published by the CRP participants as a result of their activity in the framework of the present CRP in 1994-1997. The publications are arranged along the individual laboratories, common papers are listed only once (under the laboratory of its first author).

● **Austria, IRK Vienna**

1. H. Vonach et al. " $^{207,208}\text{Pb}(n,xn\gamma)$ reactions for neutron energies from 3 to 200 MeV". Phys. Rev. C 50 (1994) 1952.
2. A. Pavlik et al. " $^{207,208}\text{Pb}(n,xn\gamma)$ reactions for neutron energies up to 200 MeV" in J.K. Dickens, ed., Proc. Int. Conf. Nuclear Data for Science and Technology, Gatlinburg, USA, 9-13 May 1994 (American Nuclear Society, La Grange Park, IL 1994) Vol. 1, p. 363.
3. H. Hitzengerger et al. "Study of $^{27}\text{Al}(n,x\gamma)$ up to $E_n=400$ MeV" in J.K. Dickens, ed., Proc. Int. Conf. Nuclear Data for Science and Technology, Gatlinburg, USA, 9-13 May 1994 (American Nuclear Society, La Grange Park, IL 1994) Vol. 1, p. 367.
4. A. Pavlik et al. "Measurement of gamma-ray production cross sections in neutron induced reactions for Al and Pb" in C. Coceva et al., eds., Proc. Specialists' Meeting on Measurement, Calculation and Evaluation of Photon Production Data, Bologna, Italy, 9-11 Nov. 1994, Report NEA/NSC/DOC(95)1 (ENEA, Bologna 1995) p. 33.
5. A. Pavlik et al. " $^{208}\text{Pb}(n,pxn\gamma)$ reactions for neutron energies up to 200 MeV" in P. Obložinský, ed., Measurement, Calculation and Evaluation of Photon Production Data, (text of papers presented at the first research co-ordination meeting, Bologna, Italy, 14-17 Nov. 1994), Report INDC(NDS)-334 (IAEA, Vienna 1995) p. 39.
6. H. Vonach et al. "Spallation reactions in ^{27}Al and ^{56}Fe by 800 MeV protons" Phys. Rev. C 55 (1997) 2458.
7. A. Pavlik et al. " $^{27}\text{Al}(n,x\gamma)$ reactions for neutron energies from 3 to 400 MeV" submitted to Phys. Rev. C.
8. H. Vonach et al. "Spallation reactions in ^{27}Al and ^{56}Fe induced by 800 MeV protons". Proc. Int. Conf. Nuclear Data for Science and Technology, Trieste, 19-24 May 1997, in press.

● **Germany, TU Dresden**

1. H. Freiesleben et al. "An integral test of neutron-induced photon production data for iron". In Report INDC(NDS)-334 (IAEA, Vienna 1995) pp. 137-138.
2. W. Hansen et al. "Test of neutron and photon data in an iron benchmark experiment with 14 MeV neutrons". Proc. Int. Conf. on Nuclear Data, Gatlinburg (USA), 9-15 May 1994 (ed. J.K. Dickens) p. 913.
3. W. Hansen et al. "Gap influence on neutron and photon penetration of an Fe-shield irradiated with 14 MeV neutrons". Proc. Int. Conf. on Nuclear Data, Gatlinburg (USA), 9-15 May 1994 (ed. J.K. Dickens) p. 910.
4. H. Freiesleben et al. "Investigation of neutron and photon fluxes penetrating an iron shield assembly". Proc. 18th Symp. on Fusion Technology, Karlsruhe (Germany), 22-26 Aug. 1994 (ed. K. Herschbach et al.) p. 1365.
5. H. Freiesleben et al. "Experimental investigation of neutron and photon penetration and streaming through iron assemblies". Fusion engineering and design 28 (1995) pp. 545-550.
6. H. Freiesleben et al. "Report on detailed design of neutron and gamma spectra measurements". Report TUD-IKTP/95-02 (Dresden, April 1995).
7. S. Guldbakke et al. "Response matrices of NE-213 scintillation detectors for neutrons". ASTM STP 1228, American Society for Testing Materials, Philadelphia, 1995 (ed. H. Farrar et al.) pp. 310-322.
8. H. Freiesleben et al. "Measurement and analysis of spectral neutron and photon fluxes in an ITER shield mock-up". Proc. 19th Symp. on Fusion Technology, Lisbon (Portugal), 16-20 Sept. 1996 (ed. C. Varandas et al.) p. 1571.
9. H. Freiesleben et al. "Test of photon production data in integral experiments with 14 MeV neutrons". In Report INDC(NDS)-357 (IAEA, Vienna 1996) p. 51.
10. U. Fischer et al. "Test of evaluated data from libraries for fusion applications in an ITER shield mock-up experiment". Proc. Int. Conf. on Nuclear Data, Trieste, 19-24 May 1997, in press.
11. U. Fischer et al. "Improved neutron cross-section data for Fe⁵⁶ and application to an integral fusion neutronics experiment". Proc. Int. Conf. on Nuclear Data, Trieste, 19-24 May 1997, in press.

● **Italy, ENEA Bologna**

1. A. Mengoni et al. "Electromagnetic transitions in halo nuclei" Proc. Int. Conf. on Nuclear Data for Science and Technology, Trieste, 19-24 May 1997, in press (1997).
2. T. Nakamura et al. "Coulomb excitation of ^{11}Be ", Physics Letters B 394 (1997), p. 11.
3. A. Mengoni et al. "Coulomb dissociation processes and capture reaction rates of unstable nuclei". Proc. Workshop on Nuclear Astrophysics. C. Spitaleri, ed., INFN-LNS Report, in press (1997).
4. A. Mengoni et al. "Neutron capture and neutron halos". Proc. Int. Symp. on Capture Gamma-ray and Related Topics. G. Molnár, ed., Springer Verlag, in press (1997).
5. A. Mengoni et al. "Exotic structure of light nuclei and their neutron capture reaction rates". Proc. Int. Conf. "Nuclei in the Cosmos". University of Notre Dame, 20-27 June 1996, Nucl. Phys., A621 (1997) p. 323c.
6. A. Mengoni et al. "Exotic properties of light nuclei and their neutron capture cross sections". Proc. Int. Seminar on Interaction of Neutrons with Nuclei, Dubna (Russia), 27-30 April 1996. W.I. Furman, ed., Report E3-96-336 (1996) p. 165.
7. A. Mengoni "New aspects of the neutron capture of light nuclei". 1st Int. Internet Symp. on Nuclear Data, 1996.
8. A. Mengoni et al. "Exotic properties of light nuclei and their neutron capture reaction rates". In "origin of matter and evolution of galaxies". T. Kajino et al., eds., World Scientific, Singapore (1996), p. 264.
9. F. Käppeler et al. "Neutron capture cross sections of the cerium isotopes for the s- and p-process studies". Physical Review C 53 (1996) 1397.
10. A. Mengoni et al. "Direct radiative capture of p-wave neutrons". Physical Review C 52 (1995) R2334.
11. A. Mengoni "The direct radiative capture process and its role in the calculation of thermonuclear reaction rates". Proc. of the RIKEN-INFN Joint Symp., RIKEN, 22-26 May 1995. M. Ishihara et al., eds., World Scientific (1995) p. 336.
12. A. Mengoni et al. "Neutron capture of nuclei far from stability". Proc. of the 3rd JAERI Workshop on Nuclear Physics with JAERI Tandem-Booster. JAERI Report, in press (1995).
13. A. Mengoni et al. "Fermi-gas model parameterization of nuclear level density". Journal of Nuclear Science and Technology 31 (1994) p. 151.

● **Japan, JAERI Tokai-mura**

1. K. Shibata et al. "Evaluated gamma-ray production data of JENDL-3.2". In Report INDC(NDS)-334 (IAEA, Vienna 1995) pp. 127-136.
2. F. Maekawa et al., presented by K. Shibata "Benchmark test of gamma-ray production data in JENDL-3.2 and FENDL-1". In Report INDC(NDS)-334 (IAEA, Vienna 1995) pp. 139-145.
3. K. Shibata "Evaluation of light-nuclei and gamma-ray production data". Proc. The 3rd Specialists' Mtg. on Nuclear Data for Fusion Reactors, Tokai 1995, JAERI-Conf. 96-005 (1996) p. 34.
4. K. Shibata et al. "Improvement of gamma-ray production data for JENDL-3.2", J. Nucl. Sci. Technol., 34 (1997) 503.

● **The Netherlands, Alkmaar**

1. J. Kopecky et al. "Present status of experimental gamma-ray strength functions". In Report INDC(NDS)-334 (IAEA, Vienna 1995) p. 145.
2. J. Kopecky et al. "Atlas of neutron capture cross sections". Report INDC(NDS)-362 (IAEA, Vienna, April 1997), 369 pages.

● **Russia, IPPE Obninsk**

1. S.P. Simakov "Discrete photon production cross sections in light nuclei at 14 MeV neutron energy". In Report INDC(NDS)-334 (IAEA, Vienna 1995) pp. 13-27.
2. A. Dityuk et al. "The effect of collective excitations on the formation of preequilibrium gamma ray spectra for the radiative neutron capture reaction". In Report INDC(NDS)-334 (IAEA, Vienna 1995) pp. 73-80.
3. S.P. Simakov "Status of experimental and evaluated data for γ -rays production at 14 MeV neutron incident energy". In Report INDC(NDS)-357 (IAEA, Vienna 1996) pp. 45-46.
4. S.P. Simakov et al. "Status of experimental and evaluated data for discrete gamma-ray production at 14.5 MeV neutron incident energy". Report INDC(CCP)-413 (IAEA, Vienna, September 1998), 61 pages.

● **Slovakia, IP SAS Bratislava**

1. E. Běták "Hard gammas from low-energy heavy-ion collisions". Acta Phys. Slov. 44 (1994), pp. 69-73.
2. E. Běták "Exciton-model master equations and the spin mixing". Report IC/94/74 (ICTP, Trieste 1994).
3. E. Běták et al. "Spin effects in the pre-equilibrium decay". In 7th Int. Conf. on Nuclear Reaction Mechanisms, Varenna 1994. Ed. E. Gadioli (Univ. Milano, 1994), pp. 186-195.
4. E. Běták et al. "Spin effects in the pre-equilibrium gamma production". In Proc. Specialists' Meeting on Measurement, Calculation and Evaluation of Photon Production Data, Bologna, Italy, 9-11 Nov. 1994. Ed. C. Coceva et al., Report NEA/NSC/DOC(95)1 (ENEA, Bologna 1995) pp. 193-203.
5. E. Běták "Pre-equilibrium gamma emission: spin-dependent calculations". In "measurement, calculation and evaluation of photon production data". In Report INDC(NDS)-334 (IAEA, Vienna 1995) pp. 93-102.
6. S. Hlaváč et al. "Production of discrete γ rays in light nuclei at 14 MeV. In "measurement, calculation and evaluation of photon production data". In Report INDC(NDS)-334 (IAEA, Vienna 1995) pp. 29-38.
7. S. Hlaváč et al. "Study of gamma radiation from interaction of 14.7 MeV neutrons with ^{208}Pb ". Nucl. Sci. Eng. 119 (1995) pp. 195-202.
8. E. Běták "Role of spin in pre-equilibrium calculations". Acta Phys. Slov. 45 (1995) pp. 625-632.
9. E. Běták "Pre-equilibrium calculations of gamma transitions including discrete states". In Report INDC(NDS)-357 (IAEA Vienna 1996) pp. 35-36.
10. S. Hlaváč et al. "Cross sections for gamma rays produced by 14 MeV neutrons in ^{23}Na , ^{31}P and ^{51}V ". In "measurement, calculation and evaluation of photon production data". In Report INDC(NDS)-357 (IAEA, Vienna 1996) pp. 23-24.
11. E. Běták et al. "Calculated cross sections for ^{123}I formation in photon-, proton-, and helium-ion induced reactions on strongly enriched ^{124}Xe targets". Nukleonika 41 (1996), pp. 3-21.
12. E. Běták et al. "Excitation functions of pre-equilibrium discrete gamma transitions populated in nucleon radiative capture". In 9th Inter. Symp. on Capture Gamma-Ray Spectroscopy and Related Topics, Budapest, Hungary 8-12 Oct. 1996 (in press).

13. S. Hlaváč et al. "Study of gamma radiation from interaction of 14.6 MeV neutrons with ^{27}Al ". Nucl. Sci. Eng. 125 (1997), pp. 196-204.
14. S. Hlaváč et al. "Precise determination of discrete γ ray cross sections in 14.6 MeV neutron reactions". In Inter. Conf. Nuclear Data for Science and Technology, Trieste, Italy 19-24 May 1997 (in press).
15. E. Běták et al. "The 'Lamb shift' in the region of the giant dipole resonance". In Inter. Conf. Nuclear Data for Science and Technology, Trieste, Italy 19-24 May 1997 (in press).
16. E. Běták et al. "Interplay of mechanisms of hard gamma emission". In 8th Int. Conf. Nuclear Reaction Mechanisms, Varenna, Italy, 9-14 June 1997 (Proceedings, Milano University, 1997), pp. 104-113.

● **Slovenia, IJS Ljubljana**

1. F. Cvelbar et al. "Direct-semi-direct and pre-equilibrium model study of the fast nucleon radiative capture reactions". Proc. ISINN-2 Neutron Spectroscopy, Nuclear Structure and Related Topics, (JINR, Dubna 1994).
2. F. Cvelbar "Some open problems of the radiative capture in the region of the giant dipole resonance". Proc. ISINN-2 Neutron Spectroscopy, Nuclear Structure and Related Topics, (JINR, Dubna 1994).
3. F. Cvelbar et al. "Radiative capture in the region of the dipole giant resonance: status of the integrated cross section and of the activation cross section". Proc. NEA Specialists' Meeting on Measurement, Calculation and Evaluation of Photon Production Data, Bologna 1994. Ed. C. Coceva et al., Report NEA/NSC/DOC(95)1 (ENEA, Bologna 1995) p. 204.
4. F. Cvelbar et al. "Average angular distribution of 14 MeV neutron capture γ -rays". Proc. of IAEA 1st Research Co-ordination Meeting on Measurement, Calculation and Evaluation of Photon Production Data, Bologna 1994, INDC(NDS)-334 (IAEA, Vienna 1995) p. 81.
5. A. Likar et al. "On the consistency of direct-semidirect model for radiative capture of nucleons". Book of Abstracts, Int. Nuclear Phys. Conf. INPC'95, 21-26 Aug. 1995, Beijing, China.
6. A. Likar "Nuclear Dicke states in the direct-semidirect model". In INDC(NDS)-334 (IAEA, Vienna 1995) p. 63.

7. A. Likar et al. "Consistent direct-semidirect model for radiative capture of fast neutrons". Poster CR19, abstract booklet, p. 197, gamma-ray spectroscopy and related topics, Budapest, 8-12 Oct. 1996.
8. A. Likar et al. "Consistency of basic assumptions in the DSD model, invited talk". Proceedings of a specialists' meeting on measurement, calculation and evaluation of photon production data, Bologna, Italy, 9-11 Nov. 1994, ed. C. Coceva et al., NEA/NSC/DOC(95)1 p. 19.
9. F. Cvelbar et al. "Pre-equilibrium and direct-semidirect model calculations of nucleon radiative capture excitation functions on heavy nuclei". J. Phys. G: Nucl. Part. Phys. 21 (1995) pp. 377-384.
10. A. Likar et al. "Fast neutron capture through a consistent version of the direct-semidirect model". Nucl. Phys. A591 (1995) pp. 458-478.
11. A. Likar et al. "Calculation of fore-aft asymmetry of gamma-rays from fast neutron capture in ^{40}Ca ". Nucl. Phys. A591 (1995) pp. 479-488.
12. A. Likar et al. "Fast proton capture through a consistent version of the direct-semidirect model". Nucl. Phys. A593 (1995) pp. 69-79.
13. A. Likar "Nuclear Dicke states and the direct-semidirect model". Nucl. Phys. A598 (1996) pp. 235-247.
14. A. Likar et al. "Interference of isovector and isoscalar giant quadrupole resonances in Y and Pb". Nucl. Phys. A611 (1996) pp. 56-67.
15. A. Likar et al. "Fast neutron capture in ^{206}Pb , ^{165}Ho and ^{238}U ". Nucl. Phys. A619 (1997) pp. 57-64.
16. A. Likar et al. "Neutron optical potential from capture reactions". Nucl. Phys. A615 (1997) pp. 18-32.
17. A. Likar et al. "Direct neutron capture in light nuclei". Nucl. Phys. A619 (1997) pp. 49-56.

● **USA, LLNL Livermore**

1. F.S. Dietrich "Overview of reaction mechanisms for calculating the high energy component of fast-nucleon induced gamma spectra". In Report INDC(NDS)-334 (IAEA, Vienna 1995) pp. 53-62.
2. W.E. Parker et al. "Fluctuation effects in radiative capture to unstable final states: A test via the $^{89}\text{Y}(\vec{p},\gamma)$ reaction at $E_p=19.6$ MeV". Phys. Rev. C52 (1995) 252.
3. F.S. Dietrich et al. "Extended direct-semidirect mechanism and the role of multistep processes in fast-nucleon radiative capture". Proc. Int. Conf. on Nuclear Data for Science and Technology, Trieste, 18-24 May 1997 (submitted).

● **USA, ORNL Oak Ridge**

1. J.K. Dickens "Precision measurement of ^{56}Fe cross section for the 846-keV gamma transition and for E_n between threshold and 4 MeV". In Report INDC(NDS)-334 (IAEA, Vienna 1995) pp. 7-12.
2. J.C. Blacknom "Measurements of $^7\text{Li}(n,\gamma)^8\text{Li}$ cross sections at $E_n=1.5-1340$ eV", Phys. Rev. C54 (1996) 383.
3. D.C. Larson et al. "Isotopic cross sections for production of gamma rays created by neutron interactions with ^{11}B for E_n between 2 and 22 MeV: Tabulated data". Report ORNL/TM-13490 (Oak Ridge 1997).
4. J.E. White et al. "Computer programs and data libraries pertaining to photon production data". Report ORNL/RSIC-57 (Oak Ridge 1997).

Participants of the CRP

- H.K. Vonach Institut für Radiumforschung und Kernphysik
A. Pavlik Boltzmangasse 3
 A-1090 Vienna
 Austria
 E-mail: vonach@pap.univie.ac.at
 E-mail: pavlik@pap.univie.ac.at
- S. Unholzer Institut für Kern- und Teilchenphysik
 Technische Universität
 Mommsenstrasse 13
 D-01069 Dresden
 Germany
 E-mail: unholzer@physik.phy.tu-dresden.de
- A. Mengoni Applied Physics Division
 ENEA
 Via Don Fiammelli 2
 I-40129 Bologna
 Italy
 E-mail: mengoni@bologna.enea.it
- K. Shibata Nuclear Data Center,
 Japan Atomic Energy Research Institute
 Tokai-mura, Naka-gun
 Ibarai-ken 319-11
 Japan
 E-mail: shibata@cracker.tokai.jaeri.go.jp
- J.Kopecky JUKO Research
 Kalmanstraat 4,
 NL-1817 HX Alkmaar
 Netherlands
 E-mail: juko@wxs.nl
- S.P. Simakov Institute of Physics and Power Engineering
 Bondarenko Sq. 1
 249020 Obninsk, Kaluga Region
 Russia
 E-mail: simakov@ippe.rssi.ru

- E. Běták
S. Hlaváč
Institute of Physics
Slovak Academy of Sciences
SK-842 48 Bratislava
Slovakia
E-mail: betak@savba.sk
E-mail: hlavac@savba.sk
- F. Cvelbar
A. Likar
Institute Jožef Stefan
Jamova 39
1111 Ljubljana
Slovenia
E-mail: franc.cvelbar@ijs.si
E-mail: andrej.likar@ijs.si
- J.K. Dickens
ORELA
Joint Institute for Heavy Ion Research
Oak Ridge National Laboratory
PO Box 2008
Oak Ridge, TN 37831-6354
USA
E-mail: jkd@astrov.phy.ornl.gov
- F.S. Dietrich
(Chairman)
N-Division
Lawrence Livermore National Laboratory
PO Box 808, L-050
Livermore, CA 94550
USA
E-mail: dietrich2@llnl.gov
- P. Obložinský
(Scientific Secretary)
Nuclear Data Section
IAEA
Wagramerstrasse 5, PO Box 100
A-1400 Vienna
Austria
E-mail: oblozinsky@iaeand.iaea.or.at

Nuclear Data Section
International Atomic Energy Agency
P.O. Box 100
A-1400 Vienna
Austria

e-mail: services@iaeand.iaea.or.at
fax: (43-1) 26007
cable: INATOM VIENNA
telex: 1-12645
telephone: (43-1) 2600-21710

Online: TELNET or FTP: iaeand.iaea.or.at
username: IAEANDS for interactive Nuclear Data Information System
usernames: ANONYMOUS for FTP file transfer;
FENDL2 for FTP file transfer of FENDL-2.0;
RIPL for FTP file transfer of RIPL.
NDSONL for FTP access to files sent to NDIS "open" area.

Web: <http://www-nds.iaea.or.at>
